UILU–ENG–92–2012

CIVIL ENGINEERING STUDIES

STRUCTURAL RESEARCH SERIES NO. 572

AD–A257 816

ISSN: 0069–4274

DTIC
S ELECTE
NOV 1 0 1992
A D

MICROMECHANICS-BASED ANALYSIS OF FIBER-REINFORCED LAMINATED COMPOSITES

By
SHAHZAD RAHMAN
DAVID A. PECKNOLD

DEPARTMENT OF CIVIL ENGINEERING
UNIVERSITY OF ILLINOIS AT
URBANA–CHAMPAIGN
URBANA, ILLINOIS
SEPTEMBER 1992

92-29233

92 11 09 071

50272-101

REPORT DOCUMENTATION PAGE	1. REPORT NO. UILU-ENG-90-2012	2.	3. Recipient's Accession No.

. Title and Subtitle	5. Report Date
Micromechanics-Based Analysis of Fiber-Reinforced Laminated Composites	September 1992
	6.

. Author(s)	8. Performing Organization Report No.
Shahzad Rahman and David A. Pecknold	SRS 572

. Performing Organization Name and Address	10. Project/Task/Work Unit No.
University of Illinois at Urbana-Champaign Department of Civil Engineering 205 N. Mathews Avenue Urbana, Illinois 61801	11. Contract(C) or Grant(G) No. N00014-86-K-0799

12. Sponsoring Organization Name and Address	13. Type of Report & Period Covered
Center for Composite Materials Research University of Illinois at Urbana-Champaign Urbana, IL 61801	1-1-91 to 8-31-92
	14.

15. Supplementary Notes

DoD University Research Initiatives Center – ONR Grant N00014-86-K-0799 (9-15-86 to 12-30-91) and the Industrial Affiliates Program of CCMR

16. Abstract (Limit: 200 words)

A procedure for three-dimensional nonlinear material modelling of fiber-reinforced laminated composites is presented. The material modelling procedure has a two-level hierarchical structure. At the bottom level, constitutive information about the fiber and the matrix phases are synthesized using a micromechanical model to yield the effective stress-strain response of a unidirectional lamina. At the top level, a three-dimensional lamination scheme is employed which assembles the laminae within a sublaminate, and delivers the effective stress-strain response of the sublaminate. Local stresses and strains in a lamina or in fiber and matrix phases can be recovered from the effective values at any stage. The material modelling procedure enables the use of standard displacement-based finite elements. The matrix material is characterized using nonlinear-elastic Ramberg-Osgood relations. Micromechanical failure criteria are used for determining various modes of failure, including compression kink-banding. The accuracy of the micromechanical model is demonstrated by comparing its predictions with results from other micromechanical models and experimental data. Examples are also presented for laminated structures; the results are in good agreement with analytical and experimental results available in the literature.

17. Document Analysis   a. Descriptors

Composite, Compression, Fiber-Reinforced, Finite Elements, Kink-Band, Laminate, Micromechanics, Non-linear Response, Shell, Thick-Section

b. Identifiers/Open-Ended Terms

c. COSATI Field/Group

18. Availability Statement	19. Security Class (This Report) UNCLASSIFIED	21. No. of Pages 171
Release Unlimited	20. Security Class (This Page) UNCLASSIFIED	22. Price

MICROMECHANICS–BASED ANALYSIS OF
FIBER–REINFORCED LAMINATED COMPOSITES

BY

SHAHZAD RAHMAN and DAVID A. PECKNOLD

Urbana, Illinois

ACKNOWLEDGEMENTS

TABLE OF CONTENTS

CHAPTER 1

INTRODUCTION

1.1 General

A *composite* may be defined as (Lee [1]) a multi–phase material formed by combining materials differing in composition and form, in a manner that they remain bonded together and retain their identities and properties. The constituents of a composite act in concert to provide improved specific or synergistic properties not obtainable by one of the components acting alone.

Composite materials are ideally suited for products and applications where high stiffness–to–weight and strength–to–weight ratios are desirable, such as in aircraft and spacecraft structures. Composites are resistant to corrosion and fatigue, and typically have good impact tolerance. All these attributes make the use of composites an attractive option for a wide range of applications, and consequently there has been a steady rise in the use of composites in the aerospace industry, automobile industry, and sporting goods industry. A detailed account of various applications of composite materials may be found in [2].

Composites may be broadly classified as (Lee [1]):

- Fibrous (composed of fibers in a matrix)

- Laminated (layered, of different materials)

- Particulate (composed of particles or flakes in a matrix)

- Hybrid (combinations of any of the above types)

The present study focuses on developing analysis procedures for unidirectionally fiber–reinforced laminated composites. Such a composite consists of unidirectionally fiber–reinforced laminae, stacked together, with the fiber direction in each lamina being possibly different, to achieve the desired properties in each direction.

1

A typical unidirectional fiber–reinforced lamina is about 0.005–0.01 inches in thickness and its cross–section may contain numerous fine fibers arranged in a random order; although to facilitate analytical modelling, it is conveniently assumed that the fibers are arranged in neat packing–geometries, such as triangular, square, or hexagonal.

When structural analysis procedures for structures made of traditional materials of construction such as steel are compared with analysis procedures for laminated structures, two important differences stand out:

- Unlike most metals, a fiber–reinforced lamina tends to be transversely isotropic, with the axis of isotropy being parallel to the fiber direction. Furthermore, the lamina can exhibit nonlinear response, particularly when subjected to shear stress in the plane of lamina.

- In shell and plate structures made of metals, there is rarely a variation of material properties in the thickness direction. Whereas, in laminated plates and shells, the material properties vary from ply to ply because of the different orientation angle of each ply.

These two important differences affect the way in which the analysis of laminated composites is accomplished: the first bears on the *constitutive modelling* of a lamina, and the second on the *structural modelling* of the laminated structure. These two important considerations are described in greater detail in the following sections in order to bring out the motivation and aims of the present study.

1.1.1 Constitutive Modelling of the Lamina

This entails a description of the material behaviour, including a suitable strength theory or criteria employed to define the onset of various modes of failure in the material. The constitutive theories used to model the behaviour of composite materials may be classified as *Micromechanical* or *Macromechanical* in nature. Micromechanical theories predict the overall behaviour of a composite lamina from the known properties of the indi-

vidual constituents, i.e. the fiber and the matrix, and their detailed interaction. This usually involves considering a *Representative Volume Element* of the composite consisting of the fiber phase and the matrix phase. Principles of mechanics are applied to determine the local stress and strain fields within the representative element and the local fields are averaged to yield the effective or equivalent homogeneous properties of the composite lamina. Macromechanical theories on the other hand consider the lamina to be a homogeneous anisotropic material whose properties are to be determined.

One advantage of using a micromechanical theory is that no *apriori* knowledge of the lamina response is needed, since this response is predicted from the properties of the constituent fiber and matrix phases. The constituents themselves are homogeneous, and the vast amount of knowledge accumulated regarding the behaviour of homogeneous materials can be directly employed to construct the effective response of a composite lamina. A second advantage is that since only the properties of the constituents are required, the effect of using different fiber matrix combinations and different fiber volume fractions can be easily studied. Also, the interaction of the fiber and the matrix material can be accurately modelled.

1.1.2 Structural Modelling of Laminates

The laminated nature of composite structures resulting from the stacking together of laminae poses a problem because of the discontinuities in material properties across the interface of two laminae with different fiber orientations. To address this problem, various laminated plate theories have been proposed. The simplest of these theories is the Classical Laminated Plate Theory (CLPT), which is an extension of the classical Kirchhoff plate theory to laminated composites. Similar extensions to Mindlin plate theory have been proposed, and are referred to as First–order Shear Deformation Theories (FSDT) for laminates. CLPT and FSDT predict the response of thin to moderately thick laminates quite well. The perceived need for further refinement and accuracy in the analysis of thick

laminates led to the development of Higher-order Shear Deformation Plate Theories (HSDT), in which the assumed displacement-field is of a still higher polynomial order in the thickness direction than in the FSDT. Aside from the finite elements based on these various laminated plate theories, various types of hybrid elements based on hybrid stress-strain formulations have also been proposed. It is easy to see that with this approach, in order to extend the capabilities of the existing finite element analysis packages to include laminated composite structures, a major effort would be required to develop a separate element library, containing elements specifically for the analysis of laminated composite structures.

The present investigation is aimed at developing efficient and accurate procedures for constitutive modelling of fiber-reinforced composites which enable the use of standard displacement-based finite elements to model laminated structures. The aims and objectives of he present study are formally outlined in the next section.

1.2 Objectives

The aims of this study are as follows:

- To model the response of laminated composites using the properties and the state of its basic constituents, i.e. fiber and matrix. This basically means that some sort of micromechanical constitutive theory is needed to describe the material behaviour of the composite. As previously stated, micromechanical theories have certain advantages over macromechanical theories, since they provide detailed information about the state of the basic constituents, and offer greater flexibility in modelling various types of nonlinearities observed in composites.

- It is desired that the micromechanical theory chosen should be accurate, and at the same time, simple enough to render its incorporation

in a general structural analysis finite element package to be practical.

- The micromechanical model chosen should have sufficient flexibility to enable the modelling of different types of nonlinearity and damage mechanisms.

- The modelling, or the analysis procedure, should be such that the equilibrium requirements on tractions at the laminae interfaces are not violated.

- This material modelling of the laminated composite is to be done in such a manner that the standard displacement–based finite elements can be used for analyzing laminated composite structures.

Having outlined the aims of the present study, a review of the constitutive theories employed to describe the behaviour of composites will be presented next.

1.3 Constitutive Theories for Composites

In the present study it was decided to employ a micromechanical theory; therefore in the following review of constitutive theories, greater emphasis is placed on micromechanical theories.

1.3.1 Micromechanical Theories

The field of micromechanics has been an area of much research activity. The bulk of the earlier literature is devoted to micromechanical theories aimed at determination of effective elastic moduli of a composite lamina from the properties of constituent phases. The simplest micromechanical model for determination of effective elastic moduli is the *Mechanics of Materials* model (Fig. 1.1), in which the constituent phases are assumed to be either connected in a series (Reuss) arrangement, or in a parallel (Voigt) arrangement. The latter arrangement of constituents is also commonly referred to as the *Rule of Mixtures* approach. A description of the Mechanics of Materials approach can be found in the works

of Jones [3] and Harris [4]. The axial stiffness and the axial Poisson's ratio of a unidirectional composite is quite accurately predicted by the Mechanics of Materials approach. To determine the transverse direction properties, the fibers and the matrix are assumed to be connected in series; the resulting estimates of transverse modulus are considerably lower than the experimentally observed values, and in fact, the estimates so obtained define the *Reuss Lower Bound* on the transverse modulus of a unidirectional composite. To remedy this situation *Combination Type* models have been proposed, in which the constituents are arranged in such a manner that a portion of them is acting in series and the remainder is acting in parallel with one another. An example of this approach is the micromechanical model proposed by Shaffer [12]. Shaffer's model resulted in some improvement over the Reuss Lower Bound for transverse modulus. The model could also be extended to consider the response of the composite in the plastic range, i.e after the onset of yielding in the matrix.

In other related works by Evkall [15] and Abolin'sh [16], the increased transverse direction stiffness of unidirectional composites as compared to the prediction by the Mechanics of Materials approach was investigated. Abolin'sh [16] pointed out that when a unidirectional composite is stressed in the direction transverse to the fibers, the matrix is restrained in the fiber direction, because it is attached to the fiber which has high axial stiffness. Thus the apparent stiffness of the matrix is greater than the stiffness of the pure matrix in bulk. When this apparent or effective stiffness of the matrix phase is taken into account, the resulting transverse direction stiffness of composite is greater than that given by the Reuss Lower Bound. This approach is referred to as the *Restrained Matrix Concept*.

Other available schemes include the *Self-consistent Field* method, which includes the *Two-phase model* [19,20,21] (Fig. 1.2) and the *Three-phase model* [17,18,22,23] (Fig. 1.3). In the two-phase model version of the Self-consistent scheme, the effective properties of the composite are determined by solving two problems. First, an inclusion

6

of the fiber phase is considered to be imbedded in a medium whose properties are equivalent to the unknown properties of the composite. A uniform state of stress or strain is then prescribed at a distance sufficiently far from the inclusion. The average stresses and strains in the inclusion are expressible in terms of the elastic moduli of the composite. The same problem is then repeated for the inclusion made up from the matrix phase of the composite. The average stresses or strains in the two phases are then combined to yield the effective moduli of the composite. Among the short–comings of the Two–phase model cited in literature are: that it is appropriate only for low fiber volume fractions, it results in poor representation of the microstructure of the composite, and it does not take into account the interaction among the constituent phases.

The Three–phase variant of the Self–consistent field method, as applicable to fiber–reinforced composites, is attributed to Hill [17,18] in which solutions for four of the five elastic moduli associated with transversely isotropic composite lamina were given. The correct solution for the fifth property (shear modulus in the plane of isotropy) was given later by Christensen and Lo [23]. The model consists of a fiber surrounded by a matrix shell, embedded in a medium whose properties are equivalent to the composite. This model is a more reasonable representation of the microstructure of the composite lamina, as compared to the Two–phase model.

Hashin and Rosen [25] presented the solution for effective moduli of a composite comprised of circular fibers of varying diameters arranged in a random manner. The resulting composite is transversely isotropic in an overall sense. The assumed micro-structure and the corresponding representative volume element are shown in Fig. 1.4. The model is referred to in the literature as the *Composite Cylinder Assemblage* (CCA) model. Closed–form expressions for E_1 ,K_{23} ,G_1 and ν_1 were presented; closed form expressions for G_{23} ,E_2 and ν_{23} could not be obtained, and these quantities could only

be bounded. The results presented by Hashin and Rosen [25] contained some errors; these were subsequently presented in correct form by Dow and Rosen [26], and by Hashin [10,28]. An interesting relation between the Three–phase model and the CCA model was observed by Hashin [9]: the expressions for E_1 ,K_{23} ,G_1 and ν_1 obtained by Hermans [22] for the Three–phase model are exactly the same as given by the CCA model. Hermans' derivation of the expression for G_{23} contained some errors which were removed later by Christensen and Lo [23], who gave the result for G_{23} in the form of a root of a quadratic. It was concluded by Hashin [27] and Christensen and Lo [23] that the Three–phase model and the CCA model are related to one another, although a rigorous proof of the equivalence of the two methods was not given.

Various bounds on the effective elastic moduli of fiber–reinforced composites have been proposed. These include the bounds given by the CCA model [25,26] and the general bounds established by Hill [17] and Hashin [24].

To study the effect of fine details of the microstructure of a composite, such as the shape of the fibers and the fiber packing geometry, upon the effective elastic moduli, various numerical studies have been conducted, e.g. Foye [29], Adams and Doner [30,31] and Chen and Cheng [32,33]. These numerical procedures usually employ either the finite element method or the finite difference procedure in order to model a representative volume element of the composite in detail. The effective moduli of the composite are determined by applying appropriate displacement constraints and loadings on the boundaries of the representative volume element to correspond to uniform nominal strain. Such numerical procedures are far too complicated and computationally intensive for the purpose of structural analysis of composite structures. However, they provide useful and accurate results which can be used to assess the accuracy of other proposed micromechanical models. Also, they provide useful insights into the behaviour of composites as affected by the interaction of the fiber and the matrix at the fiber/matrix interface.

This completes the over–view of micromechanical models used for predicting the linear–elastic properties of fiber–reinforced composites. For detailed discussion and description of various models, the reader is referred to the works of Chamis and Sendekyj [8] and comprehensive reviews by Hashin [9] and McCullough [11]. Next, an account of the micromechanical models which have been used to describe the nonlinear behaviour of fiber–reinforced composites is given.

The earliest work to describe the nonlinear behaviour of fiber–reinforced materials in the context of micromechanics is by Hill [18]. Hill employed the Self–consistent field method to obtain the instantaneous moduli of a composite cylinder under axisymmetric loading conditions; bounds on the instantaneous moduli were also obtained.

A number of finite element based micromechanical studies have been conducted by various researchers to investigate the nonlinear behaviour of fiber–reinforced composites, e.g. Foye [35], Adams [36], and Adams and Crane[37]. Initial yield surfaces for various metal matrix composites subjected to mechanical and thermal loadings were investigated by Dvorak et al.[39,40], using the finite element method. Their results showed that matrix yielding in fibrous composites usually starts at the fiber/matrix interface. The initial yield surface was found to be an irregular ellipsoid, with its longest axis inclined towards the hydrostatic axis in the stress space. The important factors affecting the onset of yielding were found to be the ratio of fiber modulus to matrix modulus and the fiber volume fraction. It was found that relatively small temperature changes can cause yielding. An interesting find reported by them was that unlike homogeneous metals, the application of hydrostatic loading results in yielding of the composite.

Dvorak and Bahei–El–Din [41] employed the Self–consistent field method to study the elastic–plastic behaviour of fibrous composites. The Self–consistent scheme was modified to correct some of the problems associated with the Two–phase version of this method, as reported by Hutchinson [38], who observed high estimates of initial yield

9

stresses and low estimates of plastic strains. The unmodified and modified Self-consistent schemes gave similar results for axisymmetric loading. For the case of longitudinal shear loading the modified self-consistent scheme performed well, whereas the unmodified scheme gave values of initial yield stresses substantially greater than the finite element predictions. The extension of the Self-consistent schemes to handle non–symmetric loadings was found to be difficult.

In an effort to devise a micromechanical model which is simple, yet applicable to general stress states, Dvorak and Bahei–El–Din [41,42] proposed the *Vanishing Fiber Diameter Model*, in which the composite is modelled as a continuum reinforced by fibers of vanishingly small diameter without changing the fiber volume fraction. In this manner the axial strain in both phases was constrained to be the same, thus incorporating the restrained matrix approach. The transverse direction stresses in the fiber and the matrix were assumed to be the same — note that this is tantamount to arranging the fiber and matrix phases in series for loading in transverse direction, hence their observation [43] that some of the moduli given by this model at times fell below the Hashin–Rosen bounds[25].

Min and Crossman [50] presented a Mechanics of Materials based micromechanical model for describing the nonlinear behaviour of fiber–reinforced composites subjected to thermomechanical loadings. The fiber and the matrix phases were assumed to be in a state of plane–stress. The predictions from the model showed reasonable agreement with the experimental data in most cases.

Sun and Chen [55] proposed a simple micromechanical model to investigate elastic–plastic behaviour of fibrous composites. The fiber was assumed to be linearly elastic, and the matrix was modelled as elastic–plastic material following the J_2 flow–rule. A macromechanical orthotropic plasticity model was also proposed to describe the lamina response. The authors suggested that the micromechanical model could be used

to predict the responses of desired fiber matrix combinations, following which the macro-mechanical model could be calibrated and tuned to match the micromechanical predictions. The macromechanical model was used in a finite element based on First-order Shear Deformation Theory to predict the response of notched and tapered laminates [56]. In the development of the micro-model, the constituent phases were assumed to be in the state of plane-stress; thus the three-dimensional nature of the stress field was not accounted for. The matrix restraining effect of the fibers was also not fully accounted for.

A micromechanical theory based on the analysis of a typical repeating cell representing a unidirectional composite was presented by Aboudi [7,51,52,53,54]. The composite is assumed to be comprised of square fibers arranged in a doubly periodic array as shown in Fig.(1.5). The representative cell is divided into four subcells; one fiber subcell and three matrix subcells. The theory proceeds by assuming a linear displacement field in each subcell, and the continuity of displacements and tractions at the fiber/matrix interface is satisfied in an average sense. The theory has been successfully used to describe the nonlinear response of fiber-reinforced composites by using the unified viscoplastic theory of Bodner and Partom [69] to describe the matrix material. The theory is referred to as *Method of Cells*, and is quite accurate, but requires a considerable amount of calculation.

A combination type micromechanical model based on Mechanics of Materials was presented by Pecknold [57]. The model is quite simple in description, and the predictions of elastic moduli showed excellent agreement with results from detailed numerical analyses. The model can portray the three-dimensional stress state of the constituent phases, and can be used for general loading conditions. The three-dimensional matrix restraint effect is also incorporated in this model.

11

1.3.2 Macromechanical Theories

In macromechanical analyses of laminates, a lamina is modelled as an anisotropic homogeneous material; consequently it can not provide information about the state of stress and strain in the constituent phases. Hill's anisotropic plasticity theory [58,59], originally intended to model the orthotropic behavior of rolled metals, has been modified and extended by many researchers to describe the behaviour of fibrous composites. Hill used a general quadratic yield criterion; however, the yield criterion was not based on stress invariants, and consequently the criterion is applicable only in the principal axes of the material. The usual idealizations that hydrostatic stress states do not influence the yield criterion and that the plastic flow is incompressible were retained.

Griffin et al. [60] developed a three-dimensional finite element analysis program for analysis of composite materials. Hill's anisotropic yield criterion was employed along with isotropic hardening. To account for nonlinear deformation characteristics of composites, Ramberg-Osgood type relations were assumed with no stress interaction.

Petit and Waddoups [61] proposed a method for predicting the nonlinear behaviour and strength of laminated composites. The response of the lamina to each stress component was assumed to be independent of stresses in other directions (such materials are referred to as quasi-linear materials). The bimodularity of the lamina in tension and compression was also modelled. Maximum Strain criteria were used to determine failure in a lamina. After failure, the lamina was gradually unloaded in the mode in which the failure had occurred. The analysis was conducted by combining the laminae using the framework of Classical Laminated Plate Theory. Their analysis captured the nonlinear behaviour of laminates fairly well, but the strength predictions made by their procedure ranged from good to poor. The authors emphasized the need for conducting more tests to give their procedure a statistical basis as well. The presentation of results and other data pertaining to the behaviour of laminates investigated by them was quite comprehensive,

and their work still remains as one of the well documented investigations into the behaviour of laminated composites.

Hahn and Tsai [62,63] proposed constitutive equations for a lamina in plane–stress from consideration of the complementary energy density function. The complementary energy density was expressed as a fourth order polynomial in the in–plane stress components. Modifications were made to the general expression so that only shear nonlinearity remained and the response to the other stress components was linear–elastic. The model has been successfully used to describe the nonlinear behaviour of laminates.

Hashin et al. [64] modelled the nonlinear response of unidirectional composites subjected to transverse and shear loadings, using Ramberg–Osgood type relations for the transverse direction and for the case of shear loading. The constitutive relations of the lamina were incorporated into the Classical Laminated Plate Theory, to obtain responses of laminates with various stacking sequences. Their predictions of nonlinear response and failure were in good agreement with predictions from other methods and experimental data.

Dvorak and Rao [65] developed an axisymmetric plasticity theory for fiber–reinforced composites. The yield function was constructed from stress invariants valid for transversely isotropic materials. The composite was assumed to be plastically deformable in the fiber direction, and capable of exhibiting plastic dilatation. A simple hardening rule and an an associated flow rule were also proposed.

Pipkin and Rogers [66] presented a continuum theory for finite plane deformations of composites reinforced by inextensible fibers. The composite was assumed to be incompressible and the fibers were assumed to be continuously distributed. These assumptions are restrictive enough to render some of the problems of deformation kinematically determinate, and if a displacement boundary value problem is prescribed, the displacement field within the composite is determinable without the consideration of

13

constitutive relations for the composite. However, the solution of a traction boundary value problem would require information about the constitutive relations for the composite. The theory was later extended by Mulhern et al. [67] to include plastic deformations.

Mulhern et al. [67] idealized the composite as transversely isotropic, comprised of rigid–perfectly–plastic matrix reinforced by inextensible fibers. The composite material was assumed to be incompressible, non–hardening and rigid–plastic. The yield function was formulated in terms of the five invariants of the stress tensor. In a later work by Mulhern et al. [68], the theory was extended to include elastic–perfectly plastic matrix and elastic fibers.

1.4 Choice of Constitutive Theory

A broad consensus on constitutive modelling for composites has not yet emerged. Here, the merits and demerits of both types of constitutive theories are briefly discussed, and the factors influencing the choice of the constitutive theory selected in this study are presented.

The primary advantage of macromechanical theories is that they require less computational effort. The macromechanical theories are well–enough developed to adequately describe nonlinear response to mechanical loadings. Therefore, structural analysis of composite structures based upon macromechanical theories is a viable option. However, much work needs to be done to extend these theories to incorporate the effects of complex load histories, temperature changes, strain rate sensitivity and creep etc.

Micromechanical theories, besides requiring more computational effort, require the *in situ* properties of the constituent phases which have to be determined (back–calculated) out from tests on laminates. The advantage associated with micromechanical theories is that issues like complex loading histories, thermal effects, and creep and strain rate sensitivity can be addressed with less difficulty. The idea of predicting the response of

composites starting from the basic constituents is intrinsically appealing since the effect of using different fiber/matrix combinations can be studied.

In the present study a micromechanical model is used to describe the behaviour of fiber–reinforced laminated composites. A newly proposed micro–model by Pecknold [57] is investigated and further developed. Preliminary results from this model are very encouraging. It is very simple in description and in the course of this study was found to be comparable in accuracy to Aboudi's Method of Cells.

A brief account of previous studies employing micromechanical models for analysis of composite structures is presented in the next section.

1.5 Previous Studies Using Micromechanics in Structural Analysis

The earliest study of which the author is aware which employs micromechanics for general structural analysis of composites is by Bahei–El–Din et al. [43,44,45]. The Vanishing Fiber Diameter model was employed in a three–dimensional finite element analysis program to model the response of laminated plates. The matrix material was described by the von Mises yield criterion with the Prager–Ziegler kinematic hardening rule. Among the problems investigated were biaxial loading and unloading of laminated plates, and loading of a plate with a hole; stress and strain distributions, and the development of plastic zones in the vicinity of the hole. The results showed fair agreement with experiments and with detailed finite element solutions. The strains in the fiber direction were well predicted; however, the strains in the transverse direction were over–predicted, which is a characteristic of the Vanishing Fiber Diameter micro–model.

Adams and Crane [37] used the finite element method to study the response of a representative volume element of a composite lamina. Nonlinear behaviour of the matrix was taken into account, and special procedures were developed so that a more general state of stress could be applied to the representative volume element. This micromechan-

15

ical modelling procedure was employed in conjunction with Classical Laminated Plate Theory to determine the nonlinear response of simple laminates. Their micromechanical modelling procedure is of interest because it is one of the first attempts at incorporating micromechanics into structural analysis for composites, but it requires extensive computational resources, and its implementation for structural analysis purposes would be prohibitively expensive. A similar procedure was used by Wu et al. [46] to study the response of metal matrix laminates subjected to thermal loading. The analysis was performed by incorporating the *Periodic Hexagonal Array* (PHA) model of Dvorak and Teply [47] into a general purpose finite element analysis program (ABAQUS [48]). The PHA model is based on the assumption that the microstructure of a composite lamina consists of hexagonal fibers arranged in a hexagonal packing geometry; this microstructure can be represented by a triangular representative volume element. The effective response of a lamina was obtained by finite element analysis of the representative volume element. The laminate response was then calculated by modelling each lamina as a solid element. It was reported by Wu et al [46] that the laminate analysis required sizable computational resources, since obtaining the effective lamina response itself required the solution of a finite element problem.

Rufin et al. [49] developed a computer program (MLAP) which employed the Vanishing Fiber Diameter model of Dvorak and Bahei–El–Din [42,45] in conjunction with Classical Laminated Plate Theory to predict the response of metal matrix composites. They observed that, in general, MLAP tended to underestimate the elastic moduli of the composites and overestimate the magnitude of plastic strains. These errors were not significant in the fiber direction, but were more pronounced in the transverse direction. They attributed this discrepancy between the experimental results and MLAP results to two factors: the limitations of the Vanishing Fiber Diameter micro–model and the nonlinear nature of matrix hardening, which could not be captured by MLAP since it assumed linear matrix hardening.

Arenburg [70,71] examined the behaviour of fiber–reinforced metal matrix composites using Aboudi's Method of Cells. The nonlinear matrix behaviour was modelled by the unified viscoplasticity theory of Bodner and Partom[69]. The effective lamina constitutive relations provided by the Method of Cells were incorporated into a First–order Shear Deformation Plate Theory. Results were presented for tensile response of notched coupons, plates in bending, and moment–curvature responses of laminates. The numerical results showed good agreement with experimental results.

1.6 Outline of the Analysis Procedure

Fig. 1.6 shows a laminated plate structure discretized by finite elements. A typical element within the structure is also shown. Stiffnesses, strains and stresses are tracked at sampling points (material points) within each element. This information is provided by the *material model*, which interfaces with the main analysis program. The interface is called a *standard interface* since the laminated heterogeneous nature of the structure is hidden from the main analysis program, and the information being transferred between the material model and the main analysis program is essentially the same as would be required for the analysis of a structure made from a homogeneous material.

Obviously, the standard procedures for sampling the stiffness and stress are not applicable since the material in the neighborhood of a material point is heterogeneous. This problem can be solved if the material in the neighborhood of the material point is represented by an equivalent homogeneous, possibly anisotropic, material. In this study, a material modelling strategy is presented which is based on this homogenization procedure.

As shown in Fig. 1.6, the proposed material model has two components:

(1)   *The Micro–model*, which describes the response of a unidirectional lamina. The stress and strain fields within the fiber and matrix phases are combined appropriately to yield effective stresses and strains in the lamina. Similarly, the effective lamina constitutive relations are developed from the constitu-

17

tive relations of fiber and matrix. The three–dimensional nature of the stress–field in the constituent phases is accounted for, to better represent the fiber/matrix interaction phenomenon.

(2)   *The Sublaminate model,* which generates the response of a group of laminae, by combining the stress and strain fields within each lamina to yield overall stresses and strains. The constitutive properties of a group of laminae are combined in an appropriate manner to yield the constitutive properties of an effective homogeneous material, which represents the group of laminae. A three–dimensional lamination scheme taking into account the in–plane and out–of–plane stresses has been employed in the present study, since the out–of–plane stresses play a decisive role in initiation of delamination, and should be accounted for.

After the stresses, strains and constitutive properties of the effective homogeneous material representing the group of laminae has been determined, this information is passed to the structural analysis package. This process of homogenization of fields within a fiber and matrix to obtain the response of a lamina, followed by homogenization of the various fields within a group of laminae to determine the response of a ply cluster (sublaminate), may be referred to as the *composition* process.

At the end of the composition process, we have the stresses, strains and effective properties of an equivalent material representing a sublaminate. This information is passed to the structural analysis program through a standard interface. This is especially advantageous, since it makes available a large number of the elements contained in the element–libraries of most structural analysis packages. This provides the capability to analyze laminated structures without the investment of the considerable effort required to develop special purpose elements.

During loading of the structure, changes in strains occur at the material points. This change is communicated to the material model through a standard interface. The effect of this change is propagated down, first to the sublaminate model, and then to the micro–model, where the stresses, strains, and the properties of the fiber and the matrix may be updated. This process of propagating the effect of change at the material point down to the basic constituents may be referred to as the *decomposition* process.

Within this general scheme, any type of micro–model and sublaminate model can be used. In this study the micromechanical model proposed by Pecknold [57] is employed because of its simplicity. As a part of this study the micro–model was investigated and was found to be comparable in accuracy to the refined micromechanical models, such as the one presented by Aboudi [7,51,52,53,54].

In the following chapter the development of the micro–model is presented. Examples are presented to demonstrate its accuracy. Chapter Three presents the sublaminate model. In the fourth chapter, the procedure adopted for updating the stresses at a material point is presented. In the fifth chapter, numerical examples are given; results are presented for predictions of nonlinear response of laminae and laminates subjected to uniform loadings, strength response of laminae and their initial yield surfaces are presented. The results from the proposed material model are compared to predictions from other micromechanical models. Chapter Six presents structural level applications, i.e. examples of laminated structures which were solved by the material modelling procedure developed in this study. Chapter Seven is devoted to conclusions from the present study and recommendations for future work.
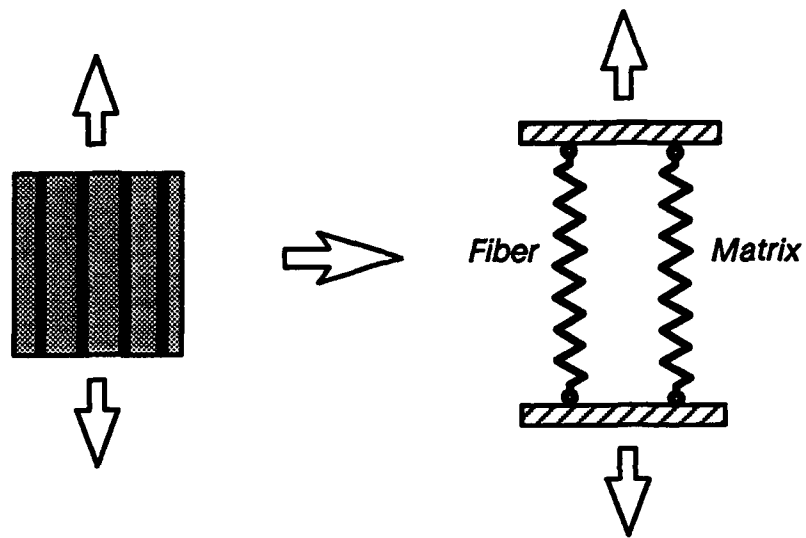
(a) Fiber and matrix in parallel (Voigt) arrangement.
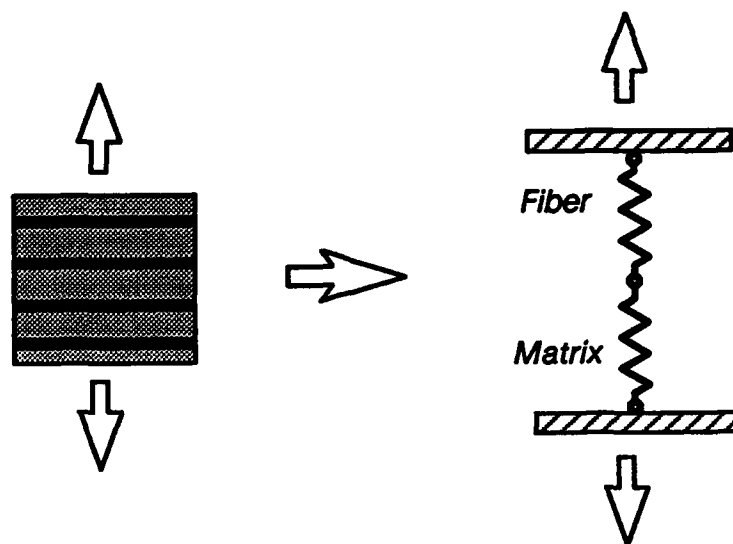
(b) Fiber and matrix in series (Reuss) arrangement.

Fig. 1.1 *Mechanics of Material models*
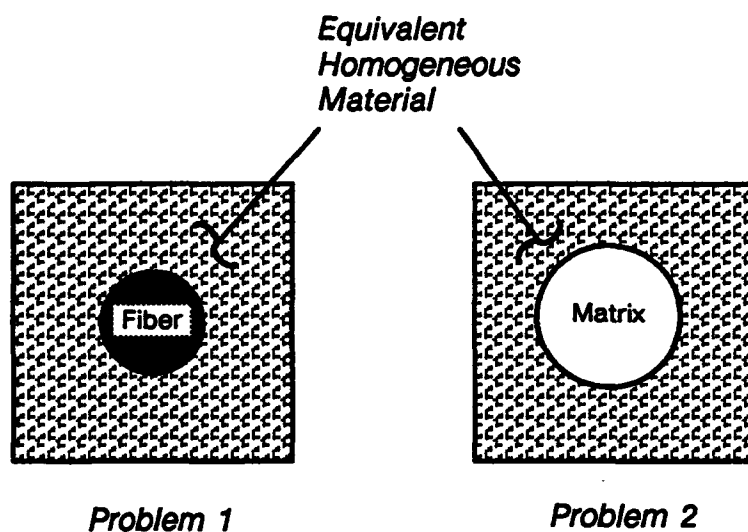
Fig. 1.2 *Description of the Two-phase model*
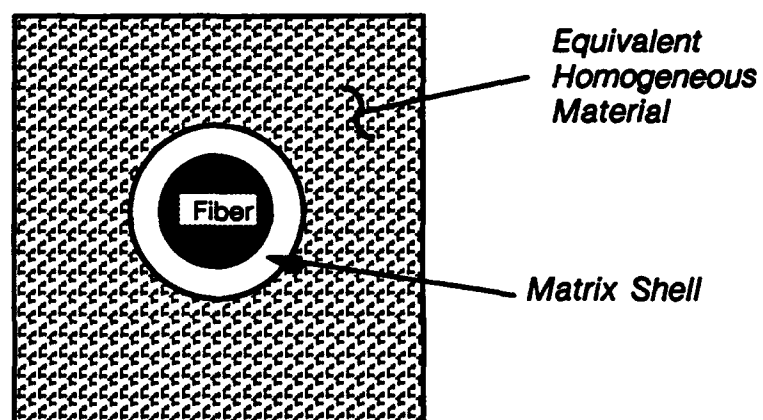
Fig. 1.3 *Description of the Three-phase model*

21

Composite Cylinder Assemblage

Representative Volume Element

Fig. 1.4 Composite Cylinder Assemblage (CCA) model

Doubly Periodic Array

Fiber

Matrix
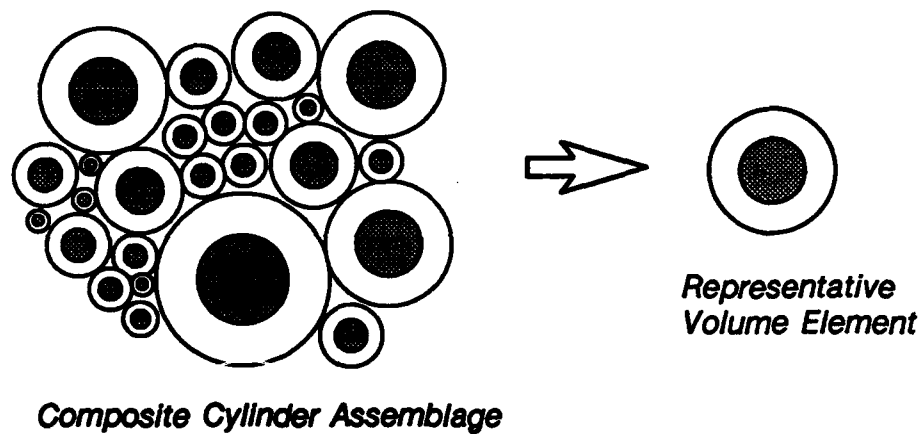
Representative Volume Element
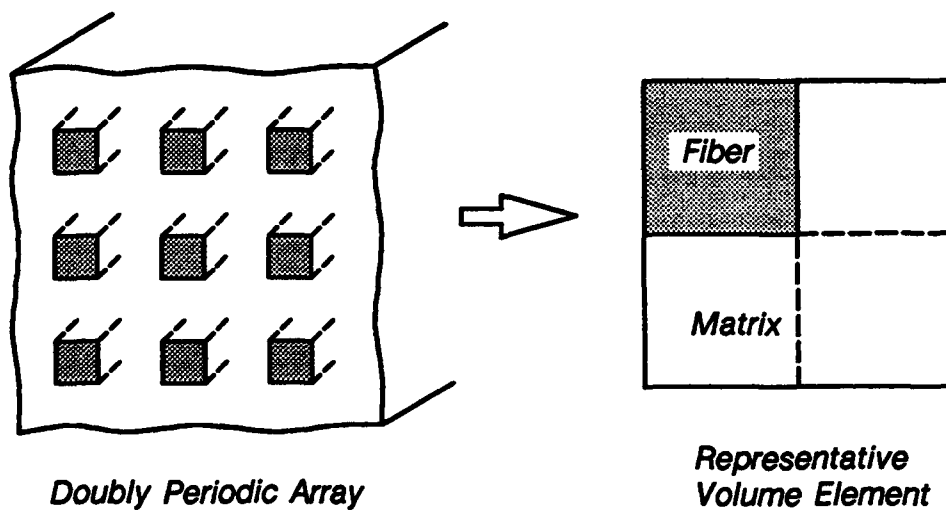
Fig. 1.5 Assumed microstructure and representative volume element in Aboudi's Method of Cells.

Structure

Element

Material Point

Standard
Interface

Equivalent Homogeneous
Material

Sublaminate
Model

Homogeneous Lamina

Fiber   Matrix
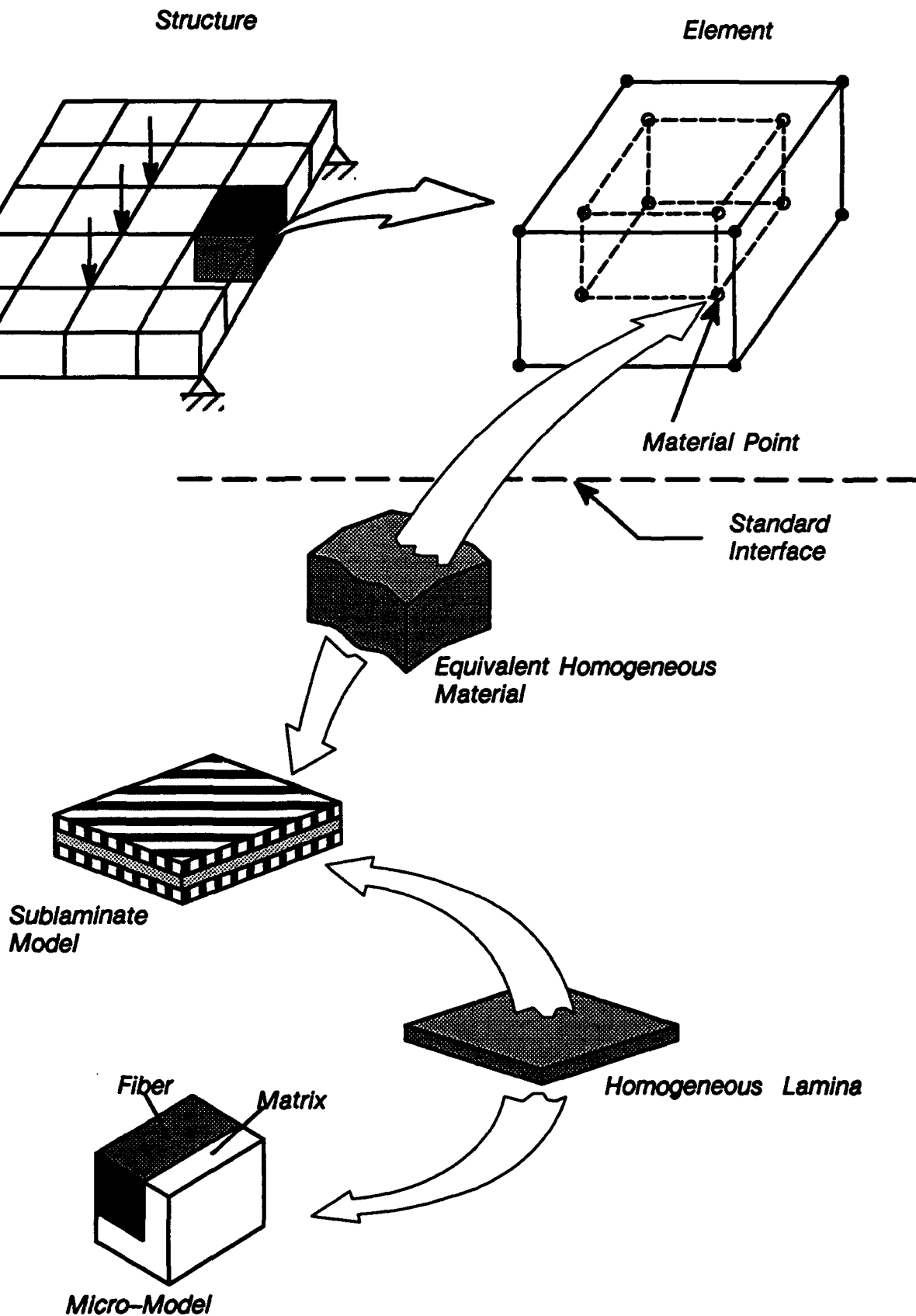
Micro-Model

Fig. 1.6 *Material modelling procedure*

23

MICRO-MODEL

In this chapter the first component of the material model, i.e. the *micro-model*, is described. The micro-model describes the response of a unidirectional lamina, starting from the fiber and the matrix constitutive descriptions. The micro-model employed here is the one proposed by Pecknold [57]. The assumptions made in order to obtain the effective stiffness of the lamina are stated, and the important features of the model are high-lighted. Constitutive relations used to model the nonlinear behaviour of the matrix material are presented. Micro-failure criteria for determination of various failure modes and procedure for incorporating the effect of damage are also presented. Examples are presented to demonstrate the accuracy of the micro-model by comparing its predictions of effective elastic moduli to results obtained from detailed numerical procedures and other established methods.

2.1 Description of the Micro-model

The proposed micromechanical model is based on the assumption that the internal microstructure of the fiber-reinforced lamina consists of square fibers arranged in a doubly periodic array, as shown in Fig. 2.1. Following Shaffer's [12] approach, it is assumed that the stress acting parallel to the x_3 axis is taken up by two strips of material: one is a strip of pure matrix enclosed by lines ll and mm, and the other is a strip of material enclosed by lines mm and nn. The material in the second strip consists of fiber and matrix phases acting in series. Together the two strips are assumed to be acting in parallel to withstand the transverse loading. For axial loading (loading in the fiber direction), both the fiber and the matrix phases are assumed to be acting in parallel.

Also shown in Fig. 2.1 is the *representative unit cell* which corresponds to the assumed geometry of the idealized composite. The unit cell is further subdivided into three subcells; one fiber subcell, denoted by f, and two matrix subcells, denoted by m_A and m_B respectively. The dimensions of the unit cell are 1 unit square, hence the name unit cell. The dimensions of fiber and matrix subcells are given in terms of quantities W_f and W_m, which are defined as

$$W_f = \sqrt{V_f} \qquad , \qquad W_m = 1 - W_f \qquad (2.1)$$

where V_f = Fiber Volume Fraction.

In the following section the assumptions made in homogenizing the stresses and strains will be presented. however before that, for the sake of convenience, the three subcells are grouped to define two elements: *Material Element A*, consisting of the fiber subcell f and the series–or–parallel connected matrix subcell m_A, and *Material Element B*, consisting of the remaining matrix subcell m_B.

2.2 Stress and Strain Homogenization in Unit Cell

The effective stresses and strains in the lamina are determined from the subcell values in two stages: first, fiber subcell f and matrix subcell m_A are used to construct Material Element A; then Material Element A and Material Element B are used to construct the unidirectional lamina. The procedure that is used is shown in Fig. 2.2 by means of spring analogs.

The stress and strain homogenization procedure is now set down more formally in the next section.

2.2.1 Homogenized Stresses and Strains in Material Element A

Within Material Element A, the axial (11) components are treated differently from the remaining components. In order to express the equilibrium and compatibility conditions compactly, the stress and strain vectors are partitioned as follows:

25

$$\{\sigma\} = \begin{Bmatrix} \sigma_{11} \\ \text{---} \\ \sigma_{22} \\ \tau_{12} \\ \sigma_{33} \\ \tau_{23} \\ \tau_{13} \end{Bmatrix} \equiv \begin{Bmatrix} \sigma_L \\ \text{---} \\ \\ \sigma_T \\ \\ \end{Bmatrix} \quad , \quad \{\epsilon\} = \begin{Bmatrix} \epsilon_{11} \\ \text{---} \\ \epsilon_{22} \\ \gamma_{12} \\ \epsilon_{33} \\ \gamma_{23} \\ \gamma_{13} \end{Bmatrix} \equiv \begin{Bmatrix} \epsilon_L \\ \text{---} \\ \\ \epsilon_T \\ \\ \end{Bmatrix} \qquad (2.2)$$

Thus σ_L and ϵ_L are (1x1), and σ_T and ϵ_T are (5x1) matrices. Note that the components of the vectors are not listed in conventional order. Although this particular ordering of components is not necessary for micro–model computations, it is most convenient for subsequent computations at the sublaminate model level.

It is assumed that the axial (fiber) direction strain (ϵ_L) are the same in the fiber and the matrix, and the remaining five "transverse" stress components (σ_T) are the same in the fiber and the matrix. These relations are expressed compactly as

$$\begin{Bmatrix} \epsilon_L \\ \text{---} \\ \sigma_T \end{Bmatrix}_A = \begin{Bmatrix} \epsilon_L \\ \text{---} \\ \sigma_T \end{Bmatrix}_f = \begin{Bmatrix} \epsilon_L \\ \text{---} \\ \sigma_T \end{Bmatrix}_{m_A} \qquad (2.3a)$$

The complementary stress and strain components (i.e. σ_L and ϵ_T) in Material Element A are weighted averages of these stress and strain components in the fiber and the matrix, i.e.

$$\begin{Bmatrix} \sigma_L \\ \text{---} \\ \epsilon_T \end{Bmatrix}_A = W_f \begin{Bmatrix} \sigma_L \\ \text{---} \\ \epsilon_T \end{Bmatrix}_f + W_m \begin{Bmatrix} \sigma_L \\ \text{---} \\ \epsilon_T \end{Bmatrix}_{m_A} \qquad (2.3b)$$

2.2.2 Homogenized Stresses and Strains in Unit Cell

Material Elements A and B are connected in parallel for all component directions, i.e. their strains are the same and the unit–cell–average stresses are weighted averages of the stresses in Elements A and B, i.e.,

$$\left\{ \epsilon \right\}_C = \left\{ \epsilon \right\}_A = \left\{ \epsilon \right\}_B \qquad (2.4a)$$

$$\left\{ \sigma \right\}_C = W_f \left\{ \sigma \right\}_A + W_m \left\{ \sigma \right\}_B \qquad (2.4b)$$

in which the stresses and strains are (6x1) vectors, the subscript C stands for the unit–cell averages.

Eqs. (2.3) and (2.4) are the homogenization relationships that completely define the micromechanical model. These relationships are also valid for incremental stresses and strains. The development of the tangent stiffness of the unit cell follows as a consequence of assumptions made in these relations. The tangent stiffness of the unit cell is also the tangent stiffness of the lamina since the unit cell represents the idealized composite lamina.

2.3 Tangent Stiffness

The tangent stiffness relates incremental (unit–cell–average) stresses and strains. The tangent stiffness of the unit cell is built up from tangent stiffness relations for the two constituent phases; these may be linear relationships or they may reflect various types of nonlinearities.

The incremental stresses and strains within a material are related to each other by relations of the form

$$
\begin{Bmatrix} d\epsilon_{11} \\ d\epsilon_{22} \\ d\gamma_{12} \\ d\epsilon_{33} \\ d\gamma_{23} \\ d\gamma_{13} \end{Bmatrix}
=
\begin{bmatrix}
S_{11} & S_{12} & S_{13} & S_{14} & S_{15} & S_{16} \\
 & S_{22} & S_{23} & S_{24} & S_{25} & S_{26} \\
 & & S_{33} & S_{34} & S_{35} & S_{36} \\
 & \text{Symm} & & S_{44} & S_{45} & S_{46} \\
 & & & & S_{55} & S_{56} \\
 & & & & & S_{66}
\end{bmatrix}
\begin{Bmatrix} d\sigma_{11} \\ d\sigma_{22} \\ d\tau_{12} \\ d\sigma_{33} \\ d\tau_{23} \\ d\tau_{13} \end{Bmatrix}
+ \Delta T
\begin{Bmatrix} a_1 \\ a_2 \\ 0 \\ a_3 \\ 0 \\ 0 \end{Bmatrix}
\qquad (2.5)
$$

where

$$a_1,\ a_2,\ a_3\ =\ \text{Coefficients of thermal expansion in } x_1, x_2 \text{ and } x_3$$
directions respectively.

$$\Delta T\ =\ \text{Change in Temperature.}$$

The above equation can be compactly written in partitioned form in accordance with Eq. (2.2) as

$$\left\{\frac{d\epsilon_L}{d\epsilon_T}\right\} = \left[\begin{array}{c|c} S_{ll} & S_{lt} \\ \hline S_{tl} & S_{tt} \end{array}\right] \left\{\frac{d\sigma_L}{d\sigma_T}\right\} + \Delta T \left\{\frac{a_L}{a_T}\right\} \tag{2.6}$$

The tangent compliance matrix is now partially inverted to provide relations of the form

$$\left\{\frac{d\sigma_L}{d\epsilon_T}\right\} = \left[\begin{array}{c|c} P_{ll} & P_{lt} \\ \hline -P_{lt}^T & P_{tt} \end{array}\right] \left\{\frac{d\epsilon_L}{d\sigma_T}\right\} + \Delta T \left\{\frac{P_{a_L}}{P_{a_T}}\right\} \tag{2.7a}$$

in which P_{ll} is (1x1), P_{lt} is (1x5), and P_{tt} is (5x5), and they are given by:

$$P_{ll} = (1/S_{ll})$$

$$P_{lt} = -(1/S_{ll}) \cdot S_{lt} \tag{2.7b}$$

$$P_{tt} = S_{tt} - (1/S_{ll}) \cdot S_{tl}\ S_{lt}$$

P_{a_L} and P_{a_T} define the vector of partially inverted thermal compliances, and are given by

$$P_{a_L} = -(1/S_{ll})\ a_L$$

$$P_{a_T} = a_T + P_{a_L}\ S_{tl} \tag{2.7c}$$

2.3.1 Material Element A

With the tangent relations for fiber subcell f and matrix subcells m_A expressed in the form of Eq. (2.7a), the homogenization relation Eqs. (2.3) can be applied to give the partially-inverted tangent compliance for Material Element A as

$$\left\{ \frac{d\sigma_L}{d\epsilon_T} \right\}_A = \left[\begin{array}{c|c} \mathbf{P}_{ll} & \mathbf{P}_{lt} \\ \hline -\mathbf{P}_{lt}^T & \mathbf{P}_{tt} \end{array} \right]_A \left\{ \frac{d\epsilon_L}{d\sigma_T} \right\}_A + \Delta T \left\{ \frac{\mathbf{P}_{a_L}}{\mathbf{P}_{a_T}} \right\}_A \qquad (2.8a)$$

where

$$\left[\begin{array}{c|c} \mathbf{P}_{ll} & \mathbf{P}_{lt} \\ \hline -\mathbf{P}_{lt}^T & \mathbf{P}_{tt} \end{array} \right]_A = W_f \left[\begin{array}{c|c} \mathbf{P}_{ll} & \mathbf{P}_{lt} \\ \hline -\mathbf{P}_{lt}^T & \mathbf{P}_{tt} \end{array} \right]_f + W_m \left[\begin{array}{c|c} \mathbf{P}_{ll} & \mathbf{P}_{lt} \\ \hline -\mathbf{P}_{lt}^T & \mathbf{P}_{tt} \end{array} \right]_{m_A} \qquad (2.8b)$$

$$\left\{ \frac{\mathbf{P}_{a_L}}{\mathbf{P}_{a_T}} \right\}_A = W_f \left\{ \frac{\mathbf{P}_{a_L}}{\mathbf{P}_{a_T}} \right\}_f + W_m \left\{ \frac{\mathbf{P}_{a_L}}{\mathbf{P}_{a_T}} \right\}_{m_A}$$

The partial inversion is now completed to give the tangent stiffness of Material Element A as

$$\left\{ \frac{d\sigma_L}{d\sigma_T} \right\}_A = \left[\begin{array}{c|c} \mathbf{C}_{ll} & \mathbf{C}_{lt} \\ \hline \mathbf{C}_{tl} & \mathbf{C}_{tt} \end{array} \right]_A \left\{ \frac{d\epsilon_L}{d\epsilon_T} \right\}_A + \Delta T \left\{ \frac{\beta_L}{\beta_T} \right\}_A \qquad (2.9a)$$

in which

$$\mathbf{C}_{tt} = \mathbf{P}_{tt}^{-1}$$

$$\mathbf{C}_{lt} = \mathbf{P}_{lt} \, \mathbf{C}_{tt}$$

$$\mathbf{C}_{ll} = \mathbf{P}_{ll} + \mathbf{C}_{lt} \, \mathbf{P}_{lt}^T \qquad (2.9b)$$

$$\beta_T = -\mathbf{P}_{tt}^{-1} \, \mathbf{P}_{a_T}$$

$$\beta_L = \mathbf{P}_{a_L} + \mathbf{P}_{lt} \, \beta_T$$

Eq.(2.9a) can be written compactly as

$$\left\{ d\sigma \right\}_A = \left[\mathbf{C} \right]_A \left\{ d\epsilon \right\}_A + \Delta T \left\{ \beta \right\}_A \qquad (2.10)$$

2.3.2 Material Element B

The tangent compliance relations for Material Element B, which consists of a single matrix subcell, is inverted to give the tangent stiffness relation

$$\left\{ d\sigma \right\}_{\mathrm{B}} = \left[\, c \, \right]_{\mathrm{B}} \left\{ d\epsilon \right\}_{\mathrm{B}} + \Delta T \left\{ \beta \right\}_{\mathrm{B}} \qquad (2.11)$$

2.3.3 Unit Cell

The stress and strain homogenization relations (Eqs. (2.4)) are now applied to give the tangent stiffness relation for the unit cell as

$$\left\{ d\sigma \right\}_{\mathrm{C}} = \left[\, c \, \right]_{\mathrm{C}} \left\{ d\epsilon \right\}_{\mathrm{C}} + \Delta T \left\{ \beta \right\}_{\mathrm{C}} \qquad (2.12a)$$

where

$$\left[\, c \, \right]_{\mathrm{C}} = \text{Tangent Stiffness of Unit Cell}$$

$$\left[\, c \, \right]_{\mathrm{C}} = w_f \left[\, c \, \right]_{\mathrm{A}} + w_m \left[\, c \, \right]_{\mathrm{B}} \qquad (2.12b)$$

$$\left\{ \beta \right\}_{\mathrm{C}} = w_f \left\{ \beta \right\}_{\mathrm{A}} + w_m \left\{ \beta \right\}_{\mathrm{B}} \qquad (2.12c)$$

It should be mentioned here that the assumed microstructure of the composite, as shown in Fig. 2.1, corresponds to a material possessing tetragonal symmetry, the stiffness matrix of which is described by six independent moduli. However, because of the simplifying nature of the homogenization relations assumed here the stiffness matrix given by Eq. (2.12a) corresponds to that of a transversely isotropic material, which is characterized by five independent moduli. This is in fact advantageous, since it is known that a unidirectionally reinforced lamina tends to be transversely isotropic. In the next section the procedure for determining equivalent effective moduli of the composite lamina is illustrated. The information regarding the effective moduli of the lamina is not needed for the analysis of the lamina or the laminate; this information is presented only to facilitate comparison of the predicted moduli of composite laminae with other micro-mechanical models.

2.4 Elastic Moduli and Coefficients of Thermal Expansion

With the stiffness matrix of the composite lamina determined from Eq. (2.12a), the effective elastic moduli of the composite can then be calculated by inversion of the stiffness matrix or with the help of following useful relations, which are valid for transversely isotropic materials. If C_{11}, C_{12}, C_{23} etc. are the terms of the stiffness matrix of the composite, then

$$K_{23} = \frac{1}{2} \left(C_{22} + C_{24} \right)$$

$$G_{23} = \frac{1}{2} \left(C_{22} - C_{24} \right)$$

$$G_{12} = G_{13} = G_1 = C_{33}$$

$$E_1 = C_{11} - \frac{C_{12}^2}{K_{23}}$$

$$\nu_{12} = \nu_{13} = \nu_1 = \frac{1}{2} \frac{C_{12}}{K_{23}}$$

$$E_2 = E_3 = \frac{4 \, G_{23} \, K_{23}}{K_{23} + \psi \, G_{23}}$$

(2.13a–f)

where

$$\nu_{23} = \frac{K_{23} - \psi \, G_{23}}{K_{23} + \psi \, G_{23}}$$

$$\psi = 1 + \frac{4 \, K_{23} \nu_1^2}{E_1}$$

(2.13g–h)

K_{23}, G_{23}, E_2 and ν_{23} are the plane strain bulk modulus, shear modulus, transverse Young's modulus and Poisson's ratio in the $x_2 - x_3$ plane, respectively. E_1 and G_1 are the Young's modulus and the shear modulus, in the direction parallel to the fibers and ν_1 is the Poisson's ratio when a uniaxial stress is applied in the direction of the fibers.

Coefficients of thermal expansion for the composite lamina can be extracted by inverting Eq. (2.12a), yielding

$$\left\{ d\epsilon \right\}_C = \left[\, s \, \right]_C \left\{ d\sigma \right\}_C + \Delta T \left\{ a \right\}_C$$

(2.14a)

where

$$[s]_C = \text{Tangent Compliance of Composite} = [c]_C^{-1}$$

$$\{a\}_C = \begin{Bmatrix} a_1 \\ a_2 \\ 0 \\ a_3 \\ 0 \\ 0 \end{Bmatrix}_C = \text{Coefficients of Thermal expansion of Composite lamina.} \qquad (2.14b)$$

$$\{a\}_C = -[s]_C \{\beta\}_C$$

and a_1, a_2 and a_3 are coefficients of thermal expansion in x_1, x_2 and x_3 directions respectively.

Having described the procedure for obtaining effective lamina stiffnesses and compliances, attention is now focused on the procedure for incorporating and modelling various types of nonlinearities in the lamina response. It is often assumed that the fibers within a lamina behave linearly up to the point of fracture, and that the observed nonlinearity in lamina response is caused by the nonlinear response of the matrix material. With this in mind, constitutive descriptions for the matrix material are presented in the next section.

2.5 Constitutive Descriptions of Matrix Nonlinearity

Nonlinear matrix behaviour can be an important factor, since a degrading shear modulus may result in premature buckling of composite shells. Furthermore, matrix softening in shear may interact with or initiate kink-banding. It has also been observed that the nonlinear response of thick laminates is essentially reversible over a substantial loading range (Camponeschi [72,73]). Keeping these considerations in view, a nonlinear elastic description for the matrix material is proposed as a reasonable first step towards describing the nonlinear response of composite laminae. A Ramberg-Osgood type stress-strain relation is proposed here, and is described in the next section.

32

2.5.1 Ramberg-Osgood Relations

A Ramberg–Osgood type stress–strain relation which is valid for general multi-axial stress states may be expressed as

$$\epsilon_{ij} = \epsilon_{ij}^{e} + \frac{a}{3K}\left(\frac{p_e}{p_0}\right)^{m-1} p\, \delta_{ij} + \frac{b}{2G}\left(\frac{\tau_e}{\tau_0}\right)^{n-1} s_{ij} \tag{2.15}$$

The first term on the right hand side is the elastic strain, the second term corresponds to nonlinear pressure–volume change and the third term corresponds to the nonlinear shear softening effects. In the above expression K and G are elastic bulk and shear moduli, a, b, p_0, τ_0, n and m are material constants to be determined and

$$p \equiv \frac{1}{3}\sigma_{kk} \qquad s_{ij} \equiv \sigma_{ij} - p\, \delta_{ij}$$

$$p_e \equiv |p| \qquad \tau_e \equiv \sqrt{\frac{1}{2} s_{ij}\, s_{ij}} \tag{2.16}$$

The quantity p is recognizable as one–third of the first invariant of the stress tensor, and τ_e is the second invariant of the deviatoric stress tensor.

The incremental form of Eq. (2.15) is

$$d\epsilon_{ij} = d\epsilon_{ij}^{e} + \frac{a}{3K}\, m\, \left(\frac{p_e}{p_0}\right)^{m-1} dp\, \delta_{ij} + \frac{b}{2G}\left(\frac{\tau_e}{\tau_0}\right)^{n-1} ds_{ij}$$

$$+ \frac{b}{2G}\, \frac{n-1}{2}\left(\frac{\tau_e}{\tau_0}\right)^{n-1} \bar{s}_{ij}\, \bar{s}_{kl}\, ds_{kl} \tag{2.17}$$

where $\bar{s}_{ij}$ are the normalized deviator stresses defined as,

$$\bar{s}_{ij} \equiv \frac{s_{ij}}{\tau_e} \tag{2.18}$$

Eqs. (2.15) and (2.17) can be expressed in matrix form as

$$\left\{\epsilon\right\} = \left[\, c_1\, [S_1] + c_2\, [S_2]\, \right] \left\{\sigma\right\} \tag{2.19}$$

$$\left\{d\epsilon\right\} = \left[\, d_1\, [S_1] + d_2\, [S_2] + d_3\, [S_3]\, \right] \left\{d\sigma\right\} \tag{2.20}$$

33

The the stress and strain vectors are ordered as in Eq. (2.2), and the matrices S_1, S_2, S_3 are:

$$[S_1] = \begin{bmatrix} 1 & & & & & \\ 1 & 1 & & \text{Symm} & & \\ 0 & 0 & 0 & & & \\ 1 & 1 & 1 & 0 & & \\ 0 & 0 & 0 & 0 & 0 & \\ 0 & 0 & 0 & 0 & 0 & 0 \end{bmatrix} \quad , \quad [S_2] = \begin{bmatrix} 1 & & & & & \\ 0 & 1 & & \text{Symm} & & \\ 0 & 0 & 2 & & & \\ 0 & 0 & 0 & 1 & & \\ 0 & 0 & 0 & 0 & 2 & \\ 0 & 0 & 0 & 0 & 0 & 2 \end{bmatrix}$$

(2.21)

$$[S_3] = \bar{s}\,\bar{s}^T \quad , \quad \bar{s} = \begin{Bmatrix} \bar{s}_{11} \\ \bar{s}_{22} \\ 2\bar{s}_{12} \\ \bar{s}_{33} \\ 2\bar{s}_{23} \\ 2\bar{s}_{13} \end{Bmatrix}$$

and the functions c_1, c_2 and d_1, d_2, d_3 are given by

$$c_1 = \left[\frac{1}{9K}(1+a_1) - \frac{1}{6G}(1+b_1)\right]$$

$$c_2 = \frac{1}{2G}(1+b_1)$$

$$d_1 = \left[\frac{1}{9K}(1+m\ a_1) - \frac{1}{6G}(1+b_1)\right]$$

$$d_2 = c_2$$

(2.22a–g)

$$d_3 = \frac{1}{2G}\frac{n-1}{2}b_1$$

$$a_1 = a\left(\frac{p_e}{p_0}\right)^{m-1}$$

$$b_1 = b\left(\frac{\tau_e}{\tau_0}\right)^{n-1}$$

The standard Ramberg–Osgood relations as described above can be used to describe the nonlinear response of most metal matrix composites. However, in their standard form the Ramberg–Osgood relations also result in significant nonlinearity in response to transverse loading. The limited experimental data available for polymer matrix composites seem to suggest that even though the lamina response is quite nonlinear in

shear, no significant nonlinearity exists in response to transverse normal loading. The above-mentioned relations for matrix behaviour cannot accommodate both these behaviours simultaneously. Therefore, modifications are proposed to the above proposed Ramberg-Osgood relations, to be used in the case when nonlinearity exists only in shear response. The modified constitutive relations for the matrix material are presented in the next section.

2.5.2 Modified Ramberg-Osgood Relations

The suggested modifications are as follows. Since nonlinear behaviour only in shear is sought, the pressure-volume change term can be dropped from consideration, and the response to normal loading in all three directions can be assumed to be linear. The detailed description of the modifications made to the Ramberg-Osgood relations is as follows.

It is assumed that the response to σ_{11}, σ_{22}, and σ_{33} is essentially linear, i.e.,

$$\epsilon_{ij} = \epsilon_{ij}^{e} \qquad , \qquad \text{for} \quad i = j \qquad \text{(2.23a)}$$

The response in shear is described as

$$\epsilon_{ij} = \epsilon_{ij}^{e} + \frac{b}{2G} \left(\frac{\tau_e}{\tau_0}\right)^{n-1} s_{ij} \qquad , \qquad \text{for} \quad i \neq j \qquad \text{(2.23b)}$$

The definition of τ_e is changed to

$$\tau_e = \sqrt{\frac{1}{2} s_{ij} \, s_{ij}} \qquad , \qquad \text{for} \quad i \neq j \qquad \text{(2.24)}$$

The incremental strains are given by

$$d\epsilon_{ij} = d\epsilon_{ij}^{e} \qquad , \qquad \text{for} \quad i = j \qquad \text{(2.25a)}$$

and

$$d\epsilon_{ij} = d\epsilon_{ij}^{e} + \frac{b}{2G} \left(\frac{\tau_e}{\tau_0}\right)^{n-1} ds_{ij}$$

$$+ \frac{b}{2G} \frac{n-1}{2} \left(\frac{\tau_e}{\tau_0}\right)^{n-1} s_{ij} \, s_{kl} \, ds_{kl} \quad , \qquad \text{for} \quad i \neq j \qquad \text{(2.25b)}$$

35

where the normalized deviator stresses are defined in similar fashion as before, but with respect to the new definition of τ_e given in Eq. (2.24).

Eqs. (2.23) and (2.25) can be expressed in matrix form as:

$$\{\epsilon\} = \left[c_1 \ [S_1] \ + \ c_2 \ [S_2] \right] \{\sigma\} \tag{2.26}$$

$$\{d\epsilon\} = \left[c_1 \ [S_1] \ + \ c_2 \ [S_2] \ + \ d_3 \ [S_3] \right] \{d\sigma\} \tag{2.27}$$

where the matrices S_1, S_2, S_3 are defined as:

$$[S_1] = \begin{bmatrix} 1 & & & & & \\ 1 & 1 & & \text{Symm} & & \\ 0 & 0 & 0 & & & \\ 1 & 1 & 1 & 0 & & \\ 0 & 0 & 0 & 0 & 0 & \\ 0 & 0 & 0 & 0 & 0 & 0 \end{bmatrix}, \quad [S_2] = \begin{bmatrix} 1 & & & & & \\ 0 & 1 & & & \text{Symm} & \\ 0 & 0 & 2(1+b_1) & & & \\ 0 & 0 & 0 & 1 & & \\ 0 & 0 & 0 & 0 & 2(1+b_1) & \\ 0 & 0 & 0 & 0 & 0 & 2(1+b_1) \end{bmatrix}$$

$$[S_3] = \bar{s} \ \bar{s}^T, \quad \bar{s} = \begin{Bmatrix} 0 \\ 0 \\ 2\bar{s}_{12} \\ 0 \\ 2\bar{s}_{23} \\ 2\bar{s}_{13} \end{Bmatrix} \tag{2.28}$$

and the functions c_1, c_2 and d_3 are given by

$$c_1 = \left(\frac{1}{9K} - \frac{1}{6G} \right)$$

$$c_2 = \frac{1}{2G}$$

$$d_3 = \frac{1}{2G} \frac{n-1}{2} b_1 \tag{2.29a–d}$$

$$b_1 = b \left(\frac{\tau_e}{\tau_0} \right)^{n-1}$$

It should be noted that because of the modifications made in the definition of τ_e the modified Ramberg–Osgood relations are no longer based on invariants of stress, and are applicable only in lamina coordinates.

36

2.6 Failure Criteria
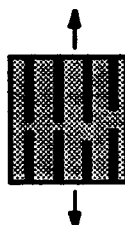
Numerous macromechanical criteria at the lamina level have been proposed, which view the lamina as an effective homogeneous anisotropic material, and describe the failure surface as a stress polynomial, e.g. the "Tsai–Wu Tensor Polynomial" criterion [88], and the "Quadratic Stress Polynomial" criterion proposed by Hashin [89]. A comprehensive survey of macromechanical failure criteria can be found in the works of Tsai [90] and Nahas [91].

Aboudi [52] employed the Method of Cells to predict the off–axis strength of unidirectional composite laminae. Failure of the composite lamina was predicted by using micro–failure criteria for the fiber and matrix phases. The lamina was subjected to off–axis loading, and stresses within the various subcells of the unit cell representing the lamina were monitored. A maximum stress failure criterion was applied to the constituent phases, to define the failure of the lamina. Aboudi's analytical results were in good agreement with experimental results.

Here, an attempt is made to employ micromechanical failure criteria to detect damage and failure in the lamina, since the stresses and strains in the constituent fiber and matrix phases are readily available through the micro–model. Attention is focused on in–plane failure mechanisms only. A brief description of these damage mechanisms and failure modes along with the criteria defining their initiation are presented in this section.

2.6.1 Fiber Fracture in Tension

A unidirectional lamina subjected to tensile loading in the fiber direction may fail by fiber fracture. If $X_t^{(f)}$ denotes the tensile strength of the fiber, then the fiber fracture mode of failure is determined by

$$\sigma_{11}^{(f)} \geq X_t^{(f)} \implies \textit{Fiber Fracture} \qquad (2.30)$$

2.6.2 Matrix Shearing

If $S^{(m)}$ is the shear strength of the matrix, then the matrix shearing failure criterion is

$$\max\left(\left|\tau_{12}^{(m_A)}\right|, \left|\tau_{12}^{(m_B)}\right|\right) \geq S^{(m)} \Longrightarrow \text{Matrix Shearing} \qquad (2.31)$$

2.6.3 Matrix Cracking in Transverse Tension

The criterion determining matrix cracking in transverse tension is taken as

$$\max\left(\sigma_{22}^{(m_A)}, \sigma_{22}^{(m_B)}\right) \geq Y_t^{(m)} \Longrightarrow \begin{array}{l}\text{Matrix Cracking in} \\ \text{Transverse Tension}\end{array} \qquad (2.32)$$

where $Y_t^{(m)}$ is the tensile strength of the matrix material.

2.6.4 Matrix Crushing in Transverse Compression

The failure of a lamina in transverse compression is assumed to be a result of compressive failure of the matrix material. If $\sigma_{22}^{(m_A)}$ and $\sigma_{22}^{(m_A)}$ are compressive stresses in the matrix subcells, and $Y_c^{(m)}$ denotes the compressive strength of the matrix material, then the compressive failure of the lamina in transverse direction may be determined by the following criterion

$$\max\left(\left|\sigma_{22}^{(m_A)}\right|, \left|\sigma_{22}^{(m_B)}\right|\right) \geq Y_c^{(m)} \Longrightarrow \begin{array}{l}\text{Matrix Crushing in} \\ \text{Transverse Compression}\end{array} \qquad (2.33)$$

2.6.5 Matrix Cracking in Axial Tension

One possible damage mechanism in fiber–reinforced composites is cracking of the matrix due to axial tension. Although not envisioned as a very serious damage mode, nor a very commonly occurring one, its consideration may be warranted in composites with low fiber volume fraction. The criterion indicating axial direction matrix cracking may be taken as

$$\max\left(\sigma_{11}^{(m)}, \sigma_{11}^{(m)}\right) \geq Y_t^{(m)} \implies \text{Matrix Cracking in}$$
Axial Tension
(2.34)
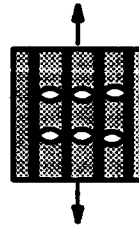
2.6.6 Lamina Failure by Kink-banding

In axial compression, the failure is assumed to be triggered by fiber micro-buckling resulting in kink-banding. At this time (1992) no adequate analytical formulations exist which can predict with consistent accuracy the compressive strength of unidirectional composites in compression. A number of micromechanics-based analytical formulae have been proposed, e.g. Rosen [92], Argon [93], Budiansky [94], and Hahn and Williams [95], but they do not correlate well with the experimental results. Although the various analytical models for prediction of compressive strength have not shown good quantitative agreement with experimental results, they have served to identify the important parameters influencing the compressive strength of composites. Based on these works the important parameters influencing the compressive strength of unidirectional composites appear to be matrix shear modulus, fiber misalignment, fiber diameter, fiber volume fraction, and fiber/matrix interface strength.
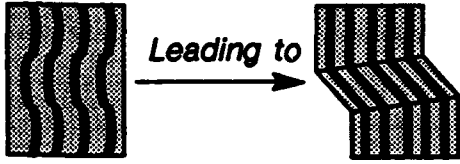
Here, a modified form of the analytical formula suggested by Hahn and Williams [95] is employed for estimating the compressive strength of the lamina. The compressive strength of a unidirectional lamina with no defects or fiber misalignment is given by Hahn and Williams as:

$$\sigma_{crit} = V_f G_{12} \qquad (2.35)$$

where, V_f is the fiber volume fraction and G_{12} is the in-plane shear modulus of the lamina. If the lamina stress-strain relations are nonlinear, then, the tangent shear modulus G_{12_T} should be used in the above relation and the critical compressive stress is given as

39

$$\sigma_{crit}^{*} \;=\; V_f \; G_{12_T} \qquad\qquad (2.36)$$
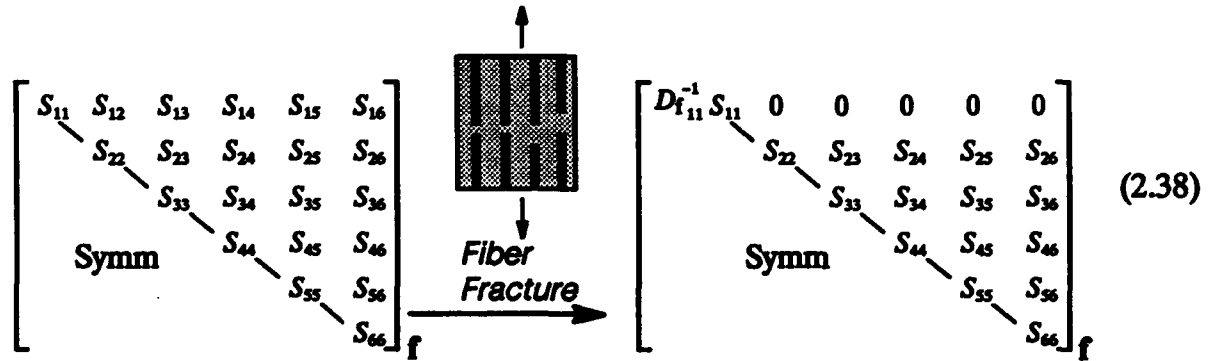
In the present analysis, micro–buckling resulting in kink–banding failure is assumed to occur if the axial compressive stress on the lamina exceeds the critical micro–buckling stress given by Eq. (2.36), i.e.,

$$\Big| \sigma_{11} \Big|_{Lamina} \;\geq\; \sigma_{crit}^{*} \;\Longrightarrow\; \qquad \xrightarrow{\text{Leading to}} \qquad\qquad (2.37)$$

Micro–buckling   *Kink–banding*

2.7 Damage Modelling

Due to the aforementioned failure modes, some degree of stiffness degradation and stress relief takes place within the lamina. The assumptions made about lamina stiffness degradation and stress relief are discussed here.

If tensile fiber fracture mode is detected then, the fiber tangent compliance matrix is modified as follows:

$$
\begin{bmatrix}
S_{11} & S_{12} & S_{13} & S_{14} & S_{15} & S_{16} \\
 & S_{22} & S_{23} & S_{24} & S_{25} & S_{26} \\
 & & S_{33} & S_{34} & S_{35} & S_{36} \\
 \text{Symm} & & & S_{44} & S_{45} & S_{46} \\
 & & & & S_{55} & S_{56} \\
 & & & & & S_{66}
\end{bmatrix}_f
\xrightarrow[\text{Fracture}]{\text{Fiber}}
\begin{bmatrix}
D_{f_{11}}^{-1} S_{11} & 0 & 0 & 0 & 0 & 0 \\
 & S_{22} & S_{23} & S_{24} & S_{25} & S_{26} \\
 & & S_{33} & S_{34} & S_{35} & S_{36} \\
 \text{Symm} & & & S_{44} & S_{45} & S_{46} \\
 & & & & S_{55} & S_{56} \\
 & & & & & S_{66}
\end{bmatrix}_f
\qquad (2.38)
$$

where $D_{f_{11}}$ is the stiffness reduction factor which serves to reduce the fiber axial stiffness and is arbitrarily assumed. Since the tensile fiber fracture failure corresponds to the opening of cracks, the axial stress in the fiber is also relieved,

$$\sigma_{11}^{(f)} \;=\; 0 \qquad\qquad (2.39)$$

In the case of matrix cracking in the axial direction, the matrix tangent compliance matrix is modified as follows

$$
\begin{bmatrix}
S_{11} & S_{12} & S_{13} & S_{14} & S_{15} & S_{16} \\
 & S_{22} & S_{23} & S_{24} & S_{25} & S_{26} \\
 & & S_{33} & S_{34} & S_{35} & S_{36} \\
 & & & S_{44} & S_{45} & S_{46} \\
\text{Symm} & & & & S_{55} & S_{56} \\
 & & & & & S_{66}
\end{bmatrix}_{m_A, m_B}
\xrightarrow{\substack{\textit{Axial Matrix} \\ \textit{cracks}}}
\begin{bmatrix}
D_{m_{11}}^{-1} S_{11} & 0 & 0 & 0 & 0 & 0 \\
 & S_{22} & S_{23} & S_{24} & S_{25} & S_{26} \\
 & & S_{33} & S_{34} & S_{35} & S_{36} \\
 & & & S_{44} & S_{45} & S_{46} \\
\text{Symm} & & & & S_{55} & S_{56} \\
 & & & & & S_{66}
\end{bmatrix}_{m_A, m_B}
\quad (2.40)
$$

where $D_{m_{11}}$ is the stiffness reduction factor which serves to reduce the axial stiffness of the matrix. Since axial tensile matrix cracking corresponds to opening of cracks, the axial stress in the matrix subcells is relieved,

$$
\sigma_{11}^{(m_A)}, \ \sigma_{11}^{(m_B)} = 0 \quad (2.41)
$$

Transverse matrix cracking is a common phenomenon in fiber-reinforced composites and it can cause significant stiffness degradation or even complete failure in laminates. Transverse cracking can occur due to transverse tensile stresses or in-plane shear stresses, or perhaps due to the combined effect of the two stresses. If the lamina fails in the transverse direction in tensile matrix cracking mode, or a matrix shearing mode, then the matrix tangent compliance matrix is modified as follows:

$$
\begin{bmatrix}
S_{11} & S_{12} & S_{13} & S_{14} & S_{15} & S_{16} \\
 & S_{22} & S_{23} & S_{24} & S_{25} & S_{26} \\
 & & S_{33} & S_{34} & S_{35} & S_{36} \\
 & & & S_{44} & S_{45} & S_{46} \\
\text{Symm} & & & & S_{55} & S_{56} \\
 & & & & & S_{66}
\end{bmatrix}_{m_A, m_B}
\xrightarrow{\substack{\textit{Transverse} \\ \textit{Matrix Cracking}}}
\begin{bmatrix}
S_{11} & S_{12} & S_{13} & S_{14} & S_{15} & S_{16} \\
 & D_{m_{22}}^{-1} S_{22} & 0 & 0 & 0 & 0 \\
 & & D_{m_{33}}^{-1} S_{33} & 0 & 0 & 0 \\
 & & & S_{44} & S_{45} & S_{46} \\
\text{Symm} & & & & S_{55} & S_{56} \\
 & & & & & S_{66}
\end{bmatrix}_{m_A, m_B}
\quad (2.42)
$$

41

where D_{m22} and D_{m44} are stiffness reduction factors which reduce the stiffness of the matrix material in the transverse direction and in in–plane shear respectively. If the failure mode is transverse matrix cracking due to tension, then since it corresponds to opening of cracks the transverse direction stress in the matrix is also relieved,

$$\sigma_{22}^{(m_A)}, \sigma_{22}^{(m_B)} = 0 \tag{2.43}$$

Since the stresses in matrix subcell m_A are related to stresses in the fiber via the constraint Eq. (2.3a) , the $\sigma_{22}^{(f)}$ stress in the fiber is also reduced to zero,

$$\sigma_{22}^{(f)} = 0 \tag{2.44}$$

The mechanics of lamina compressive failure in the transverse direction are not sufficiently clear as yet, and there exists a paucity of experimental data regarding the behaviour of unidirectional composites loaded in transverse compression. If compression failure of matrix is indicated by Eq. (2.33), then the matrix tangent stiffness is reduced in accordance with Eq. (2.42); but, since no opening of cracks is envisioned in this case, no stresses are relieved in the components of the unit cell.

Failure in a lamina can also take place due to compressive failure of the fiber or kink–banding. This is considered as a catastrophic failure, and the tangent stiffnesses of the constituent phases are reduced according to Eqs. (2.38–2.40,2.42); but no stress relieving is carried out.

In the next section numerical examples will be presented, and the predictions of the elastic moduli of composites based on the micro–model are compared to predictions from other established procedures.

2.8 Results for Elastic Moduli

The micro–model is the most important component of the material modelling procedure, and may be considered the kernel upon which the accuracy of the overall scheme depends. Therefore it is necessary that the accuracy of the micro–model be ex-

amined in detail. The first step is examination of the accuracy of the elastic moduli predicted by the model. With this in mind, the results from the micro–model are compared with a number of procedures, such as the Composite Cylinder Assemblage (CCA) model of Hashin and Rosen [9,10,25,26], numerically obtained results of Chen and Cheng [33] and Pickett [34], and predictions from Aboudi's Method of Cells [7,54].

2.8.1 Comparison with CCA Model

The CCA model model of Hashin and Rosen gives closed form expressions for E_1 ,K_{23} ,G_1 and ν_1 whereas closed form expressions for G_{23} ,E_2 and ν_{23} could not be obtained; these quantities could only be bounded.

As mentioned in the previous chapter, the Three–phase model of Hermans [22] and Christensen and Lo [23] is related to the CCA model. Again, it was noticed by Hashin [9] that the expressions for E_1 ,K_{23} ,G_1 and ν_1 obtained by Hermans are exactly the same as given by the CCA model, whereas Hermans' derivation for the expression for G_{23} contained some errors. These errors were removed later in the work of Christensen and Lo [23] and the result for G_{23} was given in the form of a root of a quadratic. Once the value of G_{23} is calculated from the Three–phase model results, E_2 and ν_{23} can be determined by using Eqs. (2.13).

Figs. 2.3–2.5 show the comparison of the effective elastic moduli as predicted by CCA model and by the micro–model. Results are presented primarily for the transverse moduli, since these are the ones which are the most difficult to predict, and they therefore serve as a measure of accuracy of the method. In instances where the CCA model does not give definite expressions for the effective moduli of the composite, Christensen and Lo's results are employed along with Eqs. (2.13). The assumed properties of the fiber and matrix are the same as used by Hashin and Rosen [25] and are given in Table 2.1 for convenience.

43

Fig. 2.3 shows the variation of the transverse Young's modulus with fiber volume fraction. Results based on Christensen and Lo's solution and the micro–model are practically coincident. In fact the micro–model results have been slightly offset to improve the readability of the graph. Both results are within the bounds given by the CCA model. Also shown in Fig. 2.3 is the transverse modulus obtained by applying a combination type model to the unit cell shown in Fig. 2.1, i.e. by using the second analog model shown in Fig. 2.2, while relaxing the matrix restraint effect induced by the compatibility of fiber direction strain in the fiber and matrix. The difference between the combination model and the Reuss lower bound arises from the fact that, in obtaining the Reuss lower bound, all of the matrix material is lumped in series with the fiber phase, whereas the combination model assumes that a portion of the matrix (Material Element B) is acting in parallel with the rest of the material of the unit cell. The latter arrangement results in increased stiffness. The difference between the micro–model values and the combination model values arises from the matrix restraining effect induced by the fibers.

Fig. 2.4 shows the longitudinal shear modulus G_1 and the transverse direction shear modulus G_{23} as given by the various analytical models and the micro–model. An interesting fact is observed in this result: the values of the longitudinal shear modulus G_1 and the transverse shear modulus G_{23} are practically the same according to both analytical models for the case when the constituent phases are isotropic. In fact, the micro–model predictions for the two shear moduli are exactly the same in this case. The values of shear moduli given by the analytical methods and the micro–model are in good agreement over the entire range of the fiber volume fraction.

Fig. 2.5 shows the micro–model results for ν_{23}, the bounds given by the CCA model and the values given by Christensen's results in conjunction with Eqs. (2.13). The micro–model results and Christensen and Lo's [23] results lie within the CCA bounds,

with Christensen and Lo's results tending to favour the lower bound and the micro-model results lying closer to the upper bound.

2.8.2 Comparison with Detailed Numerical Procedures and Aboudi's Method of Cells

Chen and Cheng [33] determined the transverse moduli of a fiber-reinforced composite with fibers arranged in a hexagonal packing arrangement, using a series-type elasticity solution. Fig. 2.6 shows the transverse Young's modulus and axial shear modulus for a composite lamina as a function of fiber volume fraction. The properties of fiber and matrix constituents are given in Table 2.2. The micro-model predictions are in excellent agreement with the results of Chen and Cheng [33].

Fig. 2.7 shows estimates of transverse and axial shear moduli for a graphite/epoxy lamina from the micro-model, the numerical procedure of Chen and Cheng [33], and Aboudi's Method of Cells [7]. The assumed properties of the graphite fibers and epoxy matrix are given in Table 2.3. The results from the three procedures are in excellent agreement.

Pickett [34] presented numerically obtained estimates for elastic moduli of a glass/epoxy lamina. The assumed properties of the glass fibers and epoxy matrix are presented in Table 2.4. Fig. 2.8 presents the variation of elastic moduli of glass/epoxy with fiber volume fraction. Results are presented for the micro-model, Pickett's procedure [34], and Aboudi's micromechanical model [7]. The micro-model results compare very well with the results by Pickett and predictions from Aboudi's model.

Figs. 2.9–2.11 show variation of elastic moduli with fiber volume fraction for a graphite/epoxy composite. Experimental results were presented by Kriz and Stinchcomb [74]. Results from the micro-model and Aboudi's Method of Cells [7] are also presented, and are in excellent agreement. The agreement between analytical predictions of elastic moduli and experimental results is very good in all the cases except for the transverse

Poisson's ratio, in which case the analytical results seem to slightly over-predict the Poisson's ratio.

2.9 Results for Thermal Expansion Coefficients

In this section, the predictions of effective coefficients of thermal expansion from the micro-model are compared with results from Aboudi [54]. Figs. 2.12 and 2.13 show the coefficients of thermal expansion in the axial and transverse directions for a glass/epoxy composite. The properties of the the glass fibers and epoxy matrix are the same as used by Aboudi [54], and are presented in Table 2.6 for convenience. Figs. 2.14 and 2.15 show the coefficients of thermal expansion of a graphite/epoxy composite. The properties of the fiber and the matrix are given in Table 2.7.

Examination of the results shows that the presence of even a small amount of fiber in the matrix results in a sharp decrease in the axial coefficient of thermal expansion, whereas the effect of fibers in reducing the coefficient of thermal expansion in the transverse direction is limited. In fact it is seen that for low fiber volume fractions there can even be an increase in the transverse coefficient of thermal expansion. This seemingly anomalous behaviour is a result of the constraining effect of the fibers. When fibers, which are axially stiff and have small thermal expansion coefficients, are added to a relatively more compliant matrix with a large expansion coefficient, the effect is a sharp drop in the axial thermal expansion coefficient even for low fiber volume fractions. This is due to high fiber stiffness in axial direction, but the tendency of the matrix to expand in the the axial direction is channeled into the transverse direction, causing an increase in the effective transverse-direction expansion coefficient. As the fiber volume fraction increases, the transverse expansion coefficient gradually decreases, more or less linearly.

The predictions of thermal expansion coefficients from the proposed micro-model and from Aboudi's refined micromechanical model are in excellent agreement, and the micro-model properly portrays the anomalous behaviour of unidirectional composites in the case of transverse thermal expansion.

46
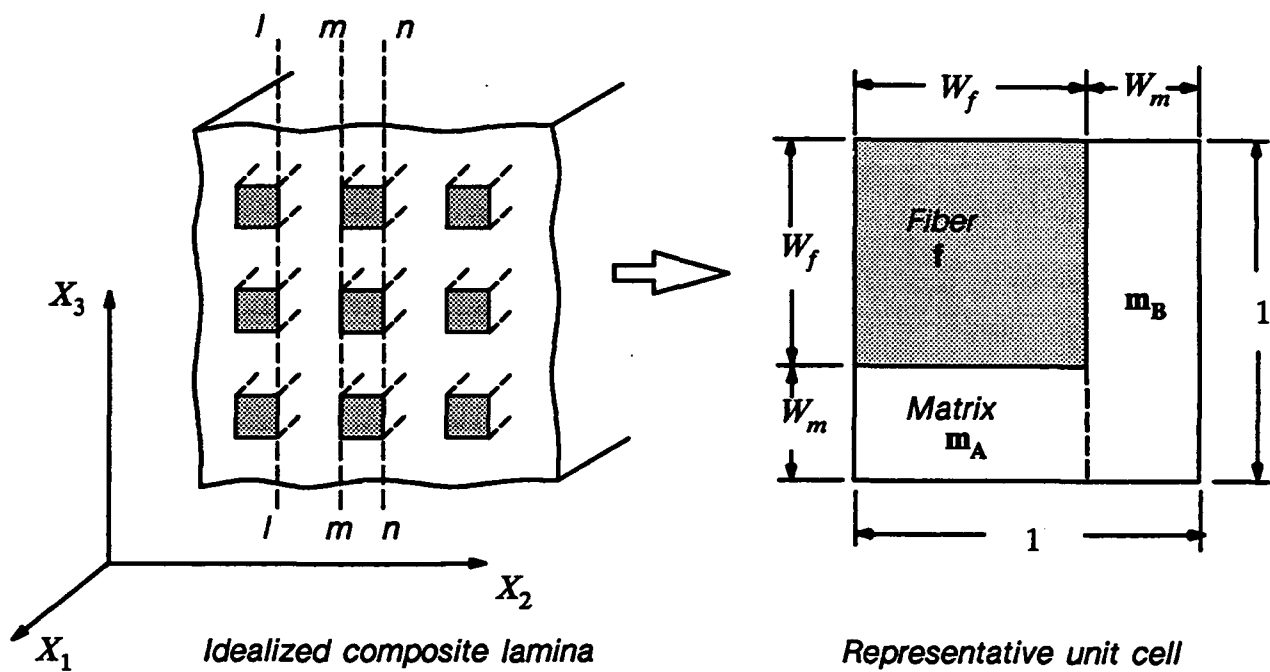
Fig. 2.1 *Idealized composite lamina and representative unit cell*
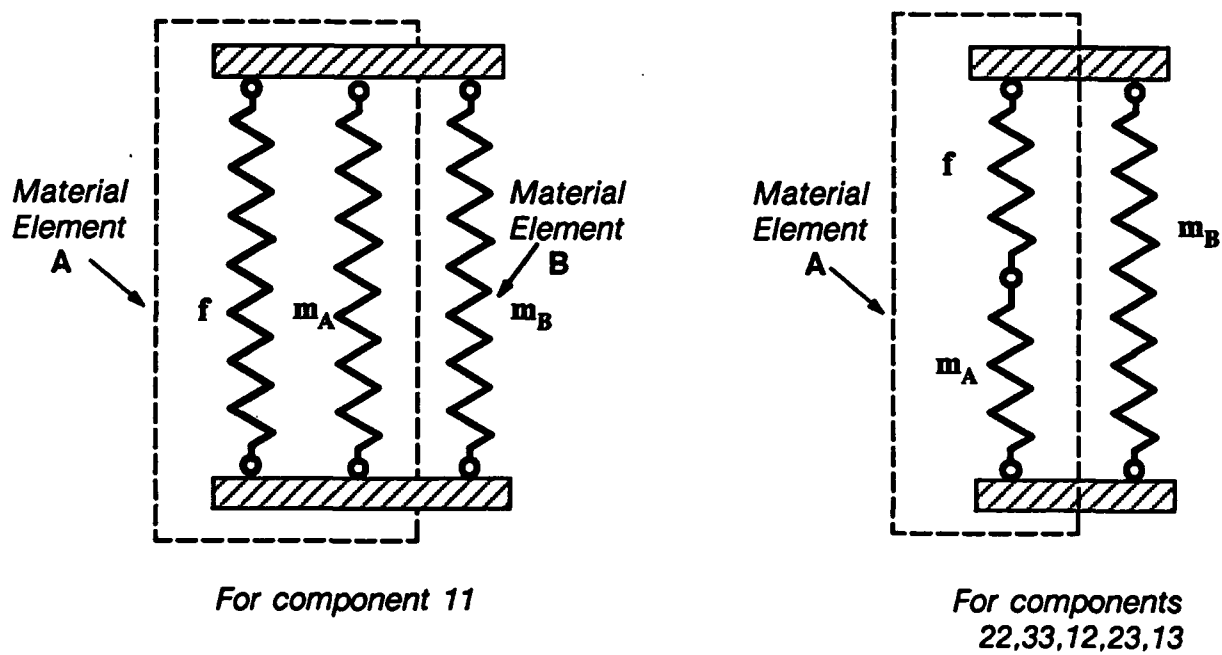
Fig. 2.2 *Analogs for stress and strain homogenization in the unit cell*

	E (Mpsi)	ν
E–Glass	10.5	0.2
Epoxy	0.4	0.35

Table 1.1 *Elastic properties of E-glass fibers and epoxy matrix used in comparing Micro-model, CCA model [26] and the Three-phase model results.*
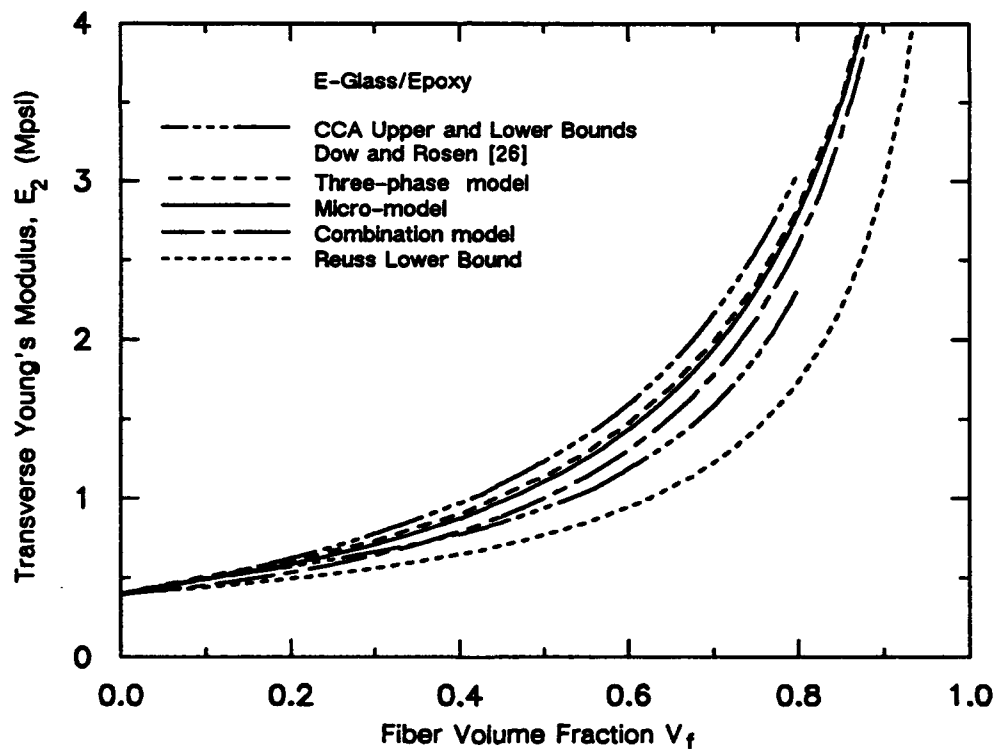
Fig. 2.3 *Comparison of transverse modulus calculated from the Micro-model, CCA model [26], and the Three-phase model[23] in conjunction with Eq (2.13).*

48
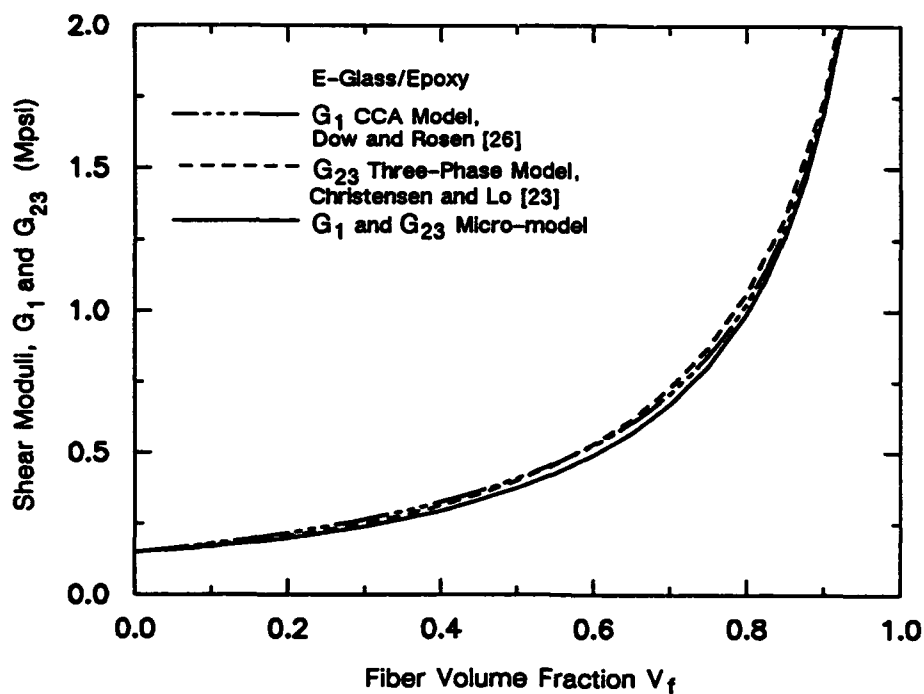
Fig. 2.4 *Shear moduli calculated from Micro-model, CCA model [26] and the Three-phase model[23].*
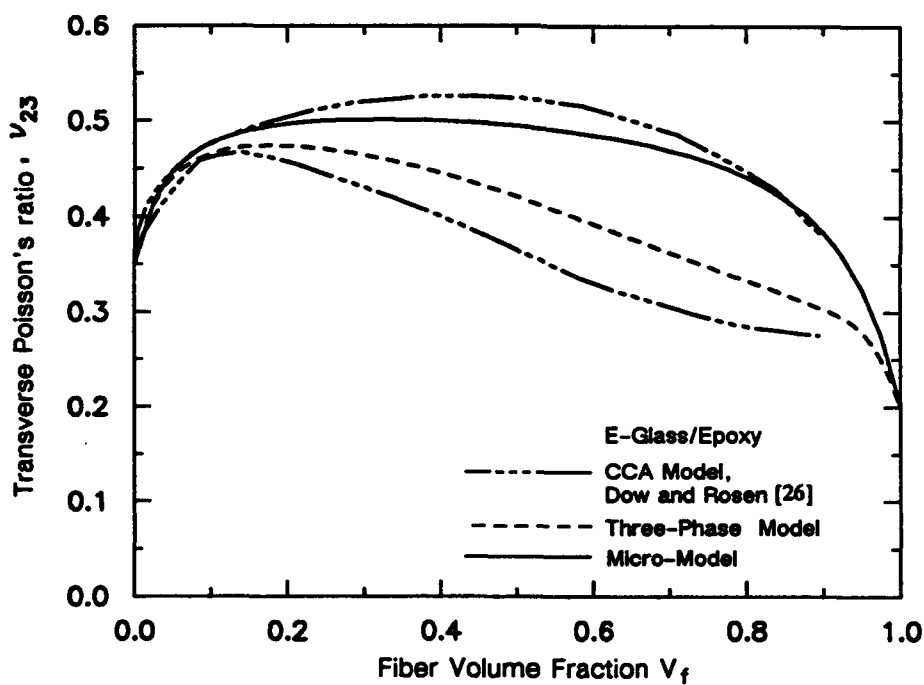
Fig. 2.5 *Transverse Poison's ratio calculated from Micro-model, CCA model [26], and the Three-phase model[23] in conjunction with Eq. (2.13).*

	E_1 (Mpsi)	E_2 (Mpsi)	G_{12} (Mpsi)	ν_{12}	ν_{23}
Fiber	50	2	10	0.2	0.15
Matrix	0.6	0.6	0.222	0.35	0.35

Table 2.2 *Elastic properties of fibers and matrix used in comparison of Micro–model predictions and results of Chen and Cheng[33].*
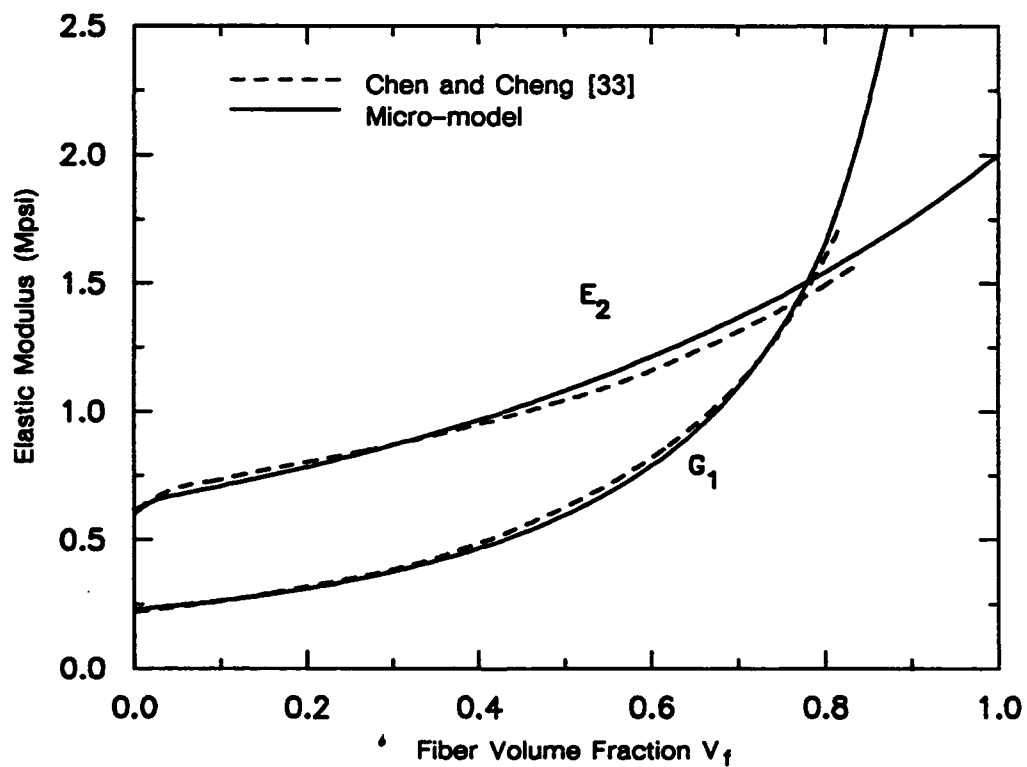
Fig. 2.6 *Comparison of Micro–Model results with numerically obtained results of Chen and Cheng[33].*

	E_1 (Mpsi)	E_2 (Mpsi)	G_{12} (Mpsi)	ν_{12}	ν_{23}
Graphite	24	2	4	0.3	0.15
Epoxy	0.6	0.6	0.231	0.3	0.3

Table 2.3 *Elastic properties of graphite fibers and epoxy matrix used in comparison of Micro-model predictions, results of Chen and Cheng [33] and Aboudi's Method of Cells [7]*
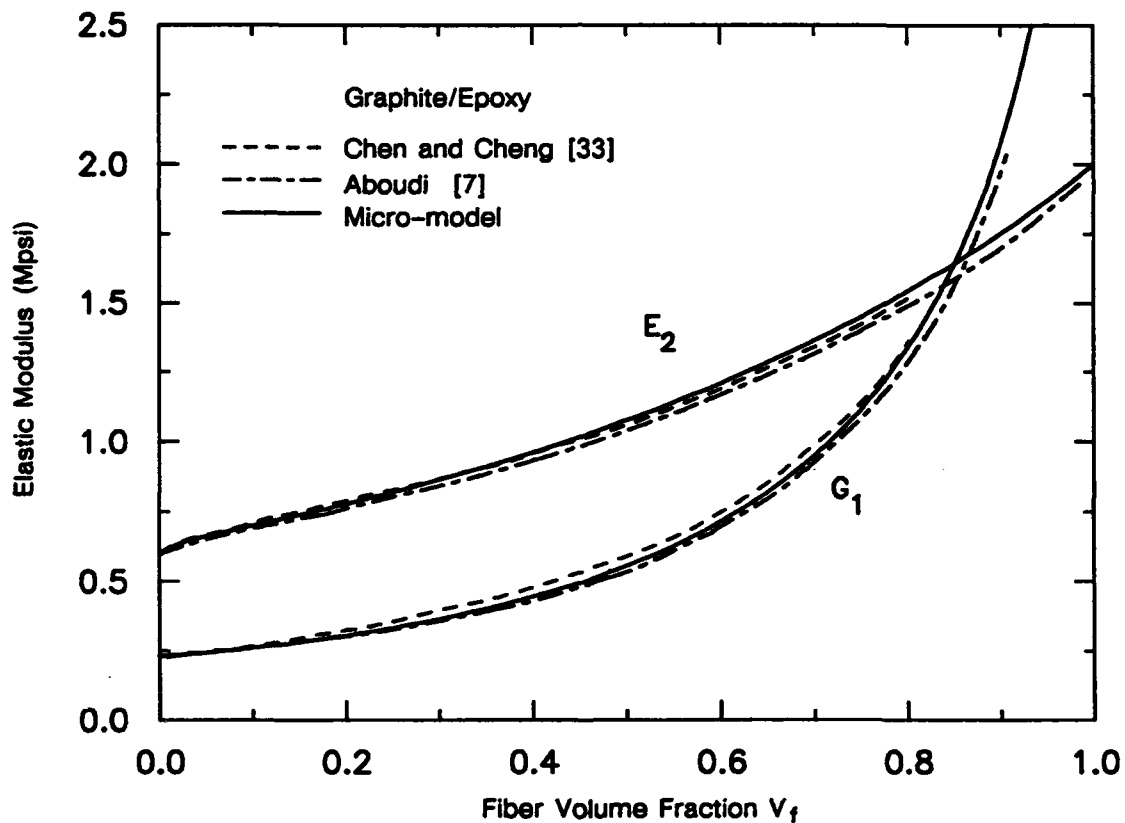
Fig. 2.7 *Comparison of Micro-model results with numerically obtained results of Chen and Cheng[33] and Aboudi's Method of Cells [7].*

	E (Mpsi)	ν
Glass	10	0.2
Epoxy	0.496	0.34

Table 2.4 *Elastic properties of glass fibers and epoxy matrix used in comparing Micro–model predictions and results of Pickett [34] and Aboudi [7].*
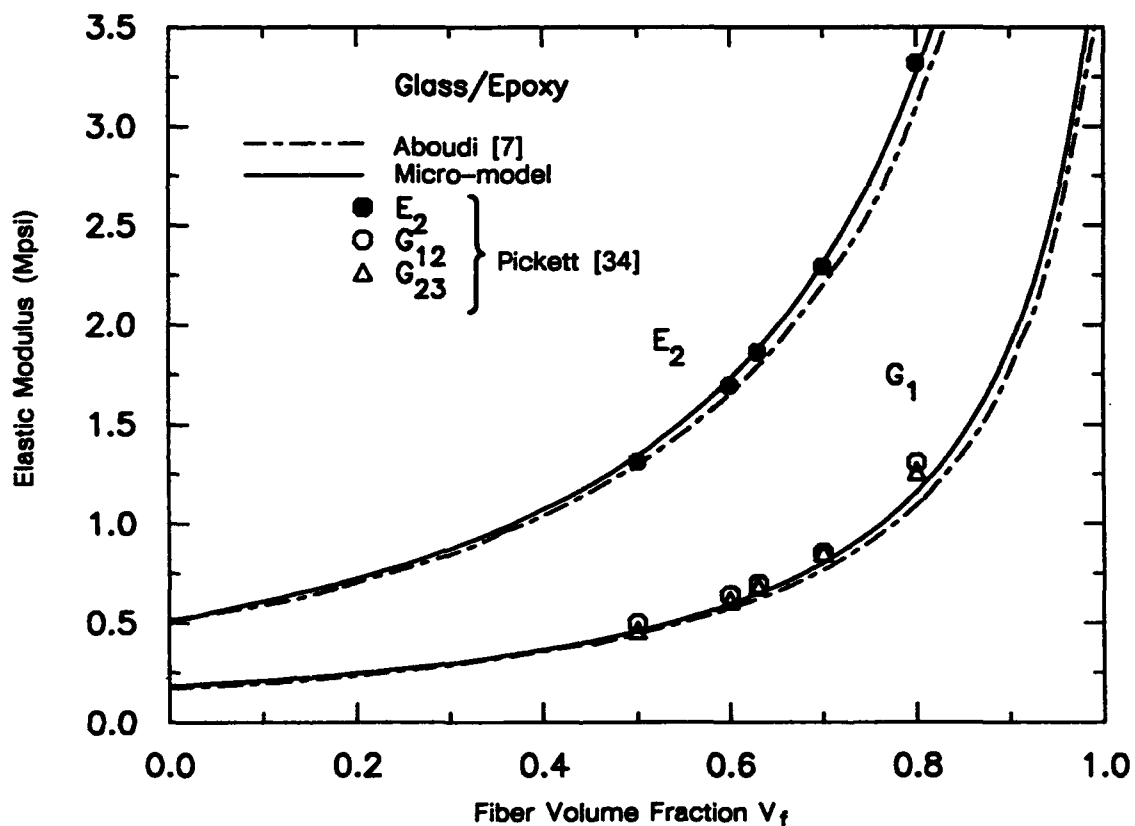
Fig. 2.8 *Comparison of Micro–model results with numerically obtained results of Pickett[34] and Aboudi's Method of Cells [7].*

	E_1 (Gpa)	E_2 (Gpa)	G_{12} (Gpa)	ν_{12}	ν_{23}
Graphite	232	15	24	0.279	0.49
Epoxy	5.35	5.35	1.975	0.354	0.354

Table 2.5 *Elastic properties of graphite fibers and epoxy matrix used in comparison of Micro–model Predictions and results from Aboudi's Method of Cells [7].*
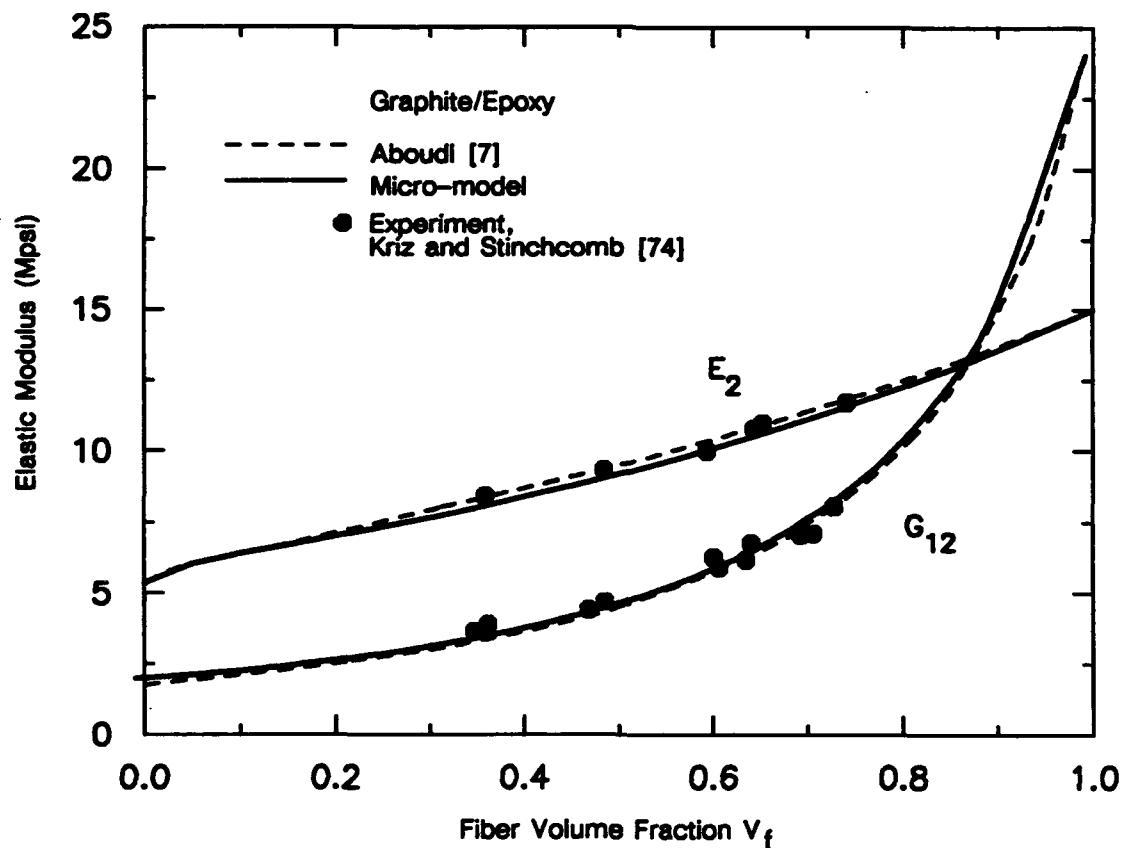
Fig. 2.9 *Comparison of transverse Young's modulus and axial shear modulus predictions from Micro–model and Aboudi's Method of Cells [7].*
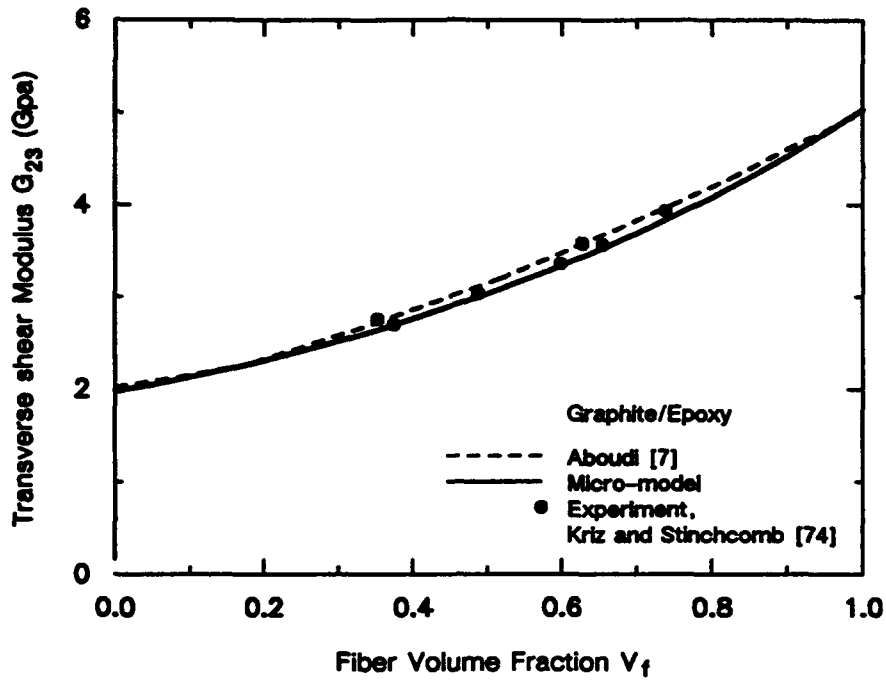
Fig. 2.10 *Comparison of transverse shear modulus predictions from Micro-model and Aboudi's Method of Cells [7].*
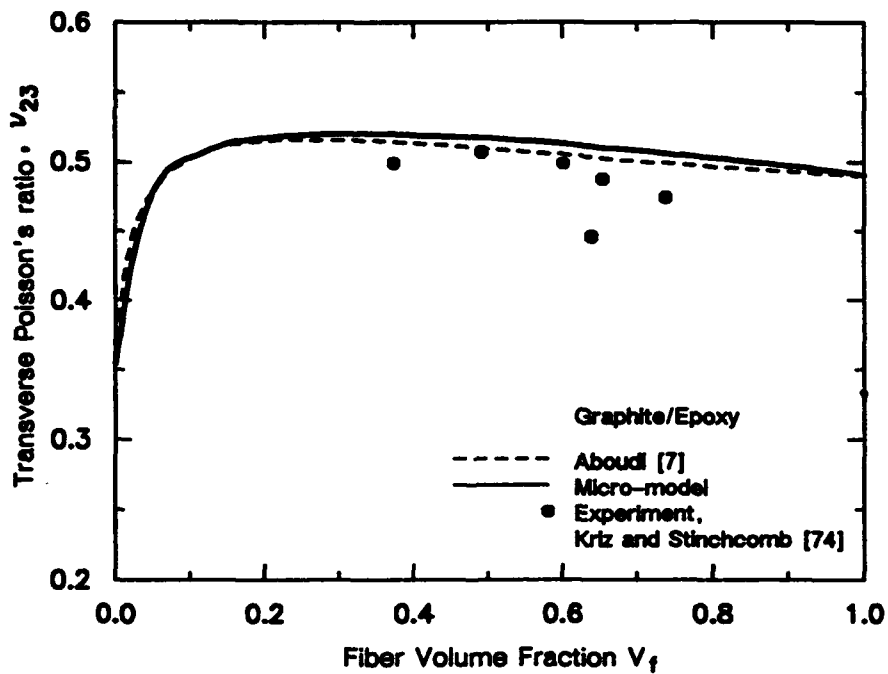
Fig. 2.11 *Comparison of transverse Poisson's ratio predictions from Micro-model and Aboudi's Method of Cells [7].*

	E (GPa)	ν	a $10^{-6}/°C$
Glass	72.38	0.2	5
Epoxy	2.75	0.35	54

Table 2.6 *Properties of glass fibers and epoxy matrix used in comparing predictions of coefficients of thermal expansion from Micro-model and Aboudi's Method of Cells [54].*
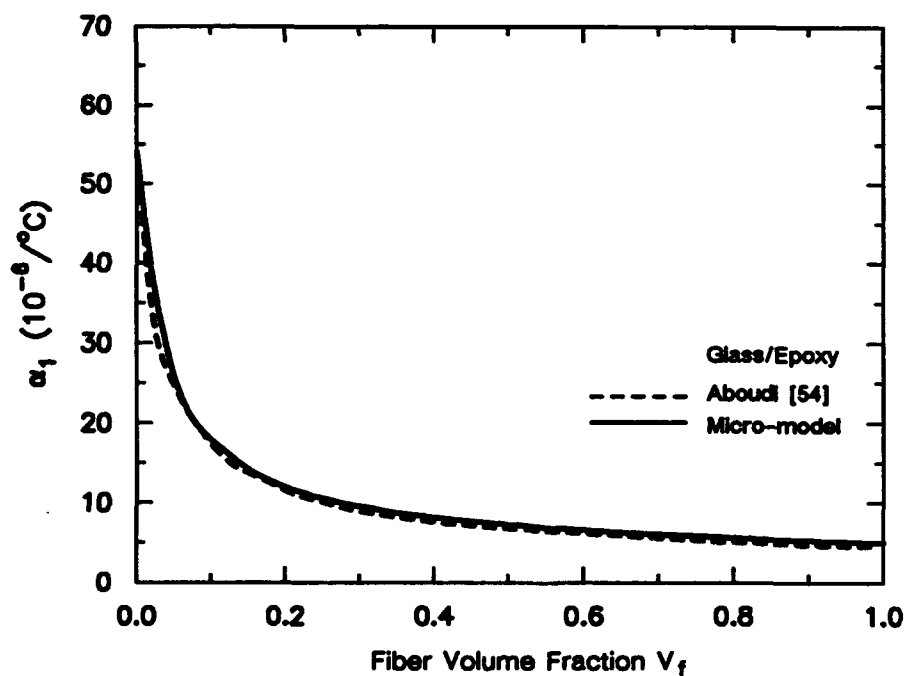
Fig. 2.12 *Prediction of axial thermal expansion coefficient of glass/epoxy from Micro-model and Aboudi's Method of Cells [54].*

55
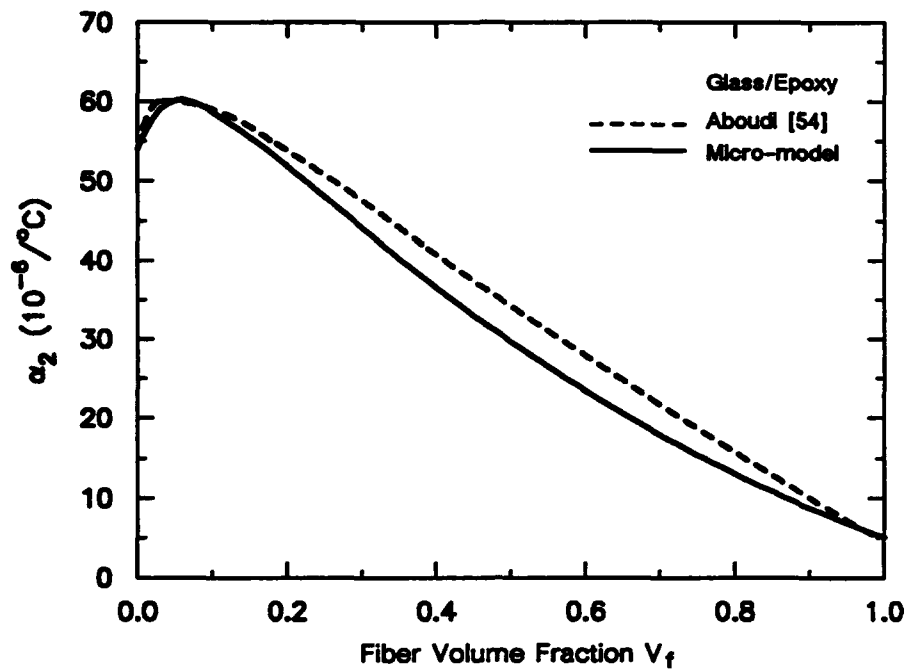
Fig. 2.13 *Prediction of transverse thermal expansion coefficient of Glass/Epoxy from Micro–Model and Aboudi's Method of Cells[54].*

	E_1 (GPa)	E_2 (GPa)	G_{12} (GPa)	ν_{12}	ν_{23}	α_1 $10^{-6}/°C$	α_2 $10^{-6}/°C$
Graphite	388	7.8	6.8	0.23	0.45	–0.68	9.74
Epoxy	3.45	3.45	1.27	0.35	0.35	36	36

Table 2.7 *Properties of graphite fibers and epoxy matrix used in comparison of coefficients of thermal expansion predictions from Micro–model and Aboudi's Method of Cells [54].*
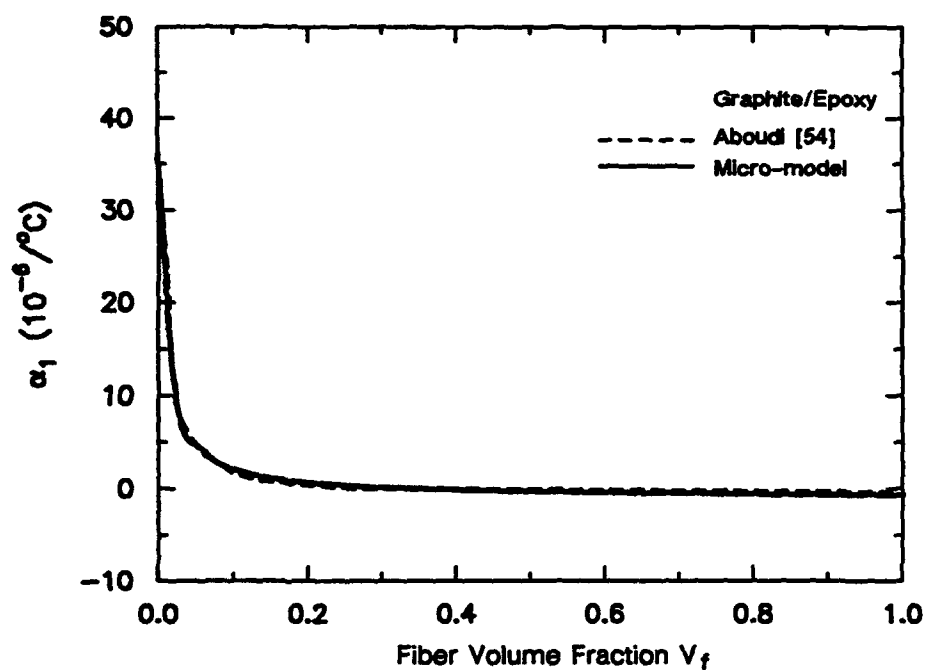
Fig. 2.14 *Prediction of axial thermal expansion coefficient of graphite/epoxy lamina from Micro-model and Aboudi's Method of Cells [54].*
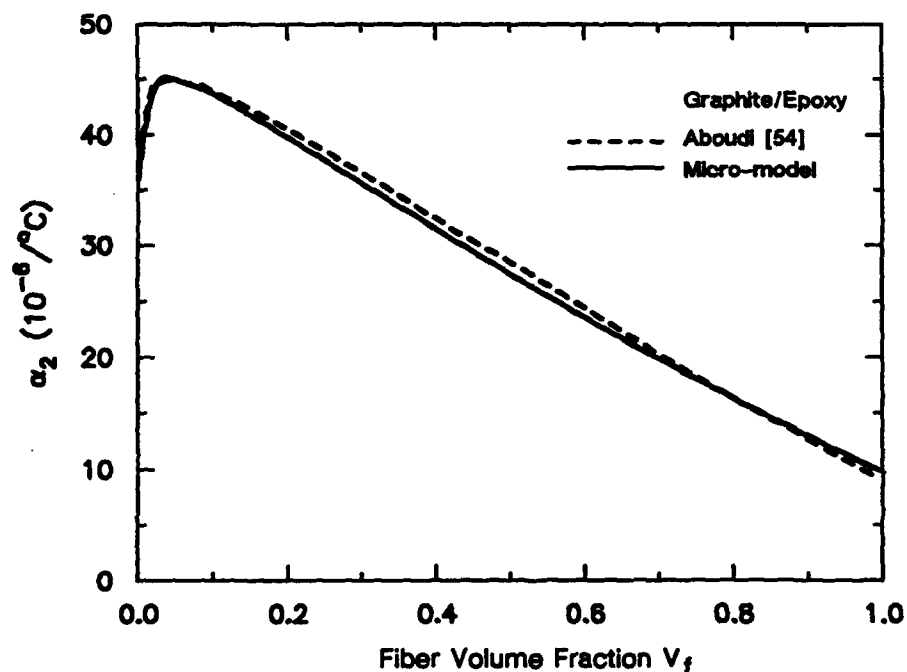
Fig. 2.15 *Prediction of transverse thermal expansion coefficient of graphite/epoxy from Micro-model and Aboudi's Method of Cells [54].*

CHAPTER 3

SUBLAMINATE MODEL

A group or a cluster of laminae, from among the total number of laminae consti-
tuting the laminate, is called a sublaminate. The micro–model combines the stresses and
strains within the fiber and matrix phases to yield the stresses, strains and stiffness of an
effective homogeneous lamina. This information is then passed onto the sublaminate
model, as shown in Fig. 3.1, which schematically describes the working of the sublaminate
model. The sublaminate model then combines the stress and strain fields within each
lamina to yield the stresses, strains and stiffness of an *equivalent homogeneous anisotropic
material*, which represents the sublaminate.

Quite often, within the stacking sequence of a laminate, a typical repeating pattern
is identifiable. This is usually the case for thick–section composites, where the symmetry
resulting from using the same pattern throughout the laminate thickness is desirable in
order to avoid the high curing stresses which would otherwise arise. An example of a
thick–section laminate with a repeating pattern is a $[0_2/90]_{16s}$ laminate, which consists of
$0_2/90$ pattern, repeated 32 times through the thickness of the laminate for a total of 96
individual laminae. Here, it can be reasonably assumed that the material in the vicinity of
a typical material point consists of 3 plies arranged in this basic pattern. If these layers are
replaced by an equivalent homogeneous material then we can employ standard finite ele-
ments and the usual sampling procedures at the material points to analyze this particular
laminate. The prospective advantages of this method also become obvious now, since we
can carry out the analysis by sampling at discrete locations through the laminate thickness,
as compared to ply–by–ply type analysis procedures which require considerably more
computational effort and storage, in order to track the nonlinear response of a laminate.

The method of representing the cluster of plies forming the sublaminate by an equivalent homogeneous continuum may be referred to as "Equivalent Continuum Modelling." In the next section the general ideas behind the method are presented.

3.1 Equivalent Continuum Modelling

The idea of equivalent continuum modelling has been applied in many different areas of mechanics and to materials other than laminated composites. Here, discussion is focused upon the method as it has been applied to laminated composites.

The basic procedure for obtaining the properties of an equivalent continuum representing a laminated material is as follows. The actual laminated material is replaced by an equivalent homogeneous material. The properties of this equivalent material are determined by requiring that the actual material and the equivalent material behave in the same way when subjected to certain fundamental patterns of stresses or strains. These fundamental patterns of stresses or strains may be thought of as *calibrating stress or strain fields*. The properties of the equivalent material so obtained can be used to analyze the structure under consideration and should yield reasonably accurate results, provided that the stress and the strain fields at the material points of the structure are not too different from the calibrating stress and strain fields.

3.2 Previous Work and Adopted Procedure

Pagano [75] gave expressions for the effective elastic moduli of laminated composites, using a three-dimensional lamination scheme. Pagano considered all the laminae within the thickness of the laminate. It was suggested that moduli so determined could be used for the purpose of structural analysis, as opposed to laminated plate type analysis procedures, which operate on a ply-by-ply basis. Once the displacement field is known, the detailed ply-by-ply solution can be determined from it. A similar procedure was employed by Sun and Li [76] to determine the effective elastic moduli of a typical repeating sublaminate within the thickness of the laminate. It was suggested that since the lami-

nate was made up from this repeating sublaminate, the elastic moduli of the laminate would be the same as the elastic moduli of the sublaminate.

A sublaminate model for determining equivalent elastic properties of a sublaminate from the properties of constituent laminae was presented by Pecknold [57]. The choice of the calibrating stress and strain fields in Pecknold's work is essentially the same as the one employed by Pagano [75] and Sun and Li [76]; therefore it was suggested by Pecknold that the results obtained by sublaminate model [57] should be identical to results from procedures proposed by Pagano and Sun and Li. However, the formulation presented in Pecknold's work is quite simple, and this author is in agreement with the assertion made in Pecknold's work [57] that the formulation presented in the works of Pagano [75] and Sun and Li [76] is such that it obscures the essential simplicity of the basic ideas which are involved. Therefore, in the present study the sublaminate model as proposed by Pecknold [57] has been employed. In this chapter, certain characteristics of the stress and strain distributions within laminated composites are first discussed, since these have a bearing on the type of calibrating stress and strain fields which are permissible. The procedure for obtaining the equivalent continuum properties of the sublaminate is then formally outlined.

3.3 Characteristics of Stress and Strain Fields in Laminates

Fig. 3.2 shows a sublaminate in assembled and disassembled forms. The coordinate axes attached to sublaminate are referred to as *laminate coordinate axes*; the primed coordinate axes attached to the lamina are the *lamina coordinate axes*. The kth lamina has also shown on its surface various stresses referred to the laminate coordinate system. The 11, 22, and 12 components of stress and strain are referred to as *in–plane* stresses and strains. Correspondingly the 33, 23, and 13 components of stress and strain are referred to as *out–of–plane* stresses and strains. The vectors of stress and strain can be partitioned using this classification of stresses and strains as follows:

$$\{\sigma\} = \begin{Bmatrix} \sigma_{11} \\ \sigma_{22} \\ \tau_{12} \\ --- \\ \sigma_{33} \\ \tau_{23} \\ \tau_{13} \end{Bmatrix} \equiv \begin{Bmatrix} \sigma_i \\ --- \\ \sigma_o \end{Bmatrix} \quad , \quad \{\epsilon\} = \begin{Bmatrix} \epsilon_{11} \\ \epsilon_{22} \\ \gamma_{12} \\ --- \\ \epsilon_{33} \\ \gamma_{23} \\ \gamma_{13} \end{Bmatrix} \equiv \begin{Bmatrix} \epsilon_i \\ --- \\ \epsilon_o \end{Bmatrix} \qquad (3.1)$$

Referring to Fig. 3.2, if there exists a perfect bond between two laminae at their interface, then the compatibility of displacements at the interface requires, not only that the displacements u_1, u_2, u_3 be continuous, but also that the in–plane derivatives of these displacements be continuous. This in turn translates into the requirement that the in–plane strains should be continuous at the lamina interface, i.e.,

$$\left. \{\epsilon_i\}^k \right|_{Interface} = \left. \{\epsilon_i\}^{k+1} \right|_{Interface} \qquad (3.2)$$

The equilibrium of tractions at the interface requires that the out–of–plane stresses be continuous across the lamina interface, i.e.,

$$\left. \{\sigma_o\}^k \right|_{Interface} = \left. \{\sigma_o\}^{k+1} \right|_{Interface} \qquad (3.3)$$

These two requirements can be written compactly as

$$\left. \begin{Bmatrix} \epsilon_i \\ --- \\ \sigma_o \end{Bmatrix}^k \right|_{Interface} = \left. \begin{Bmatrix} \epsilon_i \\ --- \\ \sigma_o \end{Bmatrix}^{k+1} \right|_{Interface} \qquad (3.4)$$

The nature of the remaining components of stress and strain, i.e. the in–plane stresses and out–of–plane strains, is dictated by these requirements, and is explained as follows.

Referring again to Fig. 3.2, it is obvious that if the elastic moduli of various laminae are referred to the global coordinates, then there will often exist a discontinuity in elastic moduli at the lamina interface, since the fiber orientations in the two layers forming the

61

interface may be different. If this is the case, and the requirement of the continuity of in-plane strains is imposed, then obviously there would be a discontinuity in the in-plane stresses at the lamina interface. If the requirement of the continuity of the out-of-plane stresses is imposed at the interface, then the out-of-plane strains may be discontinuous. The magnitude of the discontinuities in the in-plane stresses and out-of-plane strains depends upon the degree of mismatch between the elastic moduli of the two layers forming the interface and upon the nature of the imposed loading.

The problems encountered by conventional displacement-based finite elements, such as the elements based on First-order Shear Deformation Theory and Higher-order Shear Deformation Theories for laminates, can now be better realized. These elements employ smooth strain distributions within a single element. This results in assumption of smoothly varying out-of-plane strains through the laminate thickness. The computed out-of-plane stresses may then exhibit discontinuities at the laminae interfaces, violating the requirement of continuity of out-of-plane stresses. Accurate assessment of out-of-plane stresses in some cases may be important, since these stress components play an important role in causing delaminations.

In the following section the transformation of stresses, strains, and material properties from lamina coordinates to laminate coordinates is described.

3.4 Transformation of Stresses and Strains

The stresses, strains, and stiffness matrix of a lamina in lamina coordinates are denoted by σ', ϵ', and C', respectively. The same quantities when referred to the laminate coordinate system are denoted by σ, ϵ, and C, respectively. The axes X_3 and X_3' are colinear, the fiber orientation angle is denoted by θ, and the superscript k denotes the kth lamina. The stress and strain transformation laws are

$$\left\{\epsilon'\right\} = \left[T_\epsilon^k\right]\left\{\epsilon\right\} \quad , \quad \left\{\sigma'\right\} = \left[T_\sigma^k\right]\left\{\sigma\right\} \tag{3.5}$$

where the strains and stresses, in the vector of strains $\{\epsilon\}$ and stresses $\{\sigma\}$, are arranged according to the convention employed in Eq. (2.5)

The transformation laws describing the transformation of the lamina stiffness matrix and compliance matrix from lamina coordinates to laminate coordinates follow from Eq. (3.5) and the invariance of strain energy under coordinate transformation.

$$
\begin{aligned}
\left[\, C \, \right] &= \left[T_\epsilon^k \right]^T \left[\, C' \, \right] \left[T_\epsilon^k \right] \\
\left[\, S \, \right] &= \left[T_\sigma^k \right]^T \left[\, S' \, \right] \left[T_\sigma^k \right]
\end{aligned}
\tag{3.6}
$$

The strain and stress transformation matrices, $[\, T_\epsilon^k \,]$ and $[\, T_\sigma^k \,]$ are defined as:

$$
\left[T_\epsilon^k \right] \equiv
\left[
\begin{array}{ccc|ccc}
l_1^2 & m_1^2 & l_1 m_1 & 0 & 0 & 0 \\
l_2^2 & m_2^2 & l_2 m_2 & 0 & 0 & 0 \\
2 l_1 l_2 & 2 m_1 m_2 & (l_1 m_2 + l_2 m_1) & 0 & 0 & 0 \\
\hline
0 & 0 & 0 & 1 & 0 & 0 \\
0 & 0 & 0 & 0 & m_2 & l_2 \\
0 & 0 & 0 & 0 & m_1 & l_1
\end{array}
\right]
\tag{3.7a}
$$

$$
\left[T_\sigma^k \right] \equiv
\left[
\begin{array}{ccc|ccc}
l_1^2 & m_1^2 & 2 l_1 m_1 & 0 & 0 & 0 \\
l_2^2 & m_2^2 & 2 l_2 m_2 & 0 & 0 & 0 \\
l_1 l_2 & m_1 m_2 & (l_1 m_2 + l_2 m_1) & 0 & 0 & 0 \\
\hline
0 & 0 & 0 & 1 & 0 & 0 \\
0 & 0 & 0 & 0 & m_2 & l_2 \\
0 & 0 & 0 & 0 & m_1 & l_1
\end{array}
\right]
\tag{3.7b}
$$

where, l_1, l_2, m_1, m_2 are direction cosines, given by

$$
\begin{aligned}
l_1 &= \cos(X_1, X_1') = \cos(\theta^k) & , & & m_1 &= \cos(X_2, X_1') = \sin(\theta^k) \\
l_2 &= \cos(X_1, X_2') = -\sin(\theta^k) & , & & m_2 &= \cos(X_2, X_2') = \cos(\theta^k)
\end{aligned}
\tag{3.8}
$$

Some additional useful relations between the strain and stress transformation matrices [T_ϵ^k] and [T_σ^k] are

$$\left[T_\epsilon^k\right]^{-1} = \left[T_\sigma^k\right]^T \quad , \quad \left[T_\sigma^k\right]^{-1} = \left[T_\epsilon^k\right]^T \qquad (3.9)$$

3.5 Calibrating Stress-Strain Fields

In order to determine the equivalent stiffness of the sublaminate, it must be subjected to some specified calibrating patterns of stresses and strains. Also, preferably, the equivalent stiffness of the sublaminate should be determined in such a manner that the stress and strain continuity requirements specified in Eq. (3.4) are satisfied. If it is assumed that stresses and strains in each lamina within the sublaminate are constant, then the following calibrating pattern of stresses and strains can be proposed, which also satisfies the requirements in Eq. (3.4):

$$\left\{\frac{\epsilon_i}{\sigma_o}\right\}^k = \left\{\frac{\bar{\epsilon}_i}{\bar{\sigma}_o}\right\} \quad , \quad \text{for } k = 1, \ldots N \qquad (3.10)$$

where $\bar{\epsilon}_i$ and $\bar{\sigma}_o$ are homogenized in-plane strains and out-of-plane stresses in the equivalent continuum representing the sublaminate, and N is the number of laminae comprising the sublaminate. Eq. (3.10) suggests that the calibrating stress and strain fields chosen are uniform in-plane strains and uniform out-of-plane stresses.

In the next section, homogenization relations will be presented for the remaining components of stress and strain in the equivalent material.

3.6 Homogenized In-plane Stresses and Out-of-plane Strains

The in-plane stresses and out-of-plane strains in the equivalent continuum are defined as

$$\left\{\frac{\bar{\sigma}_i}{\bar{\epsilon}_o}\right\} = \sum_{k=1}^{N} \left(\frac{t^k}{t}\right)\left\{\frac{\sigma_i}{\epsilon_o}\right\}^k \qquad (3.11)$$

where t^k is the thickness of the kth lamina, t is the thickness of the sublaminate, and N is the number of laminae in the sublaminate.

Eqs. (3.10) and (3.11) are sufficient to completely characterize the sublaminate model. The above relations also apply to incremental stresses and strains. In the next section these relations are employed to obtain the tangent stiffness of the equivalent continuum representing the sublaminate.

3.7 Tangent Stiffness of Sublaminate

The tangent stiffness relations for a lamina are given by Eq. (2.12). In the lamina coordinate system, they take the form

$$\left\{ d\sigma' \right\}^k = \left[C'^k \right] \left\{ d\epsilon' \right\}^k + \Delta T \left\{ \beta' \right\}^k \tag{3.12}$$

Eq. (3.12) is transformed to the laminate coordinate system using Eqs. (3.5–3.8) to yield

$$\left\{ d\sigma \right\}^k = \left[C^k \right] \left\{ d\epsilon \right\}^k + \Delta T \left\{ \beta \right\}^k \tag{3.13}$$

The vector of thermal properties $\{\beta'\}$ transforms like the vector of stresses, i.e.,

$$\left\{ \beta \right\}^k = \left[T_\epsilon^k \right]^T \left\{ \beta' \right\}^k \tag{3.14}$$

The lamina stiffness relations in laminate coordinates can be written in partitioned form, in accordance with Eq. (3.1) as

$$\left\{ \begin{array}{c} d\sigma_i \\ \hline d\sigma_o \end{array} \right\} = \left[\begin{array}{c|c} C_{ii} & C_{io} \\ \hline C_{oi} & C_{oo} \end{array} \right] \left\{ \begin{array}{c} d\epsilon_i \\ \hline d\epsilon_o \end{array} \right\} + \Delta T \left\{ \begin{array}{c} \beta_i \\ \hline \beta_o \end{array} \right\} \tag{3.15}$$

The above lamina tangent stiffness relation is now partially inverted to give

65

$$\left\{ \dfrac{d\sigma_i}{d\epsilon_o} \right\} = \left[\begin{array}{c|c} \mathbf{P}_{ii} & \mathbf{P}_{io} \\ \hline -\mathbf{P}_{io}^T & \mathbf{P}_{oo} \end{array} \right] \left\{ \dfrac{d\epsilon_i}{d\sigma_o} \right\} + \Delta T \left\{ \dfrac{\mathbf{P}_{\beta_i}}{\mathbf{P}_{\beta_o}} \right\} \tag{3.16}$$

where

$$\mathbf{P}_{oo} = \mathbf{C}_{oo}^{-1}$$

$$\mathbf{P}_{io} = \mathbf{C}_{io}\ \mathbf{P}_{oo}$$

$$\mathbf{P}_{ii} = \mathbf{C}_{ii} - \mathbf{P}_{io}\ \mathbf{C}_{oi} \tag{3.17}$$

$$\mathbf{P}_{\beta_o} = -\mathbf{P}_{oo}\ \beta_o$$

$$\mathbf{P}_{\beta_i} = \beta_i + \mathbf{P}_{\beta_o}\ \beta_o$$

The partially inverted stiffness relations for the individual laminae within the sublaminate are assembled according to Eqs. (3.10) and (3.11) to form partially inverted stiffness relations for the sublaminate :

$$\left\{ \dfrac{d\overline{\sigma}_i}{d\overline{\epsilon}_o} \right\} = \left[\begin{array}{c|c} \overline{\mathbf{F}}_{ii} & \overline{\mathbf{F}}_{io} \\ \hline -\overline{\mathbf{F}}_{io}^T & \overline{\mathbf{F}}_{oo} \end{array} \right] \left\{ \dfrac{d\overline{\epsilon}_i}{d\overline{\sigma}_o} \right\} + \Delta T \left\{ \dfrac{\overline{\mathbf{P}}_{\beta_i}}{\overline{\mathbf{P}}_{\beta_o}} \right\} \tag{3.18}$$

where

$$\left[\begin{array}{c|c} \overline{\mathbf{F}}_{ii} & \overline{\mathbf{F}}_{io} \\ \hline -\overline{\mathbf{F}}_{io}^T & \overline{\mathbf{F}}_{oo} \end{array} \right] = \sum_{k=1}^{N} \left(\dfrac{t^k}{t} \right) \left[\begin{array}{c|c} \mathbf{P}_{ii} & \mathbf{P}_{io} \\ \hline -\mathbf{P}_{io}^T & \mathbf{P}_{oo} \end{array} \right]^k$$

$$\left\{ \dfrac{\overline{\mathbf{P}}_{\beta_i}}{\overline{\mathbf{P}}_{\beta_o}} \right\} = \sum_{k=1}^{N} \left(\dfrac{t^k}{t} \right) \left\{ \dfrac{\mathbf{P}_{\beta_i}}{\mathbf{P}_{\beta_o}} \right\}^k \tag{3.19}$$

The partially inverted stiffness relations (Eq. (3.18)) can now be partially re-inverted to obtain the tangent stiffness relations for the equivalent material representing the sublaminate

$$\left\{ \dfrac{d\overline{\sigma}_i}{d\overline{\sigma}_o} \right\} = \left[\begin{array}{c|c} \overline{\mathbf{C}}_{ii} & \overline{\mathbf{C}}_{io} \\ \hline \overline{\mathbf{C}}_{oi} & \overline{\mathbf{C}}_{oo} \end{array} \right] \left\{ \dfrac{d\overline{\epsilon}_i}{d\overline{\epsilon}_o} \right\} + \Delta T \left\{ \dfrac{\overline{\beta}_i}{\overline{\beta}_o} \right\} \tag{3.20}$$

where

$$\overline{C}_{oo} = \overline{P}_{oo}^{-1}$$

$$\overline{C}_{io} = \overline{P}_{io} \; \overline{C}_{oo}$$

$$\overline{C}_{oi} = \overline{C}_{io}^{T}$$

$$\overline{C}_{ii} = \overline{P}_{ii} + \overline{C}_{io} \; \overline{P}_{io}^{T} \qquad\qquad (3.21)$$

$$\overline{\beta}_{o} = -\overline{P}_{oo}^{-1} \; \overline{P}_{\beta_{o}}$$

$$\overline{\beta}_{i} = \overline{P}_{\beta_{i}} + \overline{P}_{io} \; \overline{\beta}_{o}$$

If the elastic moduli of the sublaminate are of interest, they can be obtained from the compliance matrix of the sublaminate, which is found by inversion of the stiffness matrix in Eq. (3.20).
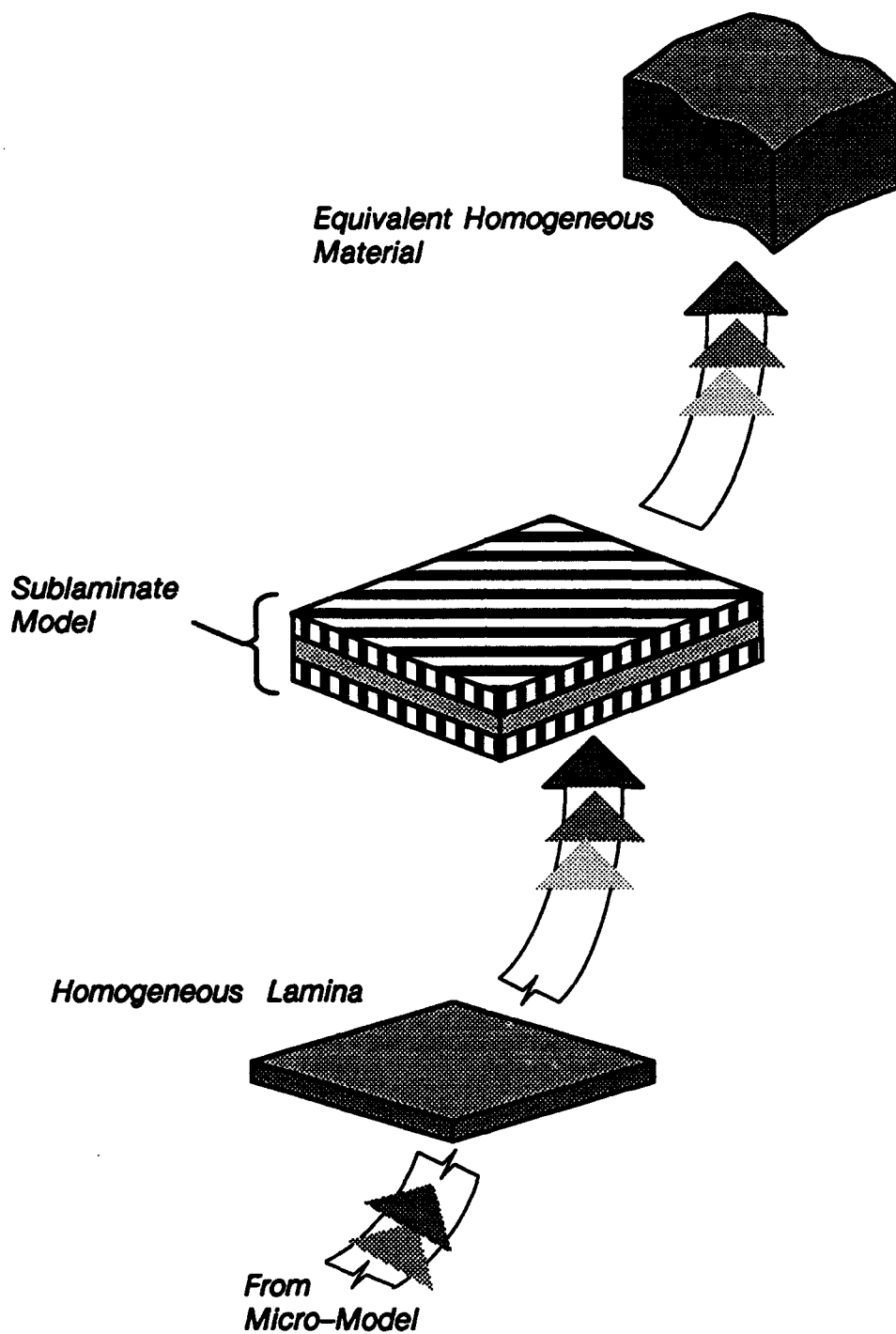
Fig. 3.1 *Schematic representation of the functioning of the Sublaminate model*
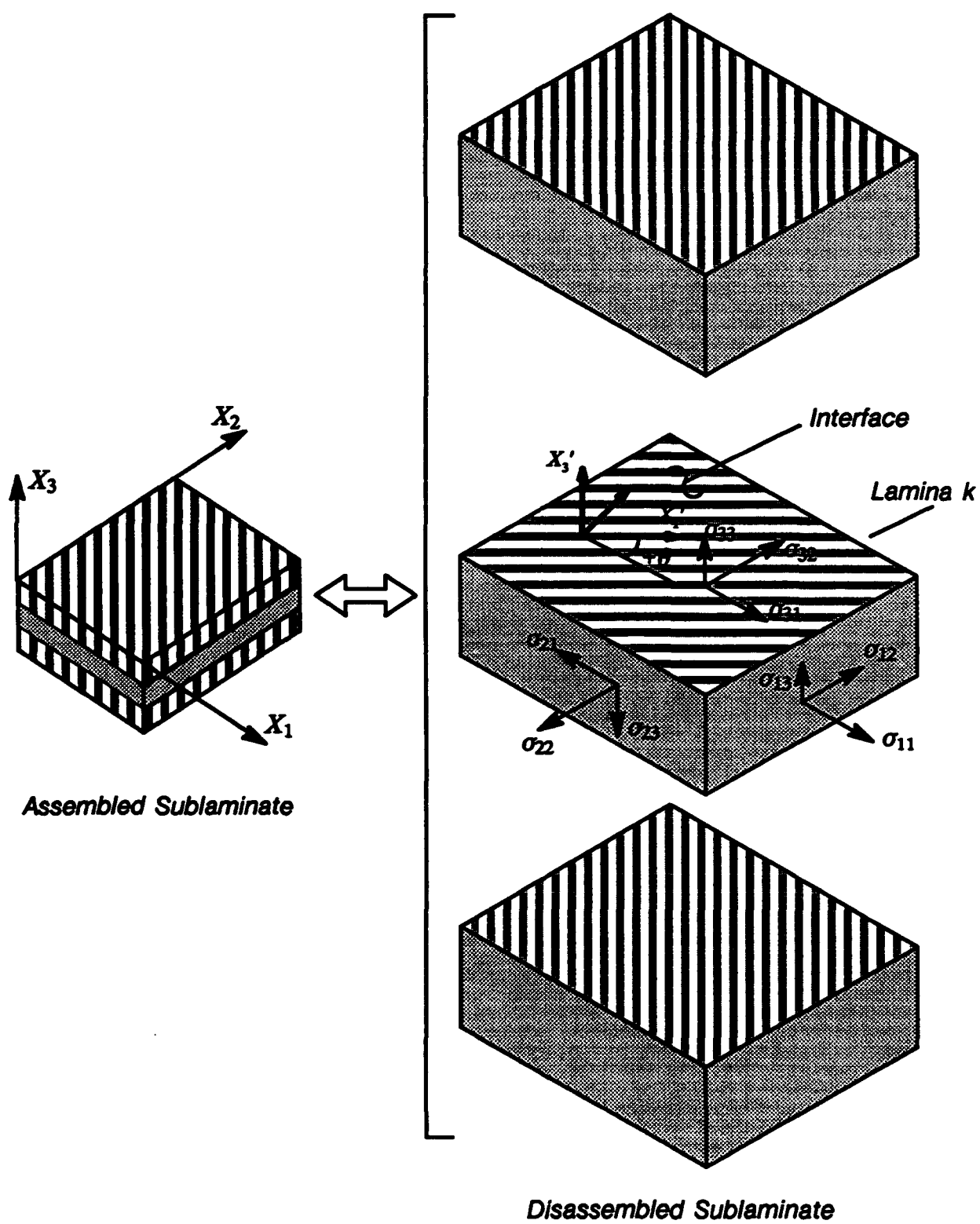
Fig. 3.2 *Stresses on laminae and the various coordinate systems.*

THE STRESS UPDATE

The solution of finite element models of nonlinear structural systems is usually obtained by applying the loading in an incremental manner. In addition, after application of each load increment, stresses are corrected and equilibrium iterations are normally performed to ensure equilibrium to within a specified tolerance. As the loading is applied to the structure, its geometry and the properties of the material may change, making the response of the structure nonlinear. These changes in material properties are monitored at the material/sampling points within each element. The effect of material property changes is reflected in the element stiffness matrices, which in turn convey the effect of these changes to the structure equilibrium equations, when element stiffness matrices are assembled to form the structure stiffness matrix. The segment of the structural analysis program which provides the constitutive description of the material at a sampling point and serves to update the material properties and the stresses at the sampling point is called the *material model*.

Specifically stated, within the framework of finite element analysis, the material model is called upon to perform the following important tasks:

1) Update the stresses at the material points, as the strains change.

2) Update the tangent stiffness of the material at the material points, if required.

3) Record and indicate other changes in the state of the material, such as the onset of yielding or failure etc.

4.1 Solution of Nonlinear Structural Systems

The solution of nonlinear systems is usually carried out by a combined incremental-iterative scheme, such as the Newton-Raphson or the Modified Newton-Raphson

method. The loads are applied in increments P_n, P_{n+1}, ... , and at each load step equilibrium iterations are performed to satisfy equilibrium to within specified tolerance. The equilibrium equations of the structure are cast in an incremental–iterative form as

$$\mathbf{K}_T \ \Delta\mathbf{U}_{n+1}^{(i)} = \mathbf{P}_{n+1} - \mathbf{I}_{R_{n+1}}^{(i-1)} = \mathbf{R}_{n+1}^{(i)} \tag{4.1}$$

in which $\mathbf{K}_T$ is the tangent stiffness matrix of the structure, $\mathbf{I}_{R_{n+1}}$ is the internal resistance vector and $\mathbf{R}_{n+1}$ is the residual load. The superscripts i and $i+1$ refer to ith and $i+1$th iterations. After each iteration the previous estimate of nodal deflections is updated as

$$\mathbf{U}_{n+1}^{(i)} = \mathbf{U}_{n+1}^{(i-1)} + \Delta\mathbf{U}_{n+1}^{(i)} \tag{4.2}$$

The graphical interpretation of the incremental–iterative scheme is shown in Fig. 4.1.

4.1.1 Role of the Material Model

The tangent stiffness matrix of the structure $\mathbf{K}_T$ and the internal resistance vector $\mathbf{I}_R$ are formed by assembling element tangent stiffness matrices $\mathbf{K}_T^{(e)}$ and internal resistances vectors $\mathbf{I}_R^{(e)}$. The element stiffness matrices and internal resistance vectors are evaluated using a numerical integration scheme such as Gaussian quadrature. The numerical integration scheme requires the material tangent stiffnesses and stresses at the material points, as is indicated in the following Eqs. (4.3):

$$\mathbf{K}_T^{(e)} = \int_{V^{(e)}} \mathbf{B}^{(e)^T} \mathbf{C}_T^{(e)} \mathbf{B}^{(e)} dV^{(e)} = \sum_{i=1}^{NP} W_i \ \mathbf{B}_i^T \mathbf{C}_{T_i} \mathbf{B}_i \ |\mathbf{J}_i|$$

$$\mathbf{I}_R^{(e)} = \int_{V^{(e)}} \mathbf{B}^{(e)^T} \sigma^{(e)} dV^{(e)} = \sum_{i=1}^{NP} W_i \ \mathbf{B}_i^T \sigma_i \ |\mathbf{J}_i| \tag{4.3}$$

where

NP = Number of Material Points or Sampling
Points within the element.

$$W_i = \text{Weighting Factor associated with the } ith \text{ Material Point.}$$

$$J_i = \text{Jacobian Matrix defining the mapping from element coordinates to parametric coordinates.}$$

The function of the material model becomes clear when Eqs. (4.3) are considered. Corresponding to a deflected state, strain increments, previous stresses and strains, and history parameters are passed to the material model, which then updates the stresses, material tangent properties, and history parameters at the material point. Geometric nonlinearities, if present, are reflected in the strain–displacement matrix $\mathbf{B}$.

The procedure for obtaining the equivalent tangent stiffness of the material at the material point has been described in detail in Chapters 1–3, and is quite straight–forward. The stress update, however, is more involved as a consequence of the "two–level micro–structure" employed in the material modelling procedure. The problems associated with updating the stresses at a material point will be outlined in detail in the next section.

4.2 Outline of the Stress Update Problem

Suppose that during the incremental–iterative solution scheme, a change $\Delta\mathbf{U}$ takes place in the nodal displacements. The displacement increment causes an increment of strain $\Delta\bar{\epsilon}$ at a material point. The state of strains at the material points within the elements is directly updated, i.e.,

$$\bar{\epsilon} \leftarrow \bar{\epsilon} + \Delta\bar{\epsilon} \qquad (4.4)$$

The stresses, however, cannot be updated directly by adding the predicted increments of stresses $\Delta\bar{\sigma}^e$ based on tangential estimates to the previous state of stress, since this would result in a cumulative error as the solution proceeds. This problem is a direct consequence of nonlinear material behaviour, as is illustrated in Fig. 4.2, which shows the difference between the stress increment based on tangential estimate $\Delta\bar{\sigma}^e$ and the true stress incre-

ment $\Delta\overline{\sigma}$. What is sought is an accurate estimate of the true stress increment $\Delta\overline{\sigma}$ consistent with the material constitutive description and the imposed strain increment $\Delta\overline{\varepsilon}$.

The procedure for determining the true increment of stress $\Delta\overline{\sigma}$ corresponding to an increment of strain $\Delta\overline{\varepsilon}$ is more complicated than for metal-plasticity. This is a result of the two-level microstructure of the material model employed here. The problem posed in updating the stresses at a material point is described in Fig. 4.3, which shows the equivalent homogeneous material at a typical material point undergoing an increment of strain. The problem is to find the corresponding true increment of stress in the equivalent material, and update the state of stress there. For this, the effect of the strain increment has to be cascaded down to the micromechanical level, where the stresses in the fiber and matrix phases are updated. Once the stresses in the fiber and matrix have been updated, the tangent stiffness and stress in the equivalent material can be evaluated using the stress and strain homogenization procedure in the micro-model and the sublaminate model. *For the homogenization procedure to be valid, it is essential that the homogenization relations are not violated during the process of transferring the effect of the strain increment to the fiber and the matrix phases. This means that the same homogenization relations used to define the Micro-model and the Sublaminate model now act as constraints which must not be violated during the stress update procedure.* Fig. 4.3 shows these constraints/homogenization relations, which have to be satisfied at the micro-model level and the sublaminate model level. It is important to note that the constraints are hybrid constraints, i.e. the constraints are specified on the strains as well as the stresses.

4.3 Stress Update Procedure

The procedure adopted here to solve the stress update problem is a relaxation type procedure. The general strategy employed is that some of the constraints are imposed while temporarily relaxing the complementary set of constraints. Residuals are then calculated by determining the imbalance in the constraints which are violated. The out of

balance constraints are satisfied by redistributing the residuals to remove the imbalance. The procedure can be repeated a number of times, until the desired degree of accuracy is achieved.

The solution scheme is a five–step process. Description of these steps and the specific tasks performed during each of these steps is presented in the following sections.

4.3.1 Tangential Update (Step 1)

In this step the effect of the strain increment $\Delta\bar{\epsilon}$, prescribed over the equivalent material at a material point, is transferred to the fiber and matrix phases at the micro–model level using tangential estimates based on material properties at the end of last converged load step. The algorithm for the Tangent Update procedure is presented schematically in Fig. 4.4, and the description of the various operations performed in this step follows next.

Given the strain increment $\Delta\bar{\epsilon}$ prescribed over the equivalent material at a material point, the in–plane strains within each lamina of the sublaminate are known via constraint (S1); but the out–of–plane strains within the individual laminae are not known. At the same time the continuity of out–of–plane stresses has to be assured. Keeping both these considerations in mind, the tangential prediction of the increment of out–of–plane stresses $\Delta\vec{\sigma_o}$ is accepted for the time being as a reasonably good estimate of the actual increment in out–of–plane stresses.

After the in–plane strains and out–of–plane stresses have been transformed to the lamina local coordinates, the complementary out–of–plane strains can be determined by forming the partially inverted tangent stiffness of the lamina as shown in Fig. 4.4, and in the following relation

$$\left\{\frac{\Delta\sigma'_i}{\Delta\epsilon_o^{'*}}\right\}^k = \left[\ \mathbf{P}^k\ \right]\ \left\{\frac{\Delta\epsilon'_i}{\Delta\sigma_o^{'*}}\right\}^k \tag{4.5}$$

74

The complete set of strains in a lamina is now known. The strain in the lamina is equivalent to the strain in the unit cell, and by virtue of constraint (M1) is equal to the increment of strain in material elements A and B. The increment of stresses in material elements A and B can be readily estimated by forming the respective tangent stiffnesses of material elements A and B,

$$\left\{\frac{\Delta\sigma_i^*}{\Delta\sigma_o^*}\right\}_{A,B} = \left[\ C_T\ \right]_{A,B} \left\{\frac{\Delta\epsilon_i}{\Delta\epsilon_o^*}\right\}_{A,B} \tag{4.6}$$

Within material element A the state of stress and strain within the fiber subcell **f** and the matrix subcell m_A can be estimated first by invoking constraint (M3) and then determining the remaining stress and strain increments by using the partially inverted compliance relations for the fiber and the matrix subcell m_A.

$$\left\{\frac{\Delta\sigma_L}{\Delta\epsilon_T^*}\right\}_{f,m_A} = \left[\ P\ \right]_{f,m_A} \left\{\frac{\Delta\epsilon_L}{\Delta\sigma_T^*}\right\}_{f,m_A} \tag{4.7}$$

This completes the Tangent Update step of the stress update procedure.

4.3.2 Constitutive Relations Update (Step 2)

After the Tangent Update step, the tangential estimates of stresses and strains within the various subcells of the unit cell are known. At this point all constraints are satisfied. However, if the material is nonlinear, the estimated stresses and the strains within the subcells are not consistent with the material constitutive description. Some of the stress or strain components have to be altered to make the stresses and strains consistent with the material constitutive description. The manner in which this is done is that some of the tangential estimates of stress and strain components are accepted, and the remaining components of stress and strain are determined, such that they are consistent with the constitutive description of the material.

For matrix subcell $\mathbf{m_B}$ the tangential estimate of strain is accepted, and the corresponding set of stresses $\{\hat{\sigma}\}_{\mathbf{m_B}}$ which is consistent with the constitutive description, is determined. The procedure which is used is *subincrementation*, in which the prescribed strain increment is divided into a pre–determined number of smaller subincrements. At the end of each subincrement the tangent stiffness of the material is updated, and a subincrement of stress corresponding to the next subincrement of strain is calculated. The subincrements of stress are summed to give the increment in stress, which is added to the previous state of stress to give the value of stresses at the end of the prescribed strain increment. The consistent stresses within matrix subcell $\mathbf{m_B}$ are then given by

$$\left\{\hat{\sigma}\right\}_{\mathbf{m_B}} = \left\{{}^{(n)}\sigma\right\}_{\mathbf{m_B}} + \sum_{i=1}^{M} \left[{}^{(i)}\mathbf{C}_T\right]_{\mathbf{m_B}} \left\{\frac{\Delta\epsilon_i/M}{\Delta\dot{\epsilon}_o/M}\right\}_{\mathbf{m_B}} \tag{4.8}$$

where M is the number of subincrements within the increment. The subincrementation procedure is illustrated in Fig. 4.5, and is adopted here because of its simplicity. The accuracy of the subincrementation method can be improved by increasing the number of subincrements; alternatively, more accurate procedures such as Runge–Kutta could be used.

Within material element A the fiber is linear–elastic, and therefore the tangential estimates of stresses and strains within the fiber are consistent with one another. It should be noted that a nonlinear constitutive relation could be used for the fiber; subincrementation scheme would then be used here also. Within matrix subcell $\mathbf{m_A}$ the tangential estimates of longitudinal strain ϵ_L and transverse stresses σ_T are accepted, and the complementary set of stresses and strains is determined by subincrementation:

$$\left\{\frac{\hat{\sigma}_L}{\hat{\epsilon}_T}\right\}_{\mathbf{m_A}} = \left\{\frac{{}^{(n)}\sigma_L}{{}^{(n)}\epsilon_T}\right\}_{\mathbf{m_A}} + \sum_{i=1}^{M} \left[{}^{(i)}\mathbf{P}\right]_{\mathbf{m_A}} \left\{\frac{\Delta\epsilon_L/M}{\Delta\dot{\sigma}_T/M}\right\}_{\mathbf{m_A}} \tag{4.9}$$

76

After determining the consistent set of stresses and strains in the various subcells of the unit cell, the material properties and stresses within the various subcells of the unit cell are updated.

4.3.3 Residual Calculation (Step 3)

The difference between the tangential estimates of stresses and strains, and the consistent stresses and strains results in violation of some of the constraints at the micro–model level and at the sublaminate model level. The process of residual calculation entails determining the amount of imbalance in those constraints which are violated, and calculating the corrective quantities needed to remove the imbalance. The process of residual calculation is shown in Fig. 4.6; it starts at the micro–model level and progresses upwards to the sublaminate model level.

At the micro–model level, within element B (matrix subcell m_B) the difference between the tangential estimates of stresses and the consistent set of stresses defines a stress residual $\{\delta\sigma\}_{m_B}$. Since the in–plane strains in material element B are in accordance with constraints (S1), only the residual $\{\delta\sigma_o\}_{m_B}$ pertaining to out–of–plane stresses need be considered, and is given as

$$\left\{\delta\sigma_o\right\}_B \equiv \left\{\delta\sigma_o\right\}_{m_B} = \left\{\hat{\sigma}_o\right\}_{m_B} - \left\{\sigma_o^*\right\}_{m_B} \qquad (4.10)$$

Stress
Residual

Similarly, within matrix subcell m_A, the difference between the consistent strains and tangential estimates define a strain residual $\{\delta\epsilon_T\}_{m_A}$ given by:

$$\left\{\delta\epsilon_T\right\}_{m_A} = \left\{\hat{\epsilon}_T\right\}_{m_A} - \left\{\epsilon_T^*\right\}_{m_A}$$

Strain
Residual

$$(4.11)$$

The strain residual within matrix subcell m_A translates into a strain residual within material element A as

$$\left\{\delta\epsilon_T\right\}_A = -W_m \left\{\delta\epsilon_T\right\}_{m_A} \tag{4.12}$$

Strain
Residual

The strain residual in material element A is the amount of strain mismatch between the material elements A and B, which ought to be removed to satisfy constraint (M1). This would require application of a corrective stress to element A given by

$$\left\{\delta\sigma_T\right\}_A \longleftarrow \left\{\overline{\overline{\delta\sigma_T}}\right\}_A = \begin{bmatrix} C_T \end{bmatrix}_A \left\{\begin{matrix} 0 \\ \delta\epsilon_T \end{matrix}\right\}_A \tag{4.13}$$

Stress
Correction

This stress correction would have to be applied to element A in order to satisfy constraint (M1), but the application of this stress correction is deferred for the time being.

In material element A the stress correction terms $\{\delta\sigma_o\}_A$ pertaining to out–of–plane stresses are calculated from $\{\delta\sigma_T\}_A$ by selecting only the out–of–plane stress terms.

The out–of–plane stresses within the lamina are now in violation of constraint (S1), and the amount of imbalance from the initial tangential estimate is given by

$$\left\{\delta\sigma_o\right\}^k \equiv \left\{\delta\sigma_o\right\}_C = -\left(W_f \left\{\delta\sigma_o\right\}_A + W_m \left\{\delta\sigma_o\right\}_B \right) \tag{4.14}$$

Stress
Residual

The out–of–plane stress residual in the lamina would result in an out–of–plane strain correction term, given by

$$\left\{\delta\epsilon_o\right\}^k \longleftarrow \left\{\overline{\overline{\delta\epsilon_o}}\right\}^k = \begin{bmatrix} P^k \end{bmatrix} \left\{\begin{matrix} 0 \\ \delta\sigma_o \end{matrix}\right\}^k \tag{4.15}$$

Strain
Correction

where $\begin{bmatrix} P^k \end{bmatrix}$ is the partially inverted lamina tangent compliance. The effect of the lamina strain correction term calculated in Eq. (4.15) is to be carried back to the fiber and the matrix phases, but its application is deferred until the next step.

The strain correction contributions from all the laminae within the sublaminate are summed up to yield a strain residual at the sublaminate level, given by

$$\{\delta\bar{\epsilon}_o\} = \sum_{k=1}^{N} \left(\frac{t^k}{t}\right)\{\delta\epsilon_o\}^k \qquad (4.16)$$

Strain
Residual

Corresponding to the sublaminate strain residual, an out–of–plane stress correction term is calculated as

$$\{\delta\bar{\sigma}_o\} \longleftarrow \left\{\frac{-}{\delta\bar{\sigma}_o}\right\} = \left[\ \bar{C}_T\ \right] \left\{\frac{0}{-\delta\bar{\epsilon}_o}\right\} \qquad (4.17)$$

Stress
Correction

This out–of–plane stress correction term is applied to the sublaminate to remove the strain residual in the sublaminate. This is explained in the next step of the stress update procedure.

4.3.4 Residual Application (Step 4)

The schematic algorithm for application of residuals to satisfy the out–of–balance constraints is shown in Fig. 4.7. The stress correction term determined in Eq. (4.17) is applied to the sublaminate, and its effect is transferred to the micro–model level. The procedure is essentially the same as that followed in the Tangent Update (Step 1) with a slight modification: the residuals calculated in the preceding step of the Residual Calculation, and whose application was deferred, are also taken into account while distributing the residuals.

4.3.5 Updated Stress Calculation (Step 5)

After all the constraints are satisfied to within acceptable tolerances, the effective stress at the material point is calculated by using the stress homogenization relations used in the definition of the micro–model and the sublaminate model. The procedure employed is shown schematically in Fig. 4.8. After the updated stresses have been calculated, this information is passed on to the main analysis program.

4.3.6 Overall Stress Update Algorithm

The overall stress update algorithm consists of the five previously described steps; step 5 is the last step in the procedure, and is taken only when the constraints are within specified tolerances. The check for satisfaction of constraints is made after Step 3 (Residual Calculation). If the constraints are not satisfied, some of the steps have to be repeated. The flowchart of the stress update procedure is shown in Fig. 4.9.

As is shown in Fig. 4.9, the prescribed strain increment $\Delta \bar{\epsilon}$ at a material point is received as input from the main structural analysis program. Step 1 (Tangent Update), Step 2 (Constitutive Properties Update), and Step 3 (Residual Calculation) are performed, following which a decision is made about the convergence of residuals. In order to ensure that the out-of-plane strain residual $\{\delta \bar{\epsilon}_o\}$ is small, the following convergence criterion is used,

$$\frac{\| \delta \bar{\epsilon}_o \|}{\| \Delta \bar{\epsilon} \|} \leq \text{Tolerance} \qquad (4.18)$$

If the above convergence criterion is satisfied, then the updated stresses are calculated and the results are conveyed to the main program. If the convergence criterion is not satisfied, then Step 4 (Residual Redistribution) is carried out, and Step 2 and Step 3 are repeated.

4.4 Comments on the Stress Update Procedure

The procedure presented in this chapter for obtaining the updated stresses was found to be quite accurate. After the stresses are updated all the constraints are satisfied, with some error remaining in the constitutive relations. This is partly the result of the subincrementation procedure adopted here, and also because of the fact that the relaxation type scheme adopted here is iterative in nature. Subincrementation is an approximate solution scheme, and therefore the results obtained contain some error. More refined integration schemes can be used for integration of constitutive relations; however, this would result in making the stress updating scheme more complex.
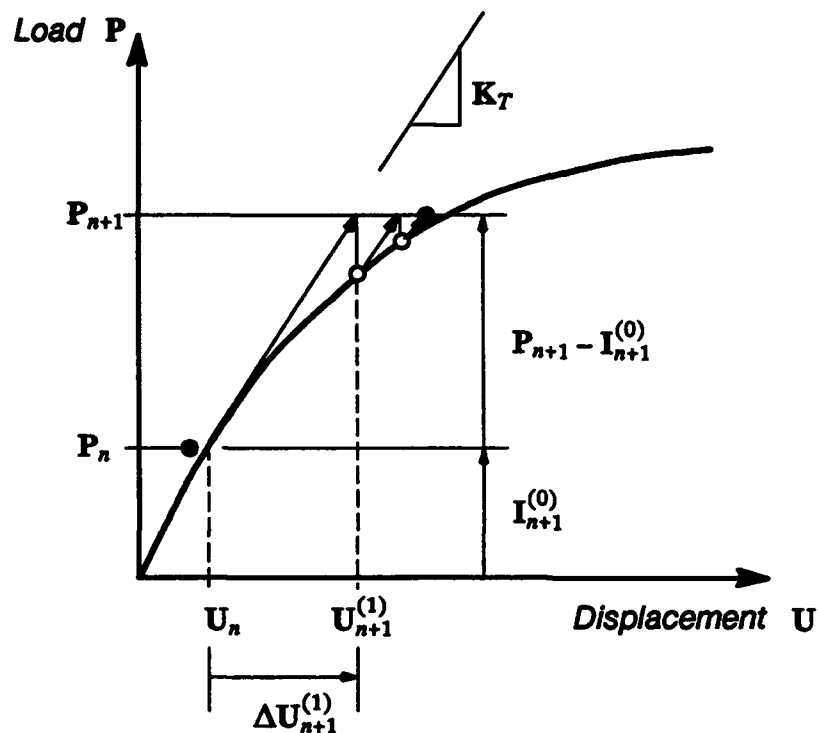
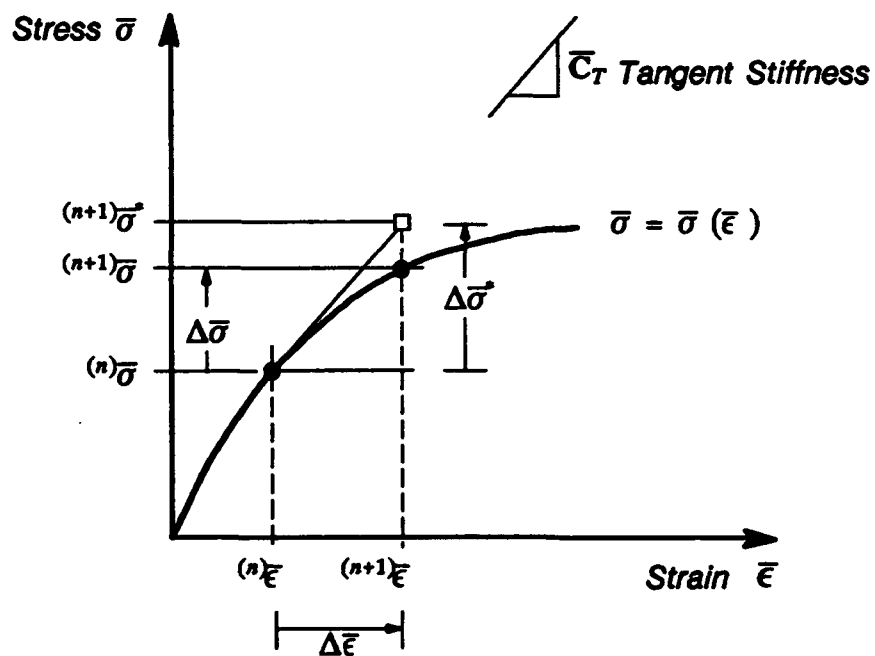**Fig. 4.1** *Incremental solution of nonlinear structural systems with Newton–Raphson iterations.*

Fig. 4.2 *Schematic view of stress update illustrating the difference between true stress increment $\Delta\bar{\sigma}$ and the tangential estimate $\Delta\bar{\sigma}^e$*
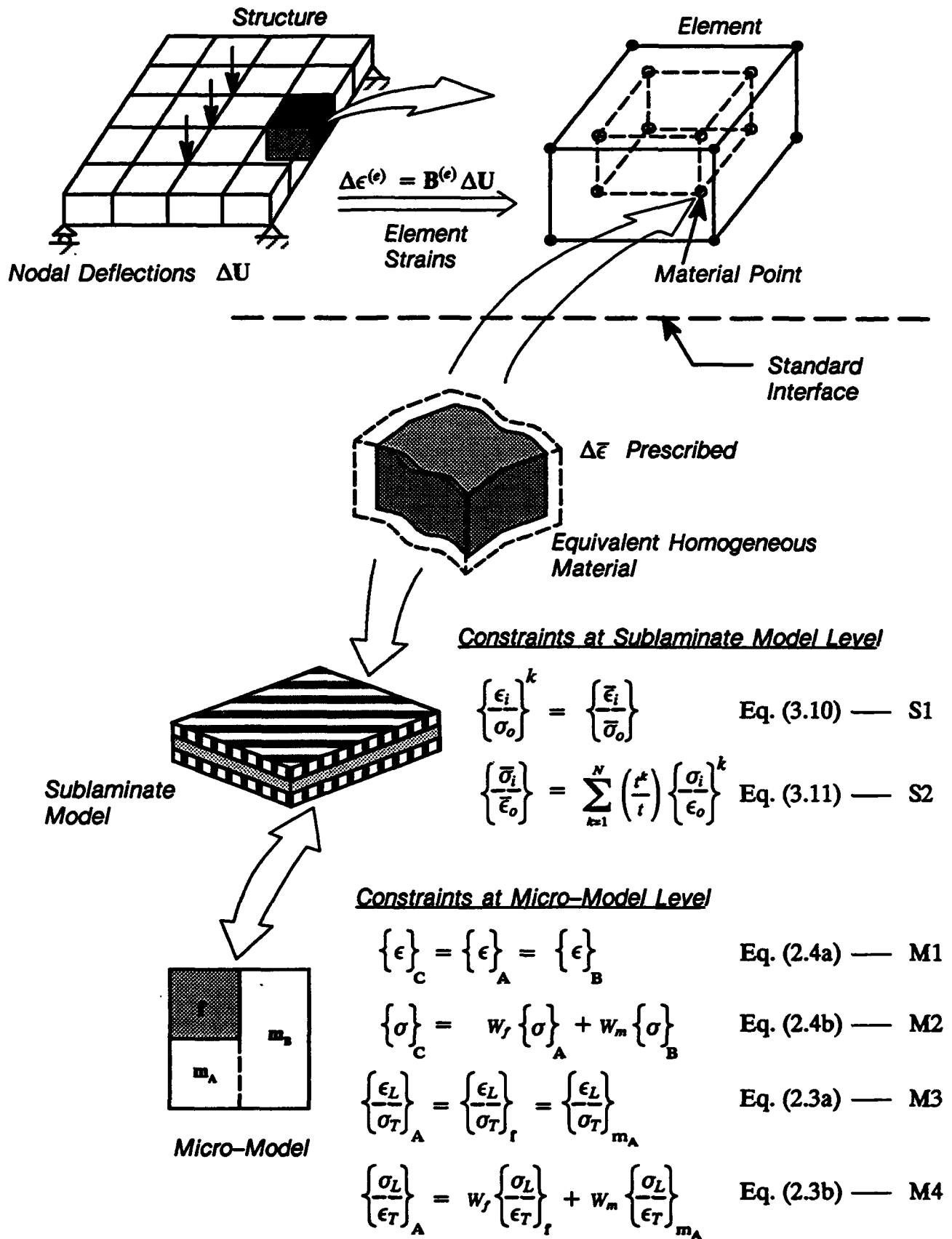
81

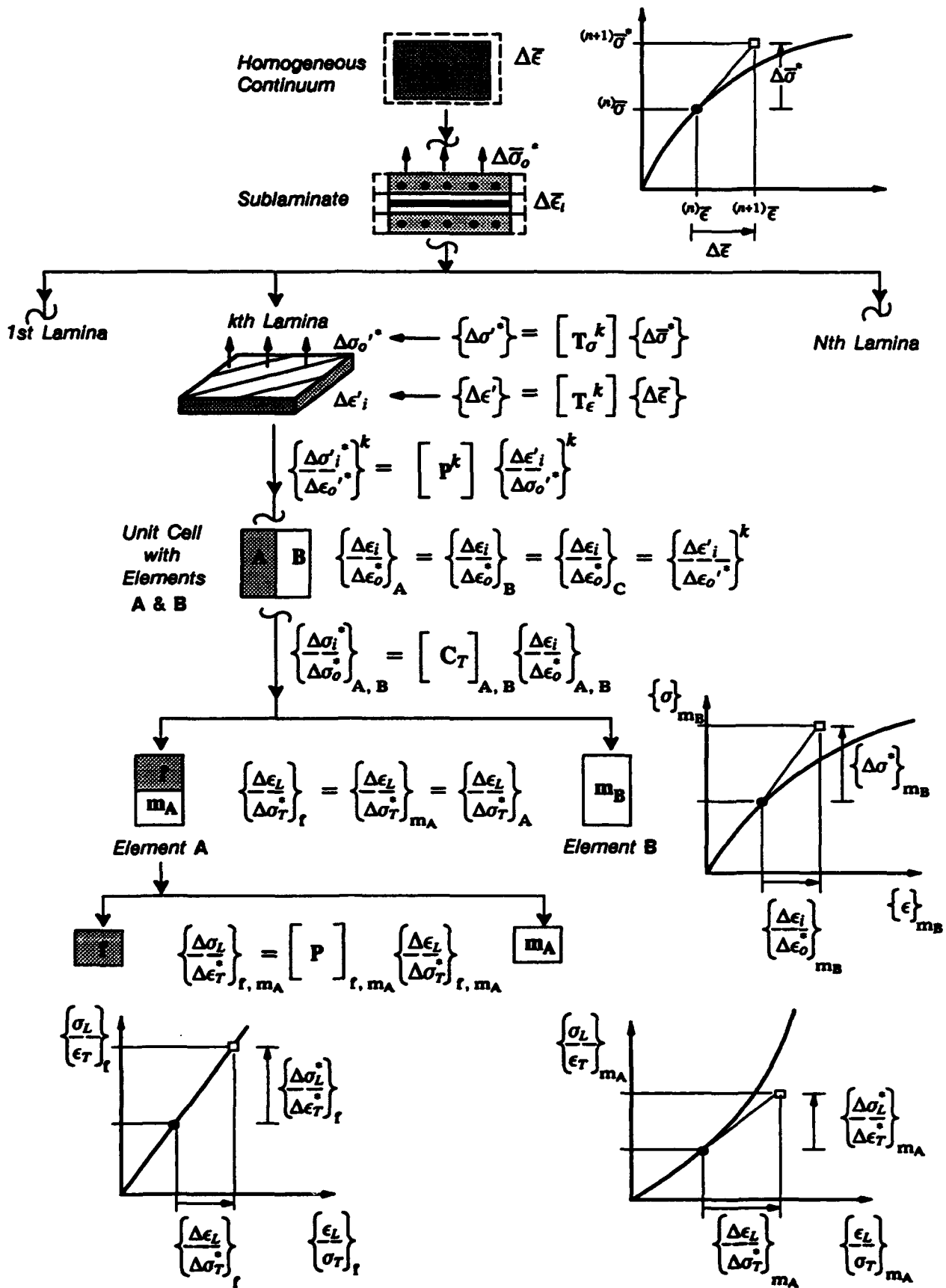**Fig. 4.3** *Schematic statement of the stress update problem.*

82

Homogeneous Continuum $\Delta\bar{\varepsilon}$

Sublaminate $\Delta\bar{\varepsilon}_i$ $\Delta\bar{\sigma}_o{}^{\bullet}$

$$(n+1)\overline{\sigma}^{\bullet}$$
$$(n)\overline{\sigma}$$
$$(n)\overline{\varepsilon} \quad (n+1)\overline{\varepsilon}$$
$$\Delta\overline{\sigma}^{\bullet}$$
$$\Delta\overline{\varepsilon}$$

1st Lamina   kth Lamina   Nth Lamina

$$\Delta\sigma_o{}'{}^{\bullet} \longleftarrow \left\{\Delta\sigma'\right\} = \left[\mathbf{T}_\sigma{}^k\right]\left\{\Delta\overline{\sigma}^{\bullet}\right\}$$

$$\Delta\epsilon'_i \longleftarrow \left\{\Delta\epsilon'\right\} = \left[\mathbf{T}_\epsilon{}^k\right]\left\{\Delta\overline{\epsilon}\right\}$$

$$\left\{\frac{\Delta\sigma'_i{}^{\bullet}}{\Delta\epsilon_o{}'{}^{\bullet}}\right\}^k = \left[\mathbf{P}^k\right]\left\{\frac{\Delta\epsilon'_i}{\Delta\sigma_o{}'{}^{\bullet}}\right\}^k$$

Unit Cell with Elements A & B

$$\left\{\frac{\Delta\epsilon_i}{\Delta\epsilon_o^{\bullet}}\right\}_A = \left\{\frac{\Delta\epsilon_i}{\Delta\epsilon_o^{\bullet}}\right\}_B = \left\{\frac{\Delta\epsilon_i}{\Delta\epsilon_o^{\bullet}}\right\}_C = \left\{\frac{\Delta\epsilon'_i}{\Delta\epsilon_o{}'{}^{\bullet}}\right\}^k$$

$$\left\{\frac{\Delta\sigma_i^{\bullet}}{\Delta\sigma_o^{\bullet}}\right\}_{A,B} = \left[\mathbf{C}_T\right]_{A,B}\left\{\frac{\Delta\epsilon_i}{\Delta\epsilon_o^{\bullet}}\right\}_{A,B}$$

$$\{\sigma\}_{m_B}$$
$$\{\Delta\sigma^{\bullet}\}_{m_B}$$
$$\{\epsilon\}_{m_B}$$
$$\left\{\frac{\Delta\epsilon_i}{\Delta\epsilon_o^{\bullet}}\right\}_{m_B}$$

$$m_A$$ $$\left\{\frac{\Delta\epsilon_L}{\Delta\sigma_T^{\bullet}}\right\}_f = \left\{\frac{\Delta\epsilon_L}{\Delta\sigma_T^{\bullet}}\right\}_{m_A} = \left\{\frac{\Delta\epsilon_L}{\Delta\sigma_T^{\bullet}}\right\}_A$$ $$m_B$$

Element A   Element B

$$\left\{\frac{\Delta\sigma_L}{\Delta\epsilon_T^{\bullet}}\right\}_{f,m_A} = \left[\mathbf{P}\right]_{f,m_A}\left\{\frac{\Delta\epsilon_L}{\Delta\sigma_T^{\bullet}}\right\}_{f,m_A}$$ $$m_A$$

$$\left\{\begin{matrix}\sigma_L\\\epsilon_T\end{matrix}\right\}_f$$
$$\left\{\frac{\Delta\sigma_L}{\Delta\epsilon_T^{\bullet}}\right\}_f$$
$$\left\{\frac{\Delta\epsilon_L}{\Delta\sigma_T^{\bullet}}\right\}_f$$
$$\left\{\begin{matrix}\epsilon_L\\\sigma_T\end{matrix}\right\}_f$$

$$\left\{\begin{matrix}\sigma_L\\\epsilon_T\end{matrix}\right\}_{m_A}$$
$$\left\{\frac{\Delta\sigma_L}{\Delta\epsilon_T^{\bullet}}\right\}_{m_A}$$
$$\left\{\frac{\Delta\epsilon_L}{\Delta\sigma_T^{\bullet}}\right\}_{m_A}$$
$$\left\{\begin{matrix}\epsilon_L\\\sigma_T\end{matrix}\right\}_{m_A}$$

Fig. 4.4   Schematic algorithm for Tangent Update($\bullet$, $\square$) procedure, Step (1)

$$\left\{\hat{\sigma}\right\}_{\mathbf{m_B}} = \left\{^{(n)}\sigma\right\}_{\mathbf{m_B}} + \sum_{i=1}^{M} \left[^{(i)}\mathbf{C}_T\right]_{\mathbf{m_B}} \left\{\dfrac{\Delta\epsilon_i / M}{\Delta\dot{\epsilon}_o / M}\right\}_{\mathbf{m_B}}$$

$$\left\{\dfrac{\hat{\sigma}_L}{\hat{\epsilon}_T}\right\}_{\mathbf{m_A}} = \left\{\dfrac{^{(n)}\sigma_L}{^{(n)}\epsilon_T}\right\}_{\mathbf{m_A}} + \sum_{i=1}^{M} \left[^{(i)}\mathbf{P}\right]_{\mathbf{m_B}} \left\{\dfrac{\Delta\epsilon_L / M}{\Delta\dot{\sigma}_T / M}\right\}_{\mathbf{m_A}}$$
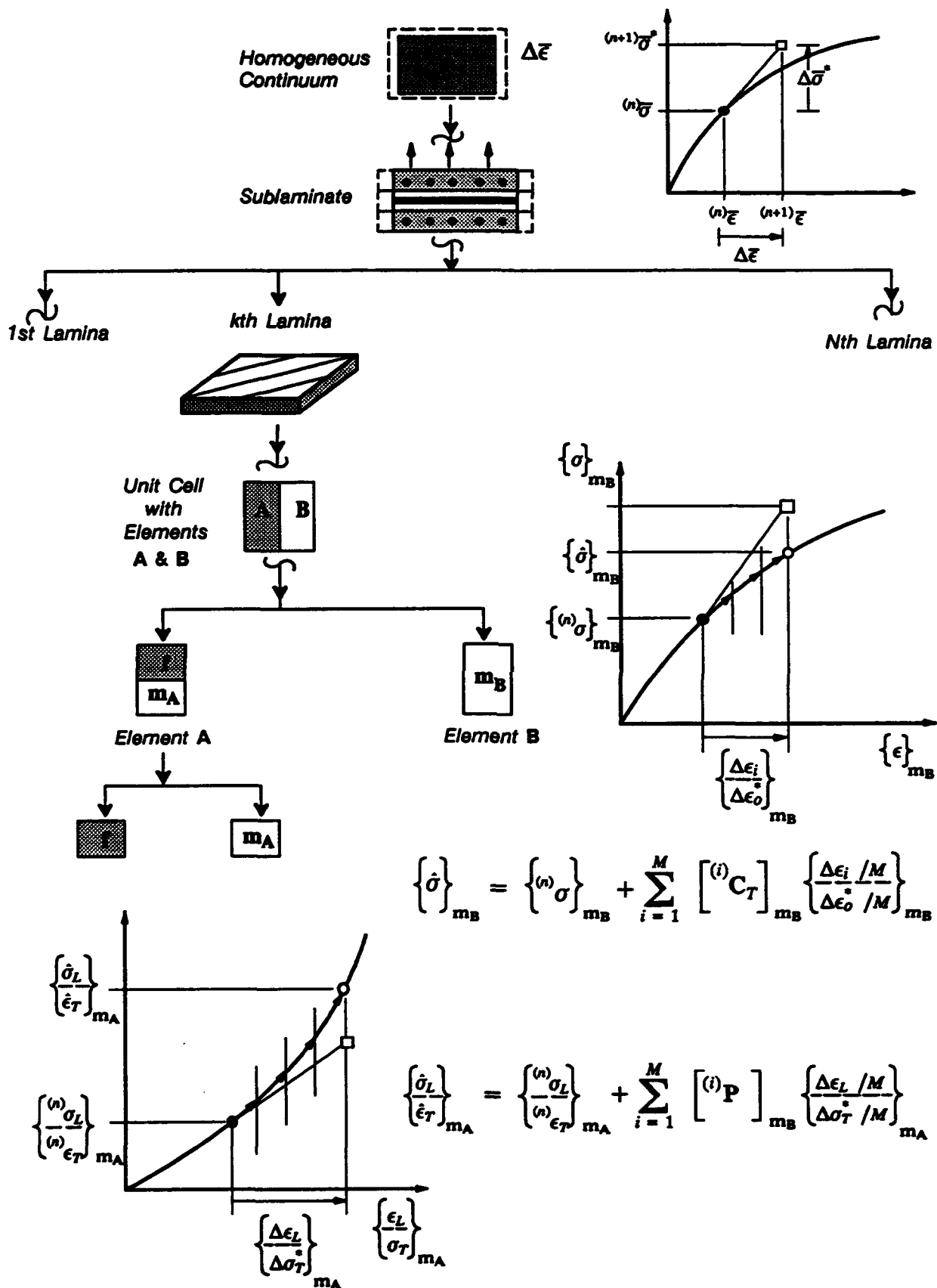
Fig. 4.5   Schematic algorithm for Constitutive Relations Update(-, o), Step (2)

84

Homogeneous Continuum $\quad \Delta\bar{\epsilon}$

$$\{\delta\bar{\sigma}_o\} \longleftarrow \left\{\frac{-}{\delta\bar{\sigma}_o}\right\} = \left[\bar{C}_T\right] \left\{\frac{0}{-\delta\bar{\epsilon}_o}\right\}$$

Stress Correction

Sublaminate

$$\{\delta\bar{\epsilon}_o\} = \sum_{k=1}^{N} \left(\frac{t^k}{t}\right) \{\delta\epsilon_o\}^k$$

Strain Residual

1st Lamina $\qquad$ kth Lamina $\qquad$ Nth Lamina

$$\{\delta\epsilon_o\}^k \longleftarrow \left\{\frac{-}{\delta\epsilon_o}\right\}^k = \left[P^k\right] \left\{\frac{0}{\delta\sigma_o}\right\}^k$$

Strain Correction

Unit Cell with Elements A & B

$$\{\delta\sigma_o\}^k \equiv \{\delta\sigma_o\}_C = -\left(W_f \{\delta\sigma_o\}_A + W_m \{\delta\sigma_o\}_B\right)$$

Stress Residual

$\{\delta\sigma_o\}_A$

$$\{\delta\sigma_T\}_A \longleftarrow \left\{\frac{-}{\delta\sigma_T}\right\}_A = \left[C_T\right]_A \left\{\frac{0}{\delta\epsilon_T}\right\}_A$$

Stress Correction

$$\{\delta\sigma_o\}_B \equiv \{\delta\sigma_o\}_{m_B} = \{\hat{\sigma}_o\}_{m_B} - \{\sigma_o^*\}_{m_B}$$

Stress Residual

$$\{\delta\epsilon_T\}_A = -W_m\{\delta\epsilon_T\}_{m_A}$$

Element A $\quad$ Strain Residual

m_A

m_B

Element B

$$\{\delta\epsilon_T\}_{m_A} = \{\hat{\epsilon}_T\}_{m_A} - \{\epsilon_T^*\}_{m_A}$$

$\left\{\sigma^*\right\}_{m_B}$

$\{\hat{\sigma}\}_{m_B}$ $\quad \{\delta\sigma\}_{m_B}$

$\{\epsilon\}_{m_B}$

$\left\{\dfrac{\hat{\sigma}_L}{\hat{\epsilon}_T}\right\}_{m_A}$

$\left\{\dfrac{\sigma_L^*}{\epsilon_T^*}\right\}_{m_A}$

$\left\{\dfrac{\delta\sigma_L}{\delta\epsilon_T}\right\}_{m_A}$

$\left\{\dfrac{\epsilon_L}{\sigma_T}\right\}_{m_A}$

Fig. 4.6 *Schematic algorithm for Residual Calculation, Step (3).*

Fig. 4.7 *Schematic algorithm for Residual Application (■), Step(4).*

Homogeneous Continuum $\Delta \bar{\epsilon}$

Sublaminate

$$\{\hat{\bar{\sigma}}_i\} = \sum_{k=1}^{N} \left(\frac{t^k}{t}\right)\{\hat{\sigma}_i\}^k$$

$$\{\hat{\bar{\sigma}}_o\} = \{\hat{\sigma}_o\}^k$$

1st Lamina   kth Lamina   Nth Lamina

$$\{\hat{\sigma}\}^k = \left[T_\epsilon^k\right]^T \{\hat{\sigma}'\}^k$$

Unit Cell with Elements A & B

$$\{\hat{\sigma}'\}^k \equiv \{\hat{\sigma}\}_C = W_f\{\hat{\sigma}\}_A + W_m\{\hat{\sigma}\}_B$$

$\{\hat{\sigma}\}_A$ $\{\hat{\sigma}\}_B$

m_A m_B

$$\{\hat{\sigma}_L\}_A = W_f\{\hat{\sigma}_L\}_f + W_m\{\hat{\sigma}_L\}_{m_A}$$

Element A $$\{\hat{\sigma}_T\}_A = \{\hat{\sigma}_T\}_{f, m_A}$$ Element B

f m_A
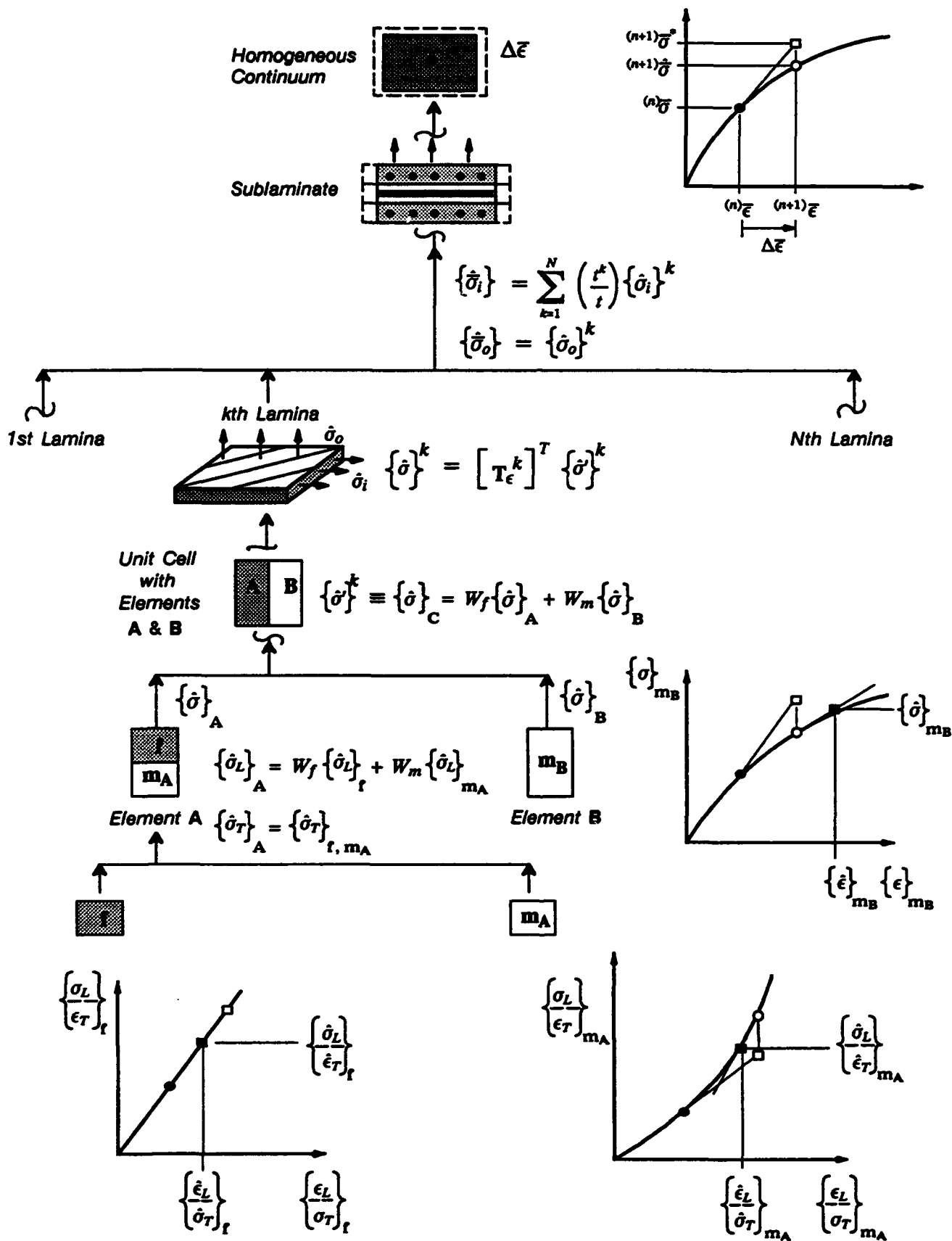
Fig. 4.8   Schematic algorithm for calculating the updated stress at a material point, Step (5).

87

Input

$\Delta \bar{\varepsilon}$, Strain increment from Main Analysis program.

↓

Step (1) Tangent Update

↓

Step (2) Constitutive Properties Update

↓

Step (3) Calculate Residuals resulting from Constitutive Properties Update.

↓

Convergence Test

Is the out-of-plane Strain Residual, $\delta \bar{\varepsilon}_o$ within Tolerance ?

Yes →

No ↓

Step (4) Residual Redistribution via Tangent Update

Step (5) Calculate the Updated Stress at the Material Point.

↓

Output

Updated Stress at the Material Point

Fig. 4.9 *Flowchart for Stress Update at a material point*

CHAPTER 5

RESPONSE OF LAMINAE AND LAMINATES
TO UNIFORM LOADINGS

$\mathbf{I}$n this chapter some applications are presented with the objective of evaluating the accuracy of the modelling procedure and demonstrating its potential. It is desirable to separate the two issues of structural modelling and modelling of the material behaviour. For this reason, the performance of the material model is evaluated in modelling and predicting the response of fiber-reinforced laminae and laminates under homogeneous loading conditions, i.e. when there is no spatial variation in the effective stresses and strains. Results are presented for:

- Response of various types of laminae, comprised of different fiber/ matrix combinations, subjected to off-axis loading, and laminates subjected to uniaxial loading. Only the effects of matrix stress-strain nonlinearity are taken into account, since the applied loading is not high enough to cause damage.

- Prediction of the off-axis strength of various types of laminae

- Initial yield surfaces of composite laminae subjected to different stress fields.

- Stress-strain response of laminates to the point of ultimate failure. In this case both the effects of matrix nonlinearity and other damage mechanisms are taken into account. Micromechanical criteria are employed for damage detection and incorporating the effect of damage.

5.1 Nonlinear Response of Laminae and Laminates

Aboudi [53], using the Method of Cells, modelled the nonlinear response of various types of laminae and laminates, comprised of different fiber/matrix combinations. A standard Ramberg–Osgood description was adopted for the matrix material. The stress–strain response of laminae and laminates predicted by Aboudi showed fairly good agreement with experimentally observed results. Here, the proposed material modelling procedure is used to predict the responses of the laminae and laminates studied by Aboudi [53], using the same elastic properties and constitutive description for the constituent fiber and matrix phases as used by him.

5.1.1 Response of Boron/Epoxy Laminae and Laminates

Fig. 5.1 shows the response of a Boron/epoxy lamina in shear. It is worth mentioning that the shear strain along the abscissa is the tensorial shear strain $\bar{\epsilon}_{12}$ and not the engineering shear strain, commonly denoted by $\bar{\gamma}_{12}$. The elastic properties of the Boron fibers and epoxy matrix are given in Table 5.1, and are the same as the ones used by Aboudi [53].

As can be seen from Fig 5.1, the results from the present formulation and Aboudi's Method of Cells are in excellent agreement. There is discrepancy between the theoretical predictions and experimental data in the vicinity of $\bar{\epsilon}_{12} = 0.75\%$; Aboudi attributed this to error in experimental data obtained from the 15° off-axis coupon.

Figs. 5.2 and 5.3 show the response of off-axis coupons $(\theta = 30^\circ, 45^\circ)$, subjected to uniaxial tension; results are shown for analytical predictions from Aboudi's Method of Cells, and the proposed material modelling procedure, along with experimental data from Cole and Pipes [78]. The predictions form both of the analytical procedures agree well with the experimental data. The predictions of $\bar{\epsilon}_{11}$ from both analytical procedures show

90

excellent agreement, but the $\bar{\varepsilon}_{22}$ strains predicted from the present formulation are slightly less than the ones predicted by Aboudi.

Figs. 5.4 and 5.5 show the response of symmetric angle-ply laminates to uniaxial loading. Results are presented for $[+30/-30]_S$ and $[+45/-45]_S$ laminates. In both cases the predictions from the present method are in excellent agreement with results from Aboudi [53]. However, for the $[+45/-45]_S$ laminate the theoretical predictions show a deviation from the experimentally observed results of Pipes, Kaminski and Pagano [80].

5.1.2 Response of E-Glass/Epoxy Laminates

Fig. 5.6 presents the shear stress–strain response of E-glass/epoxy lamina. The approximated shear stress–strain response attributed to Lifshitz was obtained by Aboudi [53] by integrating the following expression for the axial tangent shear modulus $G_{T_{12}}$ of the lamina, reported by Lifshitz [82]:

$$G_{12_T} = 6 - 692\bar{\varepsilon}_{12} + 32672\bar{\varepsilon}_{12}^2 - 539248\bar{\varepsilon}_{12}^3 \tag{5.1}$$

Also shown in Fig. 5.6 is the shear stress–strain response of the lamina as modelled by Aboudi's Method of Cells and by the present material modelling procedure. The assumed properties of E-glass fibers and epoxy matrix are given in Table 5.2, and are consistent with the properties used by Aboudi [53]. As can be seen from Fig. 5.6, the results from the two analytical modelling procedures are in excellent agreement with each other and with the derived experimental results.

Figs. 5.7 and 5.8 show the response of $[+30/-30]_S$ and $[+41/-41]_S$ laminates when subjected to uniaxial tension. The curves representing the experimental results of Lifshitz [82] are actually he upper and lower bounds of the experimentally observed results. The response of the $[+41/-41]_S$ laminate shows significant nonlinearity. The agreement between the analytical predictions and the experimental results is very good.

5.1.3 Response of Graphite/Polyimide Laminae

Fig. 5.9 shows the response of graphite/polyimide off-axis coupons. Experimental results were presented by Pindera and Herakovich [83]. Results from Aboudi's Method of Cells and the present material modelling procedure are also presented, and are seen to be in excellent agreement with each other. The agreement between analytical predictions and experimental data is fair. The properties of graphite fibers and polyimide matrix used in the analytical predictions are given in Table 5.3.

5.2 Off-Axis Strength of Composite Laminae

Off-axis strengths of various types of fiber-reinforced composite laminae were predicted by Aboudi [52], using the Method of Cells. Failure of the composite lamina was predicted by using micro-failure criteria for the fiber and matrix phases. The lamina was subjected to off-axis loading, and stresses within the various subcells of the unit cell representing the lamina were monitored. A maximum stress failure criterion was applied to the constituent phases, to define the failure of the lamina. Aboudi's analytical results were in good agreement with experimental results.

In this section, predictions of off-axis strength from the present method will be compared with the results from Aboudi's work [52]. It was assumed by Aboudi that an off-axis lamina loaded in uniaxial tension can fail in one of the following three modes: Fiber fracture, Matrix Shearing, and Matrix Cracking in transverse tension. The micro-failure criteria determining these modes of failure have already been presented in Chapter Two .

5.2.1 Strength of Boron/Epoxy Lamina

Fig. 5.10 shows the off-axis strength of a boron/epoxy lamina with variation in fiber orientation angle. Results are presented for analytical predictions from Aboudi's [52] Method of Cells and the present modelling procedure. Experimental results from Pipes and Cole [77] are also presented. The elastic properties and strengths of boron fibers and epoxy matrix are given in Table 5.4. It is seen that the predictions of both

analytical procedures agree very well over the full range of fiber orientation angle. The present model not only predicts the off-axis strength with good accuracy, but also successfully delineates the transition from fiber fracture mode to matrix shearing mode and matrix tensile failure mode. The agreement between analytical predictions and experimental results is quite good.

5.2.2 Additional Examples of Off-Axis Strength of Laminae

The off-axis strength of a graphite/polyimide lamina is shown in Fig. 5.11. The experimental results were reported by Pindera and Herakovich [83]. The properties of graphite fibers and epoxy matrix used in the analyses are listed in Table 5.5. Excellent agreement between the results from Aboudi [52] and the present method is seen again.

Fig. 5.12 shows the off-axis strength of AS/3501 graphite/epoxy lamina with variation in fiber orientation angle. The experimental results were reported by Tsai and Hahn [6]. The properties of graphite fibers and epoxy matrix, used in the micromechanics based predictions of strength are listed in Table 5.6.

The off-axis strength of a Kevlar/epoxy lamina is shown in Fig. 5.13. The experimental results are from the work of Pindera et al. [84], and the elastic properties of Kevlar fibers and epoxy matrix used in micromechanical analysis are given in Table 5.7.

Fig. 5.14 shows the off-axis strength of E-glass/epoxy lamina; the properties of E-glass fibers and epoxy matrix are presented in Table 5.8. It is interesting to note that in this case the zone in which the fiber fracture mode occurs is very small; the transition from fiber failure mode to the matrix shear failure mode occurs at about an off-axis angle $\theta \approx 1^0$. This is due to the relatively low shear strength of the epoxy matrix.

Fig. 5.15 shows the variation in off-axis strength of a boron/aluminum lamina as the fiber orientation angle changes. The experimental results presented are from the work of Becker et al. [86]. The elastic properties of the boron fibers and aluminum matrix are given in Table 5.8. The three distinct modes of failure, and the transitions from one mode

of failure to another are clearly visible in Fig. 5.15. The region in which the fiber fracture mode governs is significantly large compared to the previously presented examples, because the shear strength of the aluminum matrix is relatively high.

5.3 Initial Yield Surfaces of Metal Matrix Composites

Metal matrix composites are increasingly being used in aerospace applications, where the use of stiff fibers, such as boron or graphite in a light–weight metallic matrix like aluminum, results in a light, yet stiff and strong material. The fibers in a composite can usually be assumed to be elastic; and the yielding observed in metal matrix composites is attributable to yielding of the metallic matrix. It is of interest to see if the present micro–model can predict the initiation of yielding in metal matrix composites; therefore in this section, results for initial yield surfaces of metal matrix composites under different stress states are presented.

Results for initial yield surfaces of fiber–reinforced laminae and laminates under different stress states were presented by Dvorak et al. [40], using the finite element method to model a representative volume element of a composite lamina. Pindera and Aboudi [87] used the Method of Cells to obtain the initial yield surfaces of the composite laminae studied by Dvorak et al. In this section the results of Dvorak et al. and Pindera and Aboudi are compared to results obtained from the proposed modelling procedure.

To predict the onset of yielding in matrix material, the von Mises yield criterion is used, which is described as follows. Yielding is supposed to occur if the following condition is satisfied,

$$F(\sigma_{ij}) \geq 0 \qquad\qquad (5.2)$$

where

$$F(\sigma_{ij}) = \sqrt{3}\ \tau_e\ -\ \sigma_Y^{(m)} \qquad\qquad (5.3)$$

94

τ_e is the square root of the second invariant of the deviator stress tensor s_{ij} and $\sigma_Y^{(m)}$ is the yield stress of the matrix in uniaxial tension. Eq. (5.3) may be expressed in terms of stresses as

$$F(\sigma_{ij}) = \left\{ \frac{1}{2} \left[(\sigma_{11} - \sigma_{22})^2 + (\sigma_{11} - \sigma_{33})^2 + (\sigma_{22} - \sigma_{33})^2 \right] + 3 \left(\sigma_{12}^2 + \sigma_{13}^2 + \sigma_{23}^2 \right) \right\}^{\frac{1}{2}} - \sigma_Y^{(m)} \qquad (5.4)$$

The above yield criterion is applied to both matrix subcells, m_A and m_B, and yielding is assumed to occur if the above yield criterion is satisfied in either of the two matrix subcells. Specifically stated, yielding is assumed if either of the two following criteria are satisfied,

$$F(\sigma_{ij}^{(m_A)}) \geq 0$$

$$F(\sigma_{ij}^{(m_B)}) \geq 0$$

(5.5a–b)

Fig. 5.16 shows the initial yield surface of a boron/aluminum lamina in $(\bar{\sigma}_{22}, \bar{\sigma}_{33})$ stress space; the stresses are normalized with respect to the yield stress of the matrix $\sigma_Y^{(m)}$. The properties of the boron fibers and aluminum matrix are given in Table 5.9. The results from the present material model show very good agreement with results from Aboudi's Method of Cells and the finite elements based results of Dvorak et al. However, the yield surface predicted by Aboudi's Method of Cells contains corners which are not predicted by the detailed finite element approach.

Fig. 5.17 shows the initial yield surface of the same boron/aluminum lamina in $(\bar{\sigma}_{11}, \bar{\sigma}_{22})$ stress space. The results from the present material model agree very well with the results from Aboudi's Method of Cells and the finite element based results.

95

Fig. 5.18 shows the initial yield surface of the boron/aluminum lamina in $(\bar{\sigma}_{11}, \bar{\sigma}_{22} = \bar{\sigma}_{33})$ stress space. It is noticed that in the vicinity of the hydrostatic stress state, both the Method of Cells and the present micro–model perform poorly and predict yield stress states which are significantly higher than the finite element based results. However, the results from both models improve as the imposed stress states move away from the hydrostatic stress state.

5.4 Response and Ultimate Strength of Boron/Epoxy Laminates

Petit and Waddoups [61] presented a method for modelling the nonlinear response of laminated composites in which the nonlinear stress–strain behaviour was taken into account, but no interaction between stresses was recognized. Furthermore the bimodularity of the lamina in tension and compression was taken into account. The laminate response was derived by assembling the laminae comprising the laminate within the framework of Classical Laminated Plate Theory. A maximum strain criterion was employed to detect the onset of failure in a lamina, and the lamina was then gradually unloaded by giving it a negative tangent stiffness in the loading direction being considered (longitudinal, transverse or shear).

5.4.1 Micromechanical Modelling of Boron/Epoxy Lamina

The response of the boron/epoxy lamina as reported by Petit and Waddoups [61] is now modelled using the proposed material model. Fig. 5.19 shows the shear response of the boron/epoxy lamina; also shown is the response predicted by the material model. The properties of the constituent boron fibers and epoxy matrix were inferred from lamina responses under various loading conditions (Fig. 5.19–5.23), and are listed in Table 5.10. It should be mentioned that the properties of the fibers and the epoxy matrix are to be used in the "Modified Ramberg–Osgood Relations" (Eqs. (2.23–2.29), Chapter 2). Modified Ramberg–Osgood relations are used in order to eliminate excessive nonlinearity in transverse direction loading which is not observed in experimental results.

96

5.4.2 Failure Criteria and Damage Modelling

The employed micro–failure criteria for the various failure modes have already been presented in chapter 2 (Section 2.6). The procedure for modelling the effects of damage have also been described in chapter 2 (Section 2.7). The stiffness reduction factors used in the analysis are listed in Table 5.10.

Results for the response of boron/epoxy laminates are presented in the next section.

5.4.3 Response of Boron/Epoxy Laminates in Tension

Figs. 5.24–5.27 show the responses of boron/epoxy laminates subjected to uniaxial tension. Results are presented for the proposed material model, analytical predictions, and the experimental results of Petit and Waddoups [61].

Fig 5.24 shows the response of a $[0/90]_S$ laminate in tension. The response predicted by the proposed material model agrees well with the experimental results and the analytical results of Petit and Waddoups. According to the present analysis procedure, tensile matrix cracking in the transverse direction takes place in the 90° plies at the stress level of 70 ksi, resulting in some loss of stiffness and load redistribution. This is consistent with the analytical results of Petit and Waddoups. The ultimate failure of the laminate occurred by fiber fracture in the 0° plies at 92 ksi; the ultimate strain being 0.6 %. Experimental results indicate failure at 100 ksi, with a strain at failure of 0.71%.

The response of a $[+30/-30]_S$ laminate is shown in Fig. 5.25. The present procedure indicates some nonlinearity in response, but not as much as is indicated by Petit and Waddoups. Also, shear failure of the matrix in the plies is predicted, whereas the analysis conducted by Petit and Waddoups indicated the mode of failure to be compressive failure of the matrix in the transverse direction.

Fig. 5.26 presents the response of a $[+60/-60]_S$ laminate. The indicated mode of failure from the present analysis is tensile matrix cracking in the transverse direction at 15

ksi, the ultimate strain being 0.6%. The experimental results indicate an ultimate stress of 17.5 ksi, and strain at failure of about 0.8%.

Fig. 5.27 shows the behaviour of a $[+45/-45/90_3]_S$ laminate. The indicated mode of failure is tensile matrix cracking of the 90° plies in the transverse direction, followed by matrix shearing failure in the 45° plies. The predicted ultimate strength is 22 ksi at the ultimate strain of 0.44%. The experimental results indicated the mode of failure to be matrix cracking of the 90° plies in the transverse direction at 20 ksi.

5.4.4 Response of Boron/Epoxy Laminates in Compression

The response of a $[0/90]_S$ laminate in compression is shown in Fig. 5.28. The present analysis predicted failure of the 0° plies by compressive failure of the matrix in the transverse direction at about 230 ksi. This resulted in a slight loss of stiffness, but did not cause complete loss of load carrying capacity. The laminate finally failed at 275 ksi by micro–buckling of the 0° plies. Experimental results indicate that the laminate failed at 255 ksi by failure of the 0^0 plies.

Compression response of a $[+20/-20]_S$ laminate is shown in Fig. 5.29. No nonlinearity is observed in the laminate response, and the analytical procedure predicts laminate failure by tensile failure of the plies in the transverse direction at 117 ksi. The $[+30/-30]_S$ laminate fails in a similar fashion (Fig. 5.30). The shapes of the analytical response curves and the experimental results show very good agreement. Experimental results indicated the failure stress to be 44 ksi, as compared to 50 ksi predicted by Petit and Waddoups, and 60 ksi predicted by the present material model and micromechanical failure criteria.

The predicted response and experimental results for a $[+60/-60]_S$ laminate are given in Fig. 5.31. A significant amount of nonlinearity is observable in the response. The present analysis indicates failure at 41 ksi due to compressive failure of the matrix in the transverse direction, which is consistent with the experimental results and the analytical predictions of Petit and Waddoups. The present analysis, however, predicts an elastic–

98

plastic type response, whereas the analytical results of Petit and Waddoups show a more gradual transition to the point when the laminate loses all stiffness.

5.4.5 Comments on Modelling of Laminate Stress-Strain Response

Modelling the response of fiber–reinforced laminated composites up to the point of ultimate strength is a challenging problem, made difficult by a number of factors. The experimentally observed ultimate strengths of unidirectional composites show a considerable amount of scatter, indicating that statistically reliable properties should be used in the analysis to obtain better statistical correlation between the predicted laminate strength and the experimentally observed values. Keeping in view the observed scatter in the experimentally obtained ultimate strength values of laminated composites, the true measure of the performance of an analysis procedure for predicting the strength of composites would be its better statistical correlation with experimental results.

The choice of the failure criteria adopted in the analysis procedure can significantly affect the quality and accuracy of the predicted results. The failure mechanisms exhibited by composites are many and quite complex. Although numerous failure criteria have been proposed for strength prediction of composites, much work needs to be done in this area to develop criteria which are accurate and take into account the complex mechanisms of failure associated with composites.

Finally, the manner in which the effects of damage are accounted for in the laminate analysis also significantly affects the predicted response of the laminate. Damage mechanisms tend to dissipate the stored strain energy in the laminate and result in stiffness degradation. The manner in which the stiffness degradation and strain energy dissipation is modelled would influence the calculated response of the laminate. The field of *Damage Mechanics* aims to provide damage evolution laws and framework for incorporating the effects of damage. It is felt that incorporating a suitable damage theory would result in improved analytical predictions of laminate response.

	E (GPa)	ν	τ_0 (MPa)	a	b	n
Boron	413.6	0.15	——	——	——	——
Epoxy	5.2	0.35	157.6	0	5.74	4

Table 5.1   *Elastic properties of boron fibers and epoxy matrix, along with Ramberg-Osgood parameters for epoxy matrix.   Fiber volume fraction = 0.5*
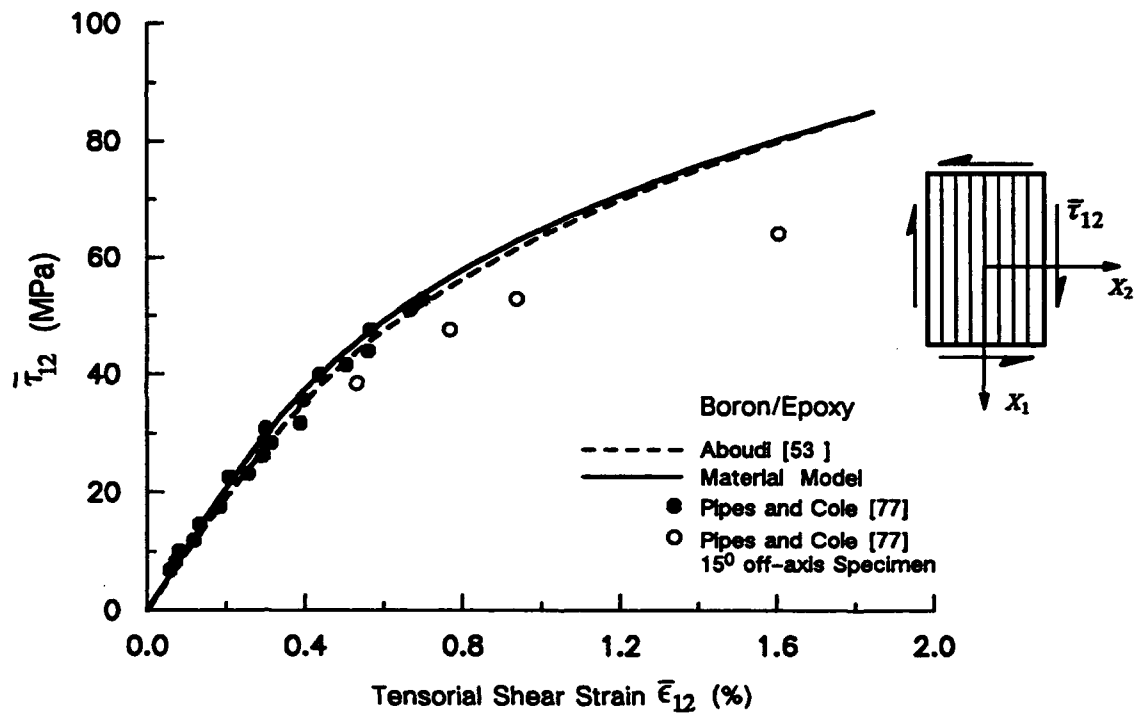
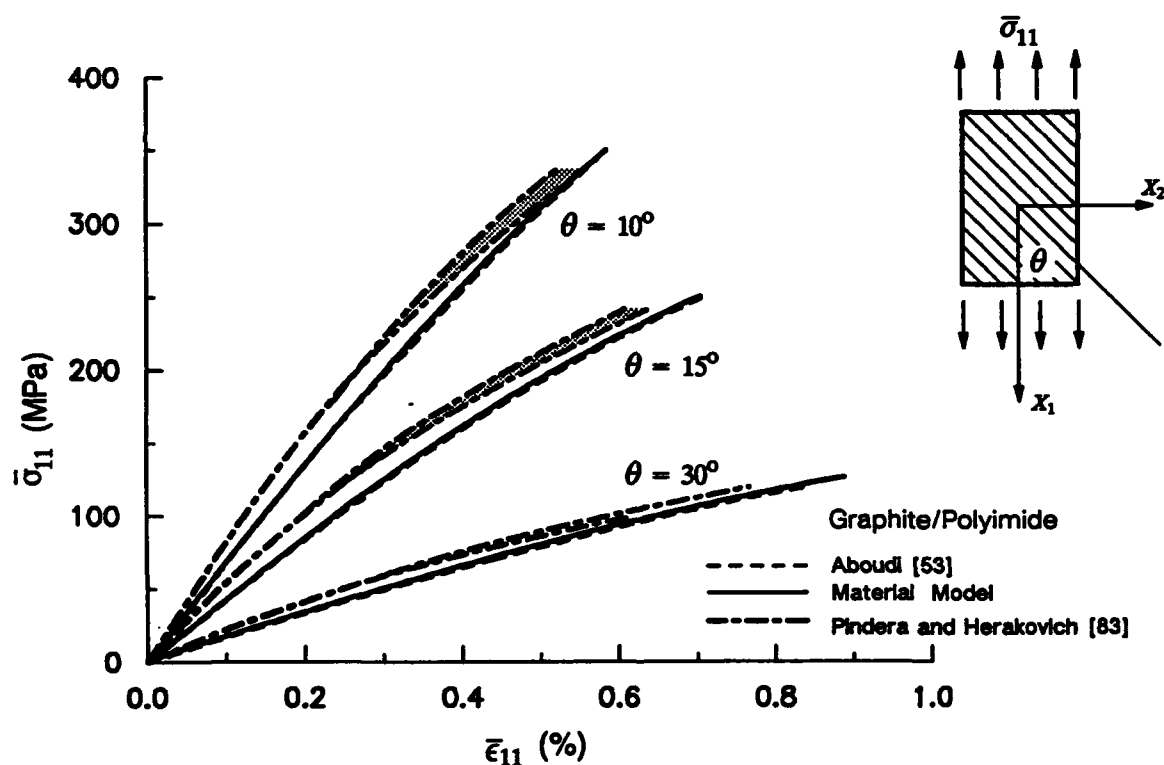**Fig. 5.1** *Shear stress-strain response of boron/epoxy lamina as predicted by Aboudi's Method of Cells and the proposed material model, along with experimental results of Pipes and Cole.*
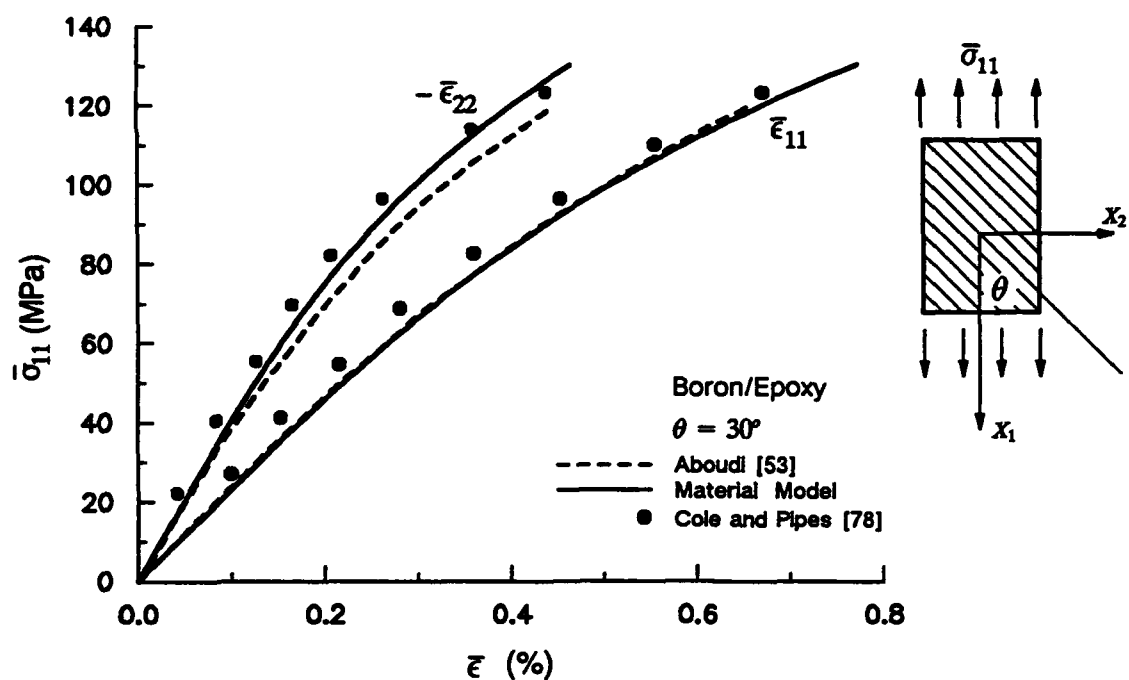
Fig. 5.2 *Uniaxial stress–strain response of 30° off-axis boron/epoxy lamina as predicted by Aboudi's Method of Cells and the proposed material model, along with experimental results of Cole and Pipes.*
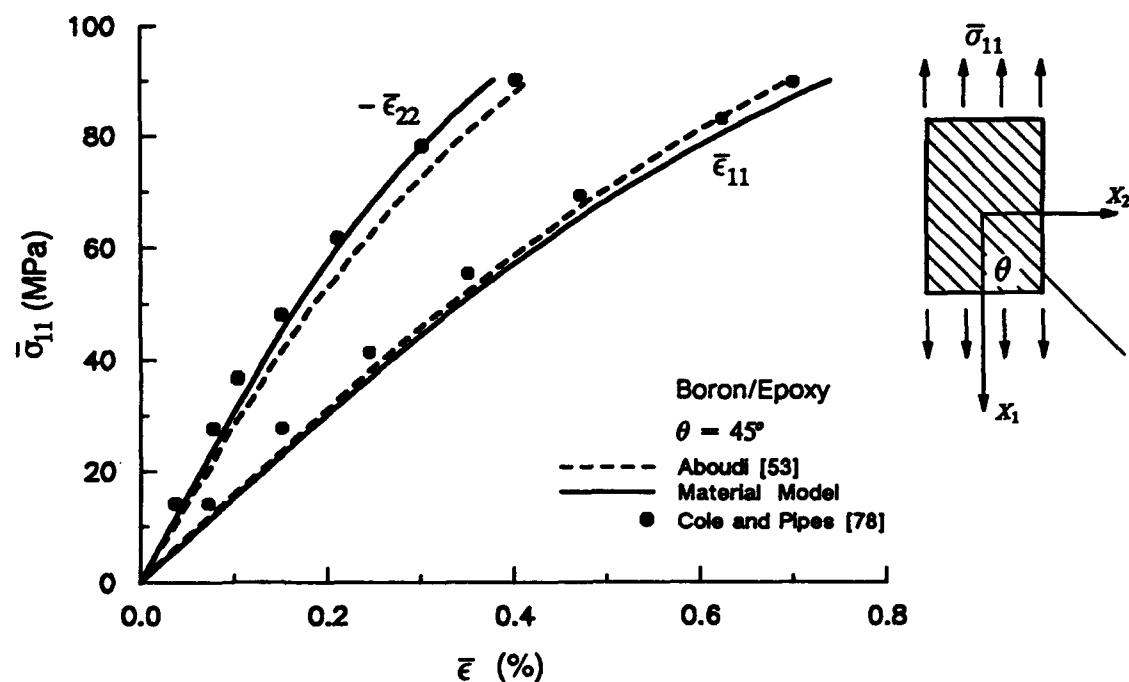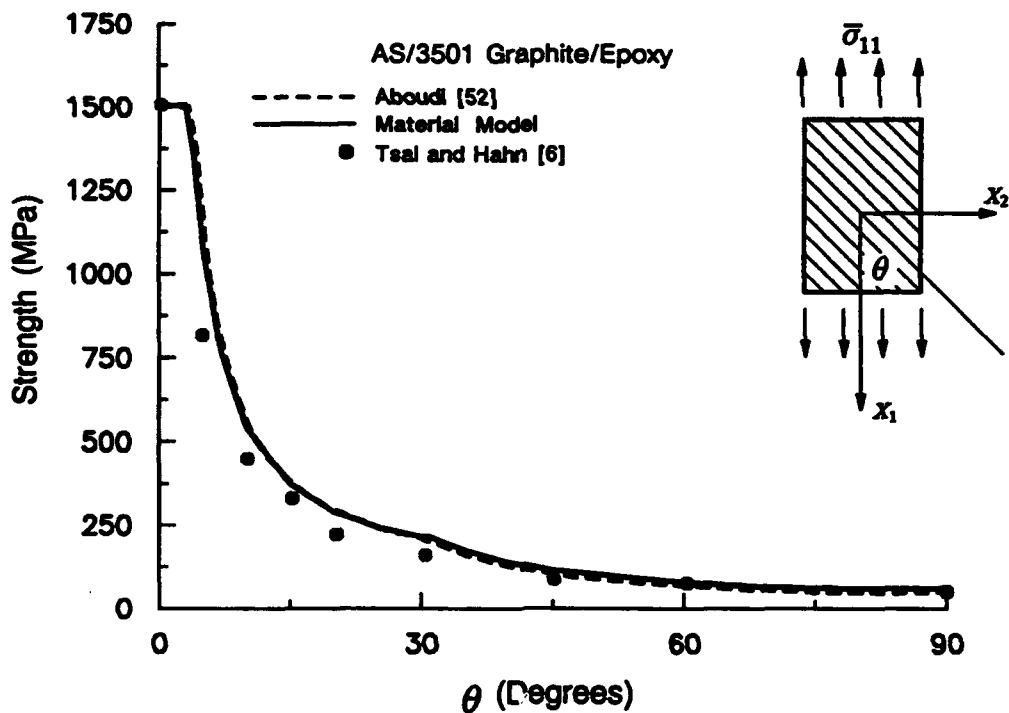

Fig. 5.3 *Uniaxial stress–strain response of 45° off-axis boron/epoxy lamina as predicted by Aboudi's Method of Cells and the proposed material model, along with experimental results of Cole and Pipes.*
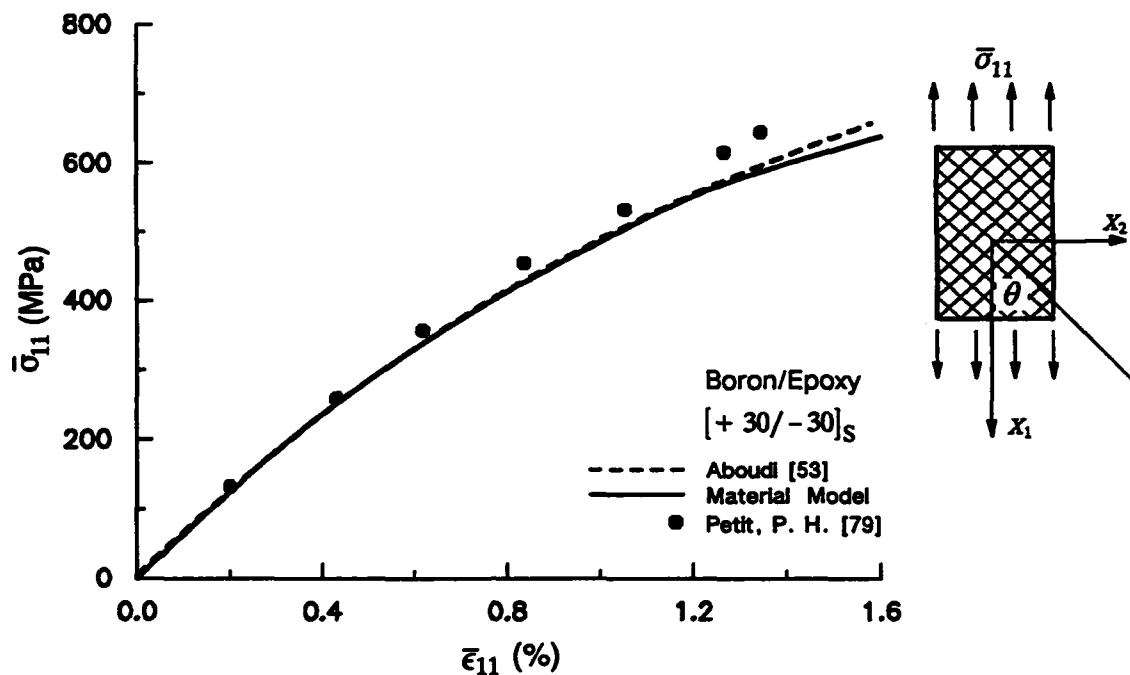
Fig. 5.4 *Uniaxial Stress–Strain Response of [+30/–30]$_S$ Boron/epoxy laminate, as predicted by Aboudi's method of cells and the proposed material model, along with experimental results of Petit.*
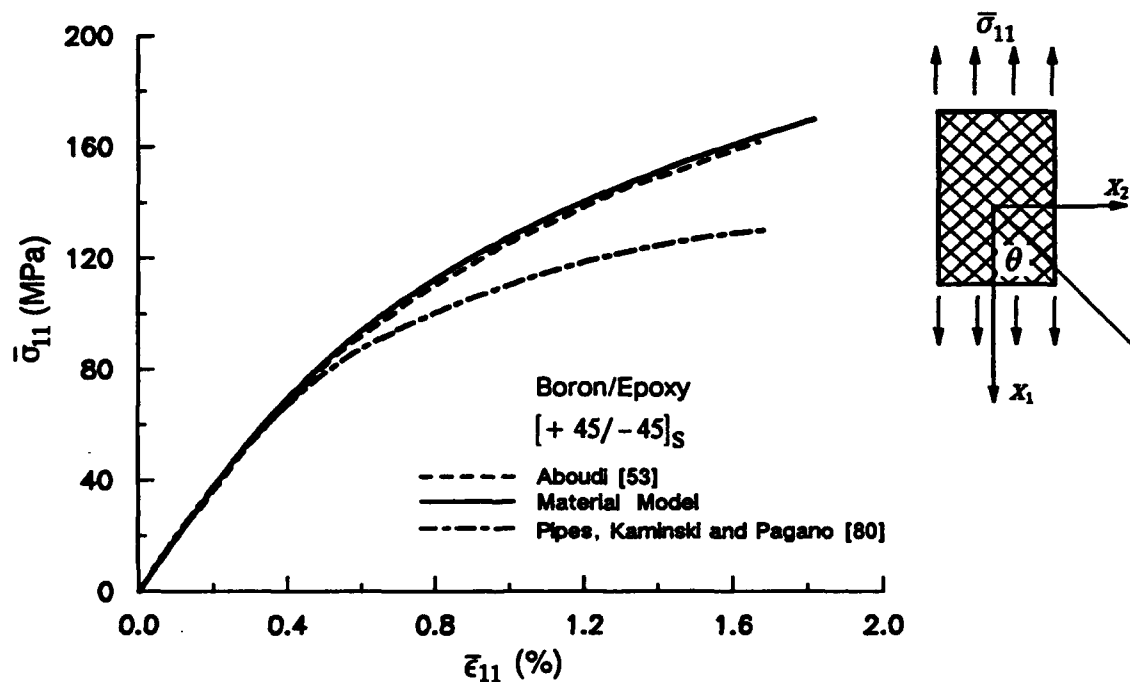
Fig. 5.5 *Uniaxial Stress–Strain Response of [+45/–45]$_S$ Boron/epoxy laminate, as predicted by Aboudi's method of cells and the proposed material model, along with experimental results of Pipes, Kaminski and Pagano.*

	E (GPa)	ν	τ_0 (MPa)	a	b	n
E–Glass	73	0.22	——	——	——	——
Epoxy	6	0.35	106	0	3.33	3

Table 5.2 *Elastic properties of E–glass fibers and epoxy matrix, along with Ramberg-Osgood parameters for epoxy matrix. Fiber volume fraction = 0.64*
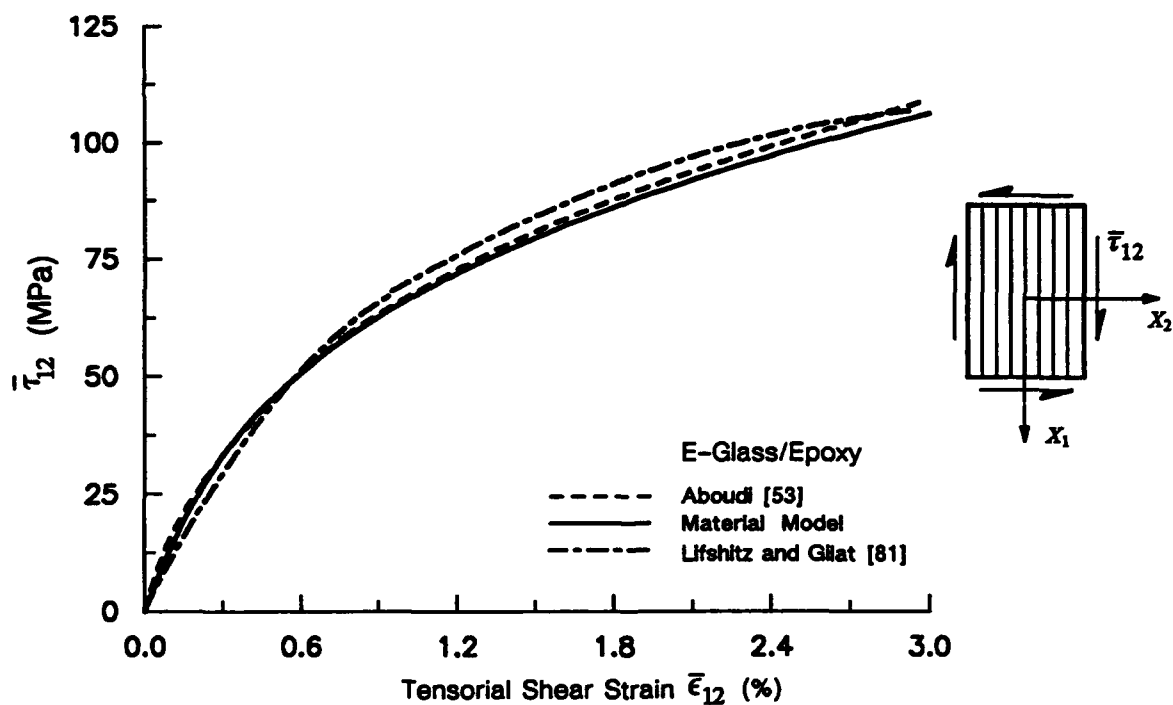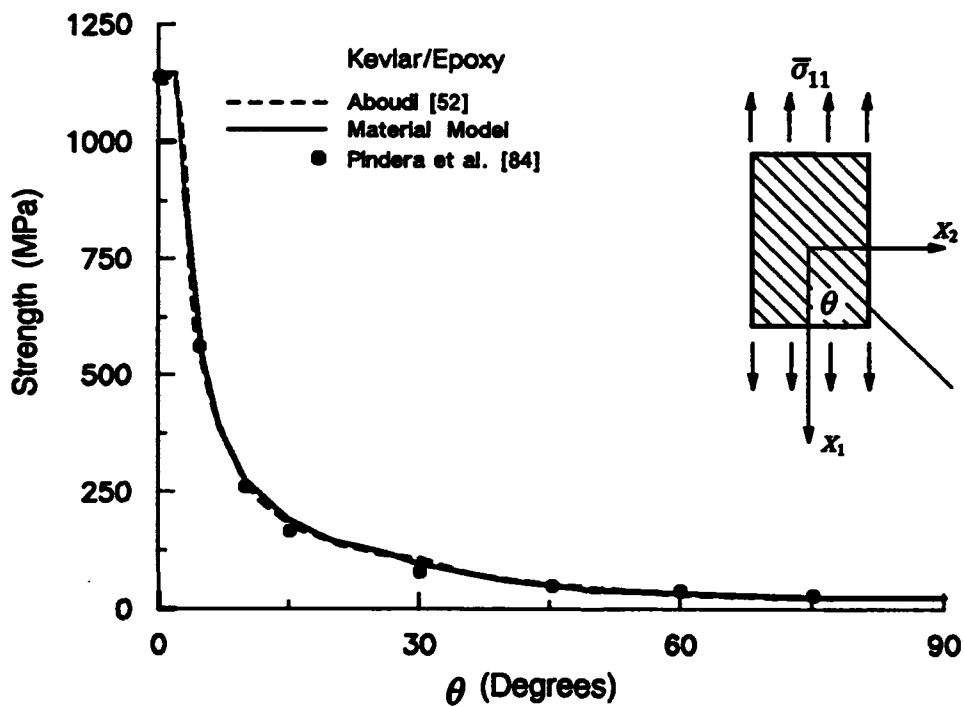

Fig. 5.6 *Shear stress–strain response of E–glass/epoxy lamina as predicted by Aboudi's Method of Cells and the proposed material model, along with derived experimental results of Lifshitz and Gilat.*
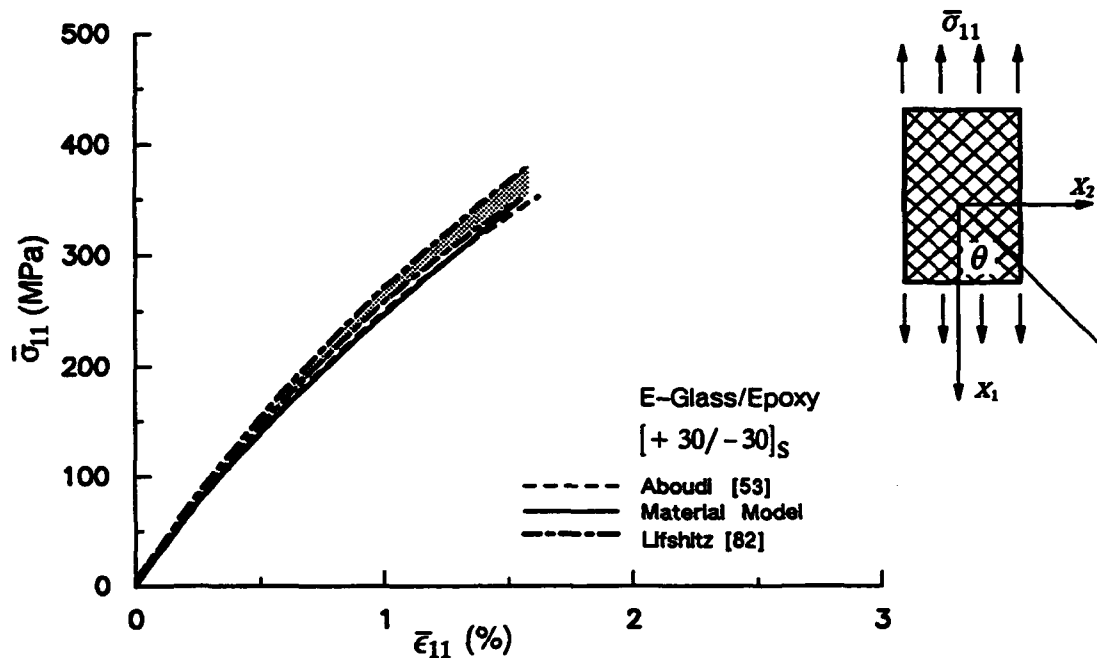
Fig. 5.7 *Uniaxial stress–strain response of [+30/–30]$_S$ E–glass/epoxy laminate, as predicted by Aboudi's Method of Cells and the proposed material model, along with experimental results of Lifshitz.*
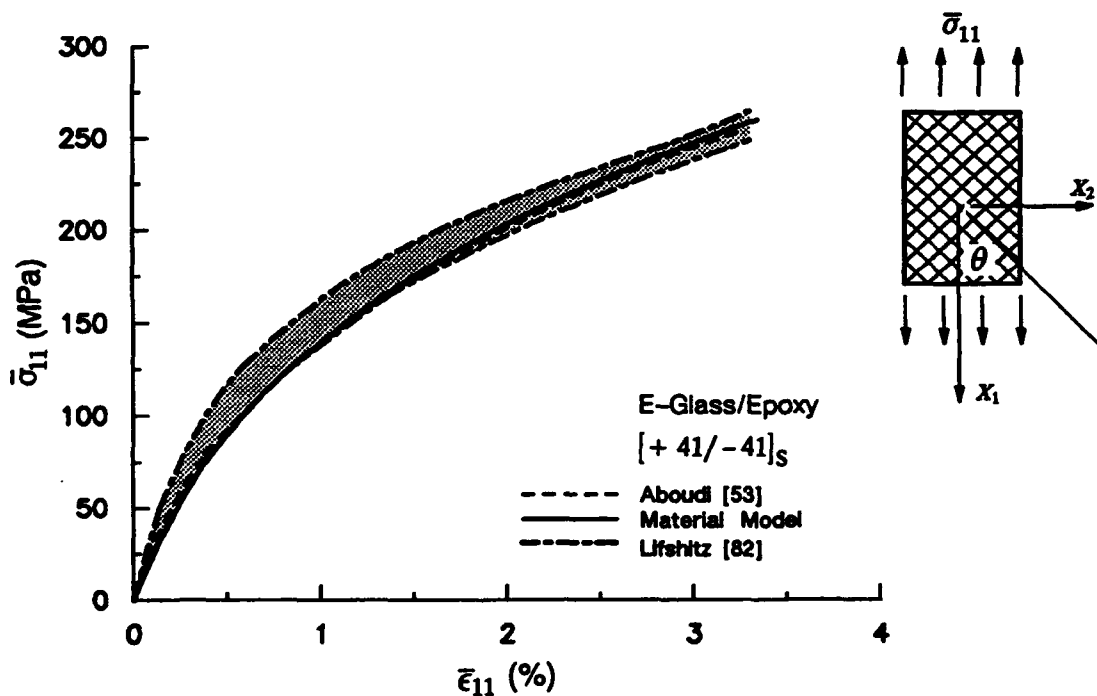
Fig. 5.8 *Uniaxial stress–strain response of [+45/–45]$_S$ E–glass/epoxy laminate, as predicted by Aboudi's Method of Cells and the proposed material model, along with experimental results of Lifshitz.*

	E_1 (GPa)	ν_1	E_2 (GPa)	ν_{23}	G_{12} (GPa)	τ_0 (MPa)	a	b	n
Graphite	222	0.33	29.5	0.73	24.1	—	—	—	—
Polyimide	3.1	0.39	3.1	0.39	1.1	186.9	0	5.61	4

Table 5.3 *Elastic properties of graphite fibers and polyimide matrix, along with Ramberg-Osgood parameters for polyimide matrix. Fiber volume fraction = 0.61*

Fig. 5.9 *Uniaxial stress-strain response of 10°,15° and 30° off-axis graphite/polyimide laminae, as predicted by Aboudi's Method of Cells and the proposed material model, along with experimental results of Pindera and Herakovich.*

	E (GPa)	ν	$X_t^{(f)}$ (MPa)	$X_t^{(m)}$ (MPa)	$S^{(m)}$ (MPa)
Boron	400	0.2	2566	—	—
Epoxy	5.2	0.35	—	93	87

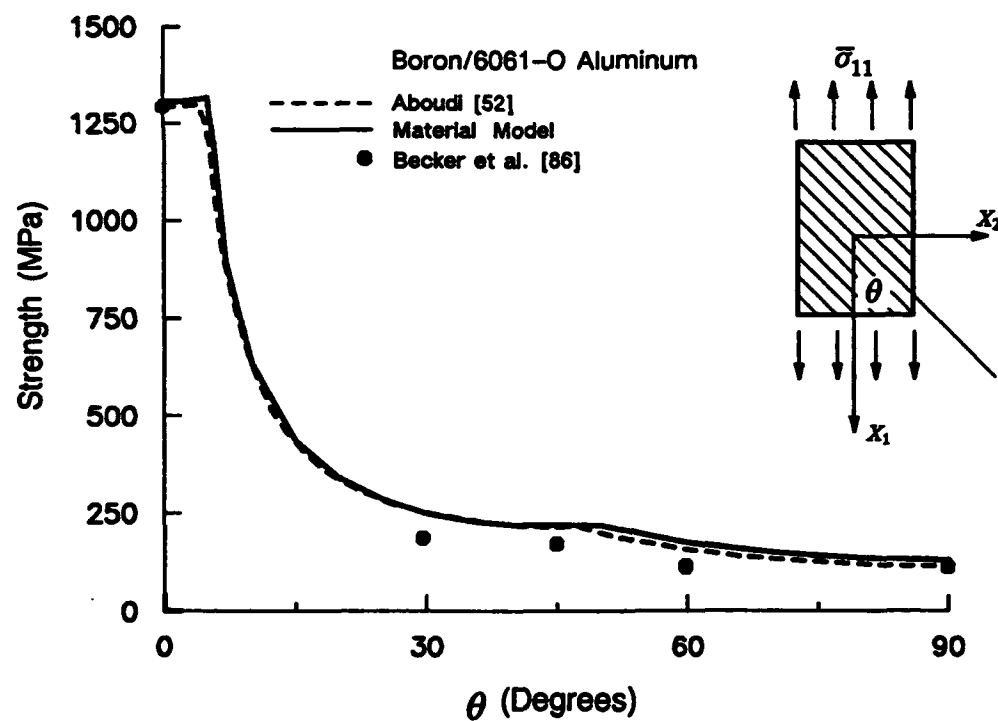**Table 5.4** *Elastic properties and strengths of boron fibers and epoxy matrix. Fiber volume fraction = 0.5*
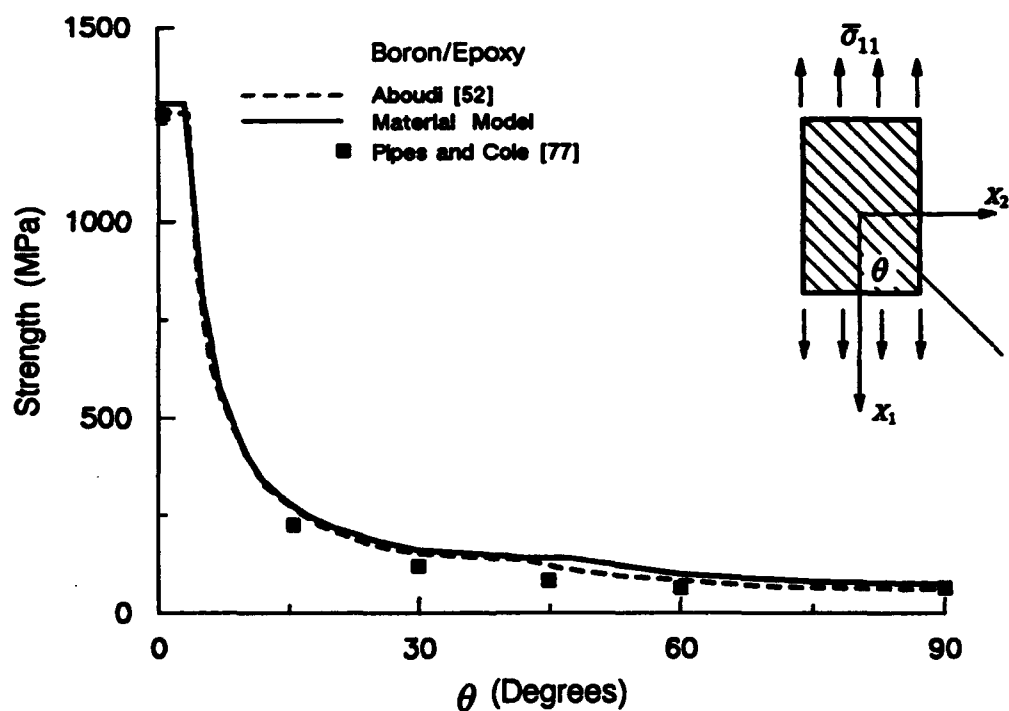
Fig. 5.10 *Off-axis strength of boron/epoxy lamina as predicted by Aboudi's Method of Cells and the proposed material model, along with the experimental results of Pipes and Cole.*

106

	E_1 (GPa)	ν_1	E_2 (GPa)	ν_{23}	G_{12} (GPa)	$X_t^{(f)}$ (MPa)	$Y_t^{(m)}$ (MPa)	$S^{(m)}$ (MPa)
Graphite	222	0.33	29.5	0.73	24.1	2517	—	—
Polyimide	3.1	0.39	3.1	0.39	1.1	—	69	71

Table 5.5 *Elastic properties and strengths of graphite fibers and polyimide matrix.*
Fiber volume fraction = 0.61
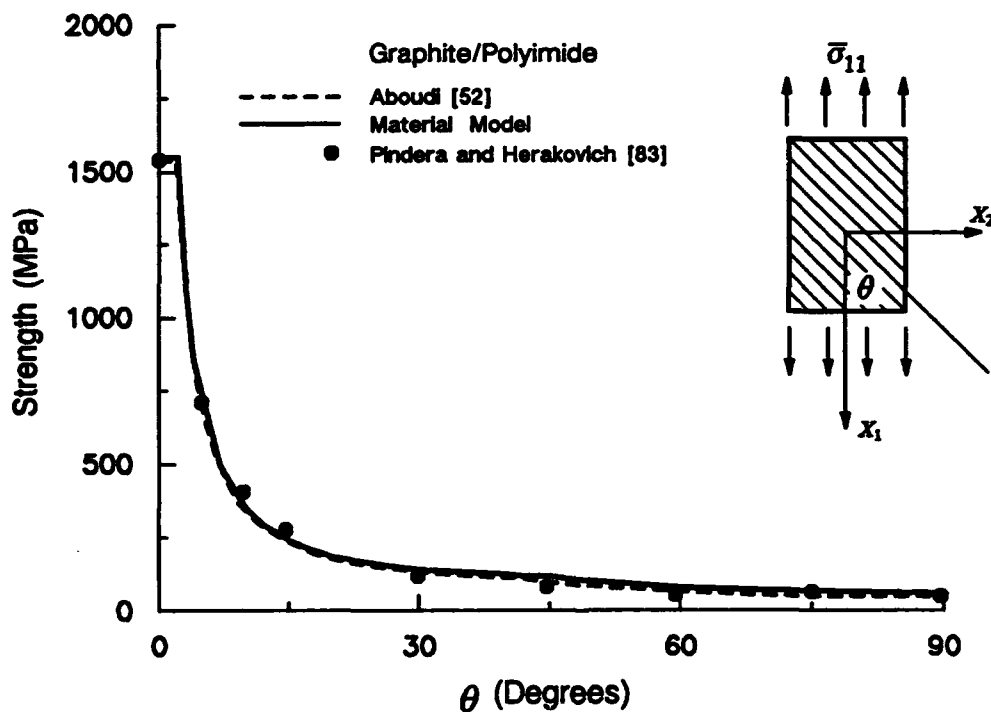
Fig. 5.11 *Off-axis strength of graphite/polyimide lamina as predicted by Aboudi's Method of Cells and the proposed material model, along with the experimental results of Pindera and Herakovich.*

	E_1 (GPa)	ν_1	E_2 (GPa)	ν_{23}	G_{12} (GPa)	$X_t^{(f)}$ (MPa)	$Y_t^{(m)}$ (MPa)	$S^{(m)}$ (MPa)
AS/3501 Graphite	213.7	0.2	13.8	0.25	13.8	2250	—	—
Epoxy	3.45	0.35	3.45	0.35	1.3	—	62.9	108

Table 5.6 *Elastic properties and strengths of graphite fibers and epoxy matrix. Fiber volume fraction = 0.66*

Fig. 5.12 *Off-axis strength of AS/3501 graphite/epoxy lamina as predicted by Aboudi's Method of Cells and the proposed material model, along with the experimental results of Tsai and Hahn.*

	E_1 (GPa)	ν_1	E_2 (GPa)	ν_{23}	G_{12} (GPa)	$X_t^{(f)}$ (MPa)	$Y_t^{(m)}$ (MPa)	$S^{(m)}$ (MPa)
Kevlar	124.1	0.35	4.1	0.35	2.9	2031	—	—
Epoxy	3.45	0.35	3.45	0.35	1.3	—	62.9	108

Table 5.7 *Elastic properties and strengths of Kevlar fibers and epoxy matrix. Fiber volume fraction = 0.55*

Fig. 5.13 *Off-axis strength of Kevlar/epoxy lamina as predicted by Aboudi's Method of Cells and the proposed material model, along with the experimental results of Pindera et al.*

109

	E (GPa)	ν	$X_t^{(f)}$ (MPa)	$Y_t^{(m)}$ (MPa)	$S^{(m)}$ (MPa)
E–Glass	73	0.22	1990	—	—
Epoxy	3.45	0.35	—	40.4	45.5

Table 5.8 *Elastic properties and strengths of E–glass fibers and epoxy matrix. Fiber volume fraction = 0.60*
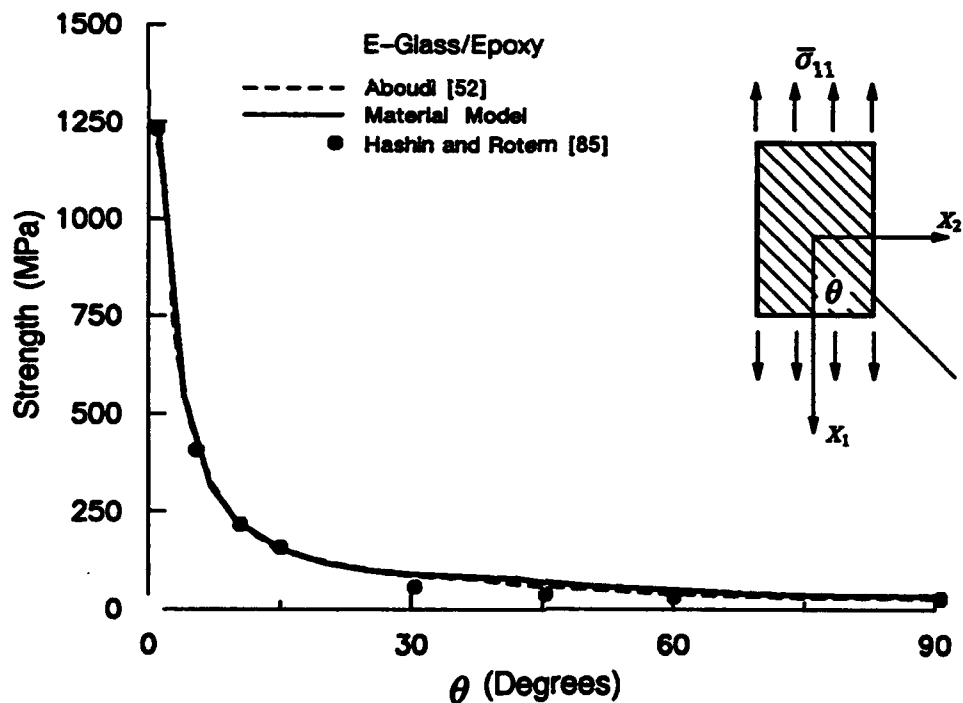
Fig. 5.14 *Off–axis strength of E–glass/epoxy lamina as predicted by Aboudi's Method of Cells and the proposed material model, along with the experimental results of Hashin and Rotem.*

110

	E (GPa)	ν	$X_t^{(f)}$ (MPa)	$Y_t^{(m)}$ (MPa)	$S^{(m)}$ (MPa)
Boron	400	0.2	2313.8	—	—
6061-O Aluminum	72.5	0.33	—	155.6	167.4

Table 5.8 *Elastic properties and strengths of boron fibers and 6061-O aluminum matrix. Fiber volume fraction = 0.46*

Fig. 5.15 *Off-axis strength of boron/6061-O aluminum lamina as predicted by Aboudi's Method of Cells and the proposed material model, along with the experimental results of Becker et al.*

	E (GPa)	ν	$\sigma_Y^{(m)}$ (MPa)
Boron	413.7	0.21	———
Aluminum	72.5	0.33	262

Table 5.9 *Elastic properties of boron fibers and aluminum matrix for calculation of initial yield surfaces of composite lamina. Fiber volume fraction = 0.3*

Boron/Aluminum

- - - - - - F. E. Results, Dvorak et al. [39]
— — — — Pindera and Aboudi [87]
———— Material Model
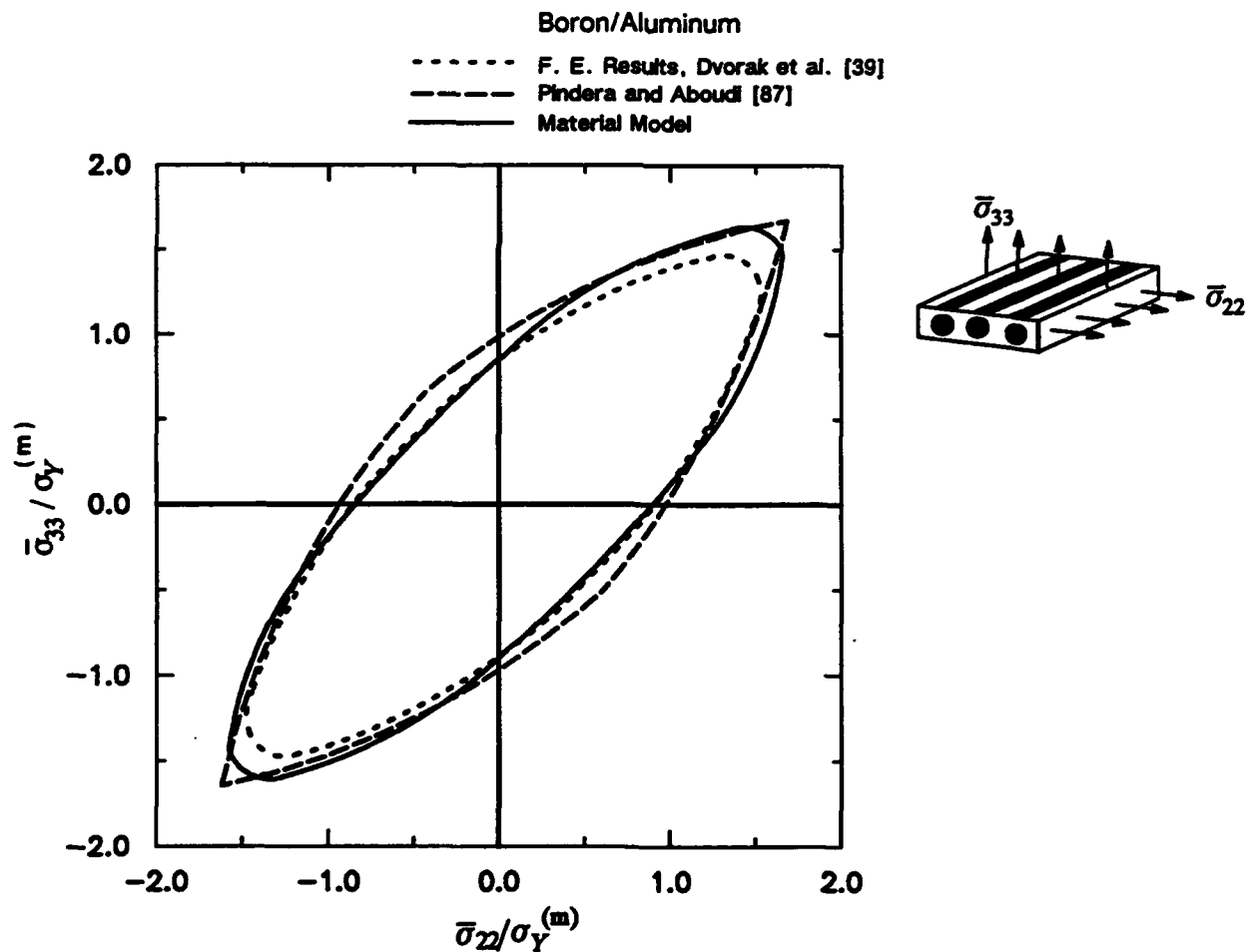
Fig. 5.16 *Initial yield surface of a boron/aluminum composite as predicted by Aboudi's Method of Cells and the proposed material model, along with finite element based results of Dvorak et al.*
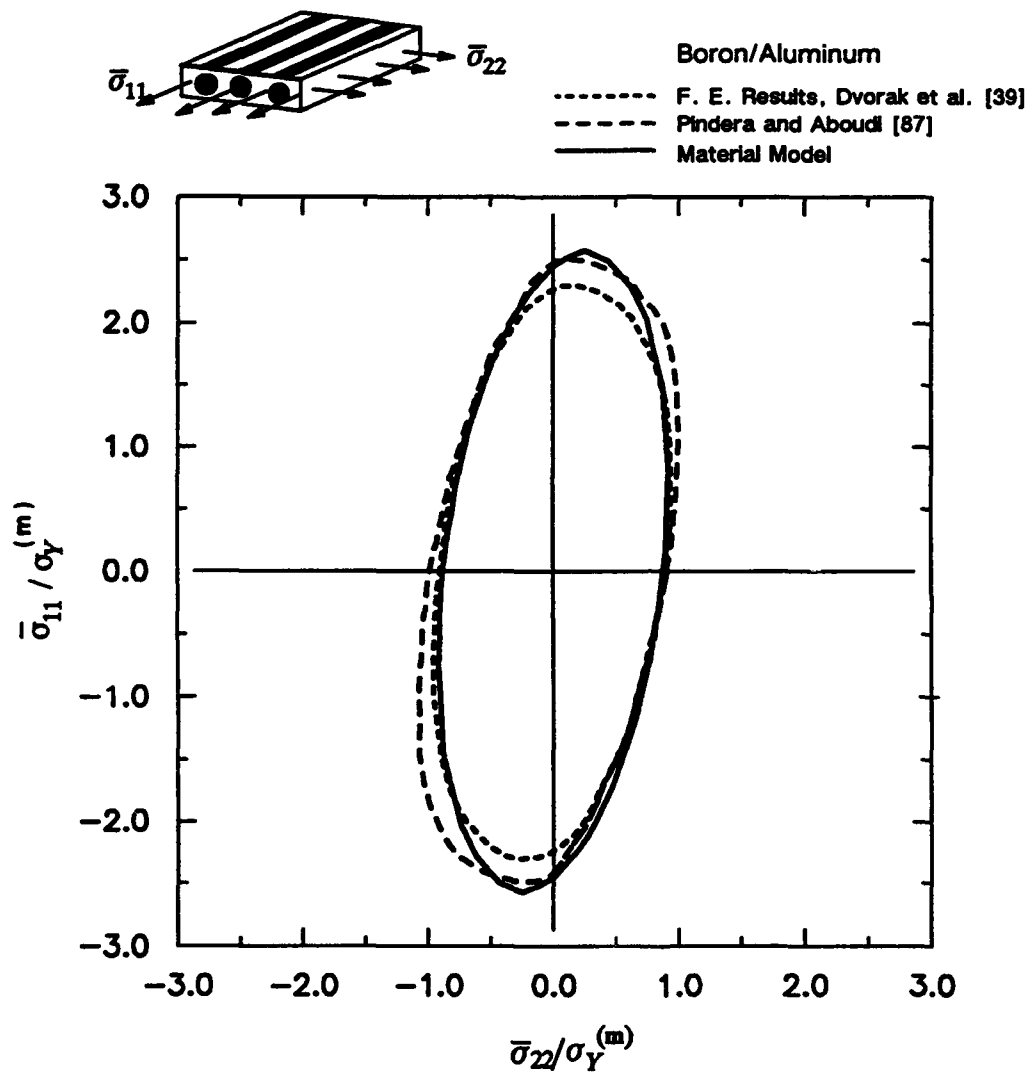
Fig. 5.17 *Initial yield surface of a boron/aluminum composite as predicted by Aboudi's Method of Cells and the proposed material model, along with finite element based results of Dvorak et al.*
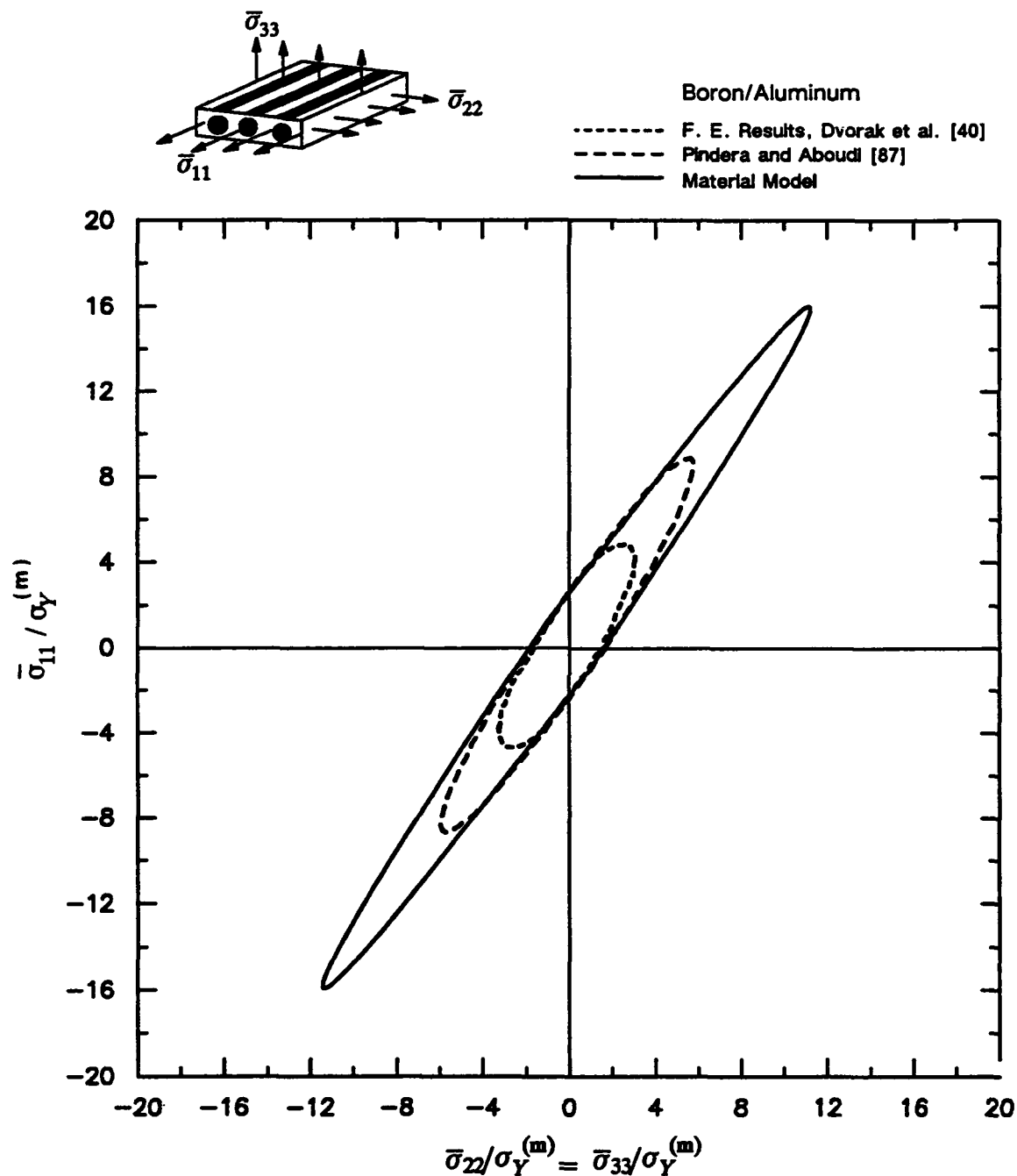
Fig. 5.18 *Initial yield surface of a boron/aluminum composite as predicted by Aboudi's Method of Cells and the proposed material model, along with finite element based results of Dvorak et al.*

114

	E (Ksi)	ν	τ_0 (Ksi)	a	b	n	$X_t^{(f)}$ (Ksi)	$Y_t^{(m)}$ (Ksi)	$Y_c^{(m)}$ (Ksi)	$S^{(m)}$ (Ksi)
Boron	59985	0.25	—	—	—	—	372	—	—	—
Epoxy	1000	0.35	13.5	0	1.0	4	—	15.5	50.0	21.0

Table 5.10 *Elastic properties of boron fibers and epoxy matrix, along with Ramberg–Osgood parameters for epoxy matrix used in modelling response of boron/epoxy laminates tested by Petit and Waddoups [61]. Fiber volume fraction = 0.5*

Stiffness reduction factors $D_{f_{11}}, D_{m_{11}}, D_{m_{22}}, D_{m_{44}} = 0.001$
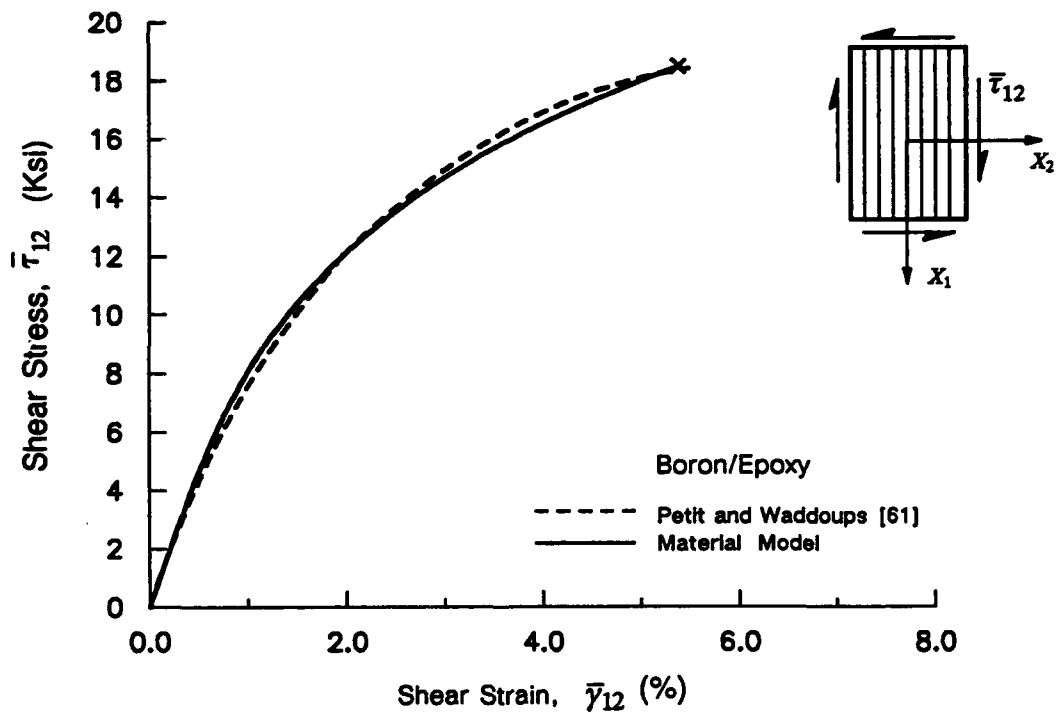
Fig. 5.19 *Shear stress–strain response of boron/epoxy lamina as modelled by the proposed material model, and by Petit and Waddoups.*
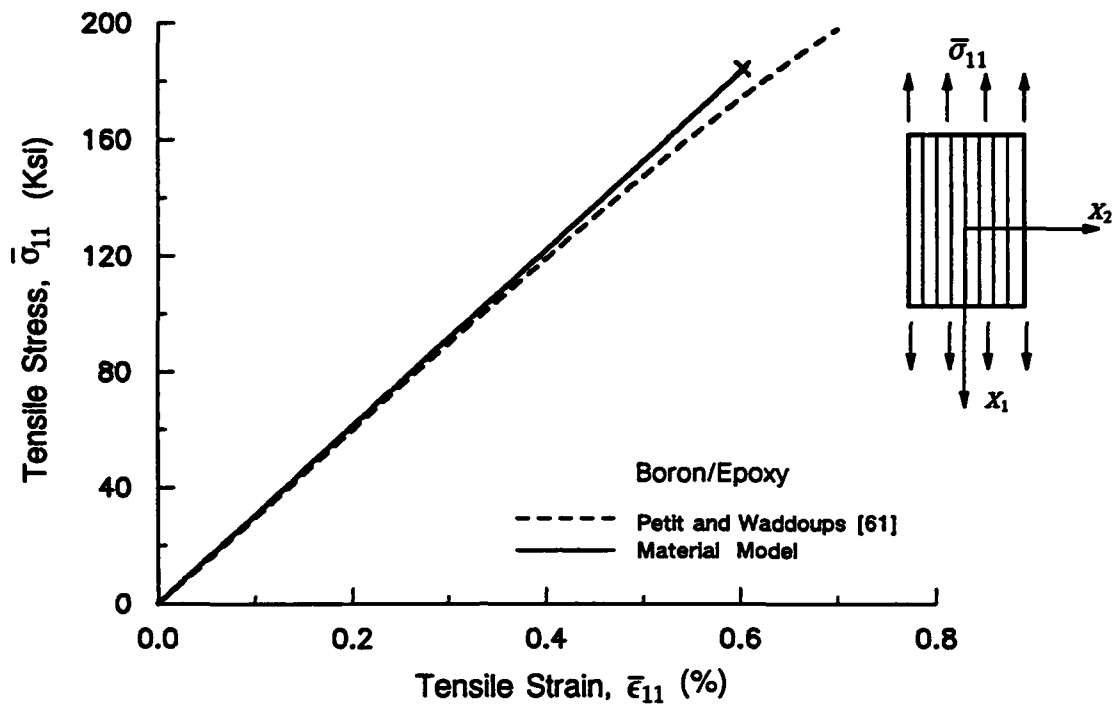
Fig. 5.20 *Response of boron/epoxy lamina in axial tension, as modelled by the material model, and by Petit and Waddoups.*
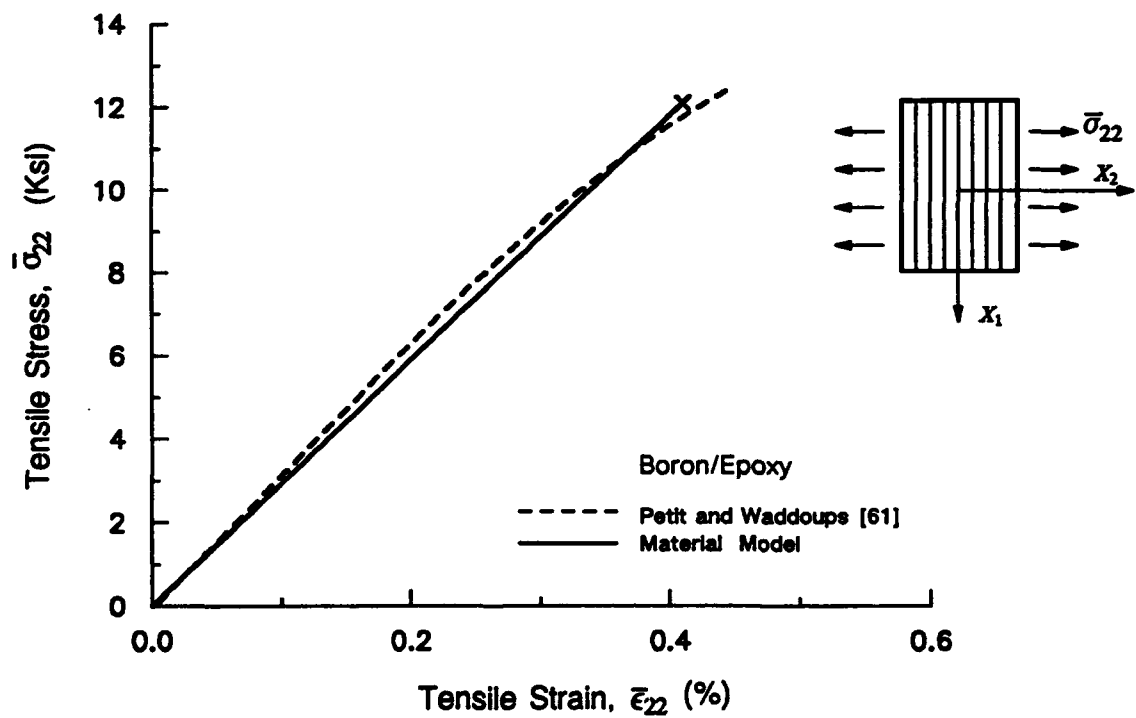
Fig. 5.21 *Response of boron/epoxy lamina in transverse tension, as modelled by the material model, and by Petit and Waddoups.*

116
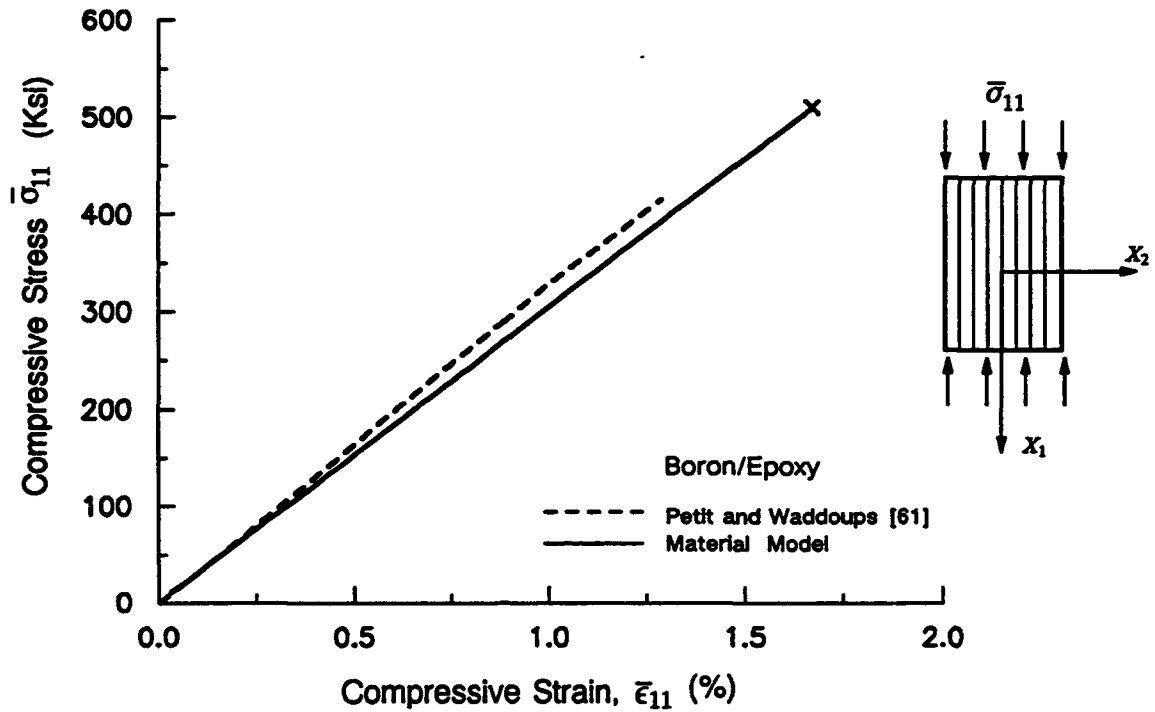
Fig. 5.22 *Response of boron/epoxy lamina in axial compression, as modelled by the material model, and by Petit and Waddoups.*
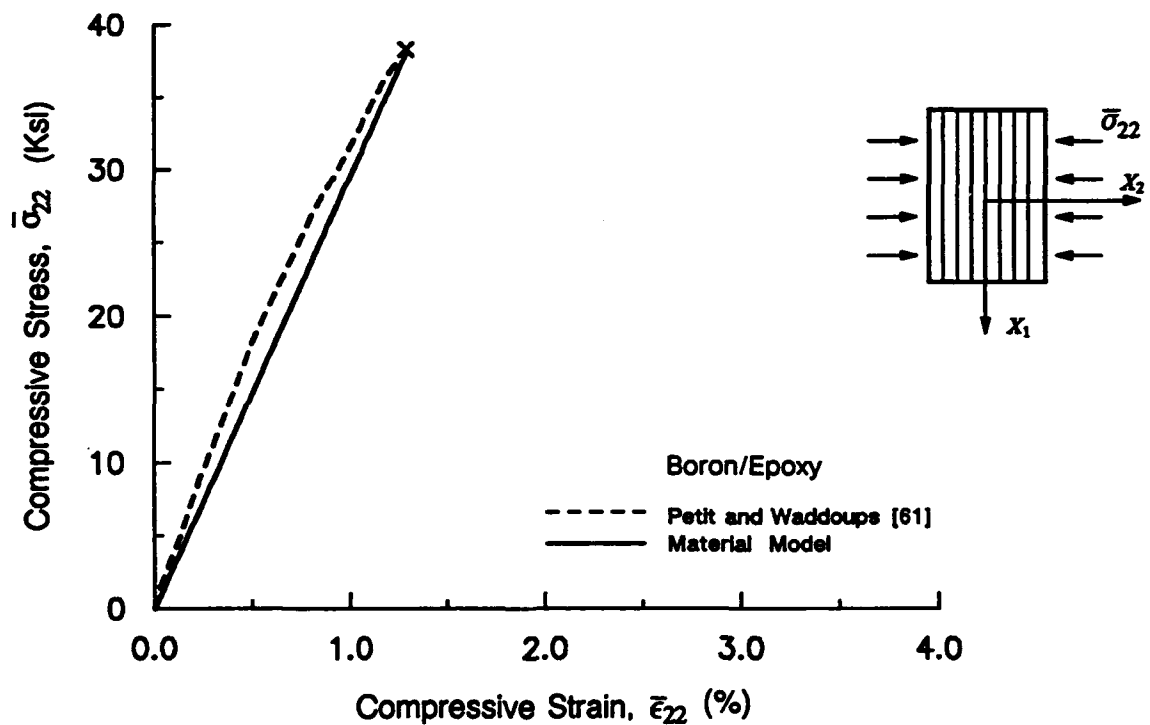
Fig. 5.23 *Response of boron/epoxy lamina in transverse compression, as modelled by the material model, and by Petit and Waddoups.*
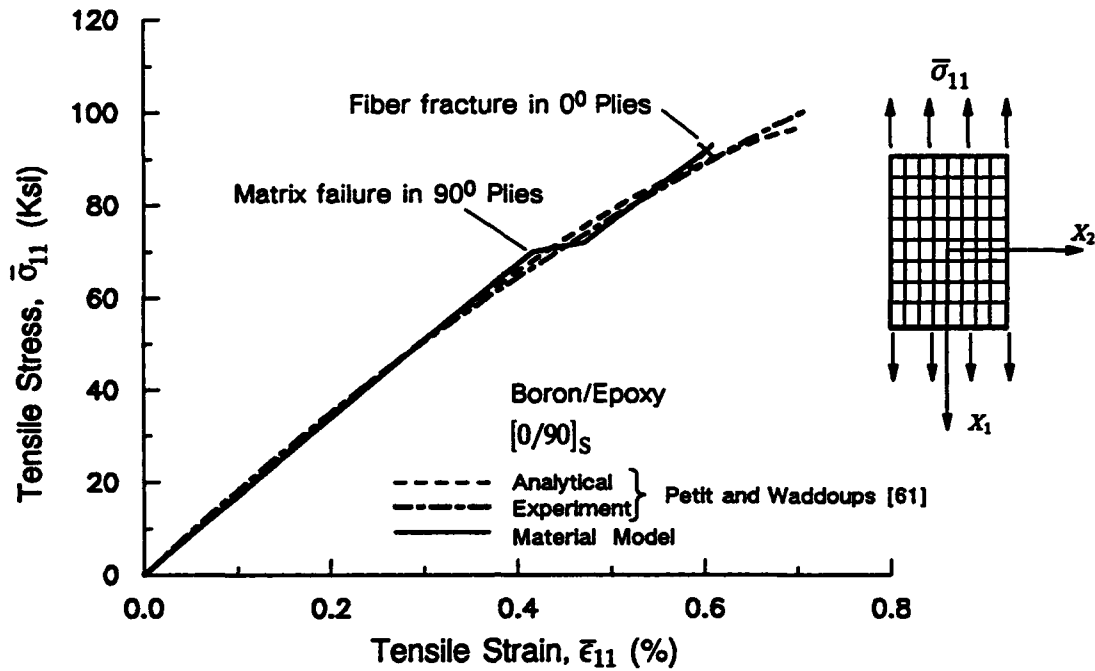
Fig. 5.24 *Response of a [0/90]$_S$ boron/epoxy laminate in uniaxial tension as predicted by the material model, along with prediction and experimental results from Petit and Waddoups.*
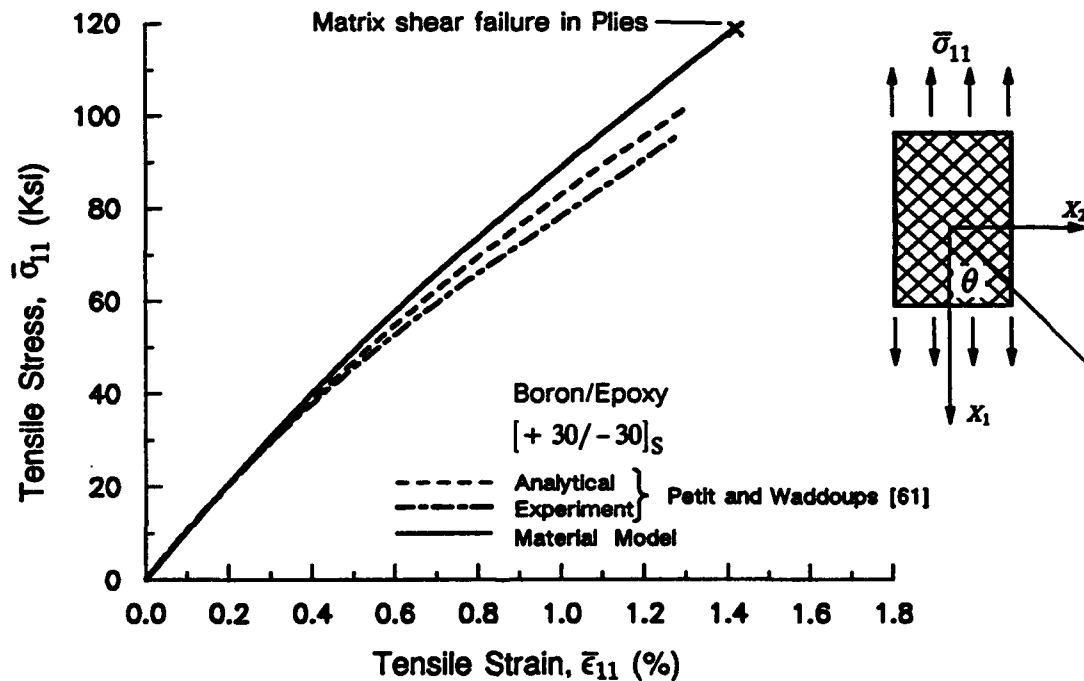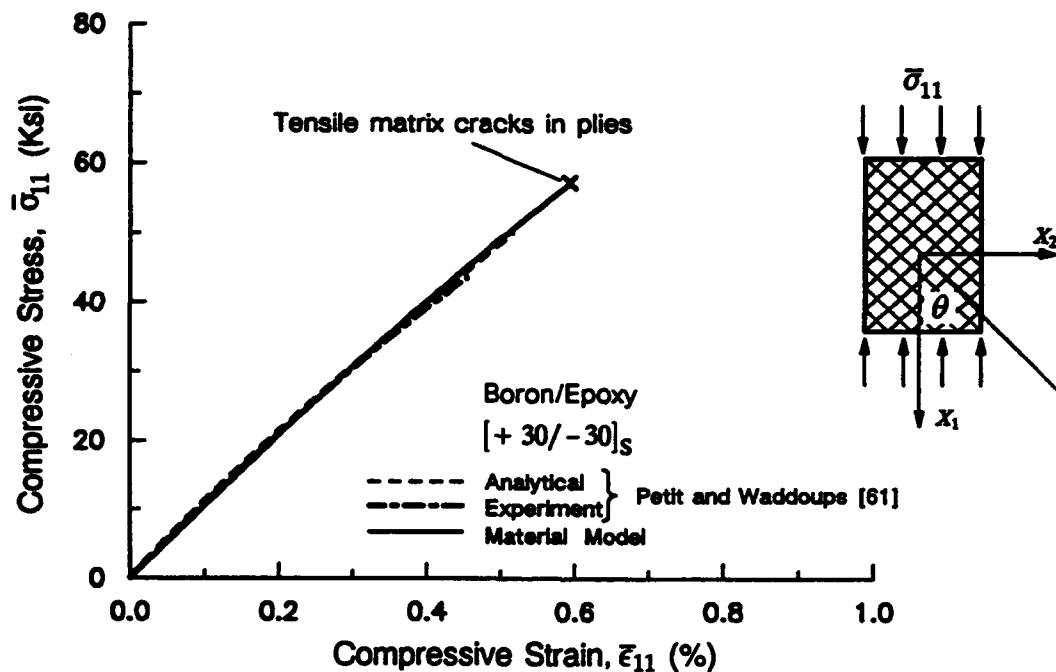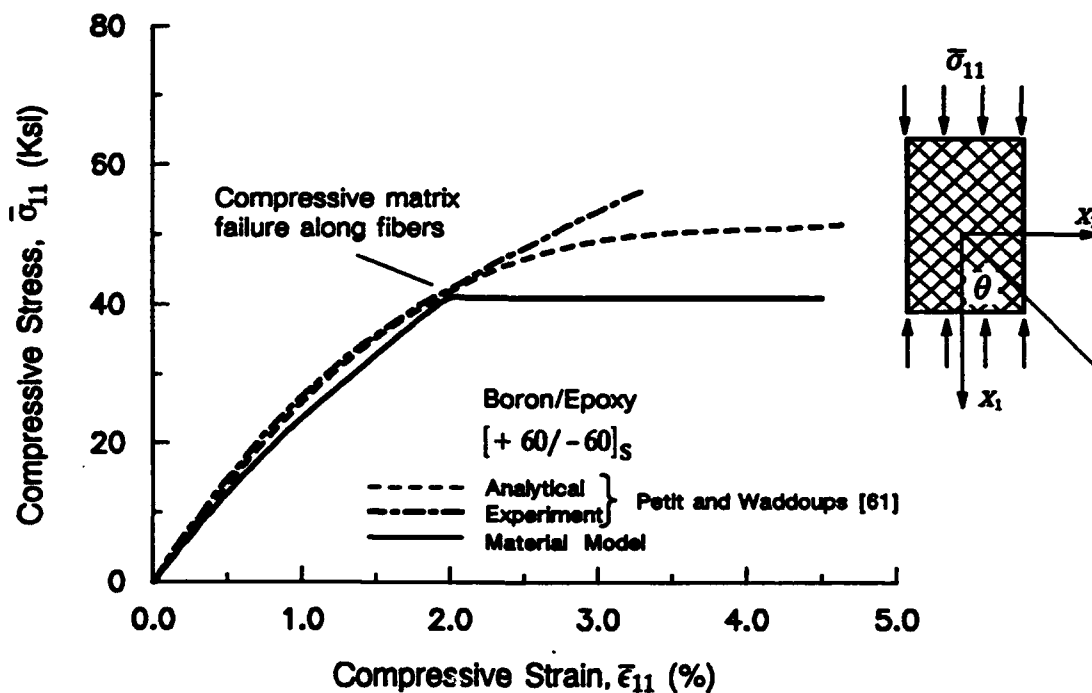

Fig. 5.25 *Response of a [+30/-30]$_S$ boron/epoxy laminate in uniaxial tension as predicted by the material model, along with prediction and experimental results from Petit and Waddoups.*

118
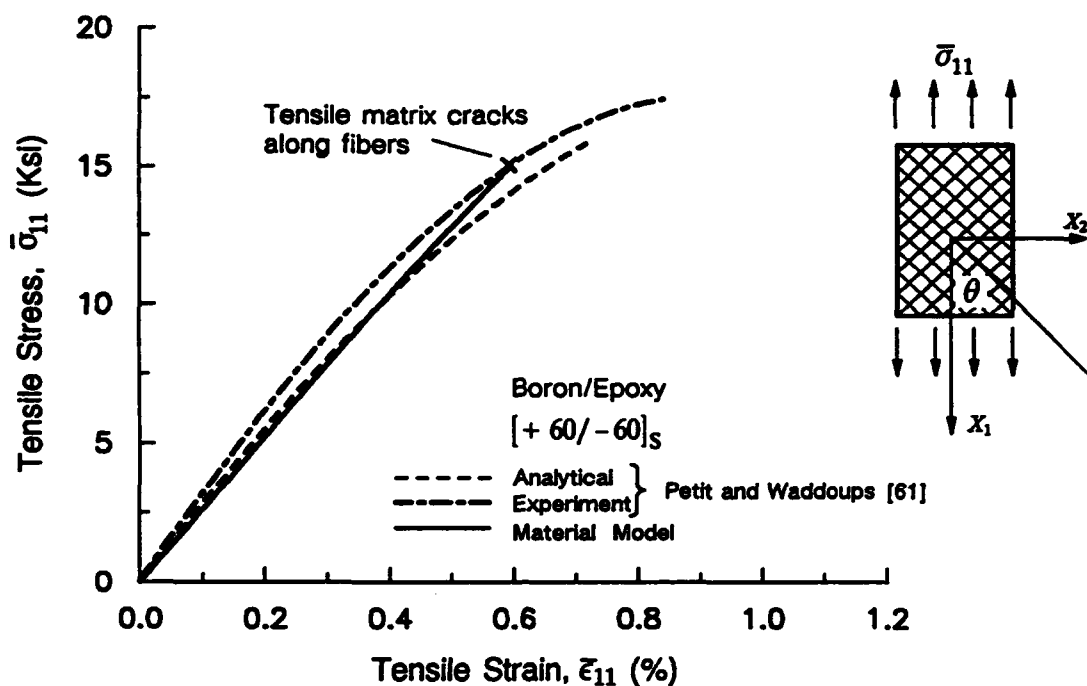
Fig. 5.26 *Response of a [+60/–60]$_S$ boron/epoxy laminate in uniaxial tension as predicted by the material model, along with prediction and experimental results from Petit and Waddoups.*
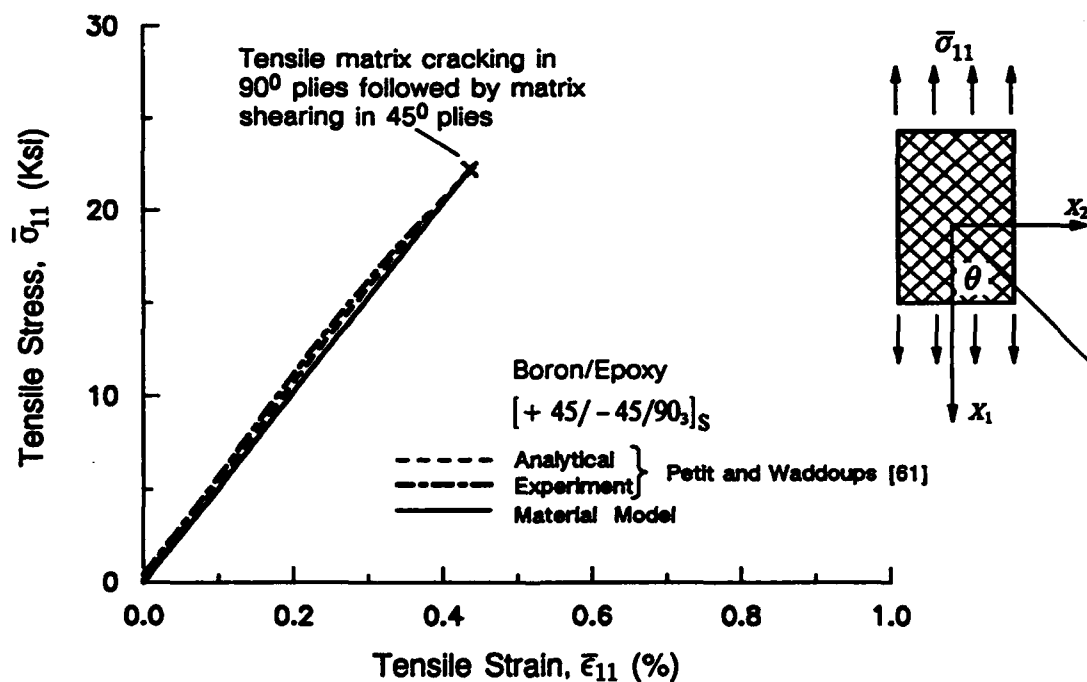
Fig. 5.27 *Response of a [+45/–45/90$_3$]$_S$ boron/epoxy laminate in uniaxial tension as predicted by the material model, along with prediction and experimental results from Petit and Waddoups.*
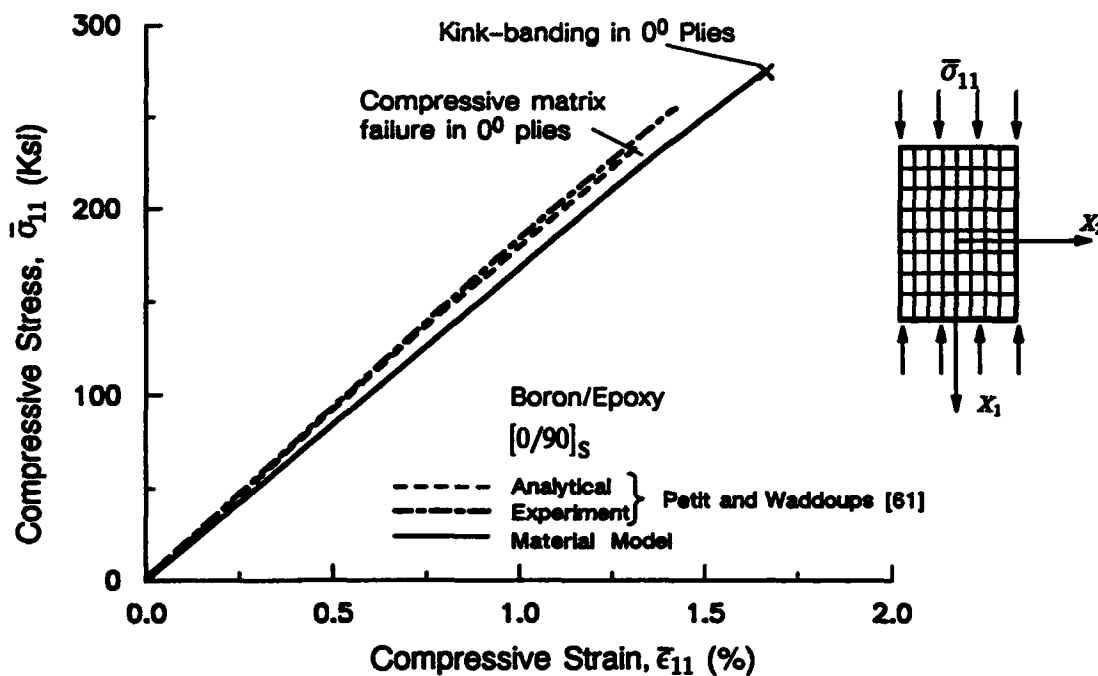
Fig. 5.28 *Response of a [0/90]$_S$ boron/epoxy laminate in uniaxial compression as predicted by the material model, along with prediction and experimental results from Petit and Waddoups.*
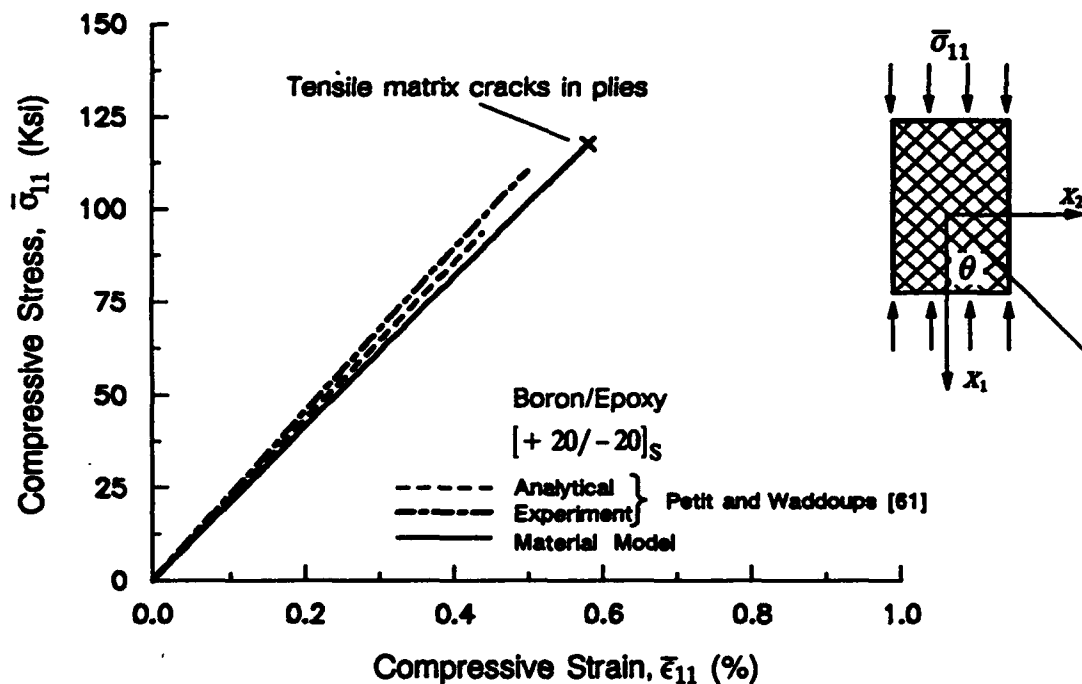
Fig. 5.29 *Response of a [+20/-20]$_S$ boron/epoxy laminate in uniaxial compression as predicted by the material model, along with prediction and experimental results from Petit and Waddoups.*

Fig. 5.30 *Response of a [+30/-30]S boron/epoxy laminate in uniaxial compression as predicted by the material model, along with prediction and experimental results from Petit and Waddoups.*

Fig. 5.31 *Response of a [+60/-60]S boron/epoxy laminate in uniaxial compression as predicted by the material model, along with prediction and experimental results from Petit and Waddoups.*

ANALYSIS OF LAMINATED STRUCTURES

The material model was incorporated in the finite element analysis package PO-LO–FINITE [96] developed at the University of Illinois. Since the material model is linked to the structural analysis program through a standard interface, a wide variety of elements in POLO–FINITE's element library are readily accessible. However, in this study only the 2–dimensional and 3–dimensional isoparametric elements were employed. A number of example problems were solved, and results are presented for:

- A thick–walled laminated cylinder in compression and in circumferential bending.

- Notched metal matrix laminates in tension.

- Bending of a simply supported plate.

- Compression of a notched laminate up to the point of failure, using micromechanics–based criteria for damage detection and loss of stiffness.

The predictions from the proposed material model are compared with experimental data and analytical predictions from sources in the literature.

6.1 Response of Thick–walled Cylinder in Compression and Bending

The geometry of the thick cylinder under consideration is shown in Fig. 6.1. It is similar to the cylinders tested at the David Taylor Research Center (DTRC) (Garala [97]) in an ongoing program to determine the compression behaviour of laminated cylinders. The loading cases which are considered are shown in Fig. 6.2: axisymmetric pressure producing compressive response in the cylinder wall; and an ovaling pressure with $p_2 \cos 2\theta$

variation which produces primarily circumferential flexure. A state of plane strain is imposed in the cylinder axis direction in both cases. Exact elasticity solution for a cylinder composed of anisotropic laminae subjected to axisymmetric pressure is given by Lekhnitskii [98]. For cross–ply laminated cylinders subjected to harmonic loading around the circumference exact elasticity solutions were presented by Ren [99]. The results from the material modelling procedure will be compared with these exact elasticity solutions.

The cylinder consists of 96 plies of AS4/3501–6 prepreg tape arranged in the stacking sequence $[0_2/90]_{16S}$. The experimentally observed properties of the prepreg tape were reported by Camponeschi [72,73] and are listed in Table 6.2. Also listed in Table 6.2 are the elastic properties of the prepreg tape as predicted by the micro–model portion of the material model. The assumed properties of the graphite fibers and the epoxy matrix are given in Table 6.1. The micro–model predicts the lamina properties quite well; better fits with experimental results can be obtained by further tuning the fiber and the matrix properties.

Table 6.3 lists the equivalent elastic properties of a typical repeating sublaminate ($[0_2/90]$) identifiable within the laminate stacking sequence. The results labelled "Sublaminate Model" are obtained by using the experimentally observed lamina properties as an input to the sublaminate model. The results labelled "Material Model" are from the complete material model, consisting of both micro–model and sublaminate model, with the constituent properties of Table 6.1 as input.

The two loading cases described above are analyzed using the finite element method in conjunction with the material modelling procedure. The results from the material modelling procedure are referred to as "Homogenized responses" since the material modelling procedure is based on homogenization of stresses, strains and the properties of the material comprising the cylinder. Exact homogenized responses are obtained by employing the material modelling procedure in an exact elasticity formulation. The accuracy

123

of the finite element solution is assessed by comparing the finite element results to the exact homogenized responses. To examine the implications of the homogenization process, the homogenized responses are compared to the results obtained from the exact ply–by–ply elasticity solution.

The finite element solution was carried out by providing as input the properties of the graphite fibers and the epoxy matrix along with the stacking sequence of the typical repeating sublaminate $([0_2/90])$. The material model generated the response of the equivalent material representing the typical repeating sublaminate via the micro–model and the sublaminate model. The exact homogenized responses were obtained by assuming that the cylinder is composed of a homogeneous material with the properties same as those of equivalent material representing the $([0_2/90])$ sublaminate.

6.1.1 Through–thickness Stress and Strain Distributions

Figs. 6.3 and 6.4 show the through–thickness stress and strain distributions in the case of axisymmetric compressive loading. In this case only a small circumferential segment of the cylinder was modelled, since it is an axisymmetric problem. For the cylinder in bending, one–quarter of the cylinder was modelled. The finite element mesh employed is shown in Fig 6.5: two elements are provided through the thickness in order to accurately capture the expected parabolic distribution of the shear stresses and strains. The stress and strain distributions for the case of cylinder in bending are shown in Figs. 6.6 and 6.7.

For the stress and strain quantities that are continuous through the laminate thickness (ϵ_θ, σ_r and $\tau_{r\theta}$), the homogenized responses are almost identical to the response calculated by exact ply–by–ply solution. Furthermore these continuous stress and strain quantities are not only continuous at the laminae interfaces but also smoothly varying throughout the laminate thickness.

For the discontinuous stress and strain quantities (σ_θ, ϵ_r and $\epsilon_{r\theta}$), it is of interest to note that although they may vary markedly from ply to ply, the distribution for each family

of plies with the same orientation is smooth, forming two envelopes of response. The homogenized response is a weighted mean of the exact ply–by–ply response. *The homogenization procedure provides excellent estimates of the exact ply–by–ply responses of continuous stress and strain quantities. The complementary discontinuous stresses and strains can then be recovered using the individual ply properties.*

6.2 Response of Notched Metal Matrix Laminates in Tension

The material model is used to predict the response of notched metal matrix laminates. Experimental results for notched laminates were presented by Shukow [100]. The geometry of the test specimens and the strain gauge locations are shown in Fig. 6.8. The specimens were formed from boron/aluminum laminae arranged in stacking sequences of $[+45/-45]_{2S}$ and $[0/+45/-45/90]_S$ respectively. The response of these notched laminates was investigated analytically by Arenburg [70], who used Aboudi's Method of Cells [7] in conjunction with First Order Shear Deformation Plate Theory for laminates to predict the laminate response. He used Bodner–Partom unified viscoplasticity theory [69] to characterize the aluminum matrix. In the present study the matrix material is characterized using Ramberg–Osgood relations (Chapter 2, Section 2.6.1), as illustrated in the next section.

6.2.1 Characterization of Boron/Aluminum Lamina

Since micromechanics is employed here to predict the lamina behaviour, material characterization in this context entails determination of the appropriate properties of the constituent fiber and matrix phases such that the lamina behaviour is accurately predicted.

The elastic properties of boron fibers and aluminum matrix provided by Arenburg [70] are listed in Table 6.4. The task of determining appropriate Ramberg–Osgood parameters for the aluminum matrix such that lamina nonlinearity is accurately portrayed was accomplished in the following way. Fig. 6.10 shows the response of a $[+45/-45]_{2S}$

unnotched laminate in tension. Appropriate Ramberg–Osgood parameters were assumed for the aluminum matrix to match the predicted response with the experimental data. The employed Ramberg–Osgood parameters are listed in Table 6.4; Fig. 6.9 shows the uniaxial stress–strain response of the aluminum matrix. Before proceeding with the analysis of the notched laminates some additional examples are presented for unnotched laminates to show that the material characterization is not limited to the case examined in Fig. 6.10.

Fig. 6.11 shows the predicted response of a $[0/+45/-45/90]_S$ laminate. The experimental results suggest a change in stiffness at about 10 ksi. This is accurately predicted by the material model and is due to the softening of the aluminum matrix in the $90°$ plies. Fig. 6.12 shows the response of a $[0/90]_{2S}$ laminate. A definite knee is again observed in the predicted response due to the yielding of the $90°$ ply. The agreement between predicted and the experimentally observed responses is very good up to 80 ksi, after which the laminate failed. Table 6.6 presents the "predicted" initial elastic moduli of the $[+45/-45]_{2S}$ and $[0/+45/-45/90]_S$ laminates. The predictions from the material model are in very good agreement with the analytical predictions from Arenburg [70] and the experimental data from Shukow [100].

6.2.2 Response of [+45/–45]₂ₛ Notched Laminate

The geometry of the test coupon is shown in Fig. 6.8. The symmetry of the test specimen is exploited so that only a quarter of the specimen is modelled (Fig. 6.13) using 20 node solid elements with 2 x 2 x 3 Gauss rule

Fig. 6.14 shows the axial strain $\bar{\epsilon}_{11}$ at the edge of the hole and at the far–field strain gauge locations, as a function of applied stress. Experimental results from Shukow [100] are also shown. The analytical results for far–field strain are in excellent agreement with the experimental results. For the strain at the edge of the hole, the analytical results from the present study are in very good agreement with the analytical results of Arenburg [70];

however, both sets of analytical results start diverging from the experimental results in the vicinity of 0.6% strain. Beyond this point both analytical models start underestimating the axial strain. Arenburg attributed this to geometric nonlinearity effects and possible delaminations, which are not accounted for in the analyses. Another source of the discrepancy could be fiber/matrix debonding, which has also not been accounted for in the analysis.

6.2.3 Response of [0/+45/−45/90]$_s$ Notched Laminate

The finite element mesh employed to analyze this laminate is shown in Fig. 6.15. It is more refined in the region near the hole because preliminary investigations indicated that the stress gradients near the hole were much greater here than in the $[+45/-45]_{2S}$ notched laminate.

Fig. 6.16 shows the computed strains at the edge of the hole and at the far–field strain gauge. The far–field strain is in good agreement with the analytical predictions from Arenburg [70], and is essentially the same as the stress–strain response of the $[0/+45/-45/90]_S$ unnotched laminate (Fig. 6.11). The axial strain at the edge of the hole is overestimated compared to analytical results of Arenburg and the experimental results of Shukow. A possible reason for the discrepancy between the analytical predictions is that different constitutive descriptions were employed in the two studies to describe the matrix material nonlinearity. Arenburg used Bodner–Partom unified viscoplasticity theory to describe the matrix material, whereas here Ramberg–Osgood relations are used for characterizing the matrix nonlinearity.

6.3 Bending of Simply Supported Square Plate

Analytical results for the response of a simply supported square plate subjected to a uniformly distributed transverse load (Fig. 6.17) were presented by Arenburg [70]. The plate is 10.0 inches square and its thickness is 0.1 inch, resulting in a span to thickness ratio of 100, so that it can be characterized as a thin plate. The plate is made of boron/alumi-

num laminae; the fibers in all the laminae are orientated in a single direction (i.e. a $[0°]_T$ laminate). The properties of the boron/aluminum lamina (Table 6.4) are same as the ones used to make the previously investigated notched and unnotched laminates. Only a quadrant of the plate is modelled for finite element analysis, using Q3DISOP solid elements. The finite element mesh and the imposed boundary conditions are also shown in Fig. 6.17. The effects of geometric nonlinearity were not by accounted Arenburg, and are neglected in this study as well.

Fig. 6.18 shows the center deflection of the plate as a function of the applied transverse load. Results are presented from the study conducted by Arenburg, and from the present study in a number of cases with different meshes and Gauss integration rules. In these cases the parameters varied were, the number of elements through the thickness, and the order of Gauss integration rule; the cases considered can be classified as follows:

- 1 Element through the thickness with 2 x 2 x 2 Gauss rule (case (1)).

- 1 Element through the thickness with 2 x 2 x 3 Gauss rule (case (2)).

- 2 Elements through the thickness with 2 x 2 x 3 Gauss rule (case (3))
  The maximum number of Gauss points that can be employed in the
  thickness direction with Q3DISOP element is restricted to 3, so in
  order to have additional Gauss points in the thickness direction, 2
  elements are employed through the thickness with 2 x 2 x 3 Gauss
  rule.

An interesting phenomenon is observed in the results presented in Fig. 6.18; i.e. the results from the different combinations of meshes and integration rules do not seem to be converging monotonically to an exact solution, rather the convergence seems to be non–monotonic. This is a result of material nonlinearity and the sensitivity of the com-

128

puted response to the location of the integration points associated with the different Gauss rules.

Fig. 6.19 shows the location of the Gauss sampling points throughout the thickness in the various cases considered. If the cross–section is undergoing flexure, the flexural stresses will be higher near the top and bottom surfaces of the plate. Case (1) will yield a lower stiffness value for the element than case (2), because in case (2) the sampling points are nearer to the top and bottom surfaces of the plate where they detect the onset of non-linearity earlier than in case (1). The integration/sampling points near the plate mid–surface do not detect significant straining and therefore do not influence the results much. Hence we see more softened response for case (2) as compared to case (1). In case (3) there is an additional layer of Guass points between the Gauss points near the plate mid-surface and the top and bottom surfaces of the plate. The Gauss points in the additional layer are sufficiently far from the top and bottom of the plate and detect the onset of non-linearity later than the extremal Gauss points in case (2). This explains the slightly stiffer response predicted in case (3) (Fig. 6.18). The results from case (3) are accepted as more accurate than cases (1) and (2), since the number of Gauss points in the thickness direction is greater and their distribution through the thickness is more reasonable.

The maximum load intensity is 12 ksi. At this load level, the analytical results of Arenburg predict the deflection at center of the plate to be 0.411 in., whereas the accepted solution in the present study (2 elements through-thickness with 2 x 2 x 3 Gauss rule) predict the center deflection to be 0.446 in.

Fig. 6.20 shows the variation in the maximum stresses at the plate top surface as the applied load increases. The maximum σ_{11} and σ_{22} stresses occur at the plate center, whereas the maximum shear stress τ_{12} occurs at the corners of the plate. The agreement with the results presented by Arenburg is fairly good. The present analysis shows more softening in the σ_{22} response than predicted by Arenburg. This is accompanied by an

129

elevation of the σ_{11} stress in order to balance the applied load. The calculated shear stresses τ_{12} from the two studies are in excellent agreement.

6.4 Compressive Strength of Notched Laminate

Chang and Lessard [102,103] conducted an experimental and analytical investigation into the compressive strength of notched laminates composed of T300/BP976 graphite/epoxy laminae. The lamina was modelled as an orthotropic material exhibiting nonlinearity only in the in–plane shear response, using the relation suggested by Hahn and Tsai [62,63]. Failure criteria for predicting the in–plane failure modes of a lamina were also given. After a lamina failed, its stiffness was reduced to reflect the damage. The laminate response was obtained by assembling the individual laminae within the frame work of Classical Laminated Plate Theory.

The material modelling procedure developed in the present study is used to predict the compression response of one of the notched laminates studied by Chang and Lessard [102,103]. The geometry of the selected notched laminate is shown in Fig. 6.21. The test specimen has an extensometer attached to it which measures the shortening over the gauge–length of 1.0 inch.

The characterization of the T300/BP976 lamina is described in the next section.

6.4.1 Characterization of T300/BP976 Lamina

The elastic moduli of the T300/BP976 lamina are given by Chang and Lessard [102]. From these lamina properties and the information available in the literature, the *in situ* elastic moduli of the constituent graphite T300 fibers and the BP976 epoxy matrix were estimated, and are given in Table 6.7. The properties of the T300/BP976 lamina used by Chang and Lessard are given in Table 6.8. The predictions of lamina properties by the material model are also presented in Table 6.8. Fig. 6.22 shows the shear response of the lamina according to Chang and Lessard. Modified Ramberg–Osgood relations (Chapter

130

2, Eqs. (2.24–2.30)) are used to model this response; the parameters are presented in Table 6.7.

The micromechanical failure criteria employed in the analysis along with the procedure for damage modelling has been described in (Chapter 2, Sections 2.7–2.8). The micro–failure criteria predict the strengths of the lamina very well (Table 6.8). The only exception is the axial compressive strength, for which the fiber micro–buckling criterion grossly over–predicts the actual compressive strength of the lamina. This discrepancy may be a result of fiber misalignment in the lamina; it may also be that a failure mechanism other than the fiber micro–buckling such as fiber compressive failure precipitates the failure.

6.4.2 Response of $[(+45/-45)_6]_s$ Notched Laminate

The notched laminate shown in Fig 6.21 is analyzed using the the mesh shown in Fig. 6.23. The properties of the of fiber and the matrix along with the stacking sequence of the typical repeating sublaminate (+45/–45) is provided as input for the material model.

Fig. 6.24 shows the load–shortening response of the notched laminate. The response is quite nonlinear since the +45/–45 stacking sequence produces primarily shear stresses within the laminae. The analysis does not predict any damage up to 2400 lbs, at which point fiber micro–buckling is predicted around the periphery of the hole. Application of additional load results in matrix shearing failure in elements lying in the vicinity of the 45° direction starting from the region of maximum stress concentration. The effect of matrix shearing failure is modelled by reducing the lamina in–plane shear stiffness. The loss of lamina shear stiffness results in prediction of fiber micro–buckling. Figs. 6.25–6.27 show the predicted state of damage at various load–levels. The predicted ultimate load is 3320 lbs, which is about 11% more than the collapse load of 3000 lbs predicted by Chang and Lessard [102]. The present investigation employed *maximum stress* failure criteria at the micromechanical level: It is speculated that application of interaction type failure criteria at the microme-chanical level would result in further improvement in the predicted results.
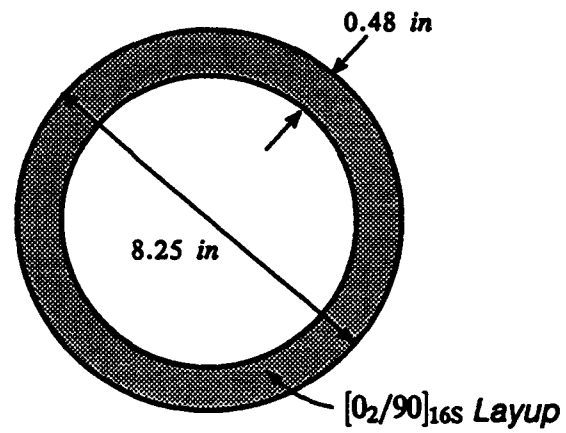
131

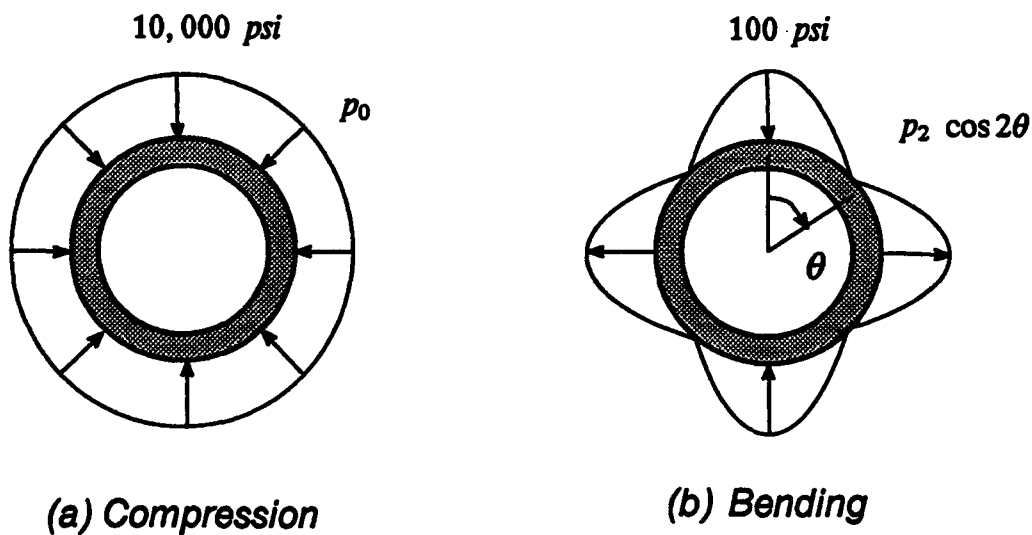**Fig. 6.1** *Geometric dimensions of the thick-walled cylinder.*

(a) Compression

(b) Bending

Fig. 6.2 *(a) Cylinder in compression, (b) Cylinder in circumferential bending.*

132

	E_1 (Mpsi)	E_2 (Mpsi)	G_{12} (Mpsi)	ν_1	ν_{23}
Graphite	27.0	2.5	5.0	0.30	0.25
Epoxy	0.728	0.728	0.26	0.40	0.40

Table 6.1 *Elastic properties of graphite fibers and epoxy matrix.*

Source	E_1 (Mpsi)	E_2 (Mpsi)	G_{12} (Mpsi)	G_{23} (Mpsi)	ν_1	ν_{23}
Experiment, Camponeschi [72,73]	16.48	1.40	0.87 [1]	0.55 [2]	0.334	0.54
Micro-model	16.50	1.56	0.87	0.53	0.337	0.468

1 From $[\pm 45]_{2S}$ tension test

2 From literature

Table 6.2 *Properties of AS4/3501-6 prepreg tape.*
Fiber volume fraction = 0.60

Source	E_1 (Mpsi)	E_2 (Mpsi)	E_3 (Mpsi)	G_{12} (Mpsi)	G_{13} (Mpsi)	G_{23} (Mpsi)	ν_{12}	ν_{13}	ν_{23}
Experiment, Camponeschi [72,73]	11.63	—	—	—	—	—	0.069	0.469	—
Sublaminate Model	11.53	6.47	1.80	0.87	0.73	0.63	0.073	0.448	0.519
Material Model	11.60	6.58	1.85	0.82	0.69	0.60	0.08	0.455	0.467

Table 6.3 *Equivalent elastic properties of* $[0_2/90]$ *repeating sublaminate.*
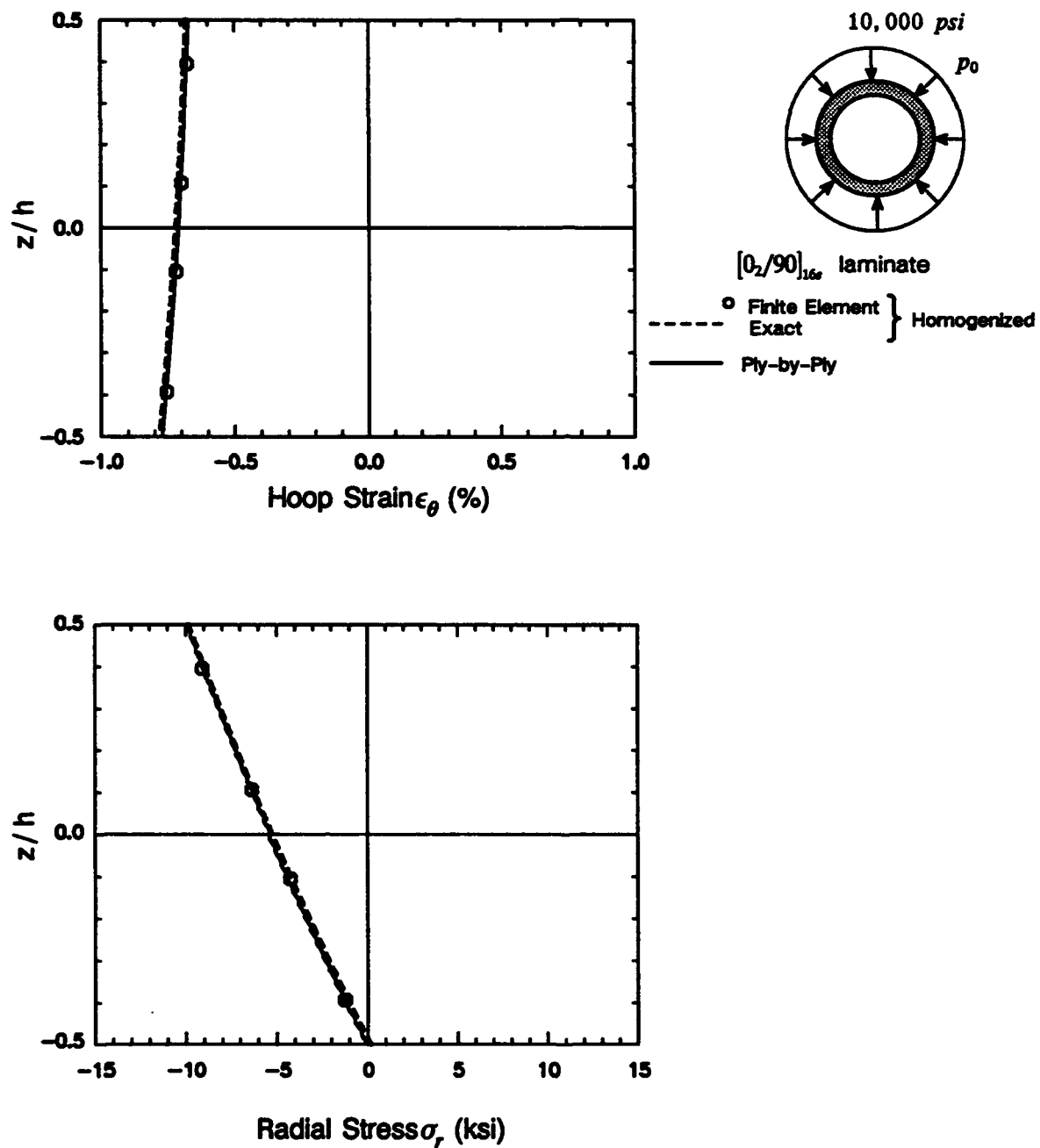
Fig. 6.3 *Response of laminated cylinder in compression, continuous quantities* $(\epsilon_\theta , \sigma_r)$

134
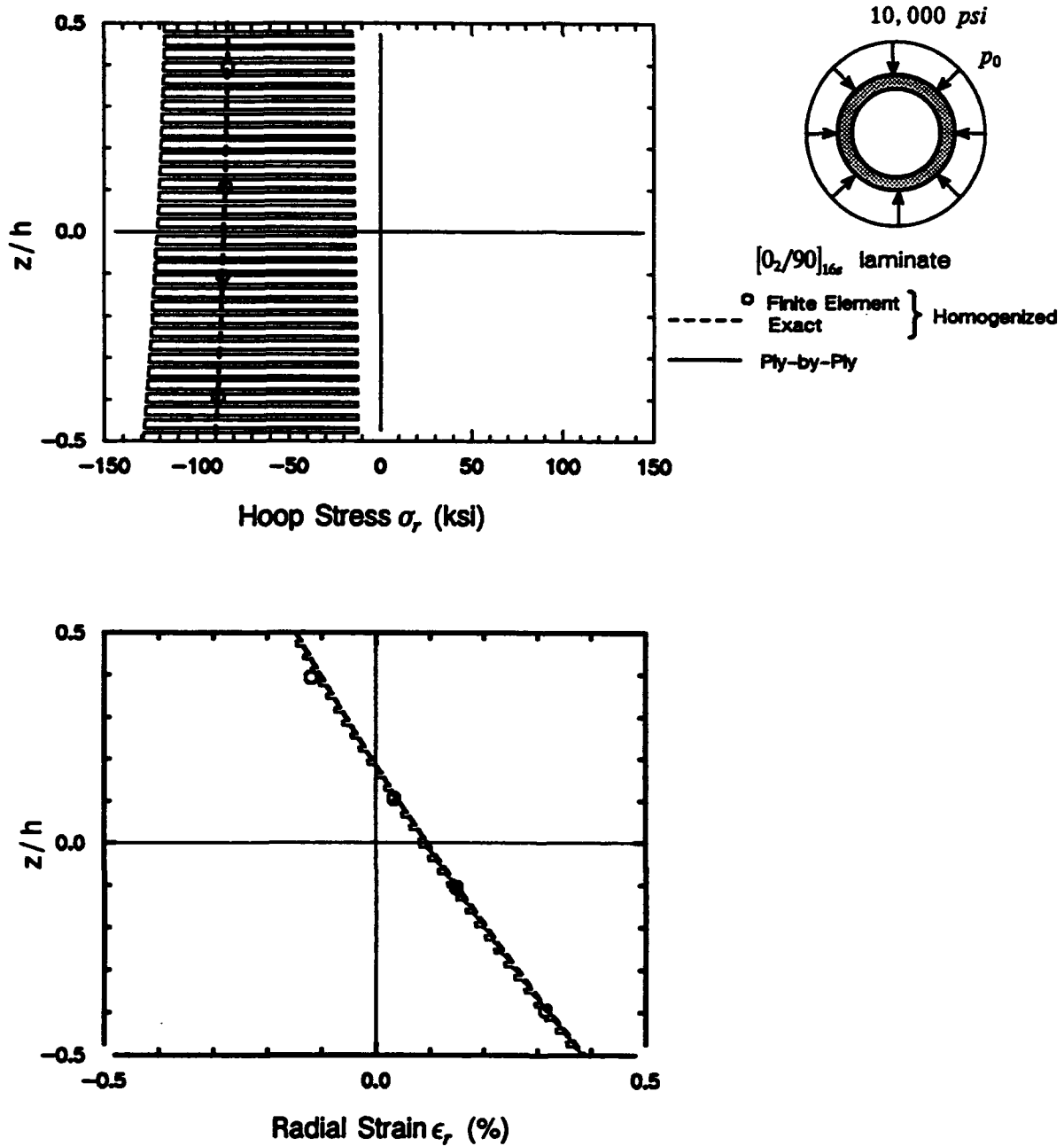
Fig. 6.4 *Response of laminated cylinder in compression, discontinuous quantities* $(\sigma_r, \epsilon_\theta)$

Mesh Size
36 Elements
355 Nodes

Typical Element,
Q3DISOP (20 Node Brick)
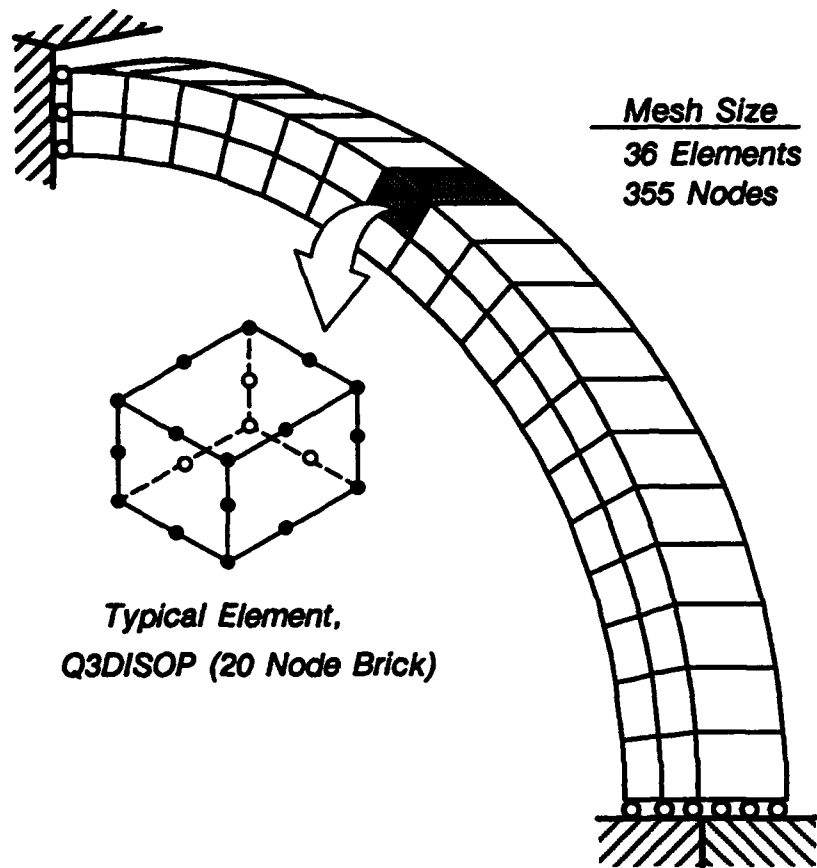
Fig. 6.5 *Finite element mesh employed in calculating the response of laminated cylinder in bending*

136
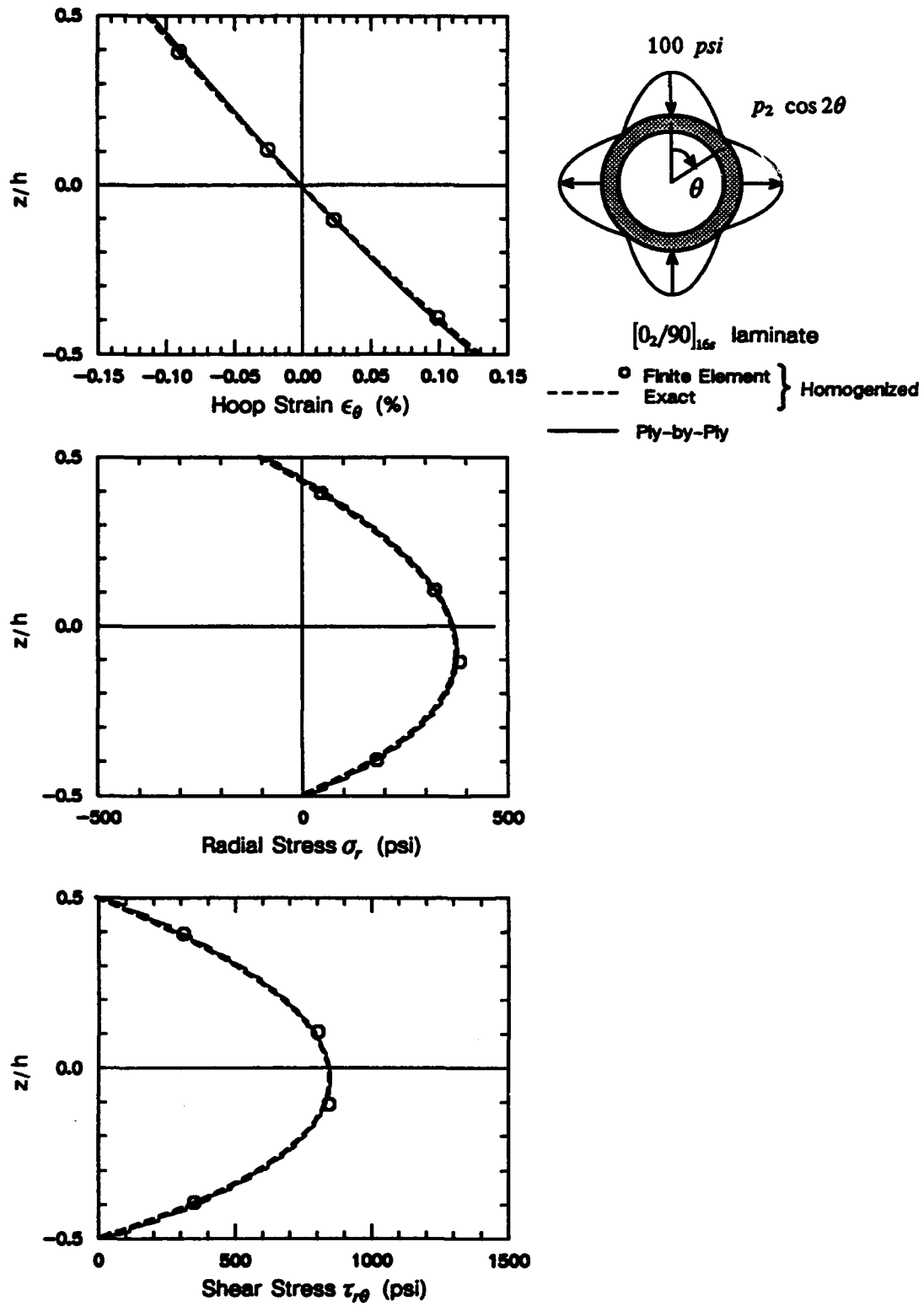
Fig. 6.6 *Response of laminated cylinder in bending, continuous quantities* $(\epsilon_\theta, \sigma_r, \tau_{r\theta})$
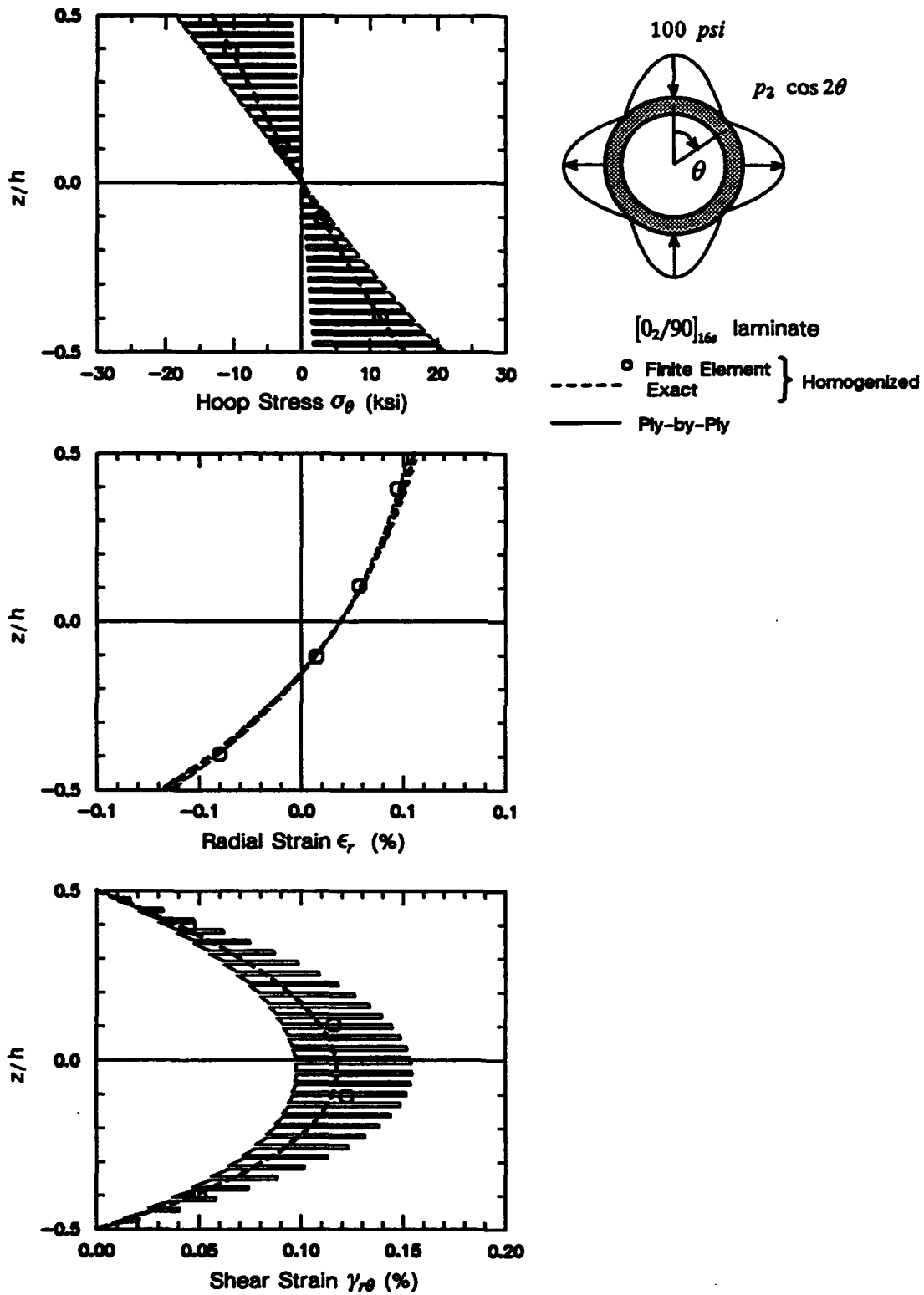
Fig. 6.7 *Response of laminated cylinder in bending, discontinuous quantities* $(\sigma_\theta, \epsilon_r, \gamma_{r\theta})$
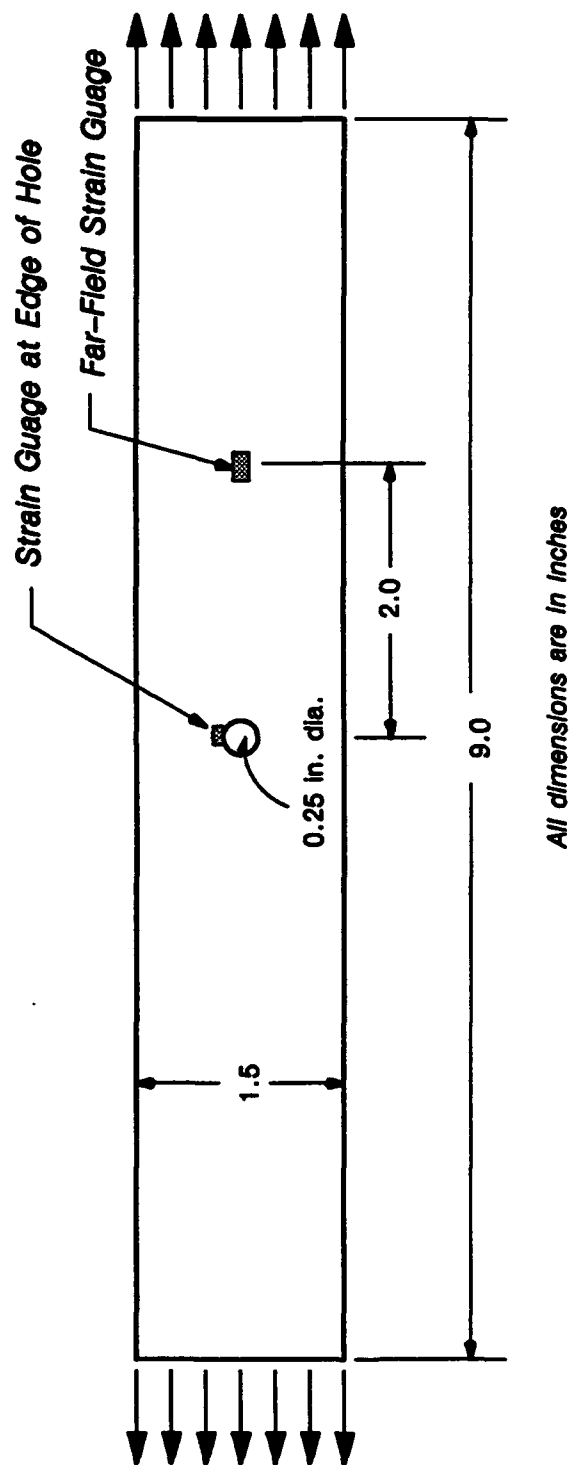
Fig. 6.8 *Geometry of the notched test coupons.*

Strain Guage at Edge of Hole

Far-Field Strain Guage

0.25 in. dia.

2.0

9.0

1.5

All dimensions are in inches

	E (Mpsi)	ν	τ_0 (Ksi)	a	b	n
Boron	58.0	0.2	—	—	—	—
Aluminum	8.69	0.25	6.0	0	1.0	5

Table 6.4 *Elastic properties of boron fibers and aluminum matrix, along with Ramberg-Osgood parameters for aluminum matrix. Fiber volume fraction = 0.44*

	E_{11} (Mpsi)	E_{22} (Mpsi)	G_{12} (Mpsi)	ν_{12}
Material Model	30.40	16.70	6.51	0.223
Arenburg [70]	30.39	16.03	6.51	0.229
Experiment Shukow [100]	30.59	19.20	6.50	0.218

Table 6.5 *Elastic properties of boron/aluminum lamina.*
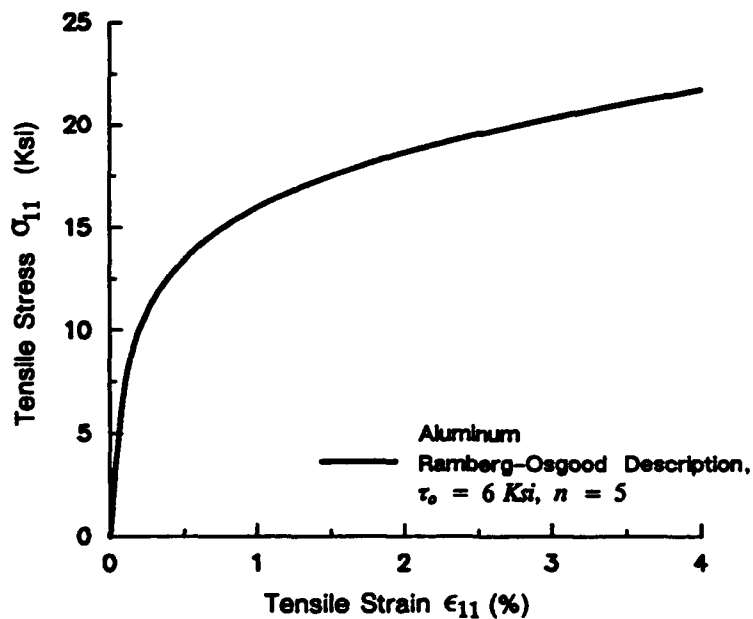
Fig. 6.9 *Back-calculated uniaxial stress-strain response of in situ aluminum matrix.*
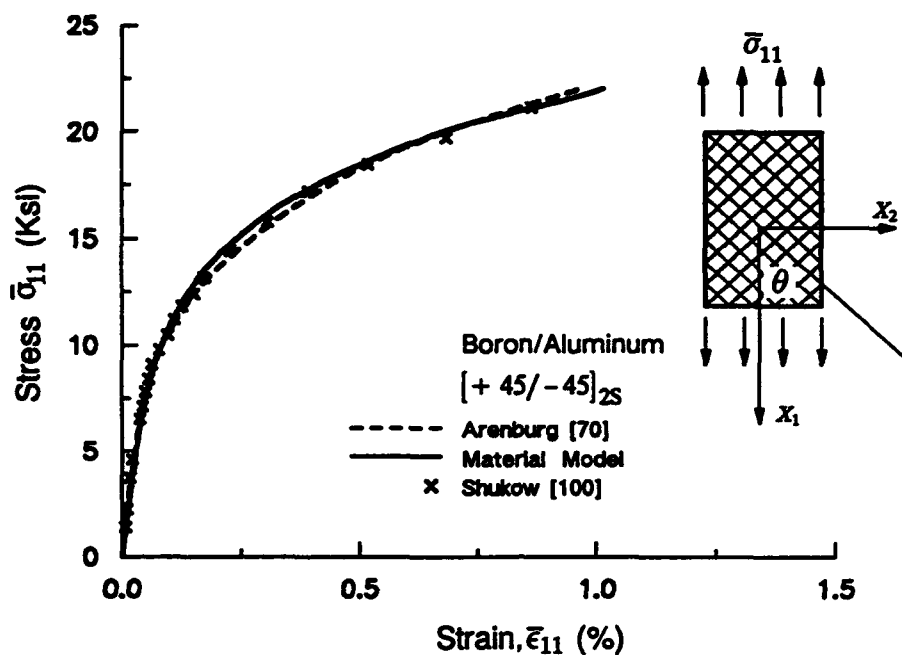
Fig. 6.10 *Response of [+45/–45]$_{2s}$ boron/aluminum laminate as predicted by the material model, along with predictions from Arenburg, and experimental data from Shukow.*
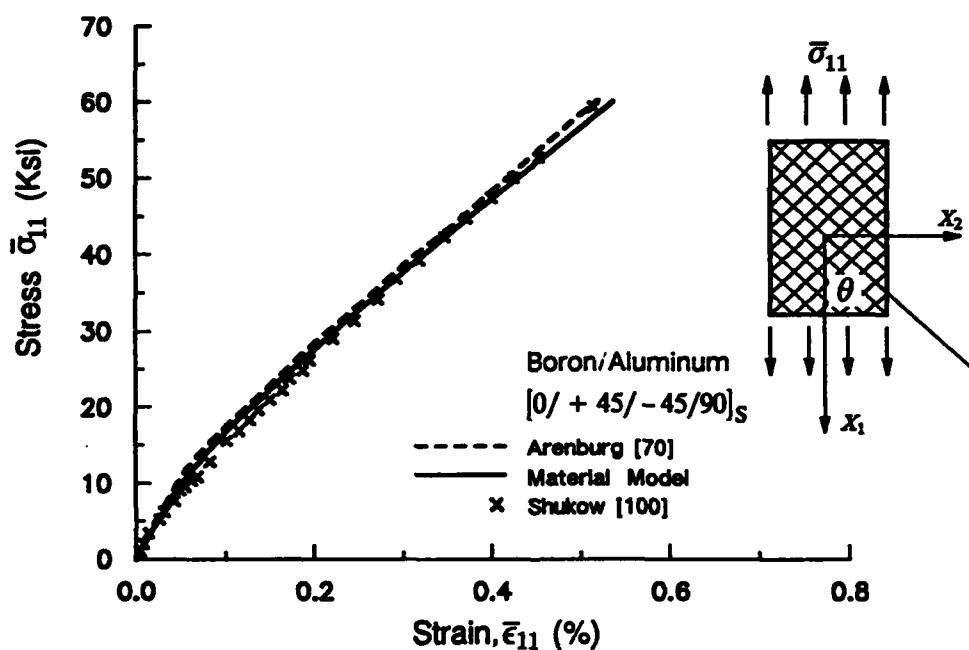
Fig. 6.11 *Response of [0/+45/–45/90]$_s$ boron/aluminum laminate as predicted by the Material Model, along with predictions from Arenburg, and experimental data from Shukow.*

141
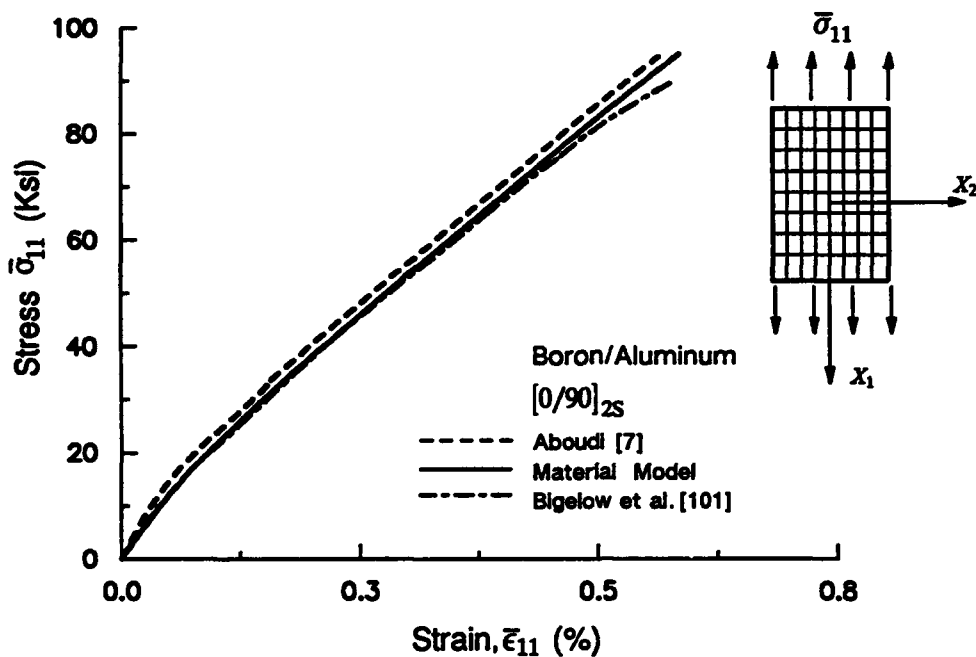
Fig. 6.12 *Response of [0/90]$_{2S}$ boron/aluminum laminate as predicted by the material model, along with predictions from Aboudi, and experimental data from Bigelow et al.*

	E_{11} (Mpsi)			ν_{12}		
Laminate	Material Model	Arenburg [70]	Experiment, Shukow [100]	Material Model	Arenburg [70]	Experiment, Shukow [100]
$[\pm 45]_{2S}$	17.77	17.67	17.36	0.366	0.358	0.373
$[0/ \pm 45/90]_S$	20.92	20.70	21.25	0.253	0.249	0.267

Table 6.6 *Elastic properties of boron/aluminum laminates.*

Mesh Size
54 Elements
471 Nodes

Typical Element,
GQ3DISOP (20 Node Brick)

X_1

X_2

X_3
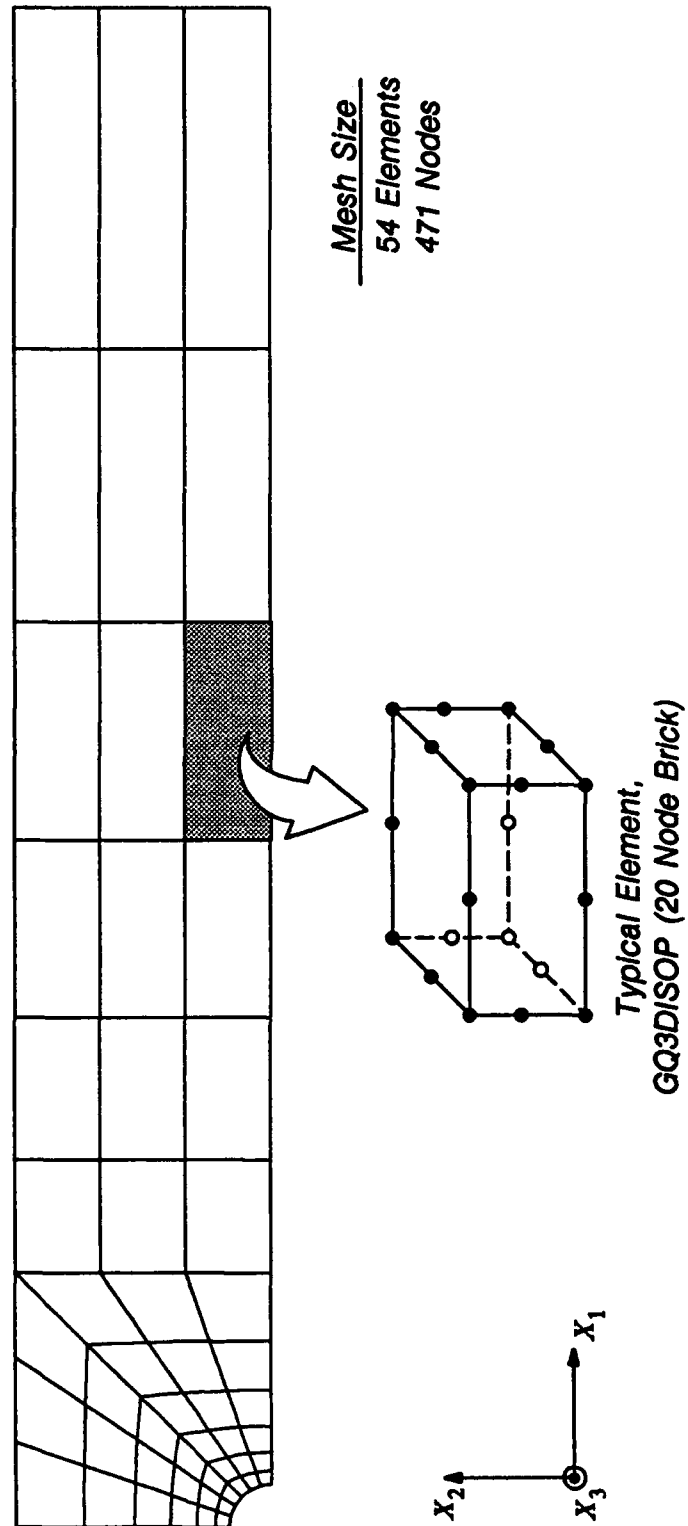
Fig. 6.13 Finite element mesh employed in the analysis of $[+45/-45]_{2s}$ notched coupon.

143
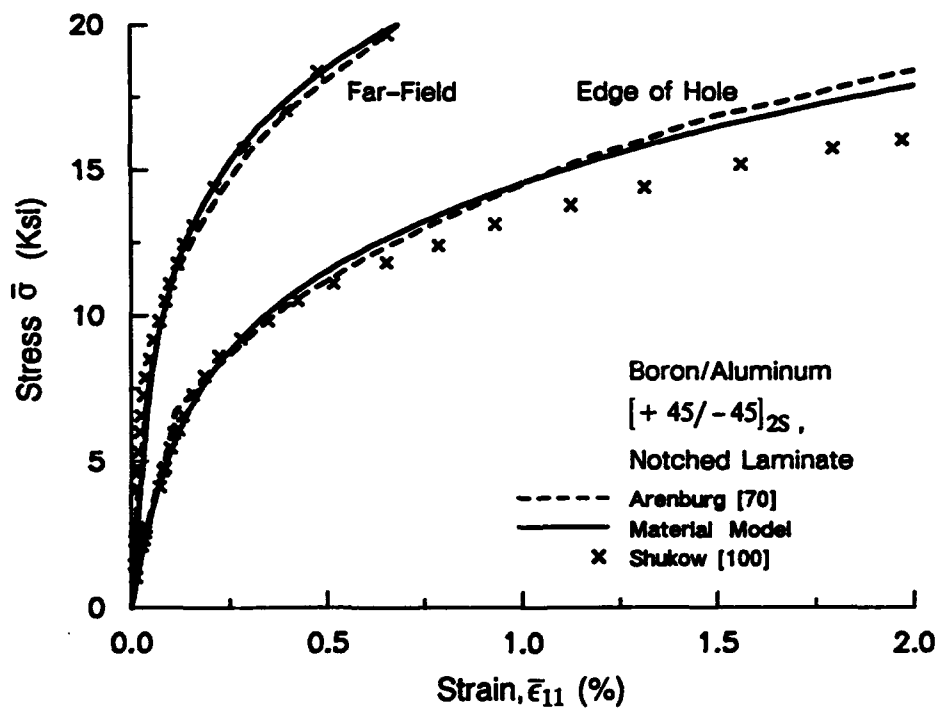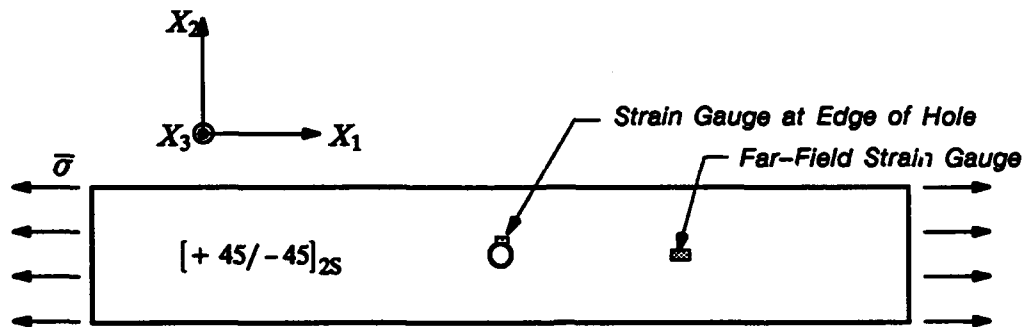
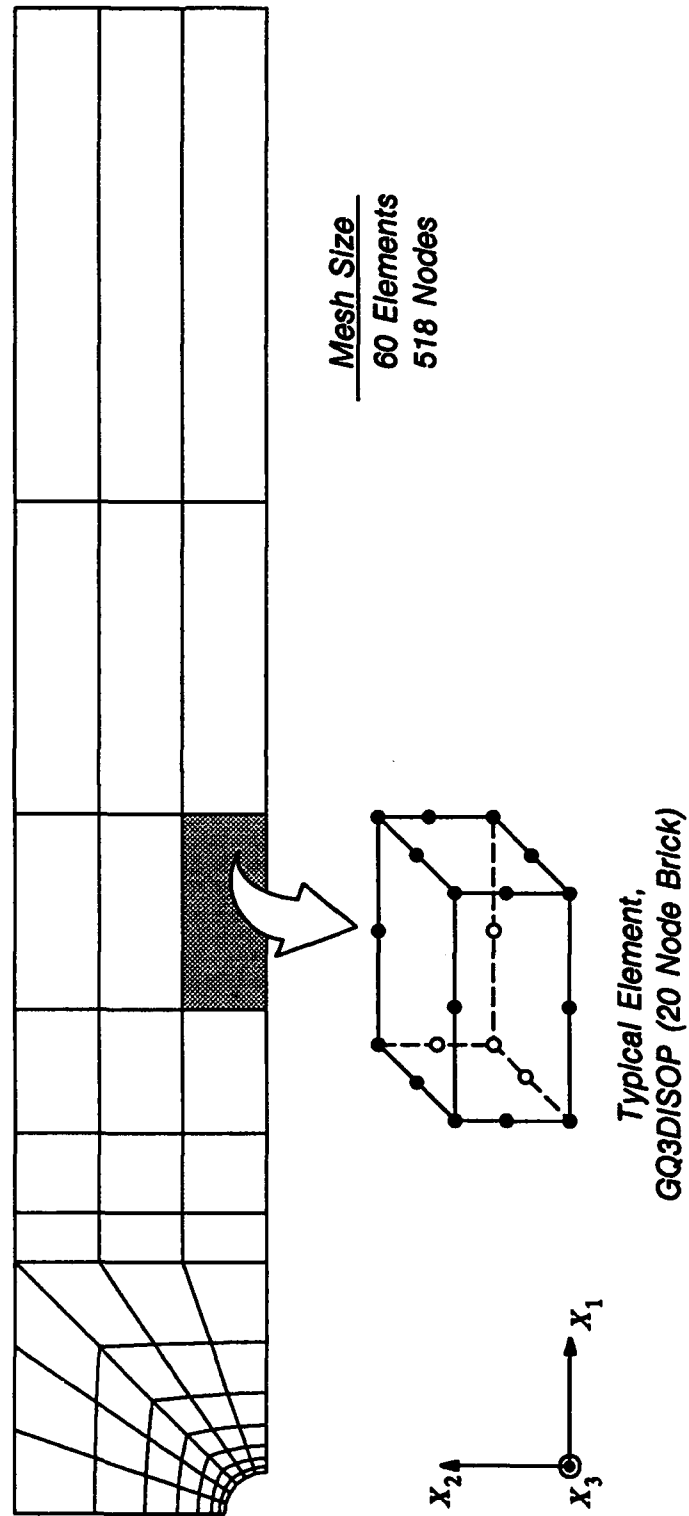Fig. 6.14 *Response of [+45/–45]$_{2s}$ notched boron/aluminum laminate.*

144

Mesh Size
60 Elements
518 Nodes

Typical Element,
GQ3DISOP (20 Node Brick)

x_1

x_2

x_3

Fig. 6.15 *Finite element mesh employed in the analysis of $[0/+45/-45/90]_s$ notched coupon.*
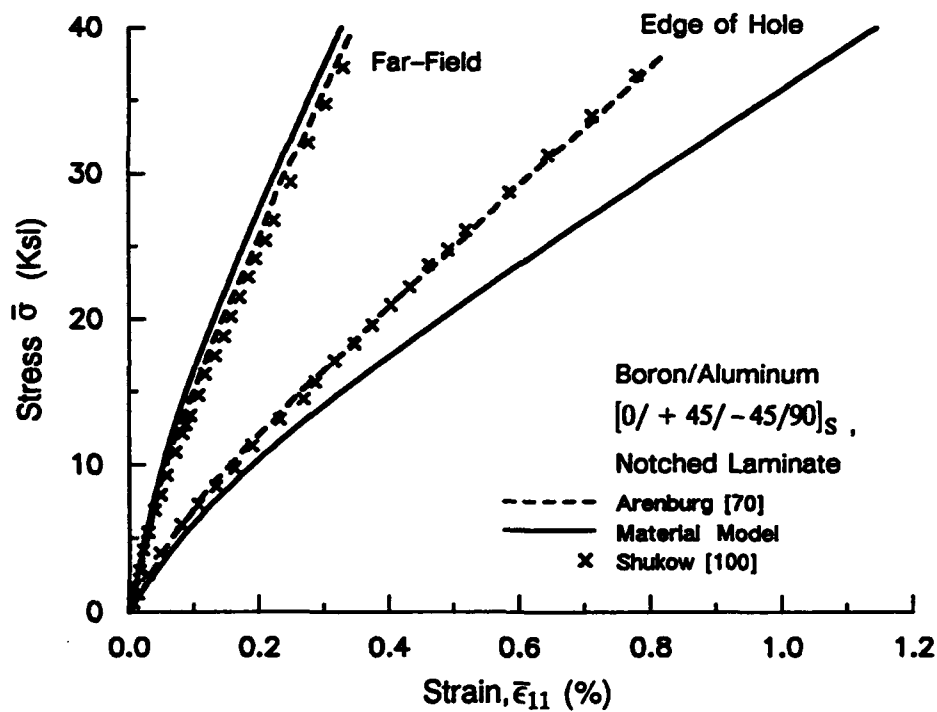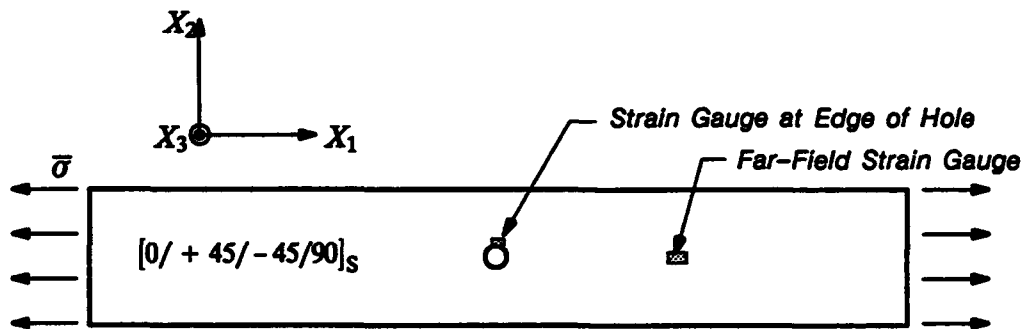
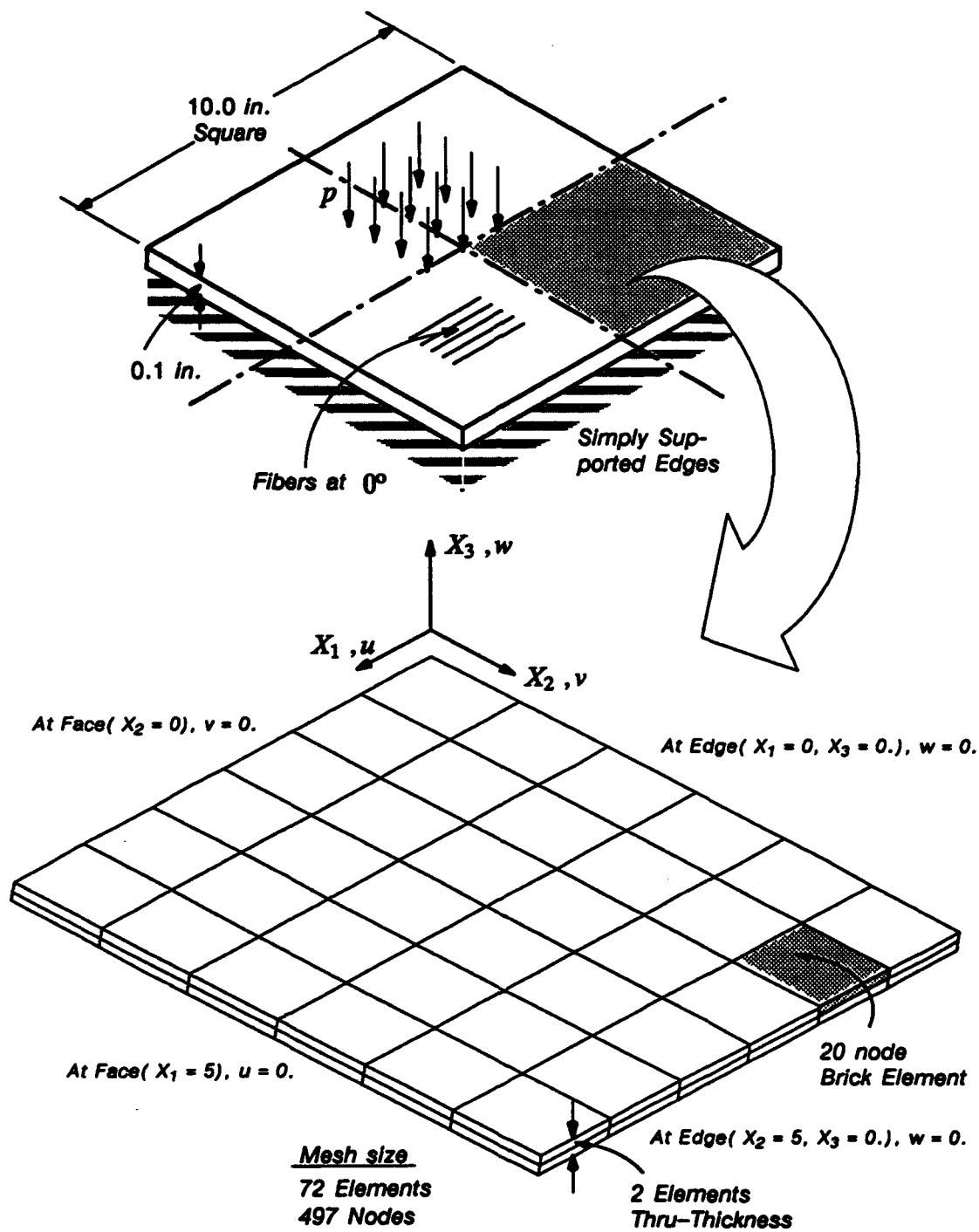**Fig. 6.16** *Response of [0/+45/-45/90]$_s$ notched boron/aluminum laminate.*

146

Fig. 6.17 *Geometry of the square plate, and the finite element mesh of the plate quadrant.*
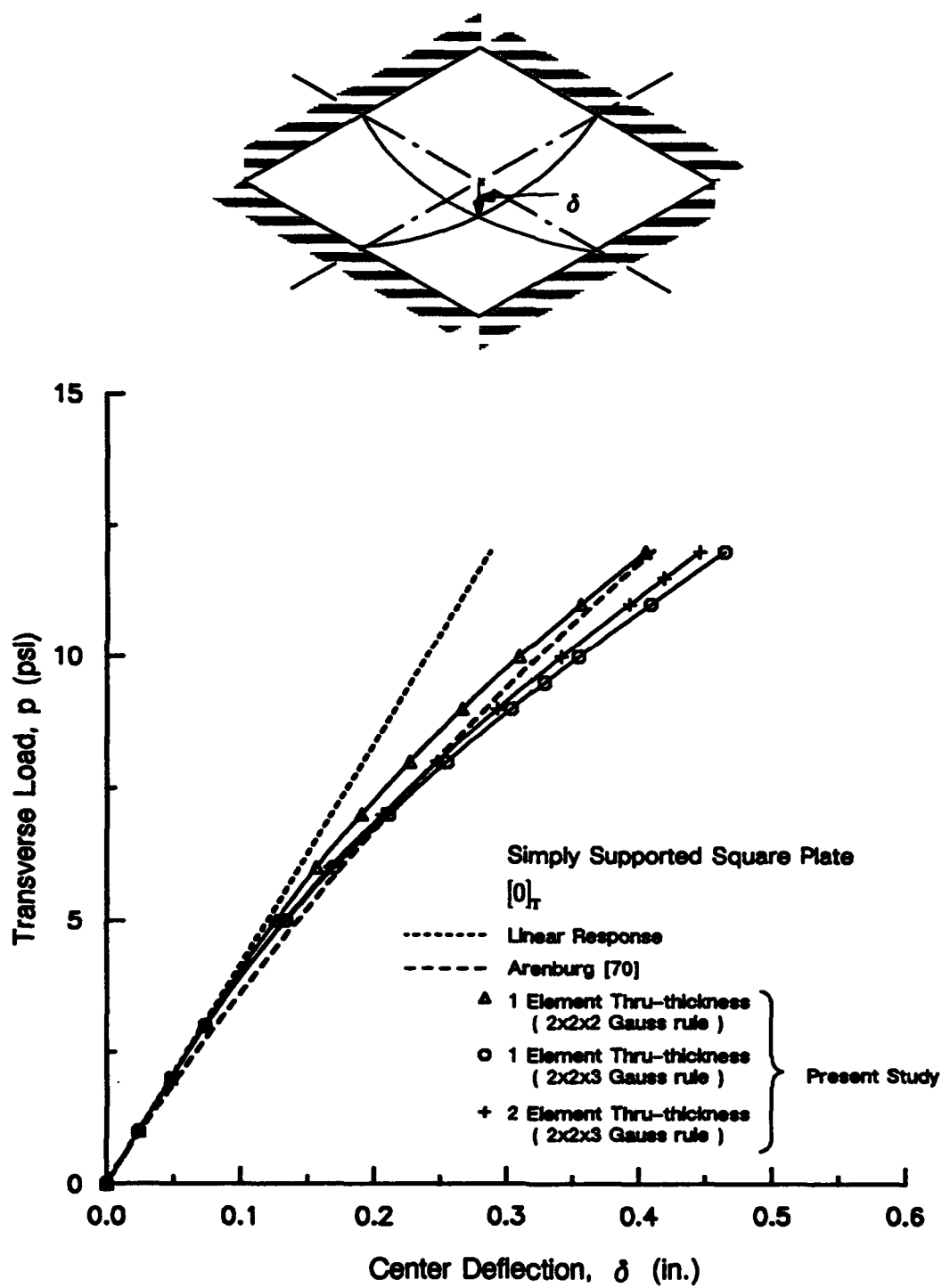
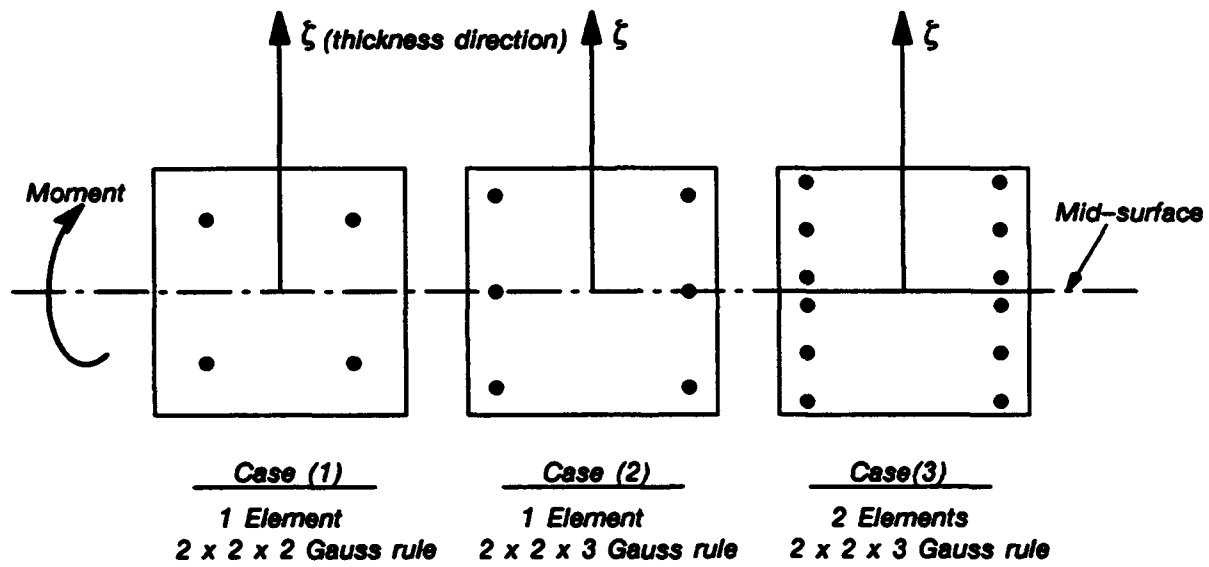Fig. 6.18 *Center deflection of simply supported square plate.*

Fig. 6.18 *Location of Gauss integration points in the thickness direction, for the various cases considered.*
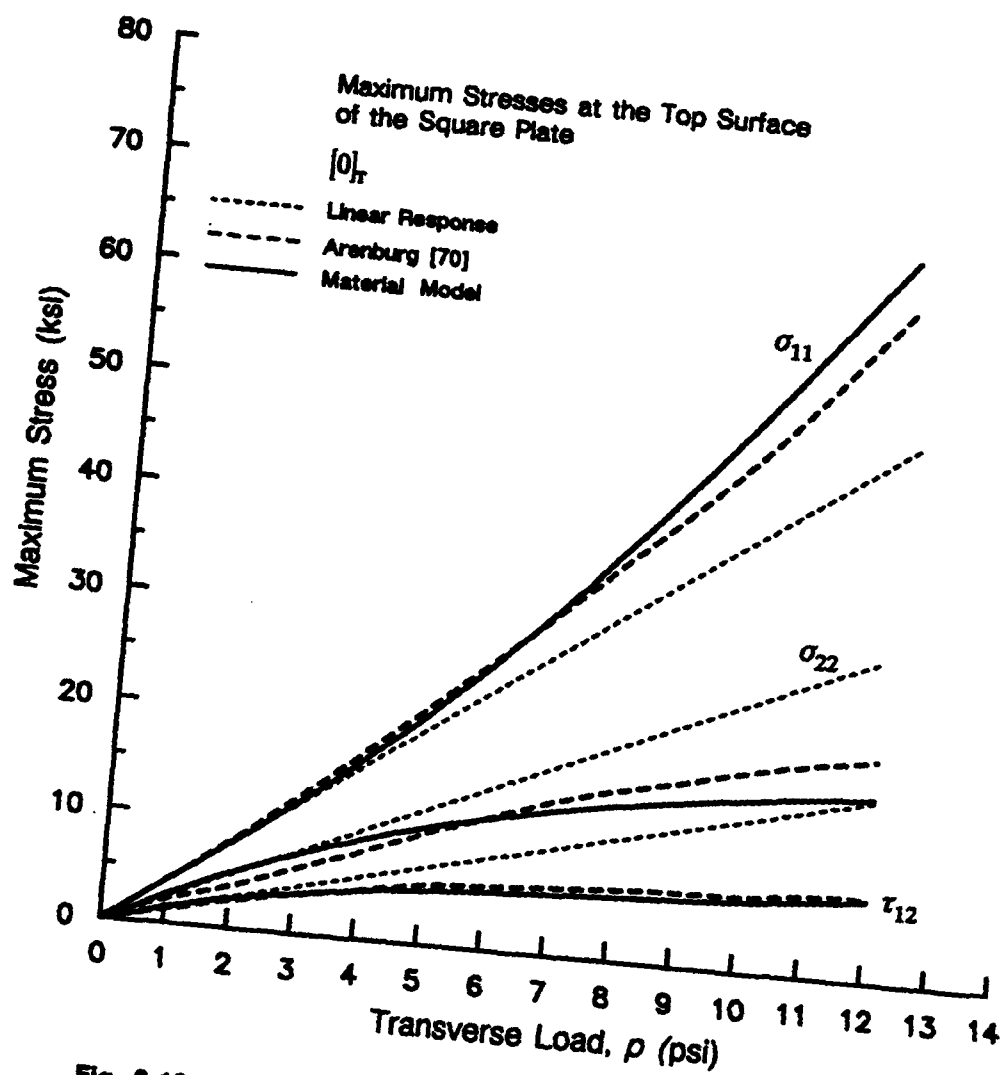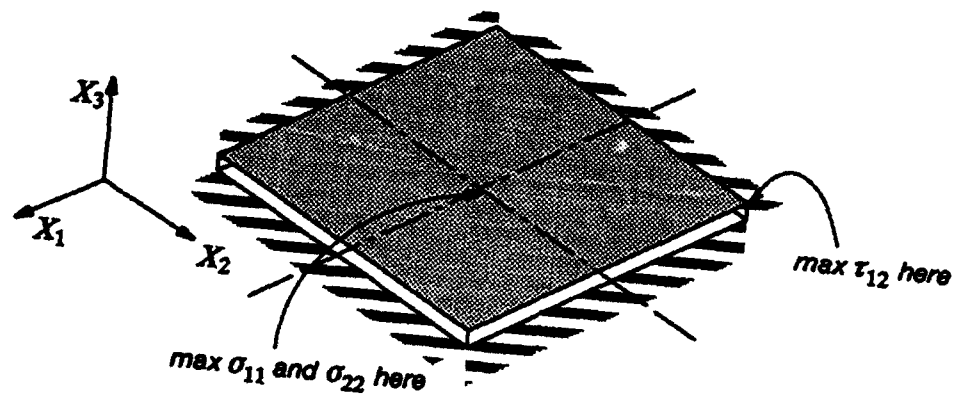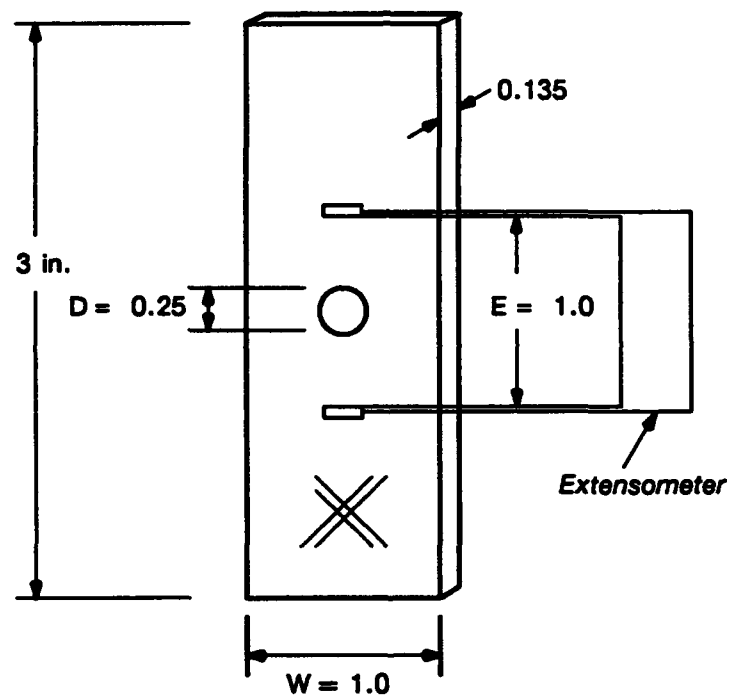
Fig. 6.19 Maximum stresses in simply supported square plate.

Fig. 6.21 *Geometry of the notched laminate tested by Chang and Lessard [102,103], stacking sequence* $\left[(+45/-45)_6\right]_S$

151

	E_1 (Mpsi)	ν_1	E_2 (Mpsi)	ν_{23}	G_{12} (Mpsi)	τ_0 (Ksi)	b	n	$X_t^{(f)}$ (Ksi)	$Y_c^{(m)}$ (Ksi)	$S^{(m)}$ (Ksi)
Graphite	33.8	0.2	3.0	0.42	1.7	—	—	—	347.0	—	—
BP976 Epoxy	0.925	0.25	0.925	0.25	0.37	9.25	1.0	4	7.5	42.0	17.0

Table 6.7 *Elastic properties of T300 graphite fibers and BP976 epoxy matrix, along with Ramberg-Osgood parameters for the matrix used in modelling the response of T300/BP976 lamina. Fiber volume fraction = 0.66*

Stiffness reduction factors $D_{f_{11}}$, $D_{m_{11}} = 0.01$, $D_{m_{22}}$, $D_{m_{44}} = 0.25$

Source	E_1 (Mpsi)	ν_1	E_2 (Mpsi)	ν_{23}	G_{12} (Mpsi)	X_t (Ksi)	X_c (Ksi)	Y_t (Ksi)	Y_c (Ksi)	S (Ksi)
Chang et al. [102]	22.7	0.23	1.88	—	1.01	220.0	231.0	6.46	36.7	15.5
Material Model	22.63	0.213	1.94	0.367	0.89	220.0	590.0*	6.5	37.0	15.5

* *The predicted compressive strength as calculated from micro-buckling criteria is much higher, probably because of some other failure-mechanism, such as fiber compressive failure.*

Table 6.8 *Elastic properties and strengths of graphite T300/BP976 lamina as given by Chang and Lessard [102], and predictions from the material model.*
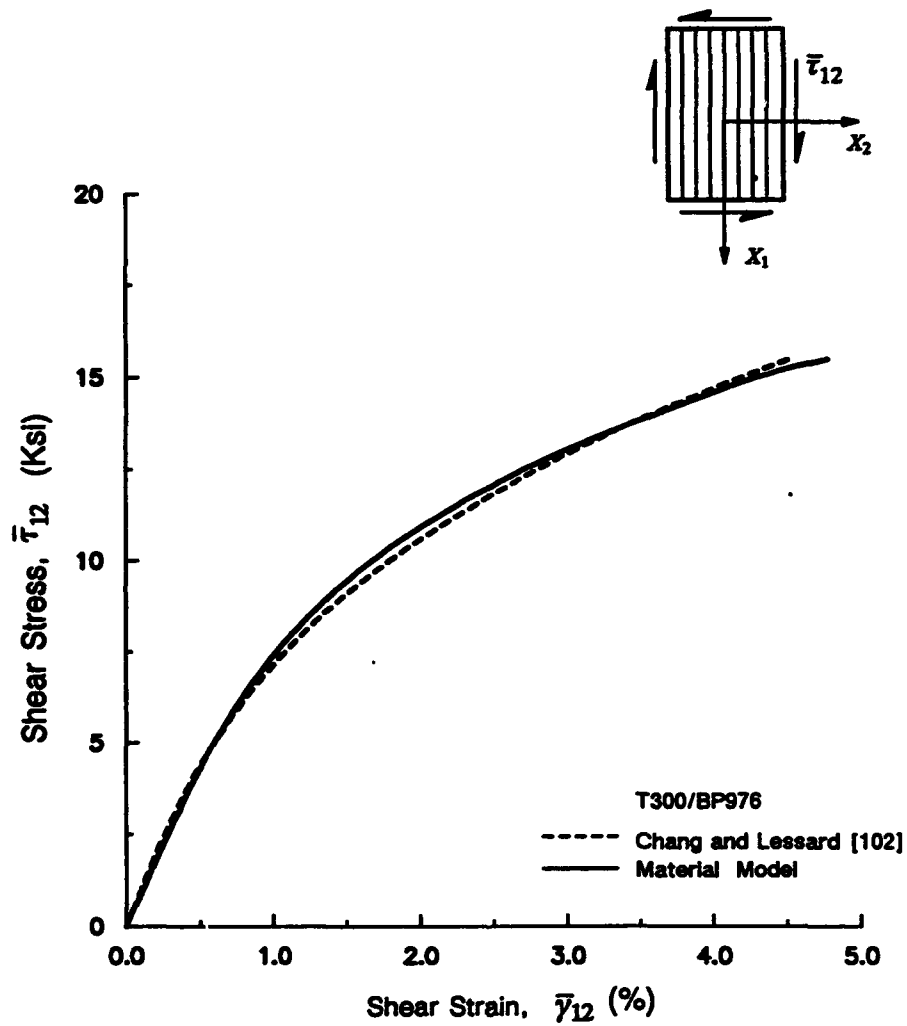
Fig. 6.22 *Shear stress-strain response of T300/BP976 graphite/epoxy lamina according to the material model, and Chang and Lessard [102].*

Mesh Size
300 Elements
981 Nodes

Typical Element,
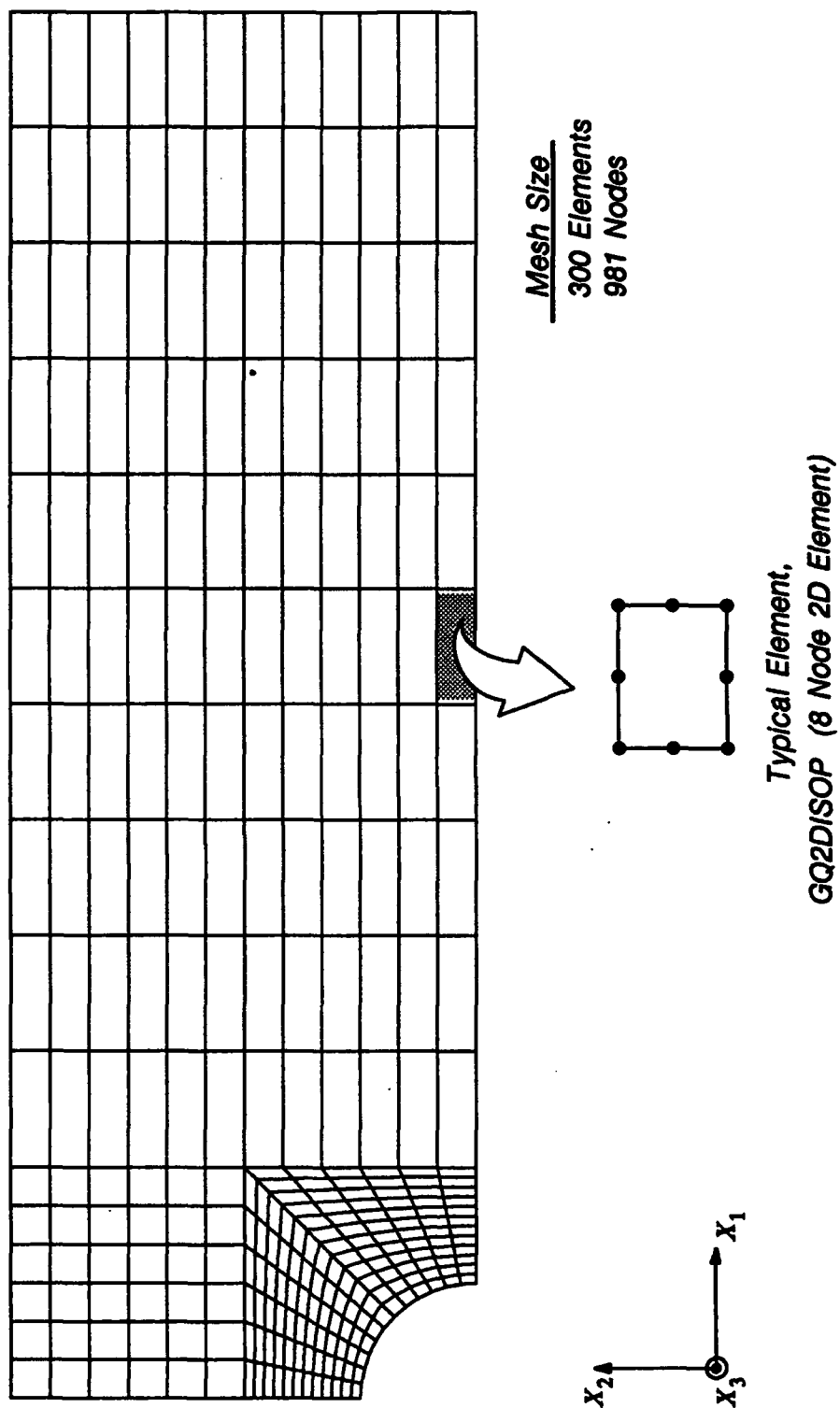GQ2DISOP (8 Node 2D Element)

X_1

X_2

X_3

Fig. 6.23 Finite element mesh employed in the analysis of $[(+45/-45)_6]_S$ notched coupon.
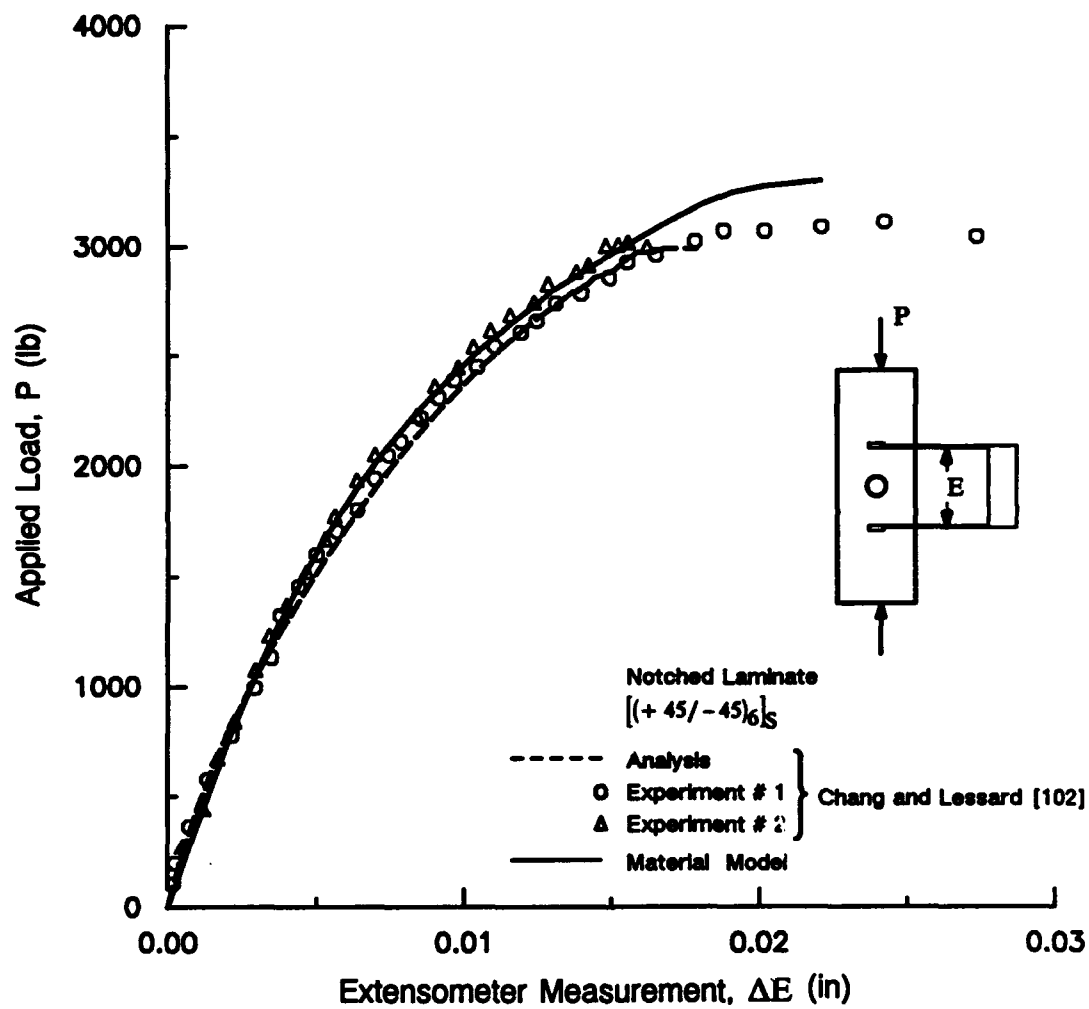
Fig. 6.24 *Load-shortening response of* $[(+45/-45)_6]_S$ *notched laminate.*

155

Applied Load-level P = 2750 lbs.

Fiber/Matrix
Shearing

Fiber Buckling

Fig. 6.25 *State of damage in* $\left[(+45/-45)_6\right]_s$ *notched laminate
at the load-level of P = 2750 lbs*

Applied Load-level P = 3200 lbs.
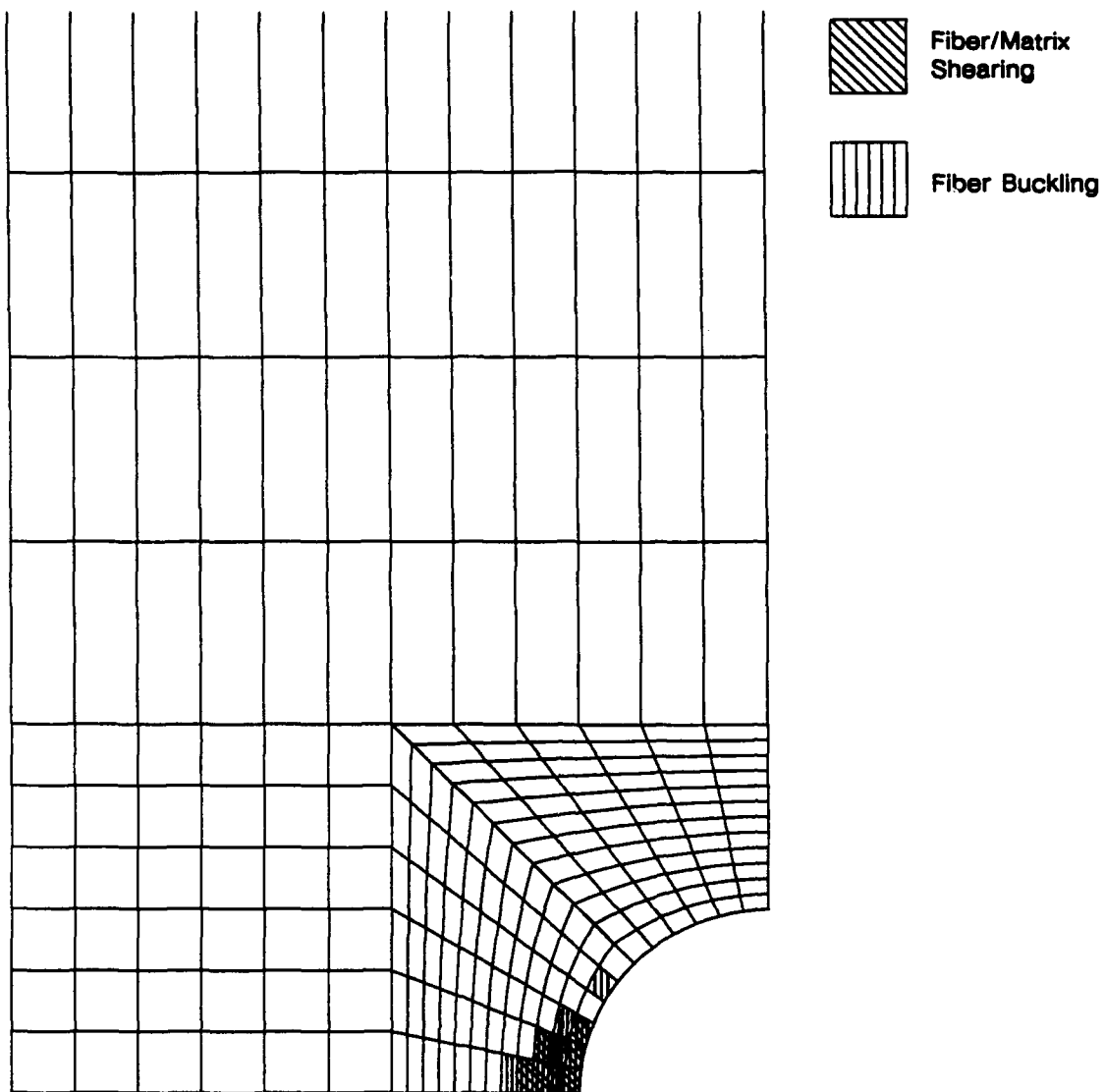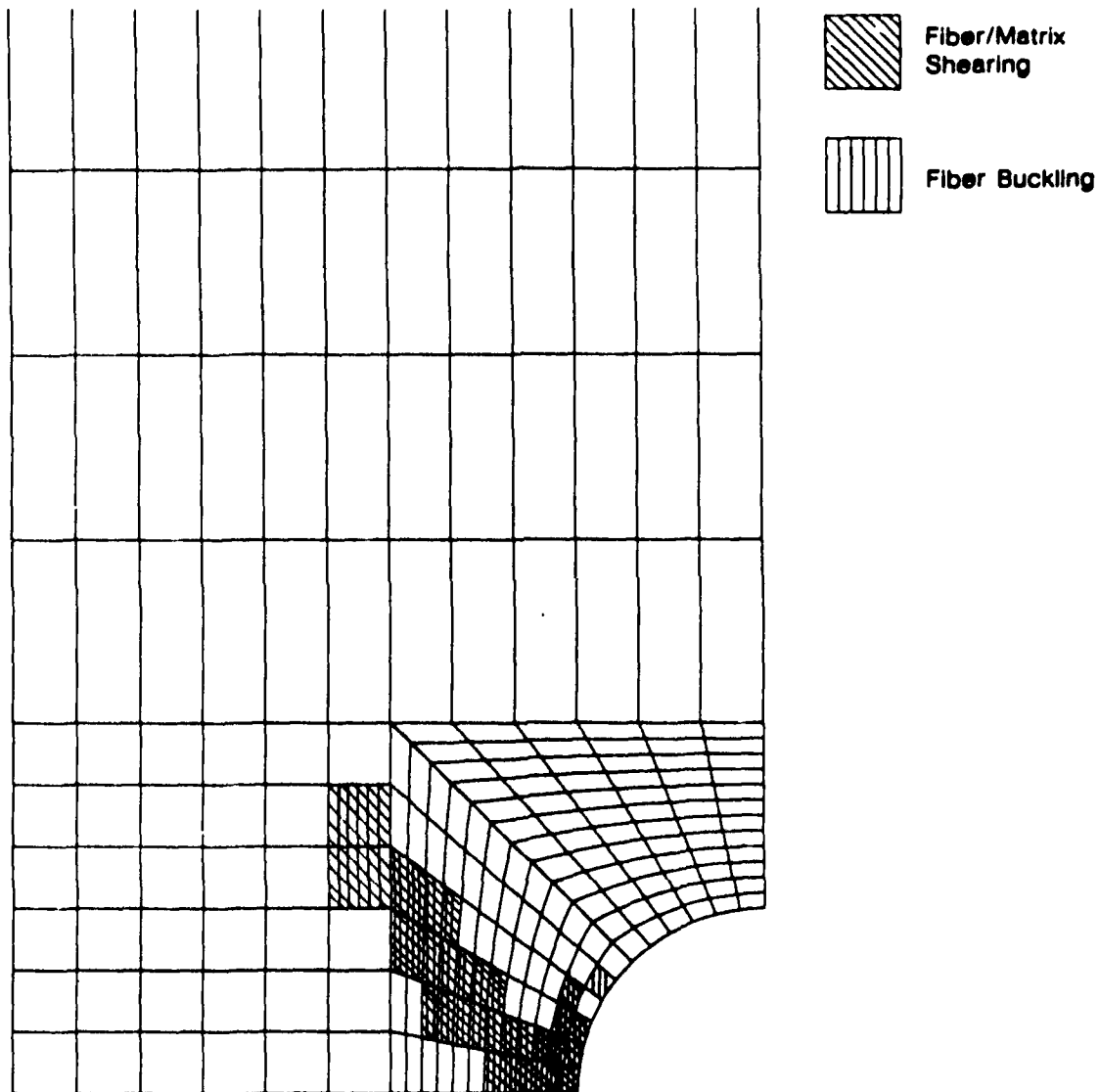

Fig. 6.26   State of damage in $[(+45/-45)_6]_S$ notched laminate
at the load-level of P = 3200 lbs
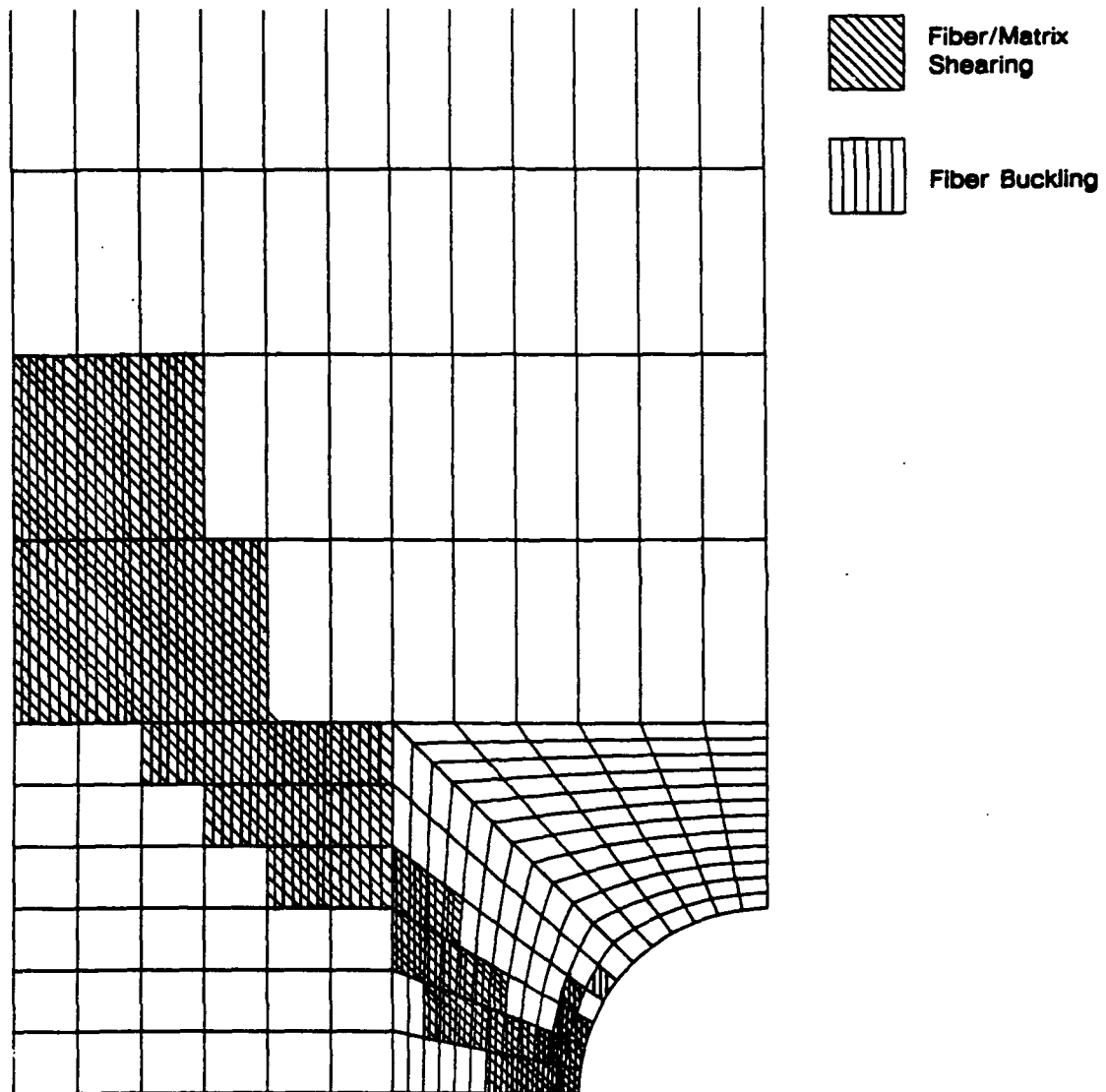
157

Applied Load–level P = 3320 lbs (Collapse–load)

Fiber/Matrix Shearing

Fiber Buckling

Fig. 6.27 *State of damage in* $[(+45/-45)_6]_s$ *notched laminate at the load–level of P = 3320 lbs (Collapse–load)*

CHAPTER 7

CONCLUSIONS AND RECOMMENDATIONS

The objective of the present study was to develop general and accurate procedures for analysis of fiber–reinforced laminated structures which also allow the use of standard displacement-based finite elements. The stress and strain fields in laminated composites can exhibit discontinuities; procedures were sought which take this phenomenon into account.

A micromechanical constitutive theory was used to characterize the composite lamina. The material model has a two–level hierarchical structure. At the bottom level, the *Micro–model* synthesizes the constitutive information about fiber and matrix phases to yield the effective stress–strain response of a unidirectional lamina. At the top level the *Sublaminate model*, using a 3–D lamination scheme, assembles the laminae forming the smallest repeating stack within the laminate to deliver the effective stress–strain response of the laminate. Local stresses and strains in a lamina or in fiber and matrix phases can be recovered from the effective values at any stage. The material modelling procedure enables the use of standard displacement based finite elements for the analysis of fiber–reinforced laminated composites.

In this study the micromechanical model presented by Pecknold [57] is employed and enhanced to model the behaviour of unidirectional lamina. It was found to yield very accurate results in spite of its simplicity.

Several conclusions based on the results of this study are discussed next.

159

7.1 Conclusions

General conclusions about the overall modelling procedure are presented first. Next, conclusions regarding the micro–model are presented. Finally, some observations on micromechanical modelling of fiber–reinforced composites are presented.

7.1.1 General

The material modelling procedure successfully enables the use of standard displacement–based finite elements for the analysis of laminated composites. The general scheme has sufficient flexibility in it so that different types of constitutive descriptions for the fiber and matrix constituents can be incorporated easily. The modelling procedure satisfies the equilibrium requirements on the tractions at the laminae interfaces.

7.1.2 Micro–model

The micro–model is the kernel on which the accuracy of the overall modelling scheme depends. Therefore, the micro–model (Pecknold [57]) was investigated in detail; conclusions are presented below.

The micro–model is quite simple in its description, but accurately accounts for the three–dimensional matrix restraining effects of the fiber reinforcement. The micro–model is valid for general multi–axial stress states. The elastic moduli of composite laminae predicted by the micro–model show excellent agreement with results from detailed numerical schemes and experimental data; it was found to be comparable in accuracy to Aboudi's Method of Cells [7], but is much simpler. The predicted effective coefficients of thermal expansion were also in very good agreement with results from Aboudi's Method of Cells.

The micro–model gives accurate results for nonlinear response of composite laminae. The results obtained compared very well with experimental data.

The results for off–axis strengths of composite laminae were in very good agreement with experimental data. The micro–model predictions of initial yield surfaces of

160

metal matrix composites compared very well with finite element based results and with the Method of Cells; the only exception being the case when the composite lamina is subjected to a hydrostatic stress state, in which case both the micro–model and the Method of Cells performed poorly. However, the results improved as the applied stress state moved away from the hydrostatic stress state.

7.1.3 Comments on Micromechanical Modelling

Micromechanics based material models are a viable option for characterizing the behaviour of composite materials and can be successfully used for analyzing structures made from such materials. The advantage of micromechanics based material models is that they predict the behaviour of composites from the fundamental properties of its basic constituents and also represent the microstructure of the composite to some extent. Therefore, they can accommodate relatively complex aspects of composite material behaviour, such as debonding at the fiber/matrix interface and matrix cracking. The complex constitutive description of composites can be obtained by synthesizing comparatively simple constitutive descriptions of its constituents and their interaction.

The problems associated with the material modelling procedure are those usually associated with the use of micromechanics. For example it is known that the *in situ* properties of the matrix material can be quite different from the properties of matrix material in bulk. Direct measurement of the in situ properties of the matrix and fiber are at this time (1992) not possible, and these properties have to be back–calculated from the lamina properties determined from simple tests.

In this study micromechanical failure criteria were employed for determining failure in the lamina. Only the in–plane failure mechanisms were considered and the failure mechanisms such as delaminations were not considered. Maximum stress failure criteria were successfully employed to determine failure modes such as fiber fracture in tension, matrix cracking in transverse direction, and matrix crushing in compression. For predic-

161

tion of axial compressive strength of lamina a micromechanics based criterion suggested by Hahn and Williams [95] was investigated, but was found to overestimate the axial compressive strength.

In the author's opinion, micromechanics based material modelling procedures have great potential, and as the problem of scarcity of experimental studies is solved and better experimental procedures are developed, the area of micromechanics should see significant improvement. Therefore, micromechanics based structural analysis procedures deserve continued investigation.

7.2 Recommendations

Here, some possible changes and enhancements that can be made to the material modelling procedure are presented. The suggested recommendations concern mostly the micromechanical modelling.

- In order to investigate problems involving thermal loading, strain rate effects and creep, incorporation of a unified viscoplasticity theory, such as the Bodner-Partom theory [69] would indeed be very useful.

- In this study relatively simple failure criteria were employed at the micromechanical level to determine the onset of failure. A possible improvement would be to employ interaction type criteria, which take into account the interaction of stresses, and at the same time provide information about the mode of failure.

- The manner in which the effect of localized damage is incorporated is an important consideration. Accurate modelling of the effect of damage is needed for accurate prediction of the laminate response and the ultimate load carrying capacity of composite structures. The field of *Damage Mechanics* provides damage evolution laws and pro-

cedures for incorporating the resulting deterioration and loss of stiffness in a material. In the present study simple procedures were employed to simulate the effect of damage. Incorporation of concepts and procedures from the area of damage mechanics within the micro–model may result in further improvements in the predictions from the material modelling procedure.

- Deterioration in the bond between the fiber and the matrix at the interface can significantly affect the overall properties of the composite lamina. This has been demonstrated by Aboudi's Method of Cells. The capability to model fiber/matrix interface failure should also be incorporated in the micro–model.

BIBLIOGRAPHY

1. Lee, S. M., *Reference Book for Composite Technology*, Lee. S. M. editor, Vol. 1-2, Technomic, 1989.

2. *Handbook of Composites*, Lubin, G. editor, Van Nostrand Reinhold Co., 1982.

3. Jones, R. M., *Mechanics of Composite Materials*, McGraw-Hill Book Co., 1975.

4. Harris, B., *Engineering Composite Materials*, The Institute of Metals, London, 1986.

5. Christensen, R. M., *Mechanics of Composite Materials*, Wiley-Interscience, New-york, 1979.

6. Tsai, S. W. and Hahn, H. T., *Introduction to Composite Materials*, Technomic, West-port, 1980.

7. Aboudi, J., *Mechanics of Composite Materials — A Unified Micromechanical Approach*, Elsevier, 1991.

8. Chamis, L. C. and Sendeckyj, G. P., "Critique on Theories Predicting Thermoelastic Properties of Fibrous Composites," *J. Composite Materials*, Vol. 2, 1969, pp. 332-358.

9. Hashin, Z., "Analysis of Composite Materials — A Survey," *ASME J. Appl. Mechanics*, Vol. 50, 1983, pp. 481-505.

10. Hashin, Z., "Theory of Fiber Reinforced Materials," NASA Report CR-1974, 1972.

11. McCullough, R. L., "Micro-Models for Composite Materials — Continuous Fiber Composites," in *The Delaware Composites Design Encyclopedia*, Vol. 2 (*Micromechanical Materials Modeling*), Carlsson, L. A. and Gillespie, J. W. editors, Technomic Publishing Co., 1990.

12. Shaffer, B. W., "Stress-Strain Relations of Reinforced Plastics Parallel and Normal to Their Internal Filaments," *AIAA Journal*, Vol. 2, 1964, pp. 348-352.

13. Halpin, J. C. and Tsai, S.W., "Effects of Environmental Factors on Composite Materials," Air Force Technical Report AFML-TR-67-423, June, 1969.

14. Ashton, J.E., Halpin, J. C. and Petit, P. H., *Primer on Composite Materials: Analysis*, Technomic Publishing Co., 1969.

15. Evkall, J. C., "Structural Behavior of Monofilament Composites," *AIAA/ASME 7th Structures, Structural Dynamics and Materials Conference* , Palm Springs, California, 1966, p. 250.

16. Abolin'sh, D. S., "Compliance Tensor for an Elastic Material Reinforced in One Direction," *Polymer Mechanics*, Vol. 1, 1965, pp. 28-32.

17. Hill, R., "Theory of Mechanical Properties of Fiber-Strengthened Materials: I. Elastic Behaviour," *J. Mechanics and Physics of Solids*, Vol. 12, 1964, pp. 199-212.

18. Hill, R., "Theory of Mechanical Properties of Fiber-Strengthened Materials: II. Inelastic Behaviour," *J. Mechanics and Physics of Solids,* Vol. 12, 1964, pp. 213-218.

19. Hill, R., "Theory of Mechanical Properties of Fiber-Strengthened Materials: III. Self-Consistent Model," *J. Mechanics and Physics of Solids,* Vol. 13, 1965, pp. 189-198.

20. Budiansky, B., "On the Elastic Moduli of some Heterogeneous Materials," *J. Mechanics and Physics of Solids*, Vol. 13, 1965, p 223.

21. Whitney, J. M. and Riley, M. B., "Elastic Properties of Fiber Reinforced Composite Materials," *AIAA Journal*, Vol. 4, 1966, pp. 1537-1542.

22. Hermans, J. J., "The Elastic Properties of Fiber Reinforced Materials When the Fibers are Aligned," *Proceedings Koninklijke Nederlandse Akademie van Wetenschappen, Series B*, Vol. 70, 1967, pp. 1-9

23. Christensen, R. M. and Lo, K. H., "Solutions for Effective Shear Properties in Three Phase Sphere and Cylinder Models," *J. Mechanics and Physics of Solids*, Vol. 27, 1979, pp. 315-330.

24. Hashin, Z., "On Elastic Behaviour of Fiber Reinforced Materials of Arbitrary Transverse Phase Geometry," *J. of Mechanics and Physics of Solids*, Vol. 13, 1965, pp. 119-134.

25. Hashin, Z. and Rosen, B. W., "The Elastic Moduli of Fiber Reinforced Materials," *ASME J. Appl. Mechanics,* Vol. 31, 1964, pp. 223-232.

26. Dow, N. F. and Rosen, B. W., "Evaluations of Filament-Reinforced Composites for Aerospace Structural Applications," NASA Report CR-207, April 1965.

27. Hashin, Z., "Assessment of the Self Consistent Scheme Approximation: Conductivity of Particulate Composites," *J. Composite Materials*, Vol. 2, 1968, pp. 284-300.

28. Hashin, Z., "Analysis of Properties of Fiber Composites With Anisotropic Constituents," *ASME J. Appl. Mechanics*, Vol. 46, 1979, pp. 543–550.

29. Foye, R. L., "An Evaluation of Various Engineering Estimates of the Transverse Properties of Unidirectional Composites," *SAMPE*, Vol. 10, 1966, p. G–31

30. Adams, D. F. and Doner, D. R., "Longitudinal Shear Loading of a Unidirectional Composite," J. Composite Materials, Vol. 1, 1967, pp. 152–164.

31. Adams, D. F. and Doner, D. R., "Transverse Normal Loading of a Unidirectional Composite," *J. Composite Materials*, Vol. 1, 1967, pp. 4–17.

32. Chen, C. H. and Cheng, S., "Mechanical Properties of Fiber–Reinforced Composites," *J. Composite Materials*, Vol. 1, 37, 1967, pp. 30–41.

33. Chen, C. H. and Cheng, S., "Mechanical Properties of Anisotropic Fiber–Reinforced Composites," *ASME J. Appl. Mechanics*, Vol. 37, 1970, pp. 186–189.

34. Pickett, G., "Elastic Moduli of Fiber Reinforced Plastic Composites," in *Fundamental Aspects of Fiber Reinforced Composites*, Schwartz, R. T. and Schwartz, H. S. editors, Interscience Publishers, 1968.

35. Foye, R. L., "Theoretical Post–Yielding Behaviour of Composite Laminates Part I — Inelastic Micromechanics," *J. Composite Materials*, Vol. 7, 1973, pp. 178–193.

36. Adams, D. F., "Inelastic Analysis of a Unidirectional Composite Subjected to Transverse Normal Loading," *J. Composite Materials*, Vol. 4, 1970, pp. 310–328.

37. Adams, D. F. and Crane, D. A., "Finite Element Micromechanical Analysis of a Unidirectional Composite Including Longitudinal Shear Loading," *Computers and Structures*, Vol. 18, 1984, pp. 1153–1165.

38. Hutchinson, J. W, "Elastic–Plastic Behaviour of Polycrystalline Metals and Composites," *Proc. of the Royal Society (London), Series A*, Vol. 319, 1970, p. 247.

39. Dvorak, G. J., Rao, M. S. M. and Tarn, J. Q., "Yielding in Unidirectional Composites Under External Loads and Temperature Changes," *J. Composite Materials*, Vol. 7, 1973, pp. 194–216.

40. Dvorak, G. J., Rao, M. S. M. and Tarn, J. Q., "Generalized Initial Yield Surfaces for Unidirectional Composites," *ASME J. Appl. Mechanics*, Vol. 41, 1974, pp. 249–253.

41. Dvorak, G. J. and Bahei-El-Din, Y. A., "Elastic–Plastic Behaviour of Fibrous Composites," *J. Mechanics and Physics of Solids*, Vol. 27, 1979, pp. 51–72.

42. Dvorak, G. J. and Bahei-El-Din, Y. A., "Plasticity Analysis of Fibrous Composites," *ASME J. Appl. Mechanics*, Vol. 49, 1982, pp. 327-335.

43. Bahei-El-Din, Y. A. and Dvorak, G. J., "Plastic Yielding at a Circular Hole in a Laminated FP-Al Plate," in *Modern Developments in Composite Materials and Structures*, Vinson, J. R. editor, ASME, 1979, p. 123.

44. Bahei-El-Din, Dvorak, G. J. and Utku, S., " Finite Element Analysis of Elastic-Plastic Fibrous Composite Structures," *Computers and Structures*, Vol. 13, 1981, pp. 321-330.

45. Bahei-El-Din and Dvorak, G. J., "Plasticity Analysis of Laminated Composite Plates," *ASME J. Appl. Mechanics*, Vol. 49, 1982, pp. 740-746.

46. Wu, J. F., Shepard, M. S., Dvorak, G. J. and Bahei-El-Din, "A Material Model for the Finite Element Analysis of Metal Matrix Composites," *Composites Science and Technology*, Vol. 35, 1988, pp. 347-366.

47. Dvorak, G. J. and Teply, J. L., "Periodic Hexagonal Array Model for Plasticity Analysis of Composite Materials," in *Plasticity Today: Modeling, Methods and Applications, W. Olszak Memorial Volume*, Sawczuk, A. and Bianchi, V., editors, Elsevier Science Publishers, Amsterdam, 1985, pp. 623-642.

48. ABAQUS User's Manual, Version 4.5(a), Hibbit, Karlson and Sorensen, Inc., Providence, RI, 1985.

49. Rufin, A. C., Rimbos, P. G. and Bigelow, S. D., "Point-Stress Analysis of Continuous Fiber-Reinforced Composites Materials with an Elastic-Plastic Matrix," *Computers and Structures*, Vol. 20, 1985, pp. 375-385.

50. Min, K. B. and Crossman, F. W., "History Dependent Thermomechanical Properties of Graphite/Aluminum Unidirectional Composites," *Composite Materials: Testing and Design(Sixth Conference), ASTM STP 787*, Daniel, I. M., editor, American Society for Testing and Materials, 1982, p. 371.

51. Aboudi, J., "A Continuum Theory for Fiber-Reinforced Elastic-Viscoplastic Composites," *Int. J. Engineering Science*, Vol. 20, 1982, pp. 605-621.

52. Aboudi, J., "Micromechanical Analysis of Strength of Unidirectional Fiber Composites," *Composites Science and Technology*, Vol. 33, 1988, pp. 79-96.

53. Aboudi, J., "The Nonlinear Behaviour of Unidirectional and Laminated Composites — A Micromechanical Approach," *J. Reinforced Plastics and Composites*, Vol. 9, 1990, pp. 13-32.

54. Aboudi, J., "Micromechanical Analysis of Composites by the Method of Cells," *Appl. Mechanics Rev.*, Vol. 42, 1989, pp. 193–221.

55. Sun, C. T., and Chen, J. L., "A Micromechanical Model for Plastic Behaviour of Fibrous Composites," *Composites Science and Technology*, Vol. 40, 1990, pp. 115–129.

56. Sun, C. T, and Yoon, K. J., "Elastic–Plastic Analysis of AS4/PEEK Composite Laminate Using One–Parameter Plasticity Model," *J. Composite Materials*, Vol. 26, 1992, pp. 293–308.

57. Pecknold, D. A., "A Framework for 3–D Nonlinear Modeling of Thick–Section Composites," *DTRC–SME–90/92*, David Taylor Research Center, Bethesda, MD, 1990.

58. Hill, R., "A Theory of the Yielding and Plastic Flow of the Anisotropic Metals," *Proc. of Royal Society (London), Series A*, Vol. 193, 1948, pp. 281–297.

59. Hill, R., *The Mathematical Theory of Plasticity*, Oxford University Press, 1950.

60. Griffin, O. H., Kamat, M. P. and Herakovich, C. T., "Three–Dimensional Finite Element Analysis of Laminated Composites," *J. Composite Materials*, Vol. 5, 1981, pp. 543–560.

61. Petit, P. H, and Waddoups, M. E., "A Method of Predicting the Nonlinear Behavior of Laminated Composites," *J. Composite Materials*, Vol. 3, 1969, pp. 2–19.

62. Hahn, H. T. and Tsai, S. W., "Nonlinear Elastic Behaviour of Unidirectional Composite Laminae," *J. Composite Materials*, Vol. 7, 1973, pp. 102–118.

63. Hahn, H. T., "Nonlinear Behaviour of Laminated Composites," *J. Composite Materials*, Vol. 7, 1973, pp. 257–271.

64. Hashin, Z., Bagchi, D. and Rosen, B. W., "Nonlinear Behaviour of Fiber Composite Laminates," NASA CR–2313, 1974.

65. Dvorak, G. J. and Rao, M. S. M, "Axisymmetric Plasticity Theory of Fibrous Composites," *Int. J. Engineering Science*, Vol. 14, 1976, pp. 361–373.

66. Pipkin, A. C. and Rogers, T. G., "Plane Deformations of Incompressible Fiber–Reinforced Materials," *ASME J. Appl. Mechanics*, Vol. 38, 1971, pp. 634–640.

67. Mulhern, J. F., Rogers, T. G. and Spencer A. J. M., "A Continuum Model for Fiber –Reinforced Plastic Materials," *Proc. of Royal Society (London), Series A*, Vol. 301, 1967, pp. 473–492.

68. Mulhern, J. F., Rogers, T. G. and Spencer A. J. M., "A Continuum Theory of a Plastic–Elastic Fibre-Reinforced Material," *Int. J. Engineering Sciences*, Vol. 7, 1969, pp. 129–152.

69. Bodner, S. R. and Partom, Y., "Constitutive Equations for Elastic–Viscoplastic Strain Hardening Materials," *ASME J. Appl. Mechanics*, Vol. 42, 1975, p. 385

70. Arenburg, R. T., "Analysis of Metal Matrix Composite Structures Using a Micromechanical Constitutive Theory," Ph.D Dissertation, Virginia Polytechnic Institute and State University, Blacksburg, Virginia, 1988.

71. Arenburg, R. T. and Reddy, J. N., "Applications of the Aboudi Micromechanics Theory to Metal Matrix Composites," in *Mechanics of Composite Materials and Structures*, ASME AMD–Vol. 100, Reddy, J. N. and Teply, J. L. editors, 1989.

72. Camponeschi, E. T. Jr., "Compression of Composite Materials — A Review," *DTRC-SME-89/67*, David Taylor Research Center, Bethesda, MD, 1989.

73. Camponeschi, E. T. Jr., "Compression Testing of Thick–Section Composite Materials," *DTRC-SME-89/73*, David Taylor Research Center, Bethesda, MD, 1989.

74. Kriz, R. D. and Stinchcomb, W. W., "Elastic Moduli of Transversely Isotropic Graphite Fibers and Their Composites," *Exp. Mechs.*, Vol. 19, 1979, pp. 41–49.

75. Pagano, N. J, "Exact Moduli of Anisotropic Laminates," in *Mechanics of Composite Materials*, Sendeckyj, G. P., editor, Academic Press, 1974, pp. 23–44.

76. Sun, C. T. and Li, S., "Three–Dimensional Effective Elastic Constants for Thick Laminates," *J. Composite Materials*, Vol. 22, 1988, pp. 629–639.

77. Pipes, R. B. and Cole, B. W., "On the Off–Axis Strength Test for Anisotropic Materials," *J. Composite Materials*, Vol. 7, 1973, pp. 246–256.

78. Cole, B. W. and Pipes, R. B., "Filamentary Composite Laminates Subjected to Biaxial Stress Fields," Technical Report AFFDL-TR-73-115, Air Force Flight Dynamics Laboratory, 1974.

79. Petit, P. H., "Ultimate Strength of Laminated Composites," Report AFML–FZM–4977, Air Force Materials Laboratory, 1967.

80. Pipes, R. B., Kaminski, B. E. and Pagano, N. J., "Influence of the Free Edge upon the Strength of Angle–Ply Laminates," *ASTM STP 521*, American Society for Testing and Materials, 1973, pp. 218–228.

81. Lifshitz, J. M. and Gilat, A., "Experimental Determination of the Nonlinear Behavior of Fiber–Reinforced Laminae under Impact Loading," *Experimental Mechanics*, Vol. 19, 1979, pp. 444–449.

82. Lifshitz, J. M., "Nonlinear Matrix Failure Criterion for Fiber–Reinforced Composite Materials," *Comp. Tech. Rev*, Vol. 4, 1982, pp. 78–83.

83. Pindera, M. J. and Herakovich, C. T., "An Endochronic Theory for Transversely Isotropic Fibrous Composites," VPI-E-81-27, Virginia Polytechnic Institute and State University, 1981.

84. Pindera, M. J., Gurdal, Z., Hidde, J. S. and Herakovich, C. T., Mechanical and Thermal Characterisation of Unidirectional Aramid/Epoxy. CCMS-86-08, VPI-86-29, Virginia Polytechnic Institute and State University, 1986.

85. Hashin, Z. and Rotem, A., "A Fatigue Failure Criterion for Fiber Reinforced Materials," *J. Composite Materials*, Vol. 7, 1973, 448–464.

86. Becker, W., Pindera, M. J. and Herkovich, C. T., Mechanical Response of Unidirectional Boron/Aluminum under Combined Loading. CCMS-87-06, VPI-E-87-17, Virginia Polytechnic Institute and State University, 1987.

87. Pindera, M. J. and Aboudi, J., "Micromechanical Analysis of Yielding of Metal Matrix Composites," *Int. J. Plasticity*, Vol. 4, 1988, pp. 195–214.

88. Tsai, S.W. and Wu., E.M., "A General Theory of Strength for Anisotropic Materials," *J. Composite Materials*, Vol. 5, 1971, pp. 58–80.

89. Hashin, Z., "Failure Criteria for Unidirectional Fiber Composites," *ASME J. Applied Mechs.*, Vol. 47, 1980, pp. 329–334.

90. Tsai, S. W., "A Survey of Macroscopic Failure Criteria for Composite Materials," *J. Reinforced Plastics and Composites*, Vol. 3, 1984, pp. 40–62.

91. Nahas, M.N., "Survey of Failure and Post–Failure Theories of Laminated Fiber–Reinforced Composites," *J. Composites Technology and Research*, Vol. 8, 1986, pp. 138–153.

92. Rosen, B. W., "Mechanics of Composite Strengthening," in *Fiber Composite Materials*, American Society for Metals, Metals Park, Ohio, 1965, pp. 37–75.

93. Argon, A. S., "Fracture of Composites," in *Treatise on Materials Science and Technology*, Vol. 1, Herman, H. editor, Academic Press, 1972, pp. 79–114.

94. Budiansky, B., "Micromechanics," *Computers and Structures*, Vol. 16, 1983, pp. 3–12.

95. Hahn, H. T. and Williams, J. G., "Compression Failure Mechanisms in Unidirectional Composites," *Composite Materials: Testing and Design(Seventh Conference)*, *ASTM STP 893*, Whitney, J., editor, American Society for Testing and Materials, 1986, pp. 115–139.

96. POLO–FINITE User's Manual, Civil Engineering Systems Laboratory, University of Illinos at Urbana–Champaign, Urbana, IL

97. Garala, H. J., "Structural Evaluation of 8–inch Diameter Graphite–Epoxy Composite Cylinders Subjected to External Hydrostatic Compressive Loading," *DTRC–89/016*, David Taylor Research Center, Bethesda, MD, 1989.

98. Lekhnitskii, S. G., *Anisotropic Plates*, Translated from the second Russian edition by Tsai, S. W. and Cheron, T., Gordon and Breach Science Publishers.

99. Ren, J. G., "Exact Solutions for Laminated Cylindrical Shells in Cylindrical Bending," *Composites Science and Technology*, Vol. 3, 1987, pp. 169–187.

100. Shukow, S. I., "Acoustic/Mechanical Characterization of Boron/Aluminum Composite Laminates," M.S. Thesis, University of Delaware, June 1978.

101. Biglow, C. A., Johnson, W. S. and Naik, R. A., " A Comparison of Various Micromechanics Models for Metal Matrix Composites," in *Mechanics of Composite Materials and Structures*, ASME AMD–Vol. 100, Reddy, J. N. and Teply, J. L. editors, 1989, pp. 21–31.

102. Chang, Fu–Kuo and Lessard, L. B., "Damage Tolerance of Laminated Composites Containing an Open Hole and Subjected to Compressive Loadings: Part I — Analysis," *J. Composite Materials*, Vol. 25, 1991, pp. 2–43.

103. Chang, Fu–Kuo and Lessard, L. B., "Damage Tolerance of Laminated Composites Containing an Open Hole and Subjected to Compressive Loadings: Part II — Experiment," *J. Composite Materials*, Vol. 25, 1991, pp. 44–64.